ELASTOSTATIC ANALYSIS OF THICK-WALLED TORI AND PIPE BENDS USING THE BOUNDARY INTEGRAL EQUATION METHOD

by

A. R. COLLE

Thesis presented to the School of Graduate Studies
as partial fulfillment of the requirements
for the degree of M.A.Sc. in
Mechanical Engineering

UNIVERSITY OF OTTAWA
OTTAWA, CANADA, 1986

ELASTOSTATIC ANALYSIS OF THICK-WALLED TORI AND PIPE BENDS USING THE BOUNDARY INTEGRAL EQUATION METHOD

Thesis Supervisor

Author

Abstract

The three-dimensional (3-D) Boundary Integral Equation (BIE) method is applied to elastostatic problems involving relatively simple and complicated thick-walled cylindrical and toroidal geometries. Verification of the suitability of the 3-D BIE mesh is made by comparing with results from the axisymmetric Finite Element (FE) method and the axisymmetric BIE method. The loading considered for the verification is internal pressure and the geometries include hollow tori of circular and elliptical cross-sections. Results from the BIE method are then presented and compared with results from the Toroidal Elasticity (TE) theory of H. A. Lang. Cases covered are internal pressure loading of a hollow torus and in-plane bending, out-of-plane bending, twist bending, in-plane end shear force, in-plane end normal force and out-of-plane end shear force of a thick-walled 90° elbow. The comparisons are useful in establishing the number of terms required in the TE solutions. Satisfactory agreement is obtained between the BIE and TE results for the first four loadings with the number of terms already developed by H. A. Lang.

The 3-D BIE method is then applied to three problems of complex geometries. The first concerns a thick walled U-bend, with straight pipes, subjected to internal pressure and in-plane bending loads. Results are presented for stresses and are compared with results previously obtained for relatively simple geometries. The second and third problems concern a pressurized thick-walled cylinder and torus with cross-bore(s). Two cylinders are considered, one cylinder having a single cross-bore while the other two cross-bores. Separate solutions for the torus are given for cross-bores located at the intrados and extrados with the cross-bores situated in the toroidal plane. Results obtained show that the stress concentration factor is smaller for a torus with cross-bores at the extrados than a cylinder with one or two cross-bores.

Acknowledgements

The author wishes to express his sincere gratitude to Professor D. Redekop for his encouragement and valuable direction throughout this study.

The author is grateful to Professor C. L. Tan of Carleton University for the use of his computer programs and also for his valuable advice on the BIE method and computer programs.

Special thanks to Mr. S. Bélanger and my fellow graduate students for their helpful advices and to my wife, Patricia, for typing this manuscript and for her encouragement.

This work was supported by a grant from the Natural Sciences and Engineering Research Council of Canada.

Contents

List of Figures

List of Tables

Nomenclature

A	Area of cross-section
a	Internal radius of cross-section
b	External radius of cross-section
$C_{ij}(P)$	Limit defined in equation (2.24)
c	Semi-major axis of an ellipse
D_{ki_j}	Third-order tensor displacement Kernel
d	Semi-minor axis of an ellipse
$d(b,c)$	Number of c^{th} node of b^{th} element
E	Young's modulus
E_1	Product of an elliptic integral of the second kind
$\overline{F}_i$	Components of the body forces
F_i	In-plane end shear force
F_n	In-plane end normal force
F_o	Out-of-plane end shear force
H	Semi length of cylinder
h	Wall thickness
I	Moment of inertia
I_p	Polar moment of inertia
$J(\varsigma)$	Jacobian of coordinate transformation
K_h	Stress concentration factor
L	Total length of the straight pipe
L_1	Maximum dimension of the physical problem
M_i	In-plane bending moment

M_o	Out-of-plane bending moment
M_t	Twist bending moment
m	Number of elements
$N^c(\zeta)$	Quadratic shape functions of intrinsic coordinates
n_i	Unit vector along outward normal to surface of body
P	Load point on surface of body
P^a	a^{th} node on surface of body
P_i	Internal pressure
p	Load point inside body
p_1	Circumference of an ellipse
Q	Field point on surface of body
q	Number of nodes
R	Domain of body under consideration, Mean toroidal radius
R_ϵ	Domain of body within a sphere of radius ϵ
R_s	Cross bore radius
r	Distance from p to Q, Radial distance from the cross-section axis
r_m	Mean cross-section radius
r, ϕ, θ	Toroidal coordinates
S	Surface of body
$S(N)$	N^{th} field of stress
S_ϵ	Surface of a sphere of radius ϵ
S_{kij}	Third-order tensor traction Kernel
T_{ij}	Second-order tensor traction Kernel
t	Thickness ratio
t_i	Boundary traction vector
U_f	Displacement factor $UE/P_i a$
U_r, U_ϕ, U_θ	Radial, circumferential and longitudinal displacement
U_x, U_y, U_z	Displacement in the cartesian coordinates
U_ρ, U_α, U_Z	Displacement in the cylindrical coordinates

U_{ij}	Second-order tensor displacement Kernel
u_i	Displacement vector
x_i	General coordinates
x, y, z	Cartesian coordinates
α	Angle of rotation about the longitudinal axis Z
γ	Toroidal radius ratio
δ_{ij}	Kronecker's delta
ϵ	Radius of small sphere centred at P
ϵ_{ij}	Strain tensor
ζ_1, ζ_2	Intrinsic coordinates
θ	Longitudinal angle
λ	Lame's coefficient
λ_1	Pipe factor Rh/r_m^2
μ	Shear modulus
ν	Poisson's ratio
ρ, α, Z	Cylindrical coordinates
σ	Actual stress
σ_f	Stress factor
σ_{ij}	Stress tensor
σ_{max}	Maximum stress factor
$\sigma_r, \sigma_\phi, \sigma_\theta$	Normal stress in toroidal coordinate
$\sigma_{r\phi}, \sigma_{r\theta}, \sigma_{\phi\theta}$	Shear stress in toroidal coordinate
$\sigma_x, \sigma_y, \sigma_z$	Normal stress in cartesian coordinate
$\sigma_{xy}, \sigma_{yz}, \sigma_{zz}$	Shear stress in cartesian coordinate
$\sigma_\theta, \sigma_z, \sigma_l$	Longitudinal stress
$\sigma_\rho, \sigma_\alpha, \sigma_Z$	Normal stress in cylindrical coordinate
$\sigma_{\rho\alpha}, \sigma_{\rho Z}, \sigma_{\alpha Z}$	Shear stress in cylindrical coordinate
σ_ϕ	Circumferential or hoop stress
$\sigma_{\phi,al}$	Hoop stress in cylinder

$\sigma_{\phi_{exact}}$	Hoop stress in cylinder (Lame's solution)
ϕ	Circumferential angle

Chapter 1

Introduction

The use of high pressures in pressure vessel and piping engineering requires the employment of thick-walled pipes, and consequently of thick-walled pipe bends. An estimation of the total number of pipe elbows in a nuclear plant is 13000 for one reactor unit and 25500 for two reactor units. Admittedly, many of these elbows are thin-walled and are part of the nuclear plant system. If the pipe is to carry fluid at an appreciable pressure, it is equally necessary to know the stress produced in a given pipe bent by internal pressure and bending loads. The ASME Boiler and Pressure Vessel Code [1] acknowledges the need for additional work in the area of end effects for curved pipe or welding elbows.

The topic of the behaviour of toroidal membranes and shells under internal pressure and bending loads has been given a great deal of attention in recent years. However, relatively few articles have appeared concerning similar analyses for thick-walled toroidal shells. The few published analytical treatments available are based on the method of successive approximations, to reduce the complexity of the problem, and are therefore only approximate. In the absence of exact analytical solutions, accurate three-dimensional treatments of thick-walled pipe bends have to be obtained numerically.

Although finite element (FE) and finite difference (FD) techniques could be used no results obtained by these techniques for incomplete thick-walled toroidal geometries are available in the literature. In view of the complexity of the problem,

the computing costs for accurate solutions would be very high using these methods. The technique employed here is the direct boundary integral equation (BIE) method, which for many applications is both more accurate and more economical in use of computer time than the FE method.

The objective of this thesis is to demonstrate the power and versatility of the direct boundary integral equation (BIE) method for three-dimensional stress analysis, to further illustrate the advantages of the BIE method by applying it to toroidal geometries, to provide stress factors for geometries and loadings not previously considered and to verify the applicability of the stress fields determined by toroidal elasticity (TE).

A background of the analytical, experimental and numerical work done on pipe bends and on thick-walled cylinders with cross-holes is given. Then a review of the basic equations of the direct boundary integral equation method is presented. This is followed by the selection of a suitable BIE mesh for toroidal geometry to obtain accurate results. This is done by comparing the three dimensional BIE results with exact and numerical results from the axisymmetric FE and axisymmetric BIE methods. Having determined a suitable mesh, results are found for a torus under internal pressure and for 90° elbows subjected separately to three in plane loads and three out of plane loads. These results are then compared with results determined by the TE method. This in turn will establish the number of terms required in the various TE solutions.

The BIE method is then used to determine the stresses in thick-walled U-bends with tangent pipes, subjected to internal pressure and in-plane bending. Next, to further illustrate the advantages of the BIE method, it is applied to a thick-walled torus with cross bores. The thesis ends with a discussion of the results for these analyses.

1.1 Pipe Bends Background

The analysis of pipeline systems to obtain the deflections, terminal reactions and stresses, was one of the earliest uses of computers in pressure vessel design. Each length of straight pipe was assumed to behave as a simple beam and hangers, mountings flanges and pumps were introduced as springs or rigid constraints. The work on pipe bends was started by Von Karman [2] who developed a solution for circular thin-walled bends under in-plane bending in 1911 and was followed by Vigness [3] for out-of-plane bending in 1943.

Pardue and Vigness [4] investigated the effect of flexibility and stress intensification factors for U-bends and 90° bends under in-plane and out-of-plane bending using a theoretical analysis and experimental test. The theoretical analysis used was an extension to Von Karman theories. The experiments consisted of tests on a series of thin-walled tube bends having a ratio of bend radius to tube radius equal to 3. The effect of the end conditions has been studied experimentally but not theoretically. The type of end constraints considered are two straight sections, one rigid flange and one straight section (this condition used for right-angle bends only) and two rigid flanges attached to the ends of the bends. They concluded that addition of constraints such as flanges at the ends of bends, greatly increases the bending rigidity which is especially true if the angle of turn is 90° or smaller.

Pardue and Vigness [5] in a second paper, experimentally investigated the effect of flanges on the maximum meridional and longitudinal stress intensification factors as well as the flexibility factors for 45°, 90° and 180° bends under in-plane and out-of-plane loads. Their investigation included bends terminated by one flange, two flanges as well as no flanges. The results indicated that the smaller the central angle of the pipe bend and the greater the number of end flanges, the larger the deviation from the axisymmetric theoretical predictions. The magnitudes of maximum meridional stress intensification and flexibility factors decreased while the maximum longitudinal stress intensification factor increased when flanges were appended to the pipe bends. However, the results for smaller angle bends appeared

to be erratic due probably to experimental difficulties.

Vissat and Del Buono [6] also investigated the effect of flanges on the stress intensification and flexibility factors, but for U-bends only. Results similar to those of Pardue and Vigness [5] were obtained.

Rodabaugh and George [7] established the flexibility and stress factors of curved pipe due to in-plane and out-of-plane bending including the effect of internal pressure using the strain energy method. They proved the adequacy of this method by means of carefully conducted tests. The theoretical formulas developed can be used for elbows of r_m/h up to 50 and R/r_m ratios ranging from 2 to infinity. Elbows of r_m/h ratios ranging from 29 to 94 ($R/r_m = 3$ to 9.5) were used for the experimental tests. They concluded that pressure in thin-walled piping subjected to in-plane and out-of-plane bending tends to reduce the effect of flexibility and stress factors, but for relatively thick-walled piping the effect is of a low order and may be neglected.

Swanson and Ford [8] experimentally studied the behaviour of stresses in thick-walled U-bends with integral straight tangent pipes under internal pressure and bending loads, both separately and together. Two pipe bends were considered, having pipe factors, λ_1 (defined as Rh/r_m^2), of 4.57 and 1.76, where the second bend had a non-circular cross section. The measured values were compared with existing theories for thin-walled bends. The theories of Turner and Ford [9] and Barthelemy [10] predicted the maximum equivalent stress up to 20% higher than those derived from the experiments. They reported that no existing theory adequately represented the stress in thick-walled pipe bends under internal pressure loading. The authors modification to Thuloup's [11] theory for internal pressure agreed fairly well with the measured stress of the pipe bend of regular cross-sections. They concluded that the stresses caused by internal pressure depend strongly on the deviations from circularity of the cross-section and that the bending and pressure stress systems were found to be superposable.

Kornecki [12] investigated the state of stress in a closed toroidal shell of uniform thick-walled circular cross section, when loaded by uniform internal and external

pressures. He used toroidal elasticity which is based on the method of successive approximations. Kronecki developed the zero, first and second order fields of stress of the series. A numerical example was given for internal pressure loading.

Smith and Ford [13] did experimental work on in-plane and out-of-plane bending of thin-walled pipe bends. The experimental results were compared with results calculated from existing theories. They indicated that although agreement between measured and calculated stresses was satisfactory for in-plane bending, it wasn't for out-of-plane bending. They acknowledged that a more exact theoretical analysis is needed for out-of-plane bending.

Then Smith [14] adapted a theoretical treatment of the elastic flexure of curved tubes already published by Turner and Ford [9] for in-plane bending to deal with out-of-plane bending. Results for both in-plane and out-of-plane are shown when acting separately and combined. Results were done for R/r_m ranging from 2 to 10 and a range of pipe thickness represented by h/r_m from 0.02 to 0.06. A design procedure is suggested to find the maximum stresses due to combined in-plane, out-of-plane and torsional bending moments.

Jones [15] developed an analysis which is an extension of Von Karman's original theory. From this analysis he obtained the stresses and flexibilities for in-plane bending of a curved thin pipe bend. He concluded that the stresses in and flexibility of pipe bends are virtually independent of the ratio r_m/R and depend almost entirely on the pipe factor λ_1.

Thailer and Cheng [16] were concerned with the analysis of 180° bends ($R/r_m = 3$), containing rigid flanges at both ends, subjected to in-plane end moments. The methods used was that of minimization of the potential energy [Raleigh-Ritz]. The tube was considered to be thin shell. The results agreed very well with the existing experimental results of Pardue and Vigness [5]. They concluded that the analytical results for a U-bend with rigid end flanges seem to be reasonably confirmed by experiments.

McGill and Rapp [17] presented results of an analysis of a thick-walled torus

subjected to internal pressure, in which displacements as well as stresses were examined. The solution was obtained by the use of axisymmetric finite difference method. He noted that the results for the stresses agreed very well with those of Kornecki [12] except for the longitudinal stress. The authors uncovered an error in Kornecki's expression for the longitudinal stress. A further case where the torus was subjected to circumferential shear was studied.

Natarajan and Blomfield [18] have used the finite element method, in conjunction with doubly curved shell elements for calculations of stress intensification and flexibility factors of curved pipes with attached pipes and flanges as end constraints subjected to in-plane bending. Various pipe bend angles were analysed (30° to 180°) and also a reversed 90° bend. They showed that the flexibility of pipe bends is dependent on both the ratio r_m/R and pipe factor (λ_1) contrary to the observation of Jones [15] and that the relationship between the bend angle and the corresponding maximum stress is non-linear. They indicated that the assumption of sections in a curved pipe remaining plane after deformation is not valid. They concluded that the flexibility of an elbow with end restraints is reduced.

Thompson [19] using Flugge's shell theory investigated the stresses produced in pipe bends ($h/r_m = 0.1$) due to internal pressure and in-plane bending. He showed that the maximum axial bending stress factor does not depend on the pipe factor alone, contrary to the conclusion of Jones.

Ohtsubo and Watanabe [20] investigated the flexibility and stress factors for 90° pipe bends ($\lambda_1 = 0.05$ to 0.5) connected with and without straight pipes and subjected to in-plane and out-of-plane bendings using the finite ring element method. The method was based on the general thin shell theory incorporating shear strains. They concluded that reductions take place in both flexibility and stress factors of bends with straight pipes as end restraints.

Whatham [21] used thin shell theory to calculate the stresses and flexibilities in curved pipes with flanged ends subjected to in-plane bending. The results were verified by experiment. His analysis showed that flanges reduce in-plane bend fle-

xibility and high circumferential stresses in curved pipe bends but produce high longitudinal stress adjacent to the flange.

Lang [22], using toroidal elasticity employed earlier by Kornecki [12], studied the same problem of a torus subjected to internal and external pressure. Lang developed the zero, first and second order fields of stress, displacement and ovalization of the series. He gave one set of numerical results for thick-walled elbows typical of heat exchangers and a steam generator.

Natarajan and Mirza [23] did work concerning stress analysis of pipe bends with end contraints subjected to out-of-plane moments.This analysis was constrained to thin shells solved by finite element method.

Lang [24] supplied details for the analysis of a pressurized elbow or torus, presented in his earlier paper [22]. The discussion was limited to the stress fields produced by internal pressure. Corrections to some constants were given. Details about displacements and ovalization were not given.

Lang [25] expanded the use of toroidal elasticity to end bending moment loading of a toroidal tube or pipe bend. Bending in the plane of the tube was considered. The analysis was limited to the first order of stress, strain and displacement fields. Later Lang [26] extended the stress fields by determining the second order. No numerical results were presented. Still using the general theory of toroidal elasticity, Lang determined the stress fields for a 90° elbow or pipe bend having several different loadings. The applied loads were twist and out of plane bending [27], out of plane bending by an end shear force [28], in plane end shear force [29] and a end normal force [30]. For these loads the zero and first order stress fields were developed. No numerical results were given. Using the same method he extended the solution to pure twist bending [31]. The series consisted of the first four orders of stress fields.

Lang [32] developed two sets of series for the mean stresses and displacements for a thin-walled elbow subjected to in-plane bending. The first set of series was based on the classical Von Karman model and the second set of series was derived

from the TE method. Result were found for typical elbows in nuclear reactors from both set of series. He concluded that the TE model generates a more complete description of mean stresses and tube flattening effects.

In the manufacturing of pipe bends it is common for cross-sectional distortion to be introduced. These shape imperfections commonly take the form of an ovality or thinning, the former being a deviation from the intended circular shape with the latter a variation in wall thickness around the cross-section. These imperfections are significant because elbows are usually critical components in piping systems due to their flexibility and the tendency for strain to concentrate in the elbow. The effects of geometric irregularities on elbows have been studied, for different kinds of loading and end restraints. Most of the elbows studied were thin and 90°.

Findlay and Spence [33] presented a theoretical solution for the flexibility and stresses in pipe bends with elliptic cross-sections under in-plane and out-of-plane bending applied separately. The theory was developed using an energy method and an assumed series expression for the radial displacement, the assumptions being similar to those in the Von Karman analysis for bends with circular cross-sections.

Arav [34] was the first to attempt to evaluate the effects of stress in the presence of local corrugations in pipe bends under in-plane bending. The investigation was both experimental and theoretical. He concluded that stresses in the corrugations in the plane of symmetry can be rather well predicted by the theoretical approach and that a considerable increase of stress level may occur in corrugations compared to smooth surfaces.

Boyle and Spence [35] used a non-linear analysis to examine the effect of internal pressure on the flexibility of a curved pipe under in-plane bending. The results were found for both circular and elliptic cross-sections of curved pipes. They compared the results with previous studies using linearized methods and suggested that the design factors normally used should be viewed with a certain amount of caution. Using the same analysis, Spence and Boyle [36] considered the stress analysis of a smooth curved pipe of non-circular cross-section under internal pressure and exter-

nal bending acting alone and together. From their results they concluded that in the presence of internal pressure, shape imperfections have a significant effect on the stresses.

Ohtsubo and Watanabe [20] investigated the effects on flexibility and stress factors of initial ovality and wall thickness variation. They considered 90° elbows under in-plane and out-of-plane moments. The finite ring element method based on thin shell theory was used. They concluded that variation of pipe wall thickness has little effect on the flexibility and stress factors whereas initial deformations have a significant effect on these factors.

Boyle and Spence [37] studied initial ovality for internal pressure and in-plane moment loadings acting alone and together using a simple elastic analysis. They concluded that a more complete analysis was required.

Spence and Findlay [38] considered the effects of typical thickness variations on bends with or without some degree of ovality for in-plane bending using a theoretical analysis based on a classical energy approach. They concluded that normal thickness variations do not appreciably affect the flexibility of curved pipes with either circular or elliptic cross-sections.

Thomas [39] determined the effects in elbow stresses arising from the presence of thickness variation, initial ovality, intrados wrinkling and longitudinal weld shrinkage for both internal pressure and in-plane moment loadings using the finite difference thin-shell analysis. End constraints were included and symmetry conditions were assumed at the interface of the pipe bend/tangent pipe assembly. He concluded that relatively simple or complicated geometric irregularities in thin-walled piping elbows do not affect the stress distribution due to in-plane moment, whereas stresses due to internal pressure are amplified in the presence of ovality, wrinkling and longitudinal weld shrinkage.

Natarajan and Mirza [40] studied the effect on the flexibility factors for bends of various included angles having non-uniform wall thickness using a finite element scheme with a doubly curved shell element. The pipe bends had straight pipes as

end contraints and were subjected to in-plane moments. They concluded that for pipe bends having λ_1 of the order 0.15 the variation in pipe wall thickness has no effect on their flexibility factors whereas for lower λ_1 of the order 0.05 the effects are considerable for bends whose included angles are more than 60°. Later, Natarajan and Mirza [41] did similar studies except that the effect of stress on pipe bends with wall variation subjected to internal pressure was studied. They concluded that variation in thickness does not produce any effect on the elbow.

Moore, Dodge and Bolt [42] studied, both experimentally and analytically, the influence of out-of-roundness and wall thickness variations on the stresses in piping elbows under internal pressure and/or in-plane, out-of-plane or torsional moment loadings. For the study, 90° piping elbows welded to short lengths of straight pipes were used. They concluded that end effects had the most influence on the stresses, followed in order by out of roundness, wall thickness variations and pressure-moment interactions.

1.2 Thick-Walled Cylinders with Cross Bores

In the field of high pressure engineering, thick-walled cylinders are used as, for example, chemical reactors, isostatic compaction chambers and gun barrels. Often connections must be made to such components, necessitating the introduction of cross bores which traverse the wall of the vessel in a radial direction. Examples include compressor heads, tee fittings and pump chambers. Sometimes because of design and lack of space the cross bore will be in an oblique direction and it also can be offset. The presence of a cross bore creates stress concentration in the cylinder at the intersection of the two bores which reduces the maximum pressure that can be safely contained. It is therefore highly desirable to know the magnitudes of the stress concentrations. Relatively little work has been done on cylinders with cross bore(s). Most of the work that has been done is experimental. The few published analytical treatments are based on simpler analyses and are therefore only approximate.

One of the first noteworthy papers was that by Fessler and Lewin [43], who

derived an approximate method based on the theoretical solution for a hole in an infinite plate under uniform tension. Their theory provided the equation to calculate the asymptotic stress-concentration factor for cylinders with sideholes sufficiently small compared with the bore. They were followed by Lake [44] and Morrison, Crossland and Parry [45] who derived the same equation in a more straightforward manner.

Fidler [46] studied the stress distribution in oblique cylinder intersection using the photoelastic technique. Elliptical opening of ratios typical of header tube joints are found in such intersection. It was shown that when the major axis of the elliptical opening is normal to the longitudinal axis of the vessel the stress distribution is less severe around the elliptical opening than around the circular opening. It was found that the optimum obliquity is approximately 56° which results in a lowering of the peak stress by 40%. This agrees well with the theoretical result (flat plate) which gives an optimum obliquity of 60°

Gerdeen [47] presented an approximate theoretical analysis for the determination of stress concentration factors in thick-walled cylinders having one and two cross bore(s). He included the transverse shear effect which had been neglected by previous investigators. The cylinders were subjected to both internal pressure and external shrink-fit pressure. The calculated concentration factors were compared with experimental data. The analysis became increasingly inacurrate as the bore diameter was reduced relatively to the cross bore diameter. Therefore, the calculations were performed only for the bore to cross bore radius ratio equal or larger than 1.5. Gerdeen concluded that the lowest stress concentration factor was expected for a cross bore diameter equal to the bore diameter.

Gerdeen and Smith [48] determined the stress concentration at the tee intersection of bores in thick-walled cylinders by experiments, to check the results with the theoretical predictions of Gerdeen [47]. Experiments were also conducted to determine the reduction of the stress-concentration factor by intersection radius at the cross bore intersection. From the experimental results it was apparent that the

lowest stress concentrations occured when the bore equaled the cross bore diameter; this confirmed the finding of the theoretical analysis of Gerdeen [47]. They concluded that an intersection radius decreased the stress concentration significantly and that the intersection radius to bore diameter ratio should be between 0.3 to 0.4 to minimize the stress concentration. Experimental results were found to agree well with theory.

Stanley and Day [49] described a photoelastic study of the stress distributions in thick-walled cylinders with offset oblique holes subjected to internal pressure. They studied the case where the major axis of the elliptical opening was parallel to the longitudinal axis of the cylinder. The possibility was examined of predicting these stresses from the results of an earlier experimental study of the stresses at oblique holes in thick flat plates subjected to in-plane forces. They concluded that for high offset parameters the predictions were underestimated.

Tan and Fenner [50] studied the effect of stress concentration in a thick-walled cylinders with a sidehole and a crosshole with or without cracks present, subjected to internal pressure using the boundary integral equation method. These problems had not been solved numerically before. They observed that a decrease in the value of stress concentration of about 3% when the diameter of the sidehole was doubled was quite consistent with the approximate solution proposed by Gerdeen [47], which gives a decrease of 3.5%. They were the first to consider cracked cross bore problems. From their results the values of the stress intensity factor for a bore to cross bore ratio of 4 was significantly higher than those for a bore to cross bore ratio of 8 with the same size of crack. They presumed that this difference was due to the reduced amount of material present, and hence reduced resistance to the crack opening. They concluded that the maximum stress concentration factors computed by the boundary integral equation approach is significantly lower than those predicted by approximate, analytical solutions.

Stanley and Day [51] described the stresses at a series of offset oblique holes in a thick-walled cylinder subjected to an axial torque. The three-dimensional

photoelastic method was used. They concluded that the stress concentrations for a wide range of hole/cylinder parameters can be reasonably well predicted from flat plate data.

Abdul-Mihsein and Fenner [52] determined the stress concentration factors of hollow and solid cylinders with cross bores subjected to axial tension and torsion using the BIE method for a range of cross bore diameter to outside diameter ratio (0.1 to 0.4). They also studied the effect on stress concentration factor of offset-oblique hole in cylinders under internal pressure. They obtained good agreement between previously published experimental results and BIE results. They demonstrated that for tension and torsion loadings, the stress concentration factor increased with increasing cross bore diameter to outside diameter ratio. They showed effectively, from the offset-oblique hole results, that the magnitude of the stress concentration factor depends mainly on the angle of obliquity. They concluded that this was due to the formation of an increasingly acute-angle corner at the intersection between the hole and the cylinder bore.

Again using the BIE method, Tan [53] has recently analysed the stress distribution in thick-walled cylinders with cross bore under internal pressure. He also considered the stress redistribution due to the introduction of a cross bore after the cylinder was partially autofrettaged. He demonstrated that the variations of the resultant residual hoop stress across the wall, in the vicinity of a cross bore introduced in an autofrettage cylinder, can be represented by a bi-linear form.

Chapter 2

BIE Method

2.1 Progress in the Use of the BIE Method

Development of the BIE method as a computational procedure for solving engineering problems has advanced considerably since Jawson and Ponter [54] and Symm [55] solved in 1963 some simple boundary value problems for Laplace's equation in two dimensions. In their formulation, they represent the boundary with straight segments and assume that over each of these the unknown function is constant. The integral equation is written at the centre of each element. The kernels of the integral equation are integrated by Simpson's Rule. They were not followed by further research until considerably later when Rizzo [56] in 1967 applied the method to problems of classical two-dimensional elastostatics. This formulation is similar to that above except the integration is done analytically.

Cruse [57,58] and Cruse and Van Buren [59] extended the solution capability to three dimensional elastostatics problems. The formulation is similar in principal to the two-dimensional elastostatics one by Rizzo [56] except that the surface is represented by plane triangular elements, over each of which the displacements and tractions are taken to be constant. These initial formulations were, however, very crude. A large number of boundary elements were necessary to give good results. Clearly, advantages would result from the reduction of the dimension of the problem by one; but the integral equations are awkward to treat numerically and, as initially formulated, the boundary integration equation method appeared to be less efficient

than the finite element method.

Meanwhile, Cruse and Rizzo [60,61] demonstrated the possibilities of extending the scope of the integral method to problems of elastodynamics, while Swedlow and Cruse [62] presented an elastoplastic analysis of anisotropic materials subjected to strain hardening. No numerical results are given in the latter paper, but Mendelson [63] and Mendelson and Albers [64] later presented, with results, an analysis of the elastoplastic problem.

Riccardella [65] and Cruse [66] improved the efficiency of the formulation by taking the displacements and tractions to vary linearly over each boundary element. The unknowns are now associated with the extremities or vertices of elements and the system of equations is obtained by writing the integral equation at these points. The integration of kernels is performed analytically, due respect being paid to the definition of the Cauchy principal value. The coefficient of the free term no longer necessarily equals $\frac{1}{2}\delta_{ij}$. For the three-dimensional problem Cruse [66] calculated the free term implicitly, by considering rigid body translation. Although this procedure improved the method, it remained inferior to that of the finite element method in many cases.

Meanwhile, researchers working on the FE method developed a useful numerical tool, known as parametric functional representation; researchers into BIE method began to consider its application in their work. Using this new numerical formulation the most significant advances in elastostatic applications are made by Boissenot, Lachat and Watson [67] – [72]. The boundary elements are allowed to be curved, with quadratic variation of geometry with respect to the intrinsic co-ordinates, while the variation of displacement and traction is defined by linear, quadratic or cubic shape functions with respect to the same co-ordinates. The integral equation is written at two, three or four nodes per element for plane elastostatic and four, eight or twelve nodes per element for three-dimensional elastostatics. Consequently, as they are impossible to integrate analytically over the curved elements, the kernel-shape functions products are accurately evaluated using Gaussian quadrature, provided

due precautions are taken when the integral tends to infinity. For three dimensional analysis the surface is represented by eight-noded quadrilateral and six-noded triangular elements, the triangular elements being considered as degenerate quadrilaterals. The domain is divided into sub-regions, for each of which an integral equation is established, obtaining a matrix of banded form. Each sub-region may have different material properties.

Rizzo and Shippy [73] using the general numerical formulation above, presented an analysis for three-dimensional linear, homogeneous, isotropic, steady state thermo-elasticity.

The progress presented above pertains to the direct formulation of the boundary integral equation method; this is hitherto the most commonly used formulation. There is however, another alternative formulation of the method.

In recent years, the development of the boundary integral equation method has been growing, to cover a wide range of complex practical problems. These range from potential flow and electromagnetism, to two and three dimensional elasticity, plates and shells, thermoelasticity, two and three dimensional elastoplasticity, fracture mechanics, vibrations, just to name a few (see, e.g. [50,52,53], [74]–[77]). Some of the developments include the application of the method to non-linear and non-homogeneous materials and also the coupling of BIE with other numerical methods.

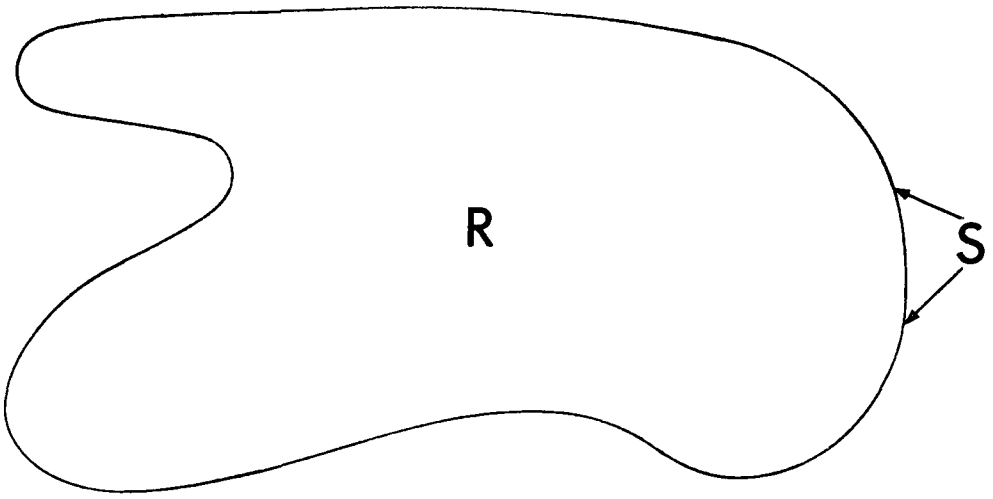

Figure 2.1: The elastic body R with surface S.

2.2 Review of the Basic Equations in 3-D Elastostatic

The analysis in this work is restricted to the analysis of linear elastostatic problems for which the material may be taken as isotropic and homogeneous. The governing differential equation of equilibrium for an element of the body can be written:

$$\sigma_{ij,j} + \overline{F}_i = 0 \qquad i,j = 1,2,3 \tag{2.1}$$

in which σ_{ij} are the stress components and $\overline{F}_i$ the components of the body forces. Hooke's Law relating the stress and strain components in an elastic body is given by:

$$\sigma_{ij} = \frac{2\mu\nu}{1-2\nu}\delta_{ij}\varepsilon_{kk} + 2\mu\varepsilon_{ij} \tag{2.2}$$

where μ and ν are the shear modulus and Poisson's ratio respectively, and δ_{ij} is Kronecker's delta symbol. The strains and displacements are related by:

$$\varepsilon_{ij} = \frac{1}{2}(u_{i,j} + u_{j,i}) \tag{2.3}$$

Substitution of Eq. (2.3) into Eq. (2.2) and using Eq. (2.1) yields Navier's equations of equilibrium in terms of displacement, which in the absence of body forces are

given by:

$$\frac{1}{1-2\nu}u_{i,ij} + u_{j,ii} = 0 \tag{2.4}$$

Eq. (2.4) represents a set of second order partial differential equations in terms of displacements valid everywhere in the domain R. Solutions are subject to appropriate boundary conditions, namely, the prescribed displacements on S_u and prescribed tractions on S_t. Traction, also known as stress vectors, represent the force per unit area acting at a point on the surface, and are given as:

$$t_i = \sigma_{ij} n_j \tag{2.5}$$

where the unit vector n_j is the outward normal vector for the body R. Substituting Eq. (2.3) into Eq. (2.2) and using Eq. (2.5) yields the traction equations in terms of displacement

$$t_i = \lambda \delta_{ij} u_{k,k} n_j + \mu(u_{i,j} + u_{j,i}) n_j \tag{2.6}$$

where

$$\lambda = \frac{2\mu\nu}{1-2\nu}$$

is known as Lamé's coefficient.

2.3 Requirements

The analytical basis of the BIE method is the transformation of the governing partial differential Eq. (2.4) applicable throughout the solution domain into an integral equation over the boundary. To do so we require:

1. A fundamental solution to Eq. (2.4), and

2. A reciprocal theorem

2.3.1 Fundamental Solution

We seek a fundamental solution giving the displacement due to a unit point load in an infinite elastic body. This is known as the Kelvin's solution [78] written in

tensor form

$$u_i^*(p,Q) = \frac{1}{4\pi\mu}\left(\frac{1}{r}\right)\left[\frac{3-4\nu}{4(1-\nu)}\delta_{ij} + \frac{1}{4(1-\nu)}r_{,i}r_{,j}\right]e_j \tag{2.7}$$

where the distance between the field point $Q(x)$ with coordinate x_{Q_i} and the load point $p(x)$ with coordinate x_{p_i} be given by:

$$r = [(x_{Q_i} - x_{p_i})(x_{Q_i} - x_{p_i})]^{1/2} \tag{2.8}$$

and e_j is the unit base vector. In Eq. (2.7) and what follows all differentiation is with respect to the field point $Q(x)$, that is:

$$r_{,i} = \frac{\partial r}{\partial x_{Q_i}} = \frac{x_{Q_i} - x_{p_i}}{r} \tag{2.9}$$

$u_i^*(p,Q)$ is the displacement in the x_i directions at point Q due to the unit point load at p in the x_j directions. The traction vectors for Kelvin's problem are determined by differentiating the displacements (Eq. (2.7)) at point Q and using Eq. (2.6)

$$t_i^*(p,Q) = \frac{-(1-2\nu)}{8\pi(1-\nu)}\left(\frac{1}{r^2}\right)\left\{\frac{\partial r}{\partial n}\left(\delta_{ij} + \frac{3}{1-2\nu}r_{,i}r_{,j}\right) - n_j r_{,i} + n_i r_{,j}\right\}e_j \tag{2.10}$$

where

$$\frac{\partial r}{\partial n} = \frac{\partial r}{\partial x_{Q_i}}n_i = \frac{1}{r}(x_{Q_i} - x_{p_i})n_i$$

and n_i is the normal at point Q. $t_i^*(p,Q)$ is the traction in the x_i directions at point Q due to the unit point load at p in the x_j directions. Both u_i^* and t_i^* are singular when r equals zero. The displacement and traction vectors can be written as:

$$u_i^*(p,Q) = U_{ij}(p,Q)e_j \tag{2.11}$$

$$t_i^*(p,Q) = T_{ij}(p,Q)e_j \tag{2.12}$$

where $U_{ij}(p,Q)$ and $T_{ij}(p,Q)$ are second order tensors given by:

$$U_{ij}(p,Q) = \frac{1}{4\pi\mu}\left(\frac{1}{r}\right)\left[\frac{3-4\nu}{4(1-\nu)}\delta_{ij} + \frac{1}{4(1-\nu)}r_{,i}r_{,j}\right] \tag{2.13}$$

$$T_{ij}(p,Q) = \frac{-(1-2\nu)}{8\pi(1-\nu)}\left(\frac{1}{r^2}\right)\left\{\frac{\partial r}{\partial n}\left(\delta_{ij} + \frac{3}{(1-2\nu)}r_{,i}r_{,j}\right) - n_j r_{,i} + n_i r_{,j}\right\} \tag{2.14}$$

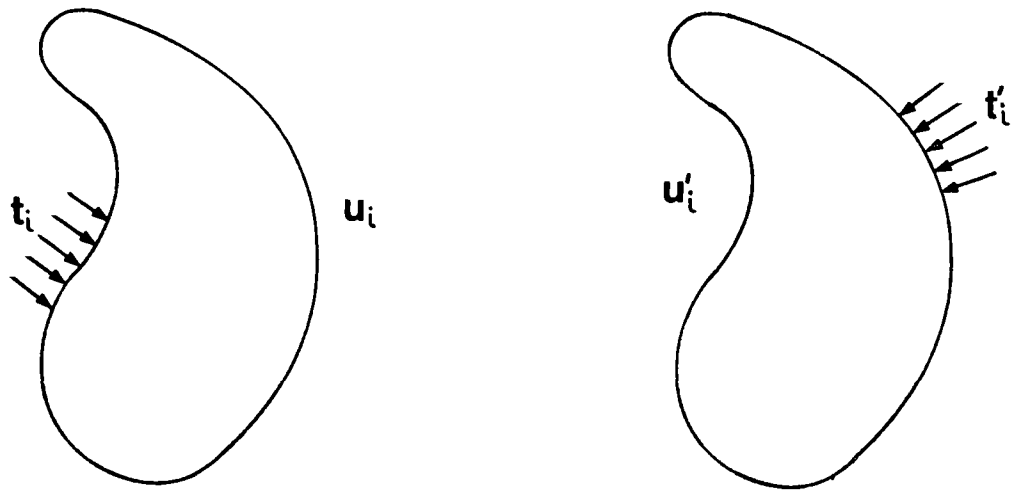

Figure 2.2: Homogeneous isotropic linear elastic body

2.3.2 Reciprocal Theorem

Consider two equilibrium states of an elastic body: one with displacements u_i and tractions t_i, and the other with displacements u'_i and tractions t'_i as shown in Figure 2.2. The Divergence theorem in tensor form is:

$$\int_R a_{i,i}\, dV = \int_S a_i n_i\, dS \tag{2.15}$$

Using Eq. (2.5) and the Divergence theorem, the work that would be done by the tractions t_i if they acted through u'_i, can be written as:

$$\begin{aligned} \int_S t_i u'_i\, dS &= \int_S \sigma_{ij} n_j u'_i\, dS \\ &= \int_R (\sigma_{ij} u'_i)_{,j}\, dV \end{aligned} \tag{2.16}$$

In this analysis body forces are assumed negligible. Then

$$\int_R \overline{F}_i u'_i\, dV = \int_R \sigma_{ij,j} u'_i\, dV = 0$$

Carrying out the indicated differentiation in Eq. (2.16) and using Hooke's law Eq. (2.2), we get:

$$\begin{aligned}\int_S t_i u_i' \, dS &= \int_R \sigma_{ij} u_{i,j}' \, dV \\ &= \int_R \left[\lambda \delta_{ij} \varepsilon_{kk} + 2\mu \varepsilon_{ij}\right] u_{i,j}' \, dV \\ &= \int_R \left[\lambda \varepsilon_{kk} u_{i,i}' + \mu (u_{i,j} + u_{j,i}) u_{i,j}'\right] \, dV \\ &= \int_R \left[\lambda \varepsilon_{kk} \varepsilon_{kk}' + \mu u_{i,j} u_{i,j}' + \mu u_{j,i} u_{i,j}'\right] \, dV \end{aligned} \tag{2.17}$$

Since

$$\mu u_{j,i} u_{i,j}' = \mu u_{i,j} u_{j,i}' = \mu u_{j,i}' u_{i,j}$$

the integral Eq. (2.16) is symmetric with respect to the prime and unprime states. Thus

$$\int_S t_i u_i' \, dS = \int_S t_i' u_i \, dS \tag{2.18}$$

This result is the well known Betti-Rayleigh reciprocal work theorem.

2.4 Displacements and Stresses at Interior Points

With no loss of generality, in Eq. (2.18) we choose the actual state of displacements and tractions as u_i and t_i respectively and the prime system as those corresponding to the fundamental solution to Navier's equation. Now we can write from Eq. (2.18),

$$\int_S t_i(Q) u_i^*(p,Q) \, dS = \int_S u_i(Q) t_i^*(p,Q) \, dS \tag{2.19}$$

where $u_i^*(p,Q)$ and $t_i^*(p,Q)$ are defined in Eq. (2.7) and Eq. (2.10). Because of the singular nature of the fundamental solution, let the load point p be surrounded by a small spherical region, R_ϵ, with the surface, S_ϵ within R as shown in Figure 2.3.

Applying Betti-Rayleigh's theorem to the domain $(R - R_\epsilon)$ gives:

$$\begin{aligned}\int_S t_i(Q) u_i^*(p,Q) \, dS \;+\; &\int_{S_\epsilon} t_i(Q) u_i^*(p,Q) \, dS = \\ &\int_S u_i(Q) t_i^*(p,Q) \, dS + \int_{S_\epsilon} u_i(Q) t_i^*(p,Q) \, dS\end{aligned}$$

Taking the limit as $\epsilon \to 0$, it is found that:

$$u_j(p) = \int_S t_i(Q) U_{ij}(p,Q) \, dS - \int_S u_i(Q) T_{ij}(p,Q) \, dS \tag{2.20}$$

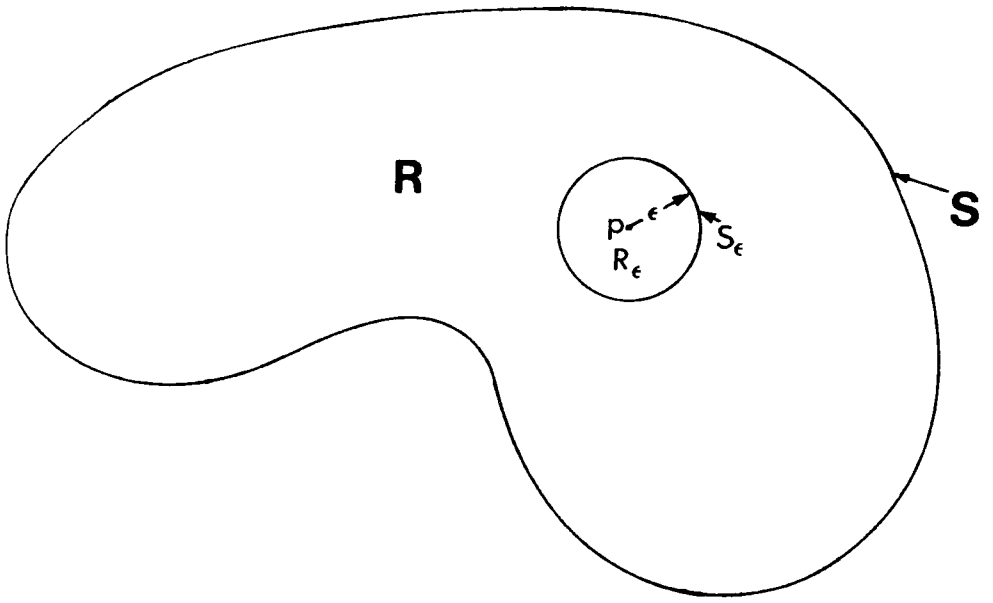

Figure 2.3: Domain R_ϵ isolating $p \in R$

This equation is known as Somigliana's identity [79] and is used to compute the displacements at points inside the body in terms of boundary values of displacements $u_i(Q)$ and tractions $t_i(Q)$. To obtain the stress state at $p(x)$, we differentiate with respect to the load point p and invoke Hooke's Law:

$$\sigma_{ij}(p) = \int_S t_k(Q) D_{kij}(p,Q)\, dS - \int_S u_k(Q) S_{kij}(p,Q)\, dS \tag{2.21}$$

By utilizing the identity

$$\frac{\partial r}{\partial x_{Q_i}} = \frac{-\partial r}{\partial x_{p_i}}$$

the third order tensors are found to be

$$D_{kij} = \frac{1-2\nu}{8\pi(1-\nu)} \left(\frac{1}{r^2}\right) \left(\delta_{ki} r_{,j} + \delta_{kj} r_{,i} - \delta_{ij} r_{,k} + \frac{3}{1-2\nu} r_{,i} r_{,j} r_{,k}\right)$$

and

$$\begin{aligned} S_{kij} = \frac{E}{8\pi(1-\nu^2)} \left(\frac{1}{r^3}\right) \Big\{ & 3\frac{\delta r}{\delta n} \left((1-2\nu)\delta_{ij} r_{,k} + \nu(\delta_{ki} r_{,j} + \delta_{kj} r_{,i}) - 5 r_{,i} r_{,j} r_{,k}\right) \\ & + n_i (3\nu r_{,j} r_{,k} + (1-2\nu)\delta_{kj}) + n_j (3\nu r_{,i} r_{,k} + (1-2\nu)\delta_{ki}) \\ & + n_k (3(1-2\nu) r_{,i} r_{,j} - (1-4\nu)\delta_{ij}) \Big\} \end{aligned}$$

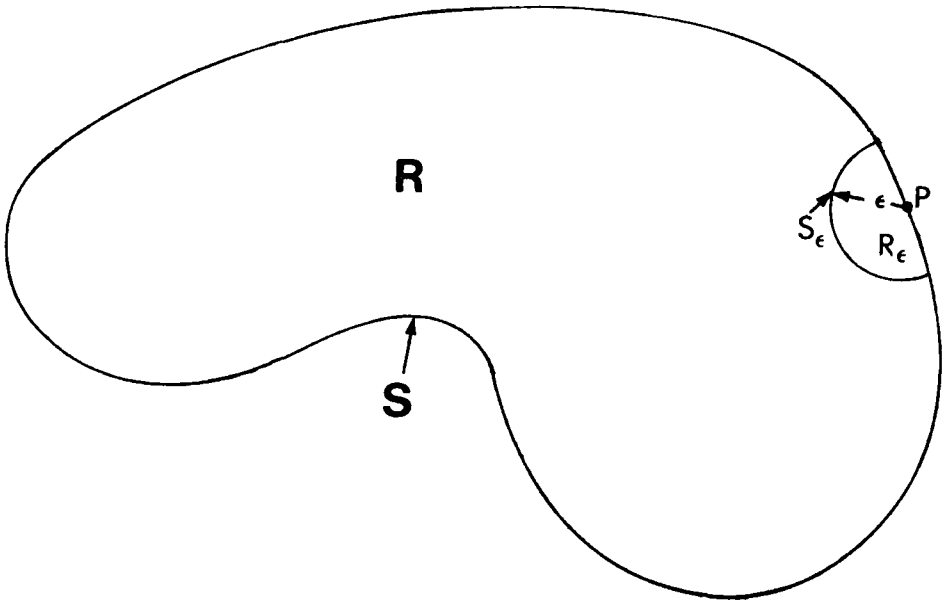

Figure 2.4: The elastic body R with surface S.

2.5 Boundary Integral Equation (BIE)

Let $p \rightarrow P$, a boundary point distinct from Q. Then Betti-Rayleigh's theorem is written for the domain $R - R_\epsilon$, where R_ϵ isolates the point P as shown in Figure 2.4:

$$\int_{S+S_\epsilon} \{t_i(Q)U_{ij}(P,Q)\,dS - u_i(Q)T_{ij}(P,Q)\,dS\} = 0 \tag{2.22}$$

Here R_ϵ is taken to be the part of R contained within a sphere of radius ϵ, centred at P. The integral equation is obtained by letting $\epsilon \rightarrow 0$.

$$C_{ij}(P)u_i(P) + \int_S u_i(Q)T_{ij}(P,Q)\,dS = \int_S t_i(Q)U_{ij}(P,Q)\,dS \tag{2.23}$$

where

$$C_{ij}(P) = \lim_{\epsilon \rightarrow 0} \int_{S_\epsilon} T_{ij}(P,Q)\,dS \tag{2.24}$$

which is dependent on the solid angle.

If the tangent plane at P is continuous

$$C_{ij} = \frac{1}{2}\delta_{ij} \tag{2.25}$$

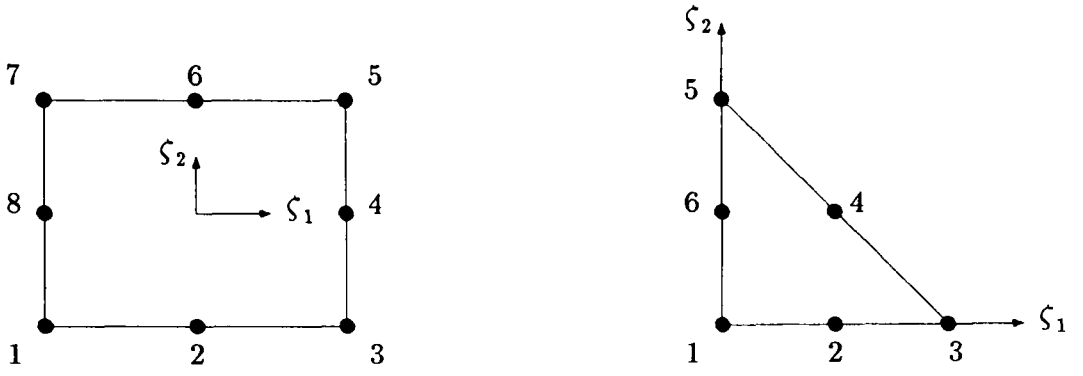

Figure 2.5: Surface elements

The BIE is a boundary constraint equation relating the boundary tractions and boundary displacements for the elastic body. Once the BIE has been solved, the surface displacements and tractions are known everywhere on the boundary, and from these data the displacements and stresses at any desired interior point may be calculated using Eq. (2.20) and Eq. (2.21).

2.6 Numerical Solution of the BIE

Since Eq. (2.23) involves only the boundary surface, the numerical solutions of the BIE are found by discretizing solely the boundary into elements. The distributions of the unknowns over these elements are expressed in term of suitable algebraic functions involving values at certain nodal points associated with the elements. The fact that only the boundary needs to be discretized means that a three dimensional volume problem becomes a two dimensional surface problem. In the computer program used in the present work, the surface is represented by an assemblage of eight-noded isoparametric quadrilateral and/or six-noded isoparametric triangular elements as shown in Figure 2.5. The geometry of each elements is defined in terms of quadratic shape functions of intrinsic coordinates [80]; they are also used to define

the variation of the unknowns over each elements. Thus:

$$x_i(\zeta) = N^c(\zeta)x_i^c$$

$$u_i(\zeta) = N^c(\zeta)u_i^c$$

$$t_i(\zeta) = N^c(\zeta)t_i^c \tag{2.26}$$

where c represent the node number.

For the rectangular elements

Corner nodes

$$N^c(\zeta) = \frac{1}{4}(1+\xi_1)(1+\xi_2)(\xi_1+\xi_2-1)$$

Mid-side nodes

$$\zeta_1^c = 0, \quad N^c(\zeta) = \frac{1}{2}(1-\zeta_1^2)(1+\xi_2)$$

$$\zeta_2^c = 0, \quad N^c(\zeta) = \frac{1}{2}(1+\xi_1)(1-\zeta_2^2)$$

where ξ_1 and ξ_2 are defined as:

$$\xi_1 = \zeta_1\zeta_1^c, \quad \xi_2 = \zeta_2\zeta_2^c$$

and

$$-1 \leq \zeta_1, \zeta_2 \leq 1$$

For the triangular elements

Corner nodes

$$N^1(\zeta) = \xi_3(2\xi_3 - 1)$$

$$N^3(\zeta) = \xi_1(2\xi_1 - 1)$$

$$N^5(\zeta) = \xi_2(2\xi_2 - 1)$$

Mid-side nodes

$$N^2(\zeta) = 4\xi_3\xi_1$$

$$N^4(\zeta) = 4\xi_1\xi_2$$

$$N^6(\zeta) = 4\xi_2\xi_3$$

where

$$\xi_1 = \zeta_1, \quad \xi_2 = \zeta_2, \quad \xi_3 = 1 - \zeta_1 - \zeta_2$$

and

$$0 \leq \zeta_1, \zeta_2 \leq 1.$$

Let the surface be represented by m such elements and a total of q distinct nodes, Eq. (2.23) then becomes:

$$C_{ij}(P^a)u_i(P^a) + \sum_{b=1}^{m} \sum_{c=1}^{6 \text{ or } 8} u_i(P^{d(b,c)}) \int_S T_{ij}(P^a, Q(\zeta)) N^c(\zeta) J(\zeta)\, d\zeta$$

$$= \sum_{b=1}^{m} \sum_{c=1}^{6 \text{ or } 8} t_i(P^{d(b,c)}) \int_S U_{ij}(P^a, Q(\zeta)) N^c(\zeta) J(\zeta)\, d\zeta \qquad (2.27)$$

where P^a is the a^{th} node, and $d(b,c)$ is the number of the c^{th} node of the b^{th} element (6 or 8). Also, $J(\zeta)$ is the Jacobian given by the modulus of the vector product of the two vectors defined by:

$$S_{ij} = \frac{\partial x_i}{\partial \zeta_j} = \frac{\partial N^c}{\partial \zeta_j} x_i^c; \qquad i \in (1,2,3), \quad j \in (1,2)$$

Eq. (2.27) represents a set of $3q$ equations and $6q$ nodal values of displacements, u_i, and tractions, t_i, half of which are known. The isoparametric representation can similarly be adopted in Eq. (2.20) and Eq. (2.21). Eq. (2.27) can be written as:

$$\left[\Delta F\right]\left[u_i\right] = \left[\Delta G\right]\left[t_i\right] \qquad (2.28)$$

where $\left[\Delta F\right]$ and $\left[\Delta G\right]$ represent matrices with known coefficients.

Applying boundary conditions, known boundary values are multiplied by their corresponding coefficient and placed in the right hand side vector. Coefficients corresponding to the unknown boundary values are placed in matrix $\left[A\right]$ to give

$$\left[A\right]\left[\overline{u}_i\right] = \left[y\right] \qquad (2.29)$$

where $\overline{u}_i$ contains the unknown values of u_i and t_i. For numerical stability, the coefficients of the matrix $\left[A\right]$ are scaled:

$\int_{S_k} T_{ij} N^c J(\zeta)\, d\zeta$ – already non dimensional, so no scaling.

$\int_{S_k} U_{ij} N^c J(\varsigma)\, d\varsigma$ – integral values are multiplied by (E/L_1).

In $\left[y\right]$ the given displacements are divided by L_1 and the given tractions are divided by E, where E is Young's modulus and L_1 is the maximum dimension of the physical problem. Eq. (2.29) is then solved by Gaussian elimination.

The numerical implementation of the BIE method will not be further discussed here. Selection of proper mesh sizes for the various problems considered herein is discussed in the chapters concerned.

2.7 Advantages of the BIE Method over Domain Methods

The numerical solutions by BIE are found by discretizing the boundary into elements, whereas for finite element (FE) and finite difference (FD) the entire domain needs to be discretized. An advantage of the BIE approach is therefore clear: a three-dimensional volume problem becomes a two-dimensional surface problem, and a two-dimensional plane problem becomes a one-dimensional line problem. This decrease in dimensionality results in a significant reduction of the numerical problem size, so there are less computer core requirements due to the smaller set of equations to be solved and less data preparations compared with the domain methods.

Another advantage of the BIE method is that no interior discretization of the domain is needed, so no approximation is imposed on the solution at the interior points. Hence, there are better resolutions of displacements and stresses. With the BIE method, only the interior points specified by the user are solved whereas the FE method calculates the solution for all nodes inside the domain even if there is no need for them. Therefore using the BIE method over the domain methods improves the use of computing resources due to the reduction of unwanted information.

Tan and Fenner [81] displayed these advantages by applying the FE and BIE methods to relatively simple three-dimensional problems. They compared the results found from both methods and then concluded that for equivalent accuracy,

the BIE method may be as much as an order of magnitude more efficient in its use of computing resources than the FE method. But they noted that probably for problems involving relatively thin structural components, the BIE approach would be less advantageous. They also noted that the BIE accuracy increased over FE as the size and the complexity of the problem increased.

2.8 Computer Program

The BIE method and computer program used here have previously been applied to a range of three-dimensional stress analysis problems (Refs. [50,52,53], [81]–[84]). In the present work the computer program used, for the BIE analysis of three dimensional problems in linear elastostatics was BIE3D4; it was written and provided by Professor C. L. Tan of Carleton University. All BIE solutions were performed at Carleton University on a Honeywell Level 66 DPS/C3 Dual Processor mainframe computer. Solution time for a typical three dimensional problem involving a torus, with three different load cases solved simultaneously, was about 150 minutes.

The physical problems are assumed to be elastic, homogeneous and isotropic. The program may be used to calculate displacements of and stresses in an elastic body subjected to a range of loading conditions. The loading conditions which may be specified by the user include uniform as well as non-uniform externally applied tractions and prescribed zero or non-zero displacements on the physical surface. If thermal effects are involved, they may be specified in terms of potential functions on the surface of the elastic body. Also, body forces due to gravity and centrifugal loads may be included in the analysis. Thermal effects and body forces are ignored in the present work. Program BIE3D4, which is executed in 53K words on the computer CP6 (DPS/C3), can handle up to:

1. 400 geometric nodes,

2. 130 surface elements,

3. 20 interior points at which results are required,

4. 5 load cases.

The physical domain is defined by the boundary and is represented by eight-noded quadrilateral and/or six-noded triangular elements. The representation of geometry and unknowns is in terms of quadratic shape functions as described in section (2.6). A graphic program is supplied with the program BIE3D4 which is used to check the geometry data. Such visual checks on the mesh data before they are used with the BIE program, reduces the possibility of erroneous results.

The numerical evaluation of the boundary integrals is carried out by Gaussian quadrature. For the problems described in this work, 4X4 point Gaussian quadrature is used throughout. With such a fixed integration scheme, it is particularly important that the boundary element mesh should be well-designed to suit the variation of stress and strain encountered, with smaller elements in regions of rapid variation. It is also important that the aspect ratio of the quadrilateral boundary elements (ratio of maximum to minimum dimension) should be relatively small. Mesh design has a major effect on solution accuracy. So, a problem with a known exact solution will be carried out by the BIE method in the following chapter to determine the mesh design and the aspect ratio that will give an accurate solution.

Chapter 3

Test Problems

3.1 Thick-Walled Cylinder

Thick-walled cylinders are used widely in industry as pressure vessels, pipes, gun tubes, etc. In many applications the cylinder wall thickness is constant, and the cylinder is subjected to a uniform internal pressure, external pressure, an axial load and a temperature change. The problem considered herein is an open cylinder with a constant thickness, subjected to internal pressure as shown in Figure 3.1.

An exact solution exists for this problem, known as Lamé's solution. The stress components [85,86] are given as:

$$\sigma_r = \frac{a^2 P_i}{b^2 - a^2}\left(1 - \frac{b^2}{r^2}\right) \tag{3.1}$$

$$\sigma_\phi = \frac{a^2 P_i}{b^2 - a^2}\left(1 + \frac{b^2}{r^2}\right) \tag{3.2}$$

$$\sigma_z = 0 \tag{3.3}$$

where the longitudinal strain is assumed to be the same for all axial fibers. In the equations above, a is the inside radius, b is the outside radius, r is the radial coordinate and P_i is the internal pressure. The radial displacement [86] is given by:

$$U_r = \frac{r}{E(b^2 - a^2)}\left[(1-\nu)a^2 P_i + \frac{(1+\nu)}{r^2}a^2 b^2 P_i\right] \tag{3.4}$$

where E and ν denotes the modulus of elasticity and Poisson's ratio.

In order to estimate the accuracy of BIE solutions obtained using a particular boundary mesh, it is appropriate to compare the numerical results with an analytical

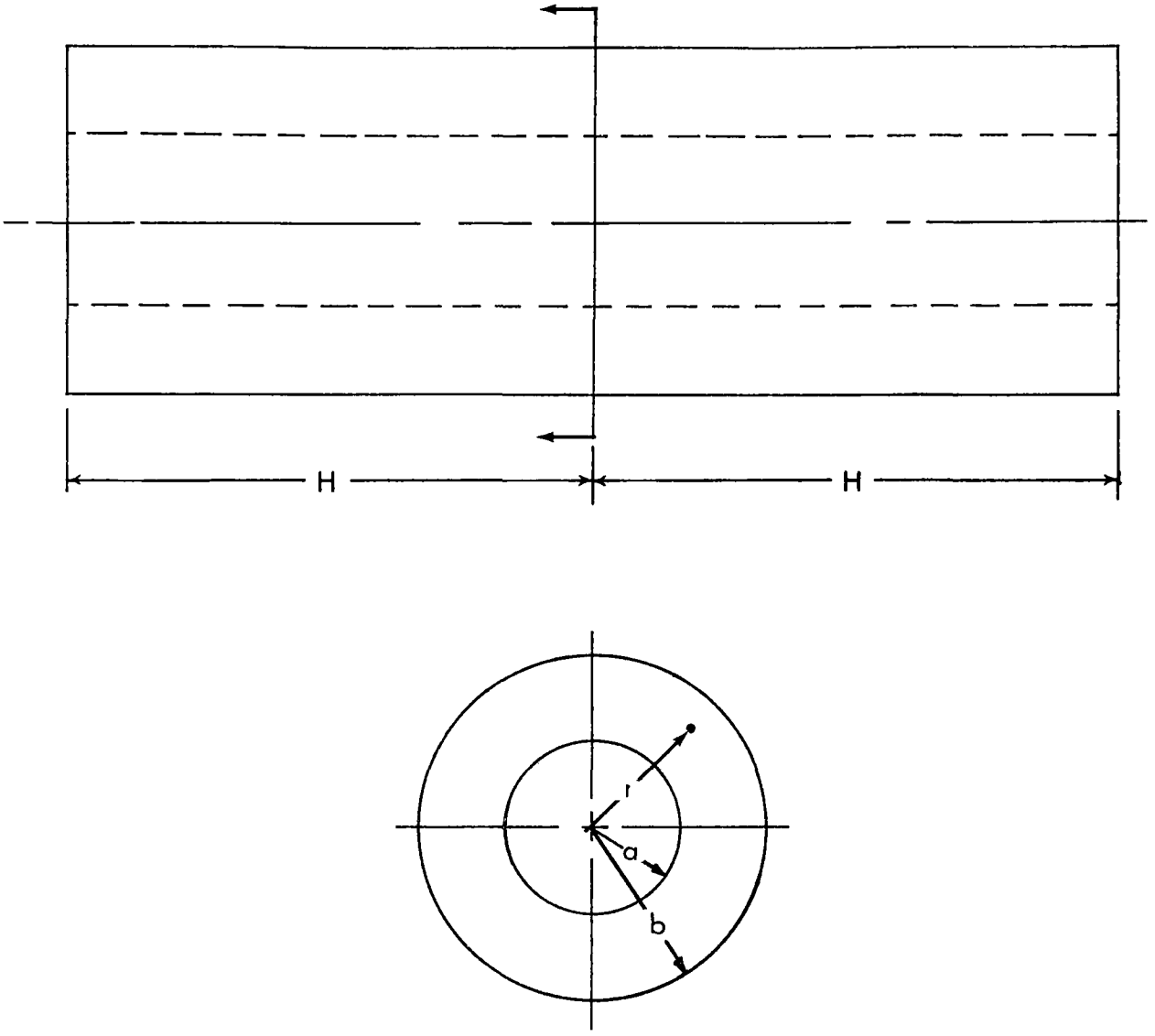

Figure 3.1: Open cylinder with internal pressure.

Case	Elements	σ_ϕ / P_i	Deviation (%)
1	6	1.8951	13.70
2	10	1.5846	4.93
3	16	1.5942	4.35
4	24	1.6586	0.49
5	32	1.6746	0.47

Table 3.1: Maximum hoop stress.

solution. The BIE mesh for thick cylinders can be used as a basis for the BIE mesh to be used subsequently for a thick torus.

Figure 3.1 illustrates the particular problem solved. The total length and the outside diameter are equal ($2H = 2b$) and the inside radius, a, is half of the outside radius, b. There are three planes of symmetry, and thus only one eight of the cylinder needs to be modelled.

This problem is solved for five different mesh distributions by the BIE method. Figures 3.2 to 3.6 show the boundary mesh arrangements of quadrilateral elements, used in the five cases. As seen from the figures the mesh distributions of the first case has only 1 element per side, then for each subsequent case the number of elements is increased. Poisson's ratio is taken to be 0.3 for all cases. The deviation of the computed hoop stress, with Lamé's solution (Eq. (3.2)) is given by:

$$\text{Deviation} = \left| \frac{\sigma_{\phi_{exact}} - \sigma_{\phi_{cal}}}{\sigma_{\phi_{exact}}} \right|$$

Table 3.1 shows the deviation of the computed peak stress, which is the hoop stress at the inside surface. The peak stress found from the exact solution is $1.6667 P_i$. Case 4 is much more accurate than cases 1, 2 and 3 whereas case 5 is not much more accurate. The mesh distribution of case 4 would be appropriate for subsequent problems. For this case the maximum aspect ratio of the quadrilateral boundary element (ratio of maximum to minimum dimension) used was 2. The next step is to use the mesh distribution of case 4 and elongate the length of the cylinder by 1.5, 2, 3 and 4 (cases 6, 7, 8 and 9). Then the computed peak stress is compared with the exact solution in order to determine the maximum aspect ratio to be used. Table 3.2 displays the deviation of the computed peak stress.

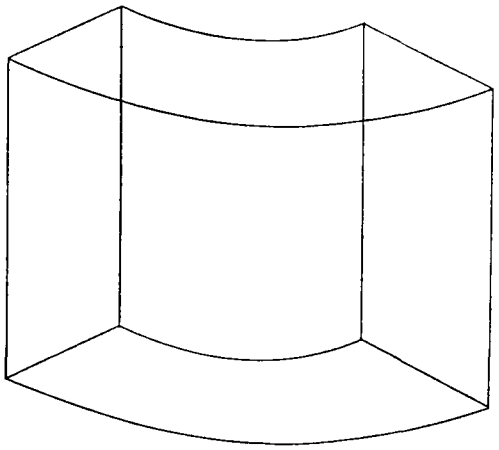

Figure 3.2: Case 1 containing 6 elements and 20 nodes

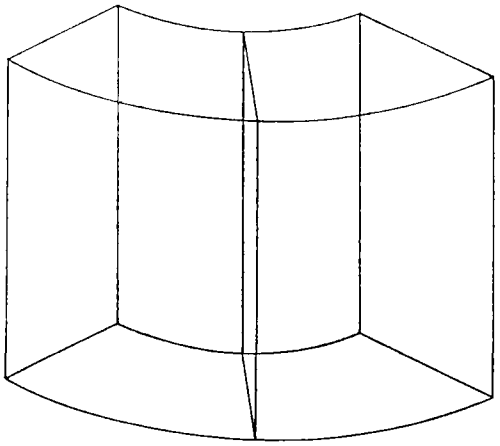

Figure 3.3: Case 2 containing 10 elements and 32 nodes

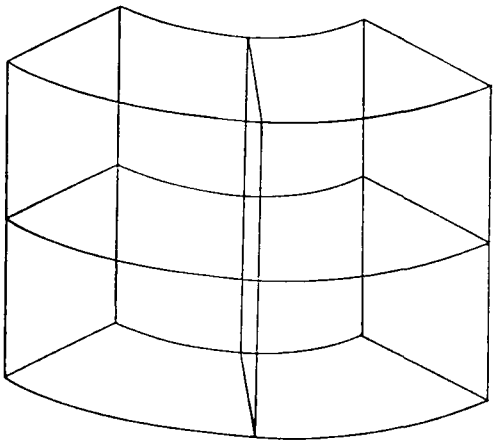

Figure 3.4: Case 3 containing 16 elements and 50 nodes.

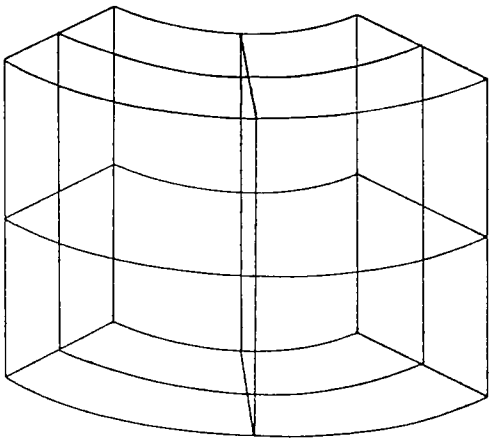

Figure 3.5: Case 4 containing 24 elements and 74 nodes.

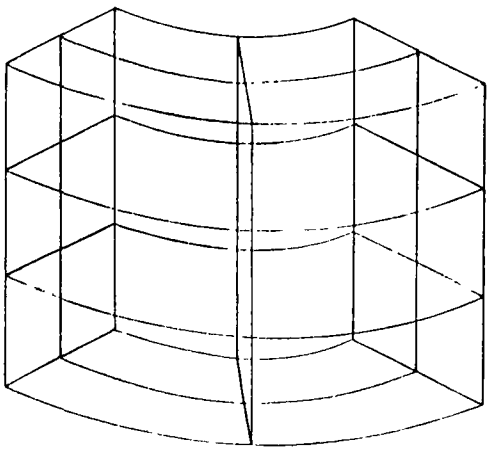

Figure 3.6: Case 5 containing 32 elements and 98 nodes.

Case	Aspect Ratio	σ_ϕ/P_i	Deviation (%)
4	2	1.6586	0.49
6	3	1.6835	1.01
7	4	1.7482	4.89
8	6	1.9684	18.10
9	8	2.1493	28.96

Table 3.2: Maximum hoop stress.

For all cases in Table 3.2 except for case 4, the maximum deviation from Lamé's solution is found to be at midside nodes. For case 7, the maximum deviation at the corner nodes is 0.92%. This is also true for the computed minimum hoop stress where for case 7 it deviates 4.47% at corner nodes, and 6.6% at midside nodes. It is seen from Table 3.2 that the aspect ratio should be relatively small, and certainly not greater than 4. This was also observed by Abdul-Mihsein and Fenner [52] for problems involving thick cylinders with cross bores. From the above observations, an aspect ratio not greater than 4 is recommended for thick shells.

The peak stress results presented in the present work are therefore believed to be accurate within 5%. Figures 3.7 and 3.8 show the radial displacement factor $\left(\frac{U_r E}{P_i a}\right)$ and the hoop stress factor (σ_ϕ/P_i) variation through the wall of the cylinder for both BIE (case 7) and analytical results. These figures confirm that the boundary mesh of case 7 achieves the accuracy desired. Note that the displacements are more accurate than the stresses. This is because the displacements and tractions are solved first and then the stresses are calculated using the tractions which increases the degree of error.

3.2 Thick-Walled Toroidal Shells

The available analytical results for the three-dimensional problems of pressurized thick-walled toroidal shells are only approximate. In the absence of exact analytical solution, accurate three-dimensional theoretical treatments of stresses in toroidal shells must be numerical. In order to verify the accuracy of three-dimensional BIE solutions obtained, using the mesh distributions chosen in the previous section to

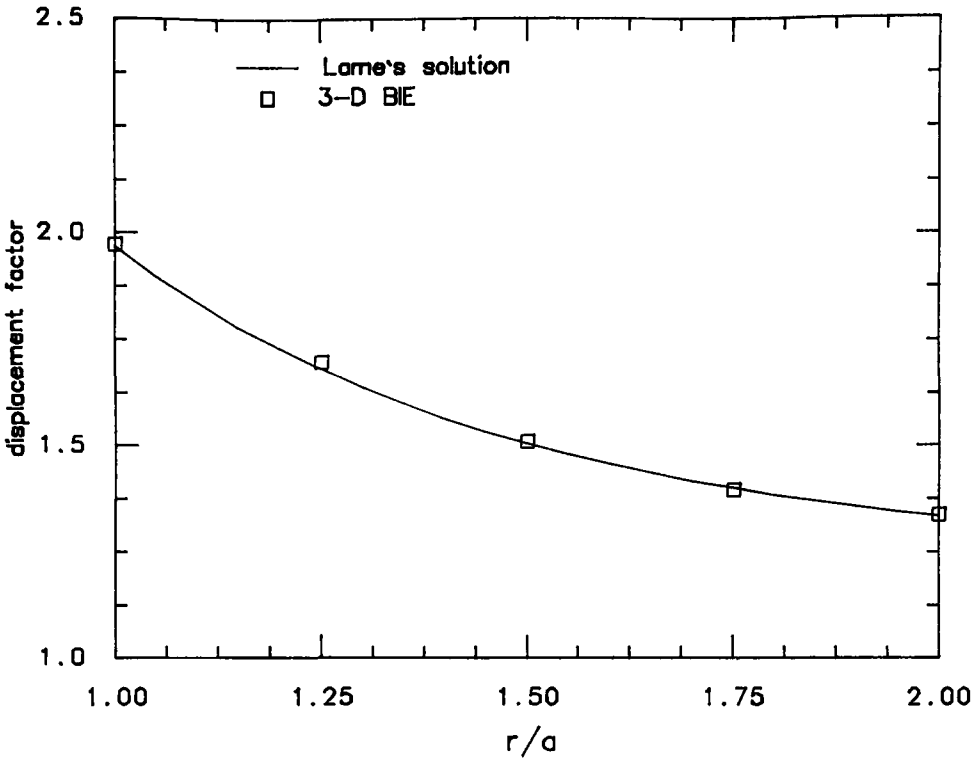

Figure 3.7: Radial displacement factor, distribution through the wall of the cylinder.

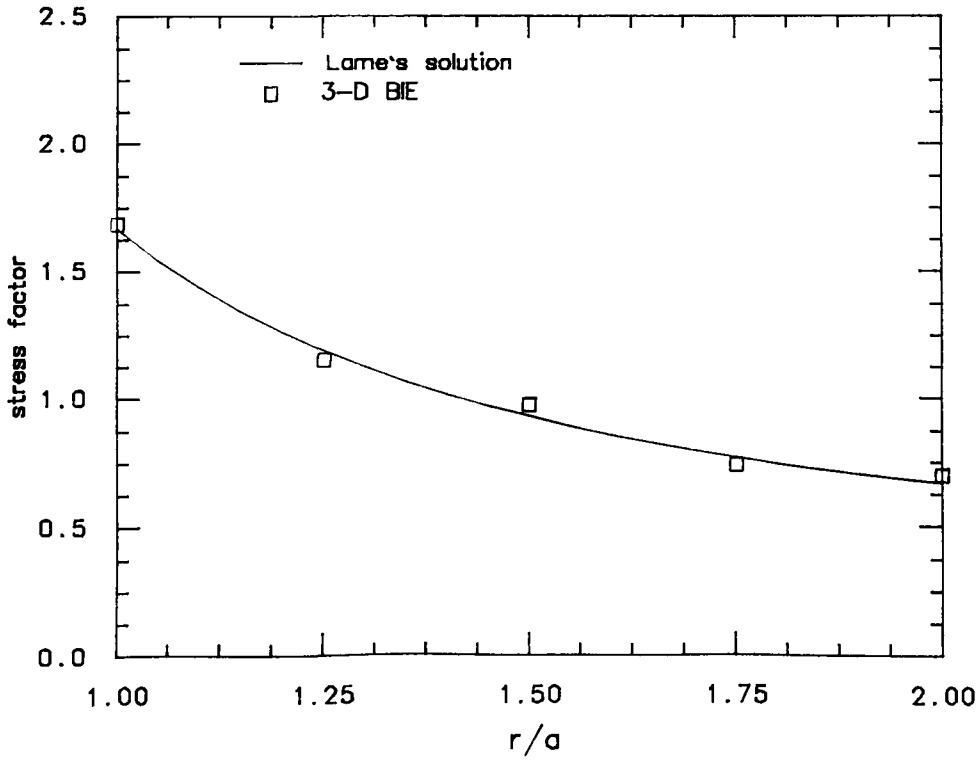

Figure 3.8: Hoop stress factor, distribution through the wall of the cylinder.

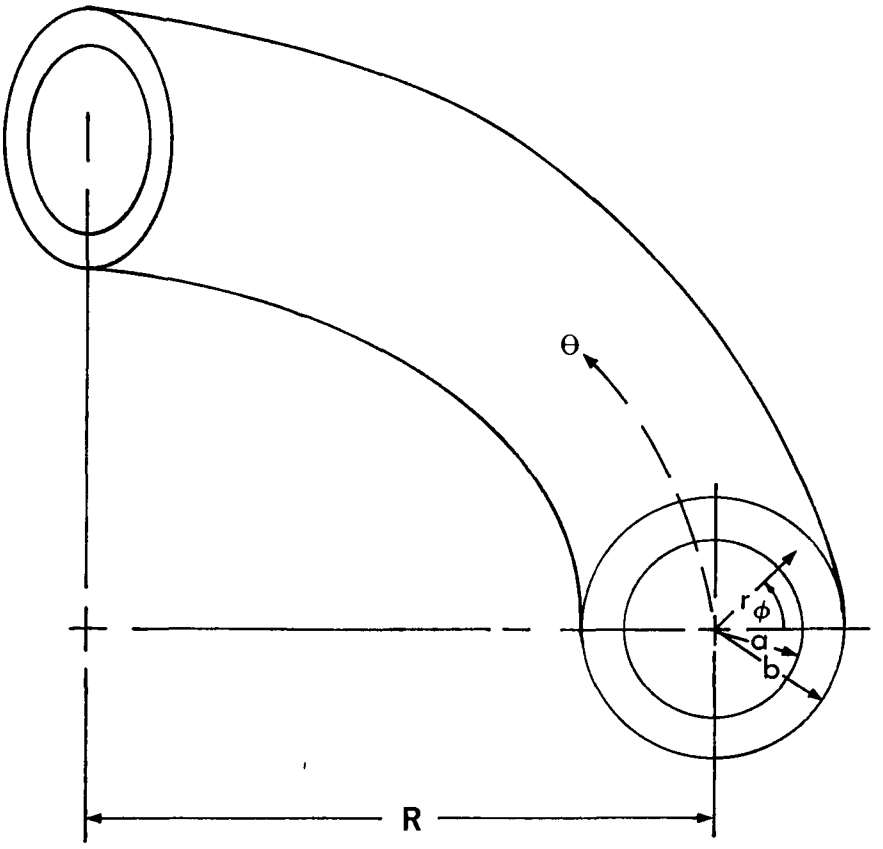

Figure 3.9: Toroidal coordinate (r, ϕ, θ).

a toroidal shell, it is appropriate to compare the results with results from other numerical methods. The other numerical methods are axisymmetric FE and axisymmetric BIE. The problems that will be analysed with these methods are tori with constant thickness subjected to internal pressure. The toroidal coordinate system (r, ϕ, θ) used in the present work is shown in Figure 3.9. In this figure, R is the mean toroidal radius, a and b are the cross-section radii, ϕ is the circumferential angle and θ is the longitudinal angle. It is convenient to define a toroidal radius ratio, γ, as R divided by a and a thickness ratio t as b divided by a.

The three dimensional BIE program gives its results in cartesian coordinates whereas the axisymmetric FE and BIE program results are in cylindrical coordinates. The results have to be transformed to toroidal coordinates. The trans-

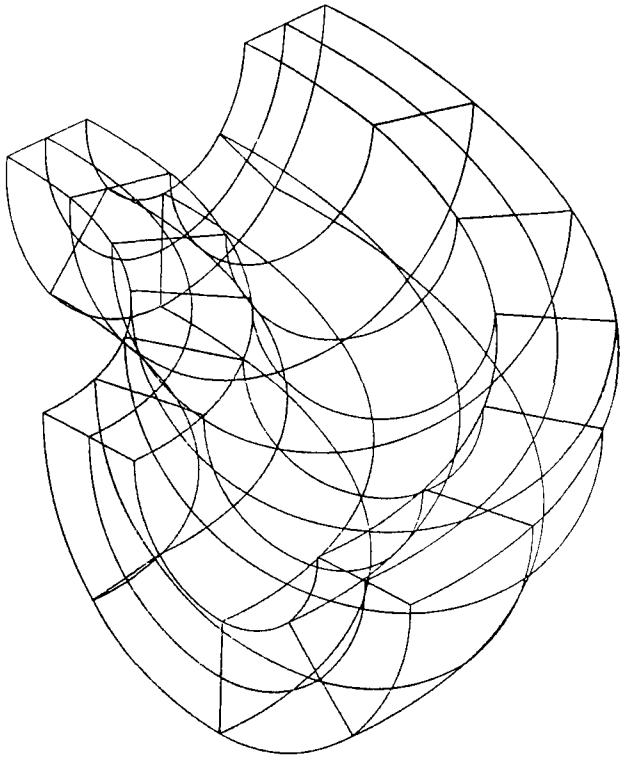

Figure 3.10: The BIE boundary mesh used for γ of 5 and t of 2, containing 88 elements and 266 nodal points.

formations for stress and displacement components from cartesian to cylindrical coordinates and then to toroidal coordinates, are giving in Appendix A.

3.2.1 Torus with Circular Cross-Section

Pressurized tori having thickness ratios, t, of 2 and 3 are analysed for two different toroidal radius ratios, γ, of 5 and 10. One eight of the torus was modelled, taking advantage of symmetry. A typical BIE boundary mesh is shown in Figure 3.10.

The element configuration was varied to suit the different toroidal radius and thickness ratios. A maximum of 124 eight-node quadrilateral elements were used. Table 3.3 gives the number of elements and nodes used for each configuration.

This problem can also be solved using an axisymmetric analysis. The cross-section of the torus is the axisymmetric surface which depends upon the longitu-

γ	t	Elements	Nodes
5	2	88	266
10	2	124	374
5	3	64	194
10	3	88	266

Table 3.3: Mesh Distribution

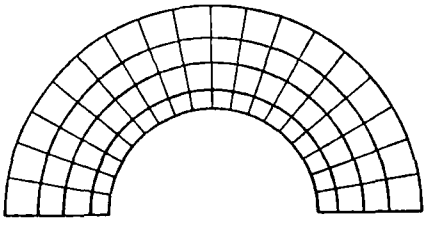

Figure 3.11: Axisymmetric FE mesh.

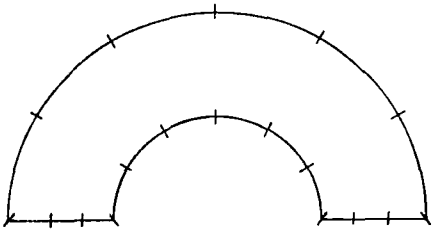

Figure 3.12: Axisymmetric BIE mesh.

dinal angle, θ and the radial coordinate, ρ, rotating around the axis perpendicular to the toroidal radius. The radial coordinate, ρ, is defined by $R + r\cos\phi$. This axisymmetric problem can be simplified by the use of symmetry in the plane of the torus, so only one-half of the cross-section plane needs to be considered. The number of elements and nodes used in the axisymmetric FE mesh are 72 and 262, respectively, and in the axisymmetric BIE mesh (where only the contour needs to be discretized) only 18 and 36, respectively. These meshes are shown in Figures 3.11 and 3.12. This clearly shows the advantage of the BIE method over FE method in significantly reducing the numerical problem. The number of elements used in the FE mesh exceed the number used in the three-dimensional BIE mesh for the case γ of 5 and t of 3.

All of the FE results shown herein are from Vogg [87] who used the ADINA program. The axisymmetric BIE results for the problem were obtained using the program AXIBIE, provided by Professor C. L. Tan of Carleton University.

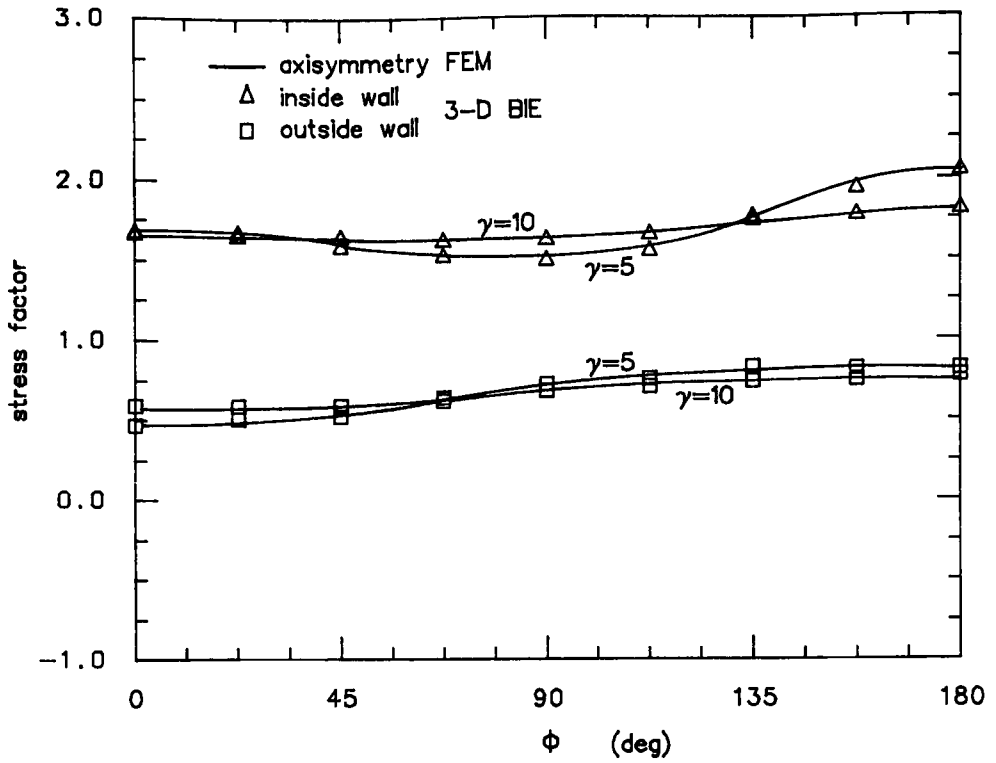

Figure 3.13: Circumferential stress factor, σ_{ϕ_f}, for t of 2.

The stress factors for the pressure loading problems are defined as

$$\sigma_f = \sigma / P_i \tag{3.5}$$

where σ is the actual stress and P_i is the applied pressure.

The results for the torus of thickness ratio of 2 and toroidal radius ratio of 5 are shown in Tables 3.4 to 3.7. These tables show the variation of the stress factors computed by the three-dimensional BIE along the longitudinal axis of the torus. The low variation of the stresses along the longitudinal axis, indicates that the mesh distribution as chosen is appropriate for the problem considered. There is excellent agreement between the three numerical methods. It is found that the maximum stress factor is the circumferential stress situated on the inside surface at the intrados (ϕ of 180°). This value calculated by three-dimensional BIE is 2.04 whereas for axisymmetric FE it is 2.1% higher and axisymmetric BIE 1.0% higher.

Figures 3.13 and 3.14 depict the effects of γ upon the circumferential and longitudinal stress factors for a constant thickness ratio of 2. Both the three-dimensional

ϕ	AXIS	AXIS	3 dimensional BIE			
deg.	BIE	FE	$\theta = 0°$	$\theta = 30°$	$\theta = 60°$	$\theta = 90°$
0	1.6733	1.6860	1.6699	1.6688	1.6690	1.6700
45	1.5867	1.5991	1.6083	1.5687	1.5684	1.6069
90	1.4777	1.4880	1.5063	1.4790	1.4790	1.5063
135	1.7351	1.7537	1.7777	1.7565	1.7565	1.7777
180	2.0566	2.0790	2.0353	2.0372	2.0371	2.0353

Table 3.4: Circumferential stress factor, σ_{ϕ_f}, at the inside surface.

ϕ	AXIS	AXIS	3 dimensional BIE			
deg.	BIE	FE	$\theta = 0°$	$\theta = 30°$	$\theta = 60°$	$\theta = 90°$
0	0.5988	0.6076	0.6244	0.6251	0.6251	0.6245
45	0.5175	0.5328	0.5177	0.5132	0.5131	0.5177
90	0.3153	0.3270	0.3108	0.3163	0.3163	0.3108
135	0.1213	0.1364	0.1139	0.1281	0.1281	0.1139
180	0.0761	0.0821	0.0679	0.0920	0.0920	0.0679

Table 3.5: Longitudinal stress factor, σ_{θ_f}, at the inside surface.

ϕ	AXIS	AXIS	3 dimensional BIE			
deg.	BIE	FE	$\theta = 0°$	$\theta = 30°$	$\theta = 60°$	$\theta = 90°$
0	0.4485	0.4592	0.4648	0.4647	0.4643	0.4645
45	0.5422	0.5400	0.5324	0.5154	0.5154	0.5324
90	0.7147	0.7107	0.7313	0.7151	0.7151	0.7313
135	0.8010	0.8121	0.8352	0.8227	0.8227	0.8352
180	0.8046	0.8118	0.8131	0.8103	0.8104	0.8131

Table 3.6: Circumferential stress factor, σ_{ϕ_f}, at the outside surface.

ϕ	AXIS	AXIS	3 dimensional BIE			
deg.	BIE	FE	$\theta = 0°$	$\theta = 30°$	$\theta = 60°$	$\theta = 90°$
0	0.3658	0.3720	0.3839	0.3791	0.3792	0.3840
45	0.3859	0.4153	0.4150	0.4051	0.4051	0.4151
90	0.4311	0.4327	0.4306	0.4316	0.4316	0.4304
135	0.2721	0.2775	0.2735	0.2798	0.2798	0.2733
180	0.1514	0.1545	0.1628	0.1647	0.1646	0.1627

Table 3.7: Longitudinal stress factor, σ_{θ_f}, at the outside surface.

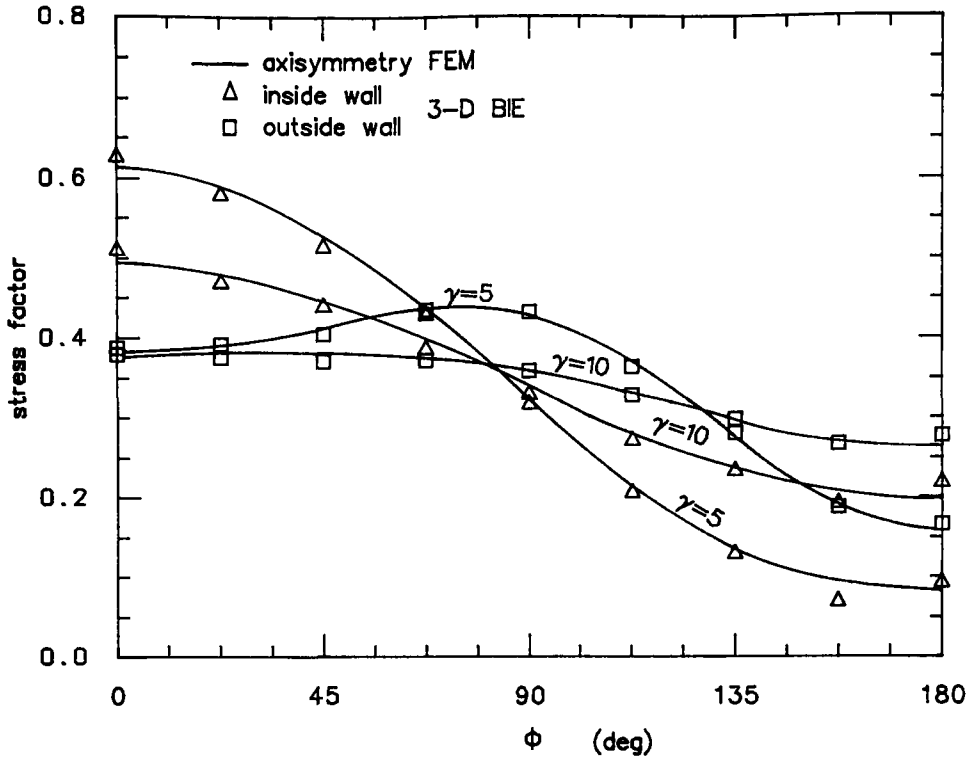

Figure 3.14: Longitudinal stress factor, σ_{θ_f}, for t of 2.

BIE and axisymmetric FE results are presented. It is seen that the maximum stress factor increases as γ decreases. This is also observed by McGill and Rapp [17]. Observing Figure 3.13, it is found that as γ increases, the circumferential stress factor becomes more uniform, approaching Lamé's solution for a cylinder, as would be expected. Around the cross-section, the circumferential stress factor at the inside surface for γ of 10 varies between 1.65 to 1.81 and for γ of 5 it varies between 1.68 to 2.07. For a cylinder of this cross-section configuration the hoop stress factor is 1.67.

Figure 3.15 shows the effect of γ on the displacement factors U_{ϕ_f} [defined as $\frac{U_\phi E}{P_i a}$] and U_{r_f} [defined as $\frac{U_r E}{P_i a}$] which are the circumferential and radial displacement factors, respectively. Note that γ has just the opposite effect compared to the maximum stress factor, namely that the maximum displacement factor increases as γ increases. Notice that the effect on U_{ϕ_f} is greater near 90° whereas U_{r_f} is greater at the extrados (ϕ of 0°). The variation of displacement factors increase as

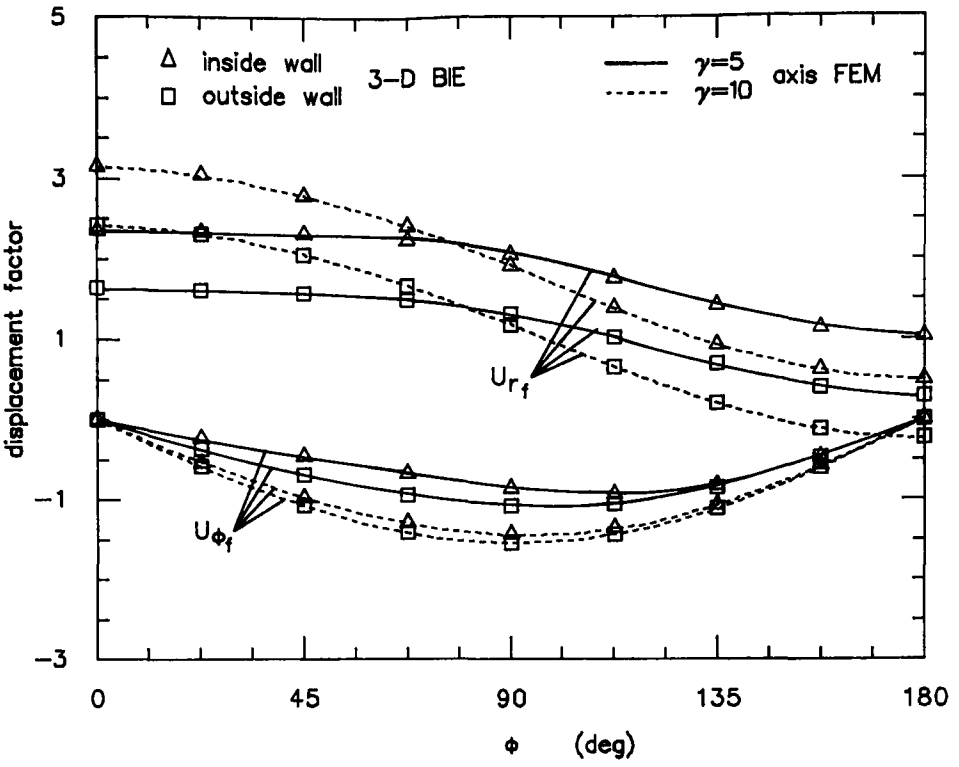

Figure 3.15: Displacement factors U_{r_f} and U_{θ_f} for t of 2.

γ increases.

Comparison between results of three-dimensional BIE and axisymmetric BIE are shown in Figures 3.16, 3.17 and 3.18. These figures demonstrate the effect of t on the stress and displacement factors for γ of 5. Observe that as t increases both maximum stress and displacement factors decrease. A similar effect can be seen in thick-walled cylinders. The minimum circumferential stress factor at the inside surface is near 90° whereas at the outside surface it is at the extrados. Note that the circumferential stress factors at the inside wall decrease almost by a constant factor when t increases. This is also true for the longitudinal stress factors at the inside wall. Figure 3.18 shows that the effect of t on U_{r_f} is significant for $0 \leq \phi \leq \pi/2$ whereas between $3\pi/4 \leq \phi \leq \pi$ it is insignificant.

The two sets of results agree very well, showing that the mesh distribution taken is adequate for the study of a torus with a circular cross-section. The results obtained for γ of 10 and t of 3 will be presented in the subsequent chapter.

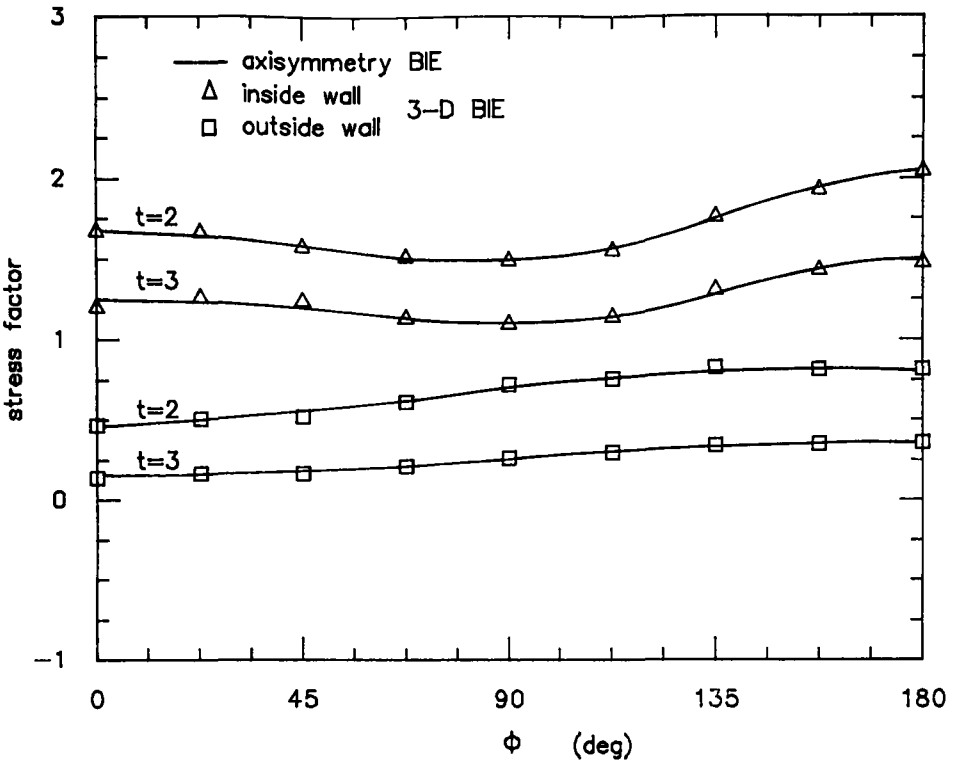

Figure 3.16: Circumferential stress factor, σ_{ϕ_f} for γ of 5.

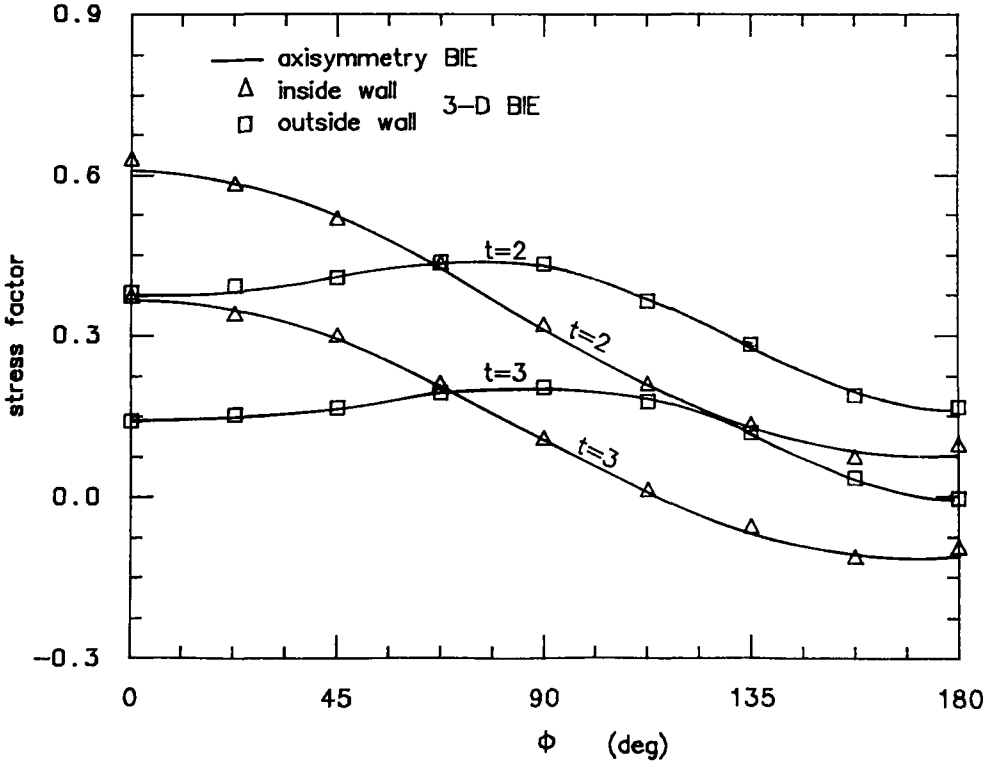

Figure 3.17: Longitudinal stress factor, σ_{θ_f}, for γ of 5.

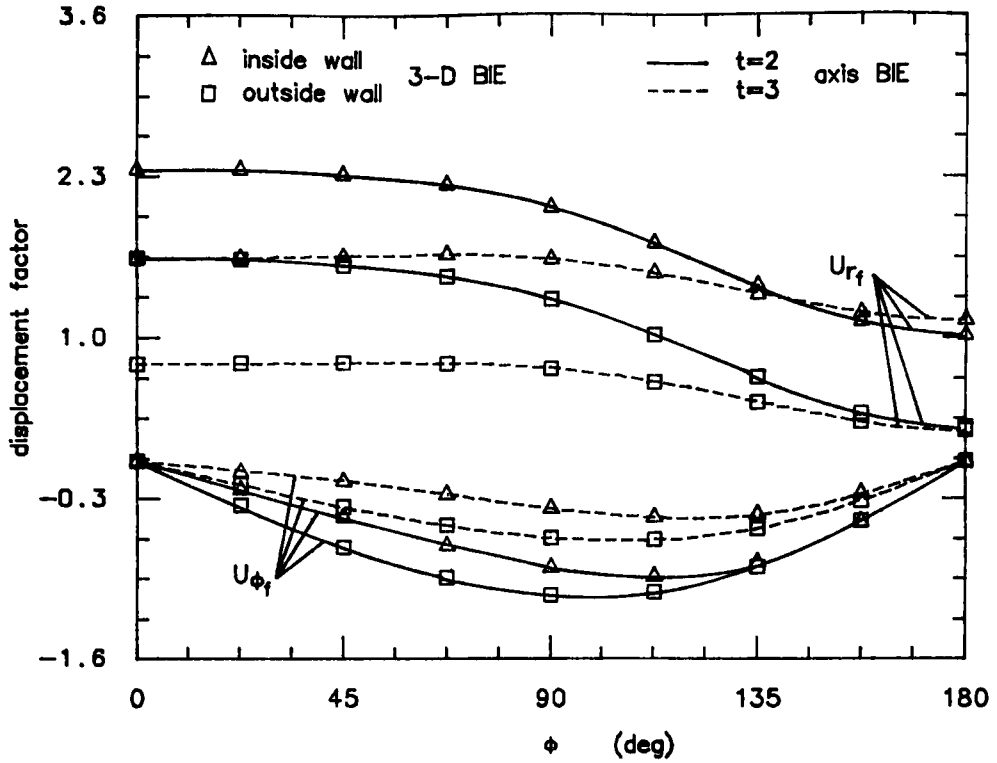

Figure 3.18: Displacement factors, U_{r_f} and U_{ϕ_f}, for γ of 5.

3.2.2 Torus with Elliptical Cross-Section

The problem solved by three-dimensional and axisymmetric BIE is shown in Figure 3.19. The cross-section is an ellipse defined by the equation $c^2x^2 + d^2y^2 = c^2d^2$, where c and d are the semi-major and semi-minor axes respectively.

At the inside wall the minor/major axes ratio is taken to be 0.6 whereas at the outside wall, it is taken to be 0.8, giving a constant thickness ratio, t of 2. This geometry was solved for two radius ratios of 5 and 10 by both BIE methods.

A difficulty arises in finding the midpoint between two points on the ellipse. The difficulty is resolved by the calculation of the circumference of the ellipse p_1 using

$$p_1 = 4cE_1$$

where E_1 is a product of an elliptic integral of the second kind, taken from function tables [88]. Knowing the coordinate ϕ_1 (defined as $(90 - \phi)$) of the two corner points of the element, E_1 is found from the tables for each corner points by extrapolation

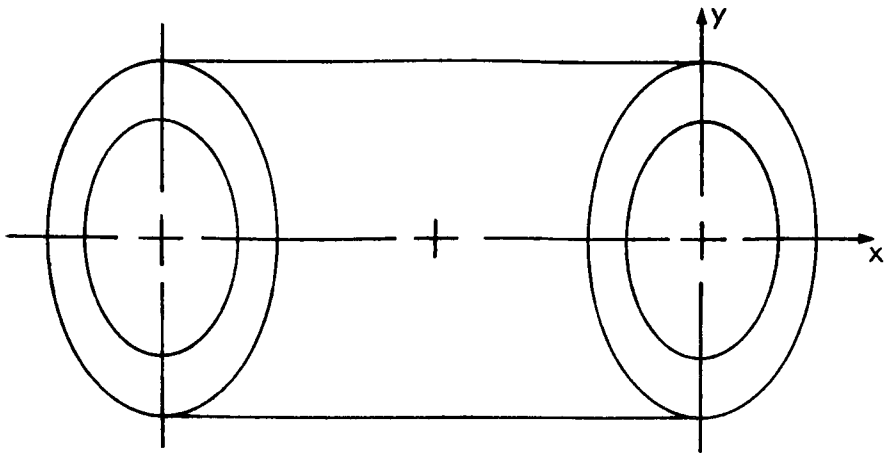

Figure 3.19: Section of elliptic cross-section

and then adding these and dividing by 2 gives E_1 for the midpoint. Again, using the tables, the corresponding angle ϕ_1 is found for the calculated E_1, by extrapolation. Due to the complexity in finding the midside nodes, more work was needed to generate the data for the oval cross-section, as compared to the circular cross-section.

For these two problems, the same mesh distribution was used as for the circular cross-section. Figures 3.20 and 3.21 depict the variation of the circumferential stress factors versus the circumferential angle for γ of 5 and 10, respectively. Both numerical results are shown. In these figures and subsequent ones, the solid curves represent a fit through the axisymmetric BIE results. Note that contrary to the case for the circular cross-section, the stress factors for the oval cross-section vary dramatically with ϕ. An increase in the maximum circumferential stress factor is observed, which is about 2.5 times greater than the one for a circular cross-section. The peak stress for the elliptic cross-section is at ϕ of 90° whereas for the circular cross-section it was at ϕ of 180°. The change of location of the peak stress factor is due to the flattening of the circular cross-section giving greater curvature in that region (ϕ of 90°). Notice contrary to the circular cross-section, as γ increases the peak stress increases. The peak stress factor increases from 4.49 to 4.92 when γ is increased from 5 to 10. For the cases shown herein, the effect of radius ratio on σ_{ϕ_f}

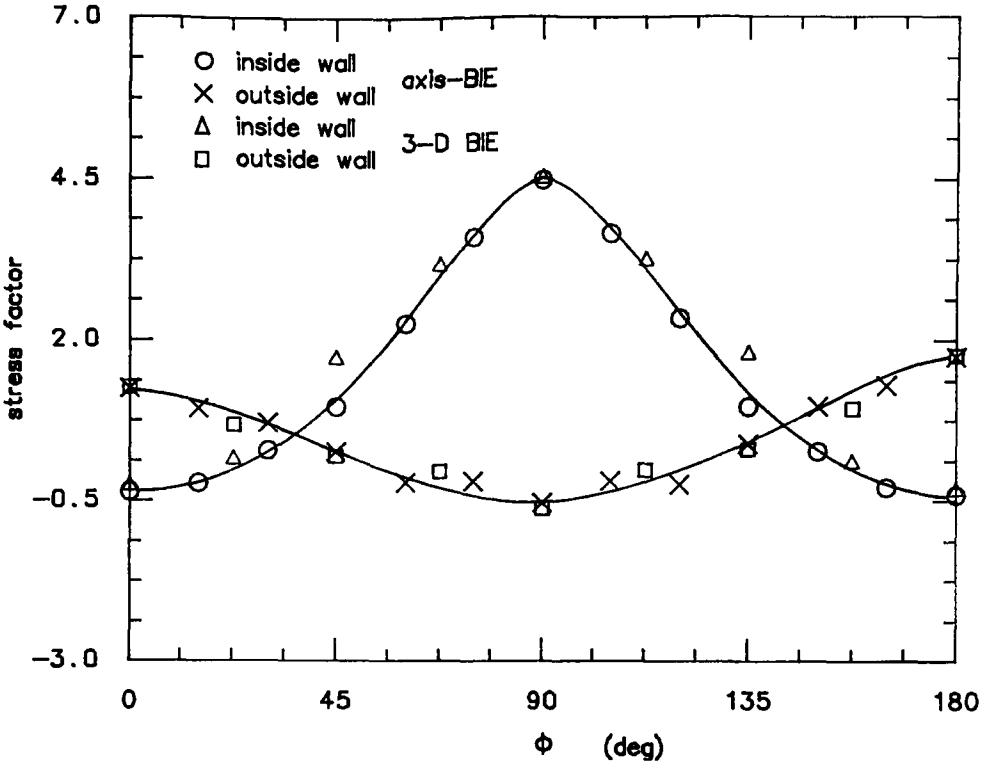

Figure 3.20: Circumferential stress factor, σ_{ϕ_f}, for γ of 5 and t of 2.

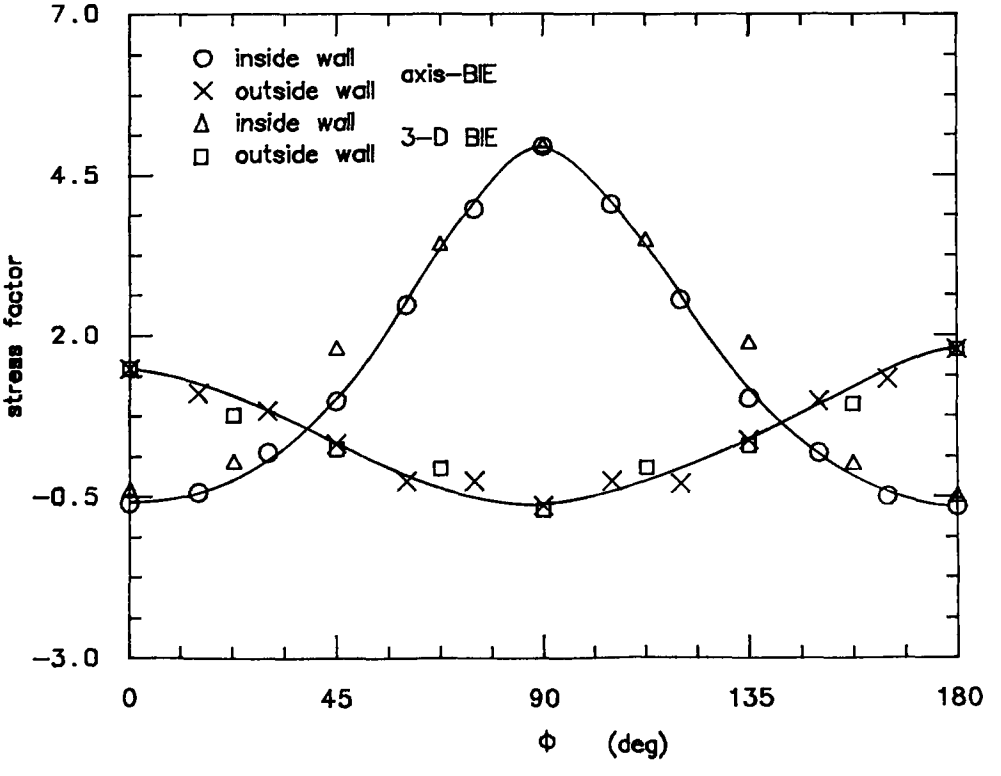

Figure 3.21: Circumferential stress factor, σ_{ϕ_f}, for γ of 10 and t of 2.

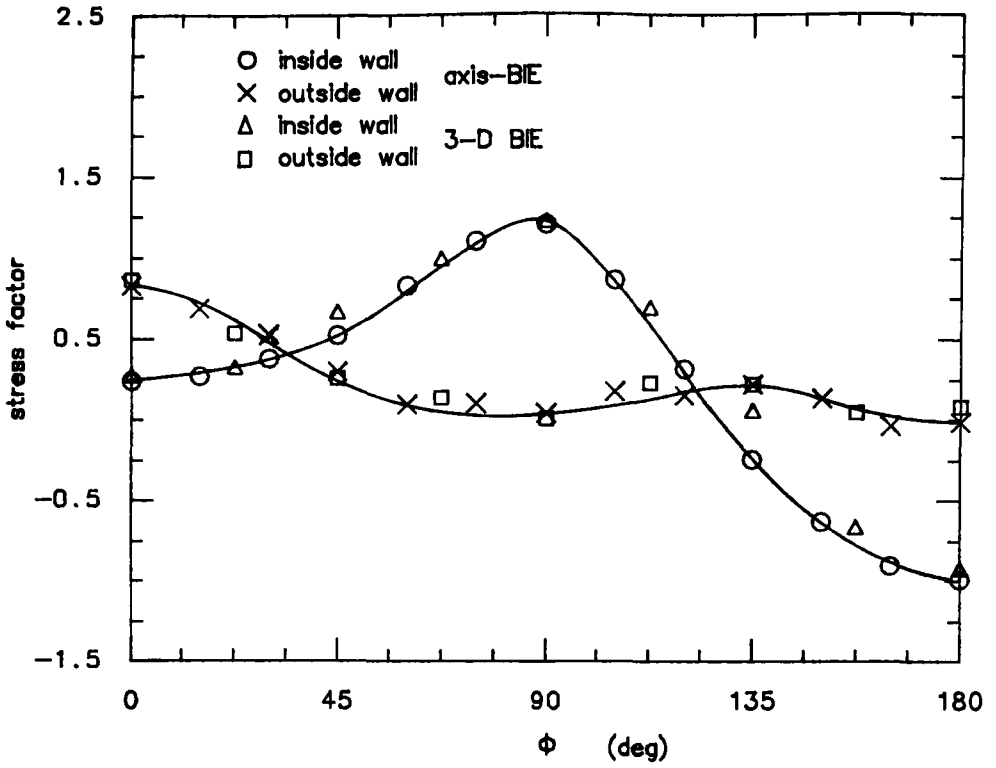

Figure 3.22: Longitudinal stress factor, σ_{θ_f}, for γ of 5 and t of 2.

on the outside surface is minimal.

The longitudinal stress factors for both cases are shown in Figures 3.22 and 3.23. Just as for the circumferential stress factors, the peak stress factor is along the inside surface at ϕ equal to 90° and the stress factors vary considerably with the circumferential angle. For both σ_{ϕ_f} and σ_{θ_f}, there is close agreement between the methods, particularly in the extreme values. Observing the above four figures, it is seen that there is a small fluctuation of the three dimensional results, mostly for small values of stress. This is also noted from the axisymmetric BIE results. This means that more elements are needed to give a better representation of the boundary due to the increase in curvature of the cross-section of the torus. However the fluctuation is small and is mostly for low values of stress which are not as important as the high values. Thus the mesh distribution used is satisfactory.

Figures 3.24 and 3.25 show the variation of the displacement factors versus the circumferential angle for γ of 5 along the inside and outside surfaces, respectively.

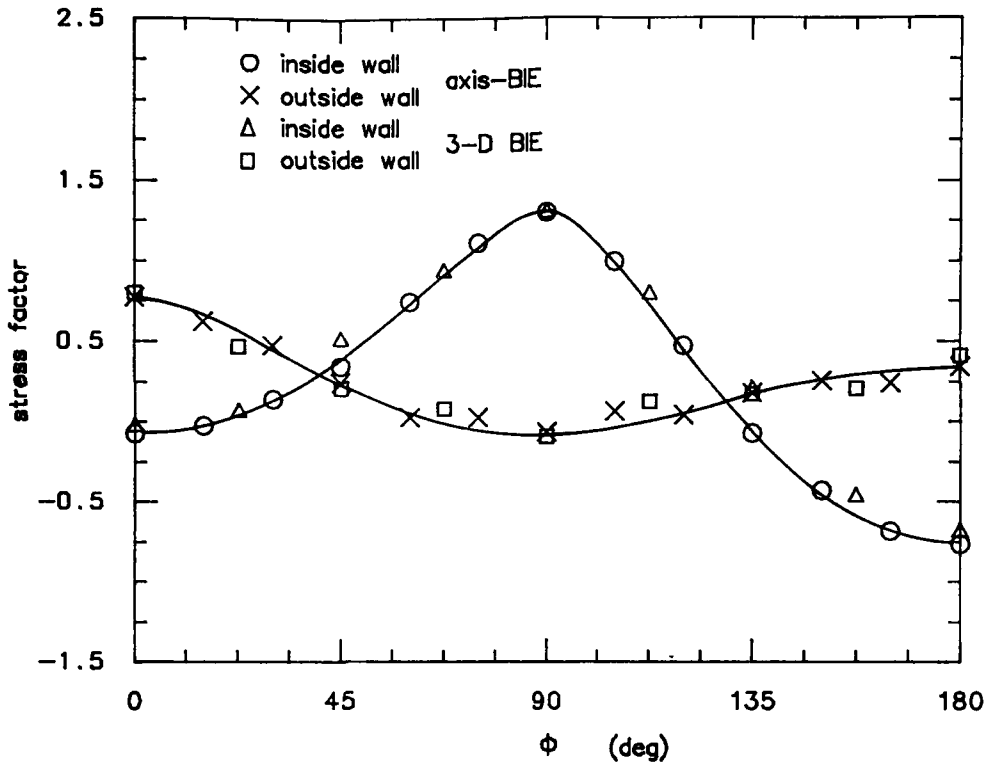

Figure 3.23: Longitudinal stress factor, σ_{θ_f}, for γ of 10 and t of 2.

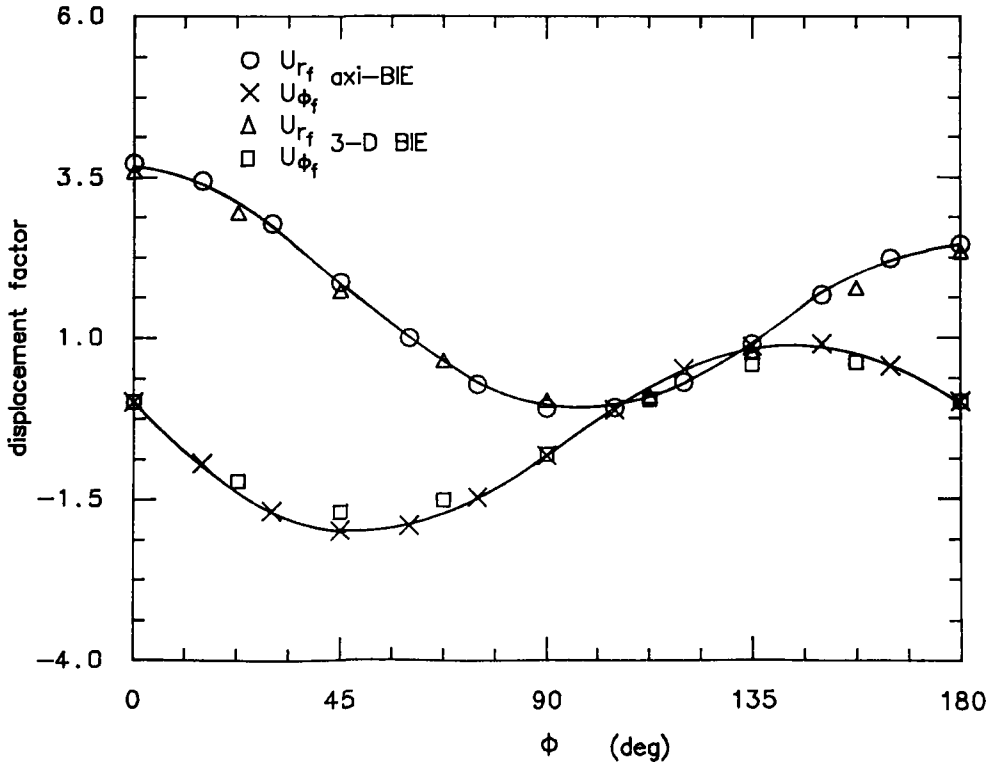

Figure 3.24: Displacement factors at the inside surface for γ of 5 and t of 2.

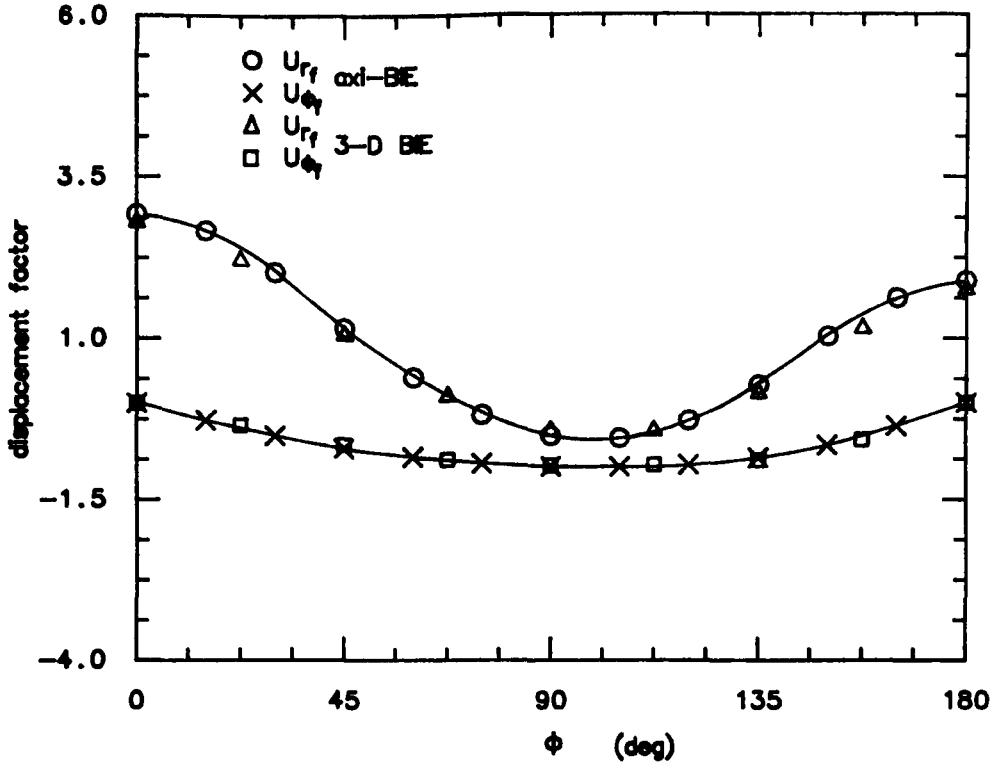

Figure 3.25: Displacement factors at the outside surface for γ of 5 and t of 2.

As for the stress factors, the displacement factors are also strongly affected in the case of an oval cross-section. Good agreement between the two methods is observed. The peak value for U_{r_f} is at the extrados on the inside surface whereas for U_{ϕ_f} it is at $\pi/4$, also on the inside surface.

The effect of radius ratio, γ (not shown herein) shows that as it increases from 5 to 10 the maximum difference between the displacement factors is in the region of $0 \leq \phi \leq 60°$. The maximum displacement factors for U_{r_f} and U_{ϕ_f} increase by 1.2 percent as γ increases from 5 to 10.

Chapter 4

Toroidal Geometries

4.1 Toroidal Elasticity

Examination of the technical literature indicated that no work prior to Göhner's work [89,90,91] used toroidal elasticity. He used a simple form of toroidal elasticity, adaptable to solid circular cross-section only, to solve the twist and pure bending of a solid circular sector. Followed by Kornecki [12] and later by Lang [22], the coordinate system was changed to suit a hollow circular cross-section of constant thickness. The coordinate system is represented by r, ϕ, θ as shown in Figure 3.9.

Toroidal elasticity makes use of the general equations of the classical linear theory of elasticity, expressed in terms of stress components. An approximate solution is obtained by expanding the stresses in power series of a small parameter (method of successive approximations). Lang used the parameter $1/R$ where R is the mean toroidal radius. Toroidal elasticity is valid for toroidal shells of arbitrary thickness with isotropic homogeneous materials.

Toroidal elasticity theory contains three equilibrium equations of the form:

$$M + \frac{1}{\rho} N = 0$$

or, in expanded form:

$$\left[M_0 + \frac{1}{R} M_1 + \frac{1}{R^2} M_2 + \cdots\right] + \frac{1}{R}\left[1 - s\cos\phi + s^2\cos^2\phi - \cdots\right]\left[N_0 + \frac{1}{R} N_1 + \frac{1}{R^2} N_2 + \cdots\right] = 0$$

There are six Beltrami-Michell compatibility equations of the form:

$$U + \frac{1}{\rho}V + \frac{1}{\rho^2}W = 0$$

or, in expanded form:

$$\left[U_0 + \frac{1}{R}U_1 + \frac{1}{R^2}U_2 + \cdots\right] + \frac{1}{R}\left[1 - s\cos\phi + s^2\cos^2\phi - \cdots\right]\left[V_0 + \frac{1}{R}V_1 + \frac{1}{R^2}V_2 + \cdots\right]$$
$$+\frac{1}{R^2}\left[1 - 2s\cos\phi + 3s^2\cos^2\phi + \cdots\right]\left[W_0 + \frac{1}{R}W_1 + \frac{1}{R^2}W_2 + \cdots\right] = 0$$

where ρ is defined as $R + r\cos\phi$, s is defined as r/R, M and N are equilibrium functions and U, V and W are compatibility functions. The equilibrium and compatibility functions for the particular problems studied herein are defined in Lang's papers which are presented in Appendix B. Each of the six stresses is represented by a series which can be expressed as:

$$S(\text{Total}) = S(0) + S(1) + S(2) + S(3) + \cdots$$

Terms of a given power in the series are grouped together and required to satisfy equilibrium, compatibility and boundary conditions. Thus a succession of approximations is developed, the higher approximations generally involving some terms of the lower approximations. A problem is solved by selecting a basic solution (first approximation) usually known from theories applicable to a straight cylinder. Higher approximations modify this first approximation, but do not change the magnitude of the applied load. When the stresses are determined, the displacements can be found by integrating the stress-displacement relations. It is generally agreed that the method of successive approximations approaches the exact solution. Unfortunately successive term becomes increasingly algebraically unwieldy. Having no formal proof of convergence, the numerical results must be viewed with some suspicion, with the effect of the next term in the series unknown. Results based on purely numerical work can serve to establish the accuracy of a TE solution at

a given level of approximation. Thus it can be determined if a given level of a TE solution is adequate or if a higher level of approximation is needed.

Lang identified ten basic TE problems for a 90° elbow. These were the internal pressure problem, three end moment problems, three end force problems and three seismic (self-weight) problems. The present work deals with the first seven of these problems.

Three programs were written by the author using the theory developed by Lang. The programming was done in FORTRAN. The computer program PRE-TORUS calculates the stresses of a pressurized torus. The second program IN-PLANE calculates the stresses for a 90° elbow subjected to in-plane loadings (symmetric about the plane of the elbow). The loadings are:

1. In-plane bending
2. End normal force
3. In-plane end shear force

The third program, OUT-PLANE, evaluates the stresses of the 90° elbow subjected to out-of-plane loadings, which are:

1. Out-of-plane bending
2. Twist bending
3. Out-of-plane end shear force

The programs are interactive and are executed within about 14K words on the computer CP6 (DPS/8-70C). Upon request they calculate the stresses in a given cross or longitudinal section of the toroidal shell.

4.2 Pressurized Torus

The problem considered in this section is a complete circular torus under internal pressure. This problem was solved by the BIE method in the previous chapter. The same geometric cases are to be studied by the TE solution. The TE solution is limited to the zero order, first order and second order stress fields. Lang [92] recommended the use of Ref. [24] in preference to Ref. [22], which has typographic errors. He has submitted two corrections for Ref. [24]. The first correction is on page 299 where $2C_0 + \alpha_3(1+\nu) - \nu\alpha_4 = 0$ replaces $2C_0 = \nu\alpha_4$, thus giving:

$$C_0 = \frac{\lambda_0 \nu(\nu-2)}{2(\nu-1)}$$

$$\alpha_4 = \frac{\lambda_0(\nu - 1 - \nu^2)}{(\nu-1)}$$

The second correction is on page 300 where the expression for λ_1 is to be replaced by

$$\lambda_1 = \frac{4B\lambda_0}{(2+\nu)} - 4\lambda_0 \frac{(1+\nu)(\nu^2+1-\nu)}{(1-\nu)(2+\nu)} \frac{1}{s_a^2+s_b^2} + 8\lambda_0 \frac{(\nu^2+1-\nu)(1+\nu)}{(2+\nu)(1-\nu)} \frac{s_a^2 \ln\left(\frac{s_b}{s_a}\right)}{(s_b^4 - s_a^4)}$$

These corrections are included in the computer program.

Figures 4.1 and 4.2 depict the effect of thickness ratio upon circumferential and longitudinal stress factors (defined in Eq. (3.5)) at the inside surface for γ of 5 and 10, respectively. TE results are compared with BIE results. The first figure shows that as t increases from 2 to 3 the agreement between TE and BIE results improves. This is also the case when γ increases from 5 to 10. The TE results presented for γ of 10 correlate well with BIE results for both thickness ratios. Note that $\sigma_{\phi_{max}}$ calculated by the BIE for the case γ of 10 and t of 3 has moved to ϕ of 135°.

It seems that additional terms in the series are needed for better accuracy when the torus radius is small. This is expected due to the fact that the problem is solved approximately by expanding the solution in the reciprocal of the toroidal radius $(1/R)$.

Table 4.1 displays the peak stress for the four cases studied. Good agreement is found between BIE and TE results. The largest deviation is only 3.03%.

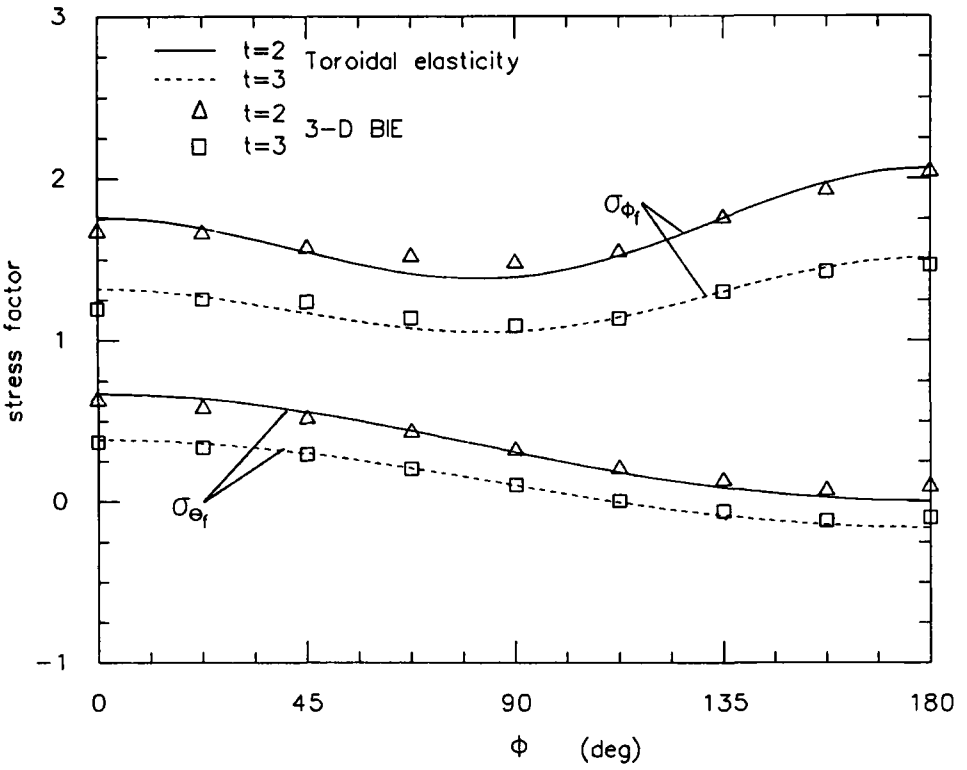

Figure 4.1: Circumferential and longitudinal stress factors at the inside surface for γ of 5.

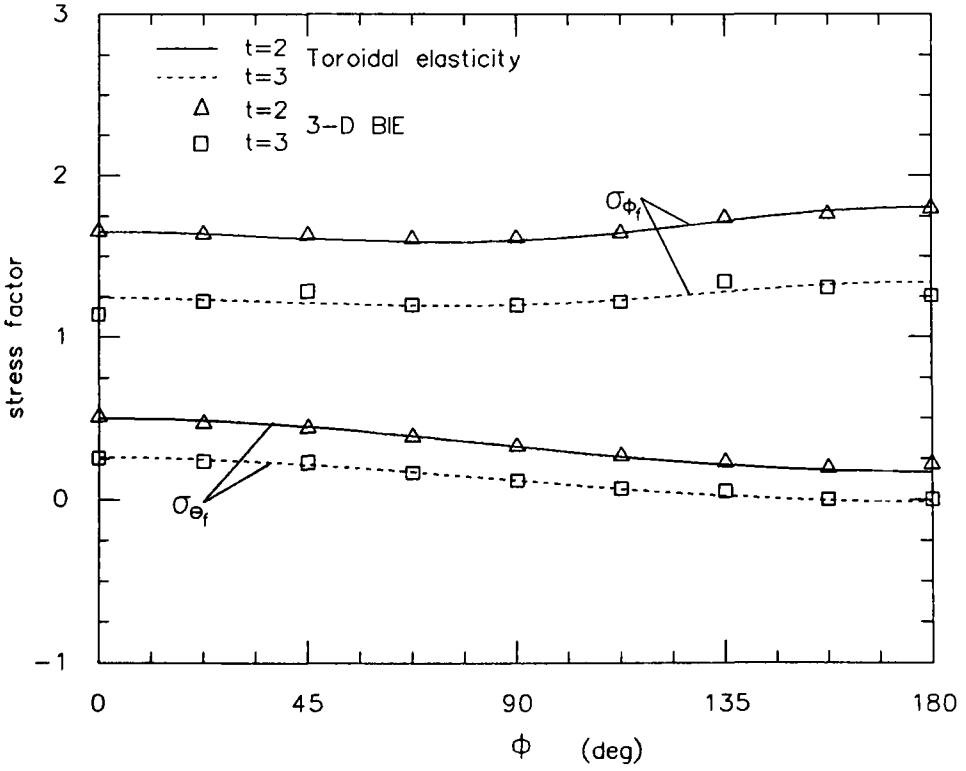

Figure 4.2: Circumferential and longitudinal stress factors at the inside surface for γ of 10.

γ	t	BIE σ_{max}	TE σ_{max}	Deviation (%)
5	2	2.0374	2.0634	1.27
10	2	1.7973	1.8040	0.37
5	3	1.4664	1.5109	3.03
10	3	1.3452	1.3393	0.43

Table 4.1: Peak stress factor for internal pressure

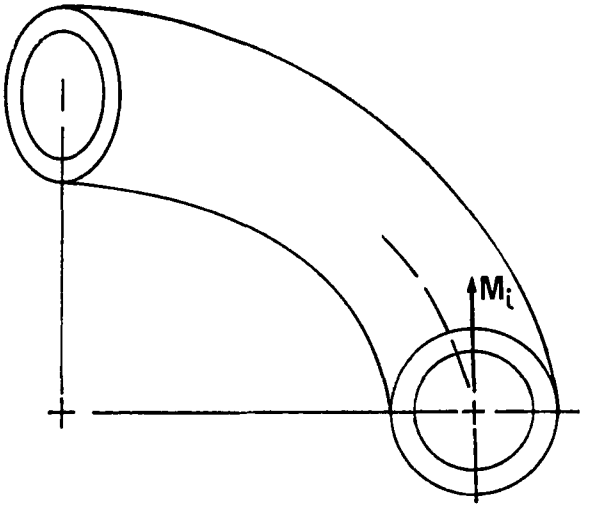

Figure 4.3: 90° Elbow subjected to in-plane moment

4.3 In Plane Bending of a 90° Elbow

The problem solved by three dimensional BIE is shown in Figure 4.3. A bending moment, M_i, is applied at the station defined by θ of 0° The elbow is fixed at the station θ of 90°, creating an opposite bending moment. For this problem, there is only one plane of symmetry, so one half of the elbow needs to be modelled. The mesh distribution is the same as for the torus subjected to internal pressure loadings.

The applied bending stress is linearly distributed over the cross-section. This gives a longitudinal stress factor equal to zero at ϕ of 90° and 270°, and a peak at ϕ of 0° and 180° at the loading station θ of 0° For the particular cases studied the applied moment is negative.

Lang [25,26] determined the first four terms in the series for a toroidal tube or pipe bend, acted upon by pure end bending moments, M_i. The stress fields are not

functions of θ. All the loadings in the TE solutions are defined by a non uniform or non linear variation of the stresses over the toroidal cross-section. It is assumed that away from the ends, the end effects due to different BIE boundary conditions and TE boundary conditions are negligible. Thus the TE results are compared with the BIE results calculated at the cross-section θ of 45° for all problems considered in this chapter.

Corrections to Ref. [26] were brought to my attention by Lang [92]. On page 98 the term $2\beta_1 s_a^2 s_b^2$ in equation (16) should be replaced by $\beta_1 s_a^2 s_b^2$. This in turn changes

$$\beta_7 = (C_0 + D_2)(1+\nu) + \nu\beta_5 s_a^2 s_b^2 + \nu\beta_1 s_a^2 s_b^2 + K_3(2+\nu)$$

In equation (24) on page 99 the number 24 replaces 96. The last correction is on page 100 where R_3 should be given as

$$R_3 = \lambda_2\overline{\beta}_7 + \lambda_3\overline{\beta}_8 + \overline{\beta}_9$$

The stress factors for in-plane and out-of-plane bending loading problems are defined as

$$\sigma_f = \sigma / \frac{Mb}{I}$$

where σ is the actual stress, b is the outside radius of the cross-section, M is the bending moment and I is the moment of inertia of the cross-section about the cross-sectional axis.

Figures 4.4 and 4.5 show the calculated values of stress factors σ_{ϕ_f} and σ_{θ_f} for a pipe bend with γ of 5 and t of 2 and 3, respectively. Agreement between TE and BIE results deteriorates as t is increased from 2 to 3. It is noted that correlation between the stress factors seems to be better for σ_{θ_f} than σ_{ϕ_f}. TE solutions overpredict σ_{ϕ_f} at the inside wall. The peak stress factor is the longitudinal stress situated at the outside surface at the intrados. The maximum circumferential stress factor is at the inside surface near ϕ of 90°. Note that as t increases the peak stress also increases.

The stress factors σ_{ϕ_f} and σ_{θ_f} for a γ of 10 are shown in Figures 4.6 and 4.7 for t of 2 and 3, respectively. The TE and BIE results are in very good agreement,

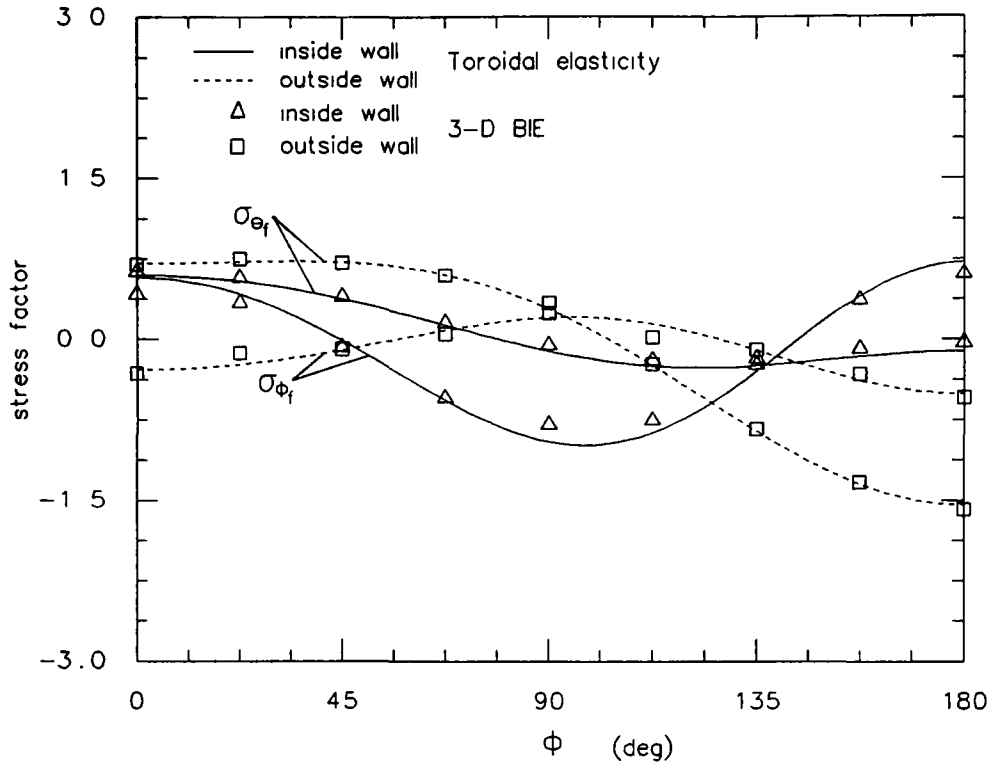

Figure 4.4: Circumferential and longitudinal stress factors for γ of 5 and t of 2.

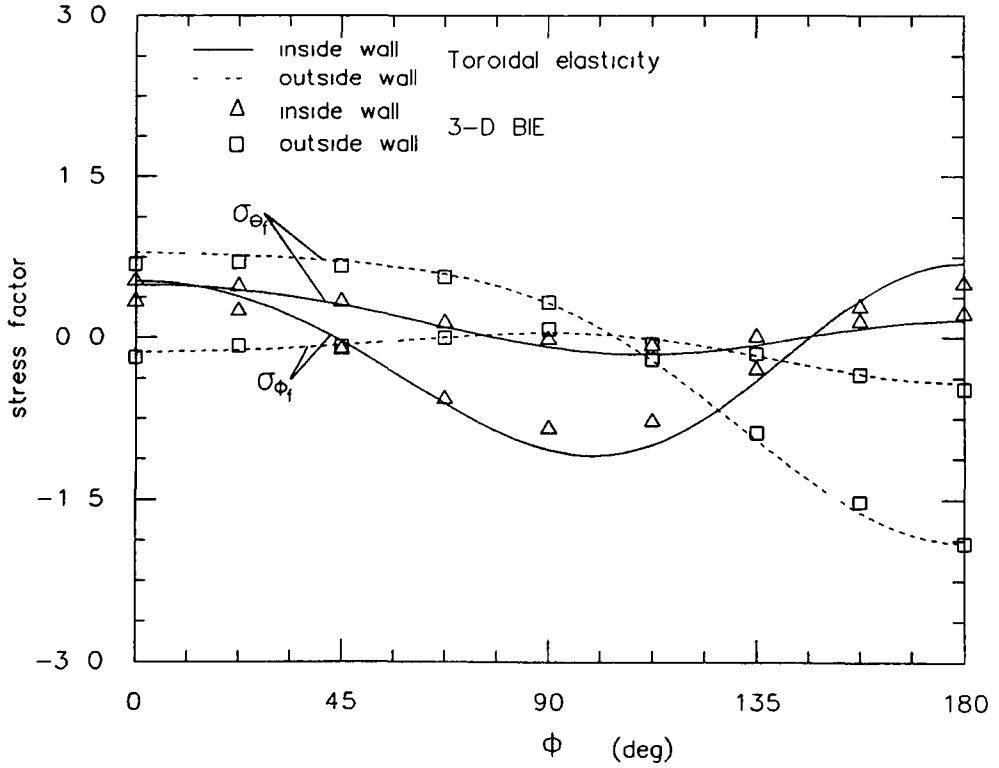

Figure 4.5: Circumferential and longitudinal stress factors for γ of 5 and t of 3.

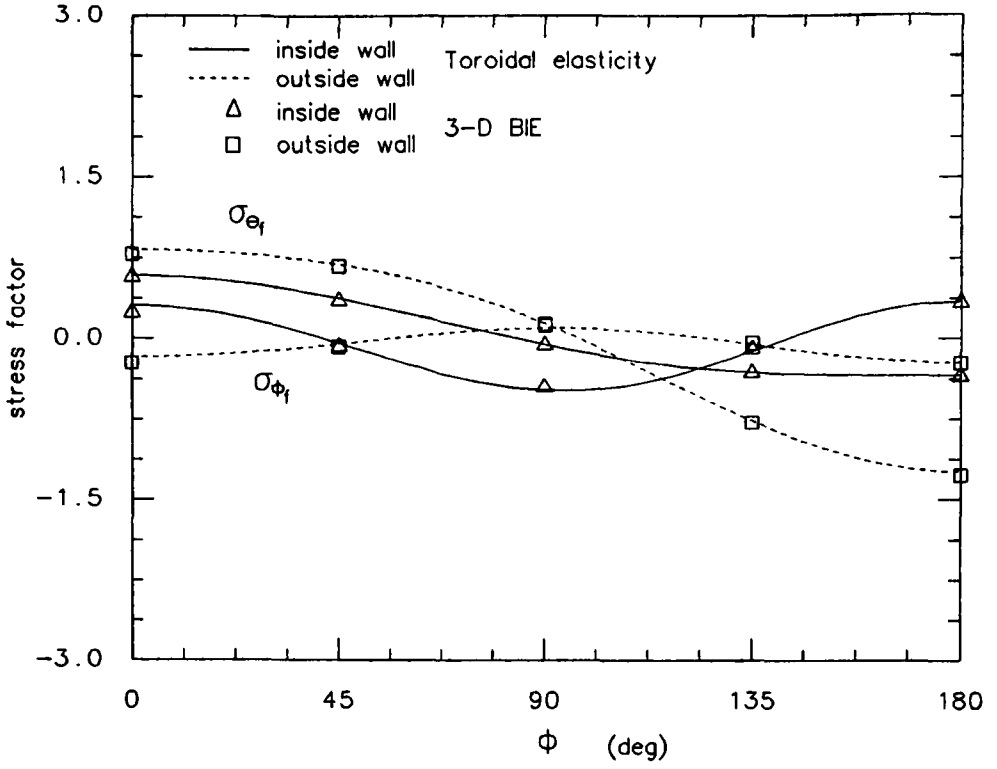

Figure 4.6: Circumferential and longitudinal stress factors for γ of 10 and t of 2.

whereas for γ of 5 the comparison was not as good. It is interesting to note that this was also true for the internal pressure problem. Comparing the figures it is seen that the maximum stresses increase with increasing t, but only by a slight amount compared to the ones for γ of 5. Thus when γ is large the effect of thickness on the size of stresses is less. Notice from the figures that σ_{θ_f} on the inside surface have a different pattern from the ones on the outside surface. This is due to the thickness effect where for thick-walled shells the distribution of stress changes significantly from one surface to the other. However, for thin-walled shells the stress on both surfaces will follow a similar pattern.

Observing Figures 4.5 and 4.7, both having the same thickness ratio but different γ of 5 and 10 respectively, it is noted that the stresses vary considerably with γ. Also note that the peak stress decreases as γ increases. Results of the peak stress factor calculated by both methods are presented in Table 4.2. Very good correlation is found between the methods, with the maximum deviation less than 3%.

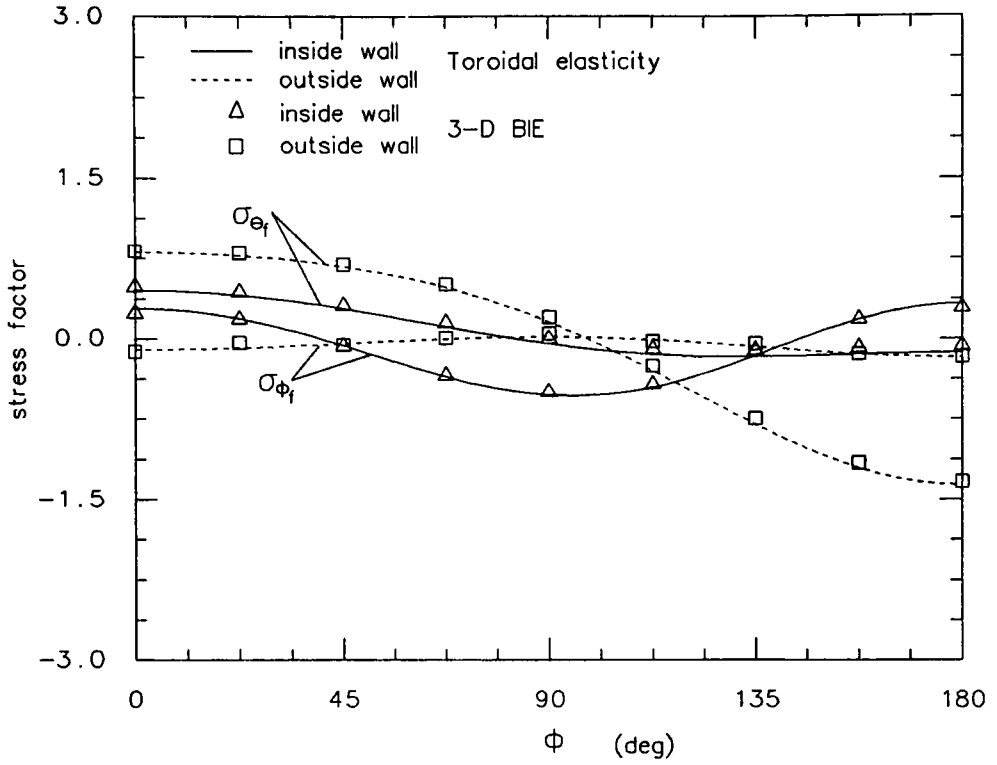

Figure 4.7: Circumferential and longitudinal stress factors for γ of 10 and t of 3.

γ	t	BIE σ_{max}	TE σ_{max}	Deviation (%)
5	2	1.5838	1.5396	2.79
10	2	1.2750	1.2390	2.82
5	3	1.9061	1.8978	0.44
10	3	1.3322	1.3633	2.33

Table 4.2: Peak stress factor for in-plane bending

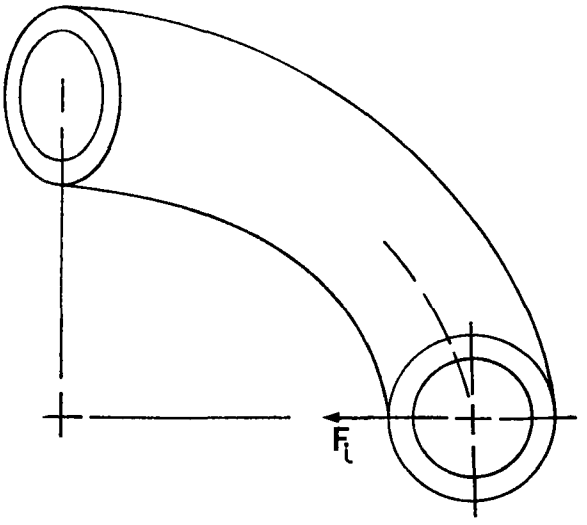

Figure 4.8: 90° Elbow subjected to an in-plane end shear force

4.4 In-Plane End Shear Force Acting on a 90° Elbow

The problem solved by the BIE is shown in Figure 4.8. An end shear force, F_i, acts inwardly at the station θ of 0°. Again the elbow is fixed at the station θ of 90° Similarly to the in-plane bending problem, there is one plane of symmetry so only one half of the elbow is modelled. The applied force, F_i, is assumed uniformly distributed over the cross-section.

A total of eight fields of stress are developed by Lang [29], three zero order fields of stress and five first order fields of stress. The elbow is maintained in equilibrium at the station θ of 90°, by an end normal force and an in-plane bending moment. For the stress field describing the bending moment, Lang used the ones determined in ref. [25]. Minor adjustments to these stress fields were done to satisfy the boundary conditions.

It was found that the term:

$$\frac{11\nu - 1}{4(1-\nu)} \frac{K_0\delta_2}{8}$$

in λ_1, of ref. [29] should not have the 4 in the denominator which was later acknowl-

edged by Lang [93]. Other corrections to ref. [29] were brought to my attention by Lang [93]. On page 273, the denominator $(1+\nu)$ of constants $\overline{\lambda}_1$ and d_0 should be replaced by $(1-\nu)$. The constant c on page 273 having a denominator $s_a^2 s_b^2$ should be replaced by $(s_a^2 + s_b^2)$. Also the term $(s_a^2 - s_b^2)$ in equation (7) on page 271 should be in fact $(s_a^2 + s_b^2)$.

The stress factors for all force loading problems considered in this chapter are defined as:

$$\sigma_f = \sigma / \frac{F}{A}$$

where σ is the actual stress, A is the cross-sectional area and F is the force.

In Figure 4.9, stress results at θ of 45° are presented for the case, γ of 5 and t of 2. Agreement between TE and BIE is poor for σ_{θ_f} and σ_{ϕ_f} whereas for $\sigma_{\phi\theta_f}$ the agreement is good. The BIE method predicts a maximum σ_{ϕ_f} at the inside surface near ϕ of 90°, whereas the TE solution predicts it at ϕ of 180°. The BIE and TE results follow a similar trend, however the results are quantitatively different especially for σ_{θ_f} at the inside surface. Apparently higher levels of approximation are needed in TE for acceptable accuracy.

It is stated at the beginning of this section that the zero and first order stress fields were determined for this particular problem. Two extra terms have been developed by Lang [26] describing the in-plane bending moment. These two terms are added to the original stress fields. Adjustments are made to these two additional terms to satisfy the boundary conditions of an end bending moment at station θ of 90°, by multiplying each term by sin θ. Now we have a shear force and a normal force defined by a zero and first order stress fields and a bending moment defined by a zero, first and second order stress fields.

Figure 4.10 shows the computed results at θ of 45° with the added stress field for a torus having γ of 5 and t of 2. Comparing with Figure 4.9, it is observed that the added stress field improves the agreement between the TE and the BIE. This is also noticed for the other geometries considered. For the other cases, only the results from the TE solution with the added stress field are presented.

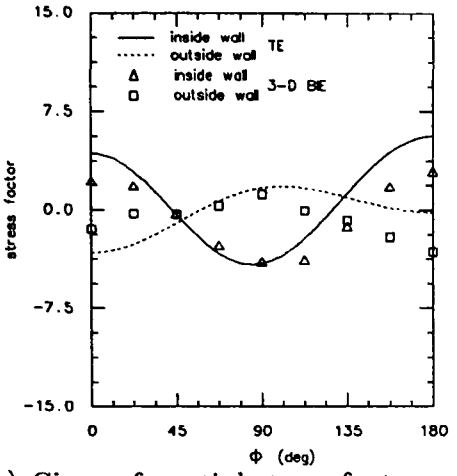

a) Circumferential stress factor

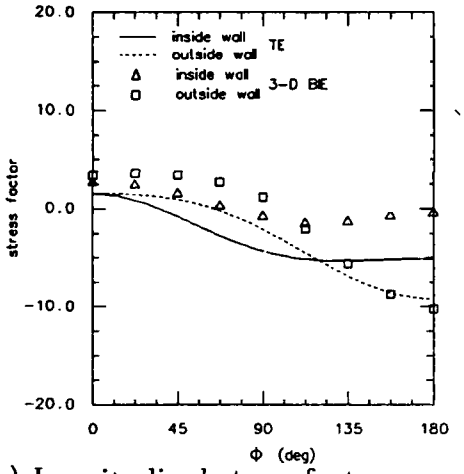

b) Longitudinal stress factor

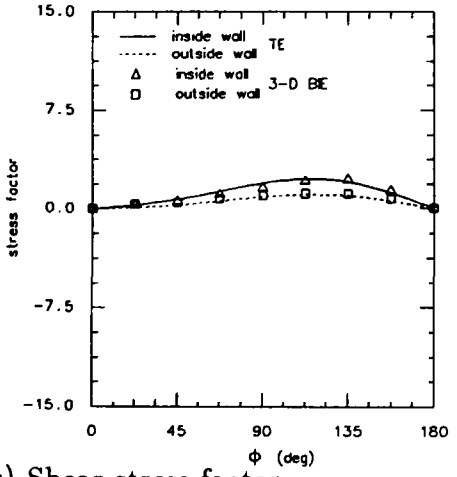

c) Shear stress factor

Figure 4.9: Stress factors for γ of 5 and t of 2.

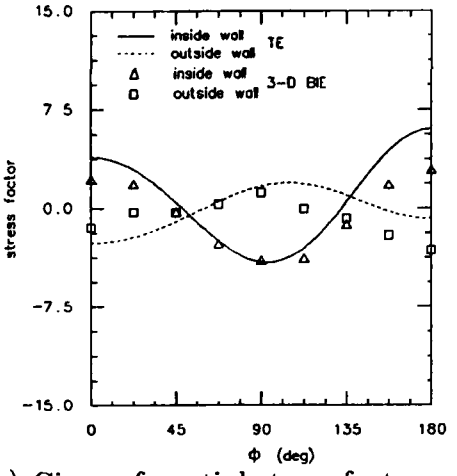

a) Circumferential stress factor

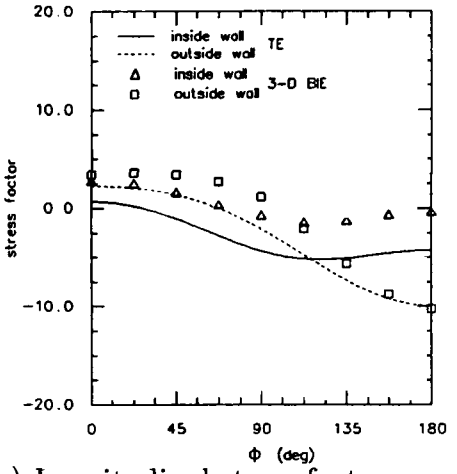

b) Longitudinal stress factor

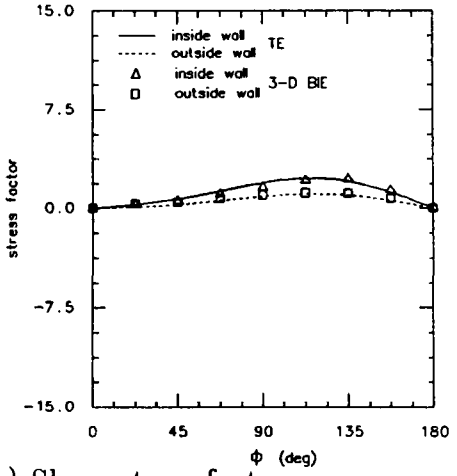

c) Shear stress factor

Figure 4.10: Stress factors with the added field for γ of 5 and t of 2.

γ	t	TE σ_{max}	Modified TE σ_{max}	BIE σ_{max}	Deviation (%)
5	2	9.218	9.914	10.247	3.25
10	2	15.010	15.359	15.560	1.29
5	3	7.501	8.953	9.735	8.03
10	3	11.890	12.617	12.304	2.54

Table 4.3: Peak stress factor for in-plane end shear force

The results at θ of 45° for γ of 5 and t of 3 and for γ of 10 and t of 2 and 3 are shown in Figures 4.11, 4.12 and 4.13. In all cases, σ_{θ_f} at the inside surface found by the TE method, follows a similar trend to the BIE results with almost a constant factor between them along the circumferential angle ϕ. For σ_{θ_f} on the outside surface, reasonable agreement between the methods is found in the region of $3\pi/4 < \phi \leq \pi$. Away from this region the agreement is poor.

Good correlation between the methods is found for σ_{ϕ_f} at the inside wall in the region $\pi/4 < \phi < 3\pi/4$ for an elbow having γ of 5. Outside this region the correlation is poor. It is noticed that for σ_{ϕ_f} at the inside surface the discrepancy between the methods decreases as γ increases between $0 \leq \phi < \pi/4$ and $3\pi/4 < \phi \leq \pi$ but increases near ϕ of 90°. Improvement of σ_{ϕ_f} on the outside surface is noticed when γ is increased from 5 to 10. Note that if a line is passed through σ_{ϕ_f} at the inside surface computed by the BIE results, $\sigma_{\phi_{max}}$ is at a point ϕ greater than 90°. This is because the neutral axis is located toward the center of curvature and not at ϕ of 90° as for a straight pipe. The TE solution predicts reasonably well the shearing stress, $\sigma_{\phi\theta_f}$.

The peak stress factor, σ_{max}, is given by the longitudinal stress on the outside wall at the intrados. Table 4.3 presents the peak stress factors at θ of 45° calculated by the TE solution with and without the added stress field and by the BIE method. The deviation in percentage between the BIE results and the modified TE results of σ_{max} are also shown. Good correlation is found between the methods with a maximum deviation less than 9%. Comparing the non-modified TE result with the BIE result of σ_{max}, it is seen that the correlation is not as good.

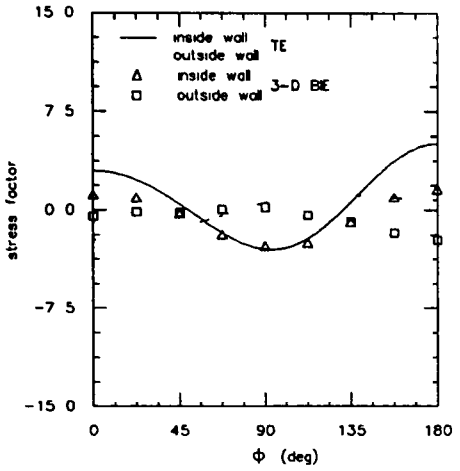

a) Circumferential stress factor

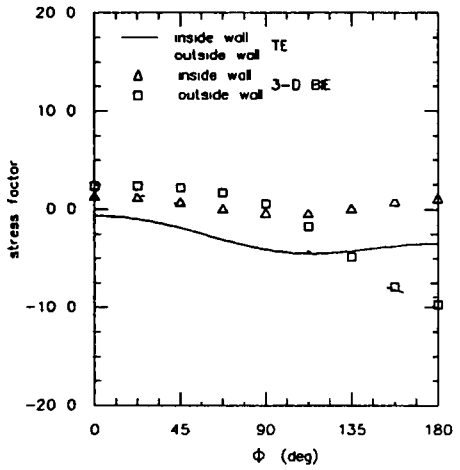

b) Longitudinal stress factor

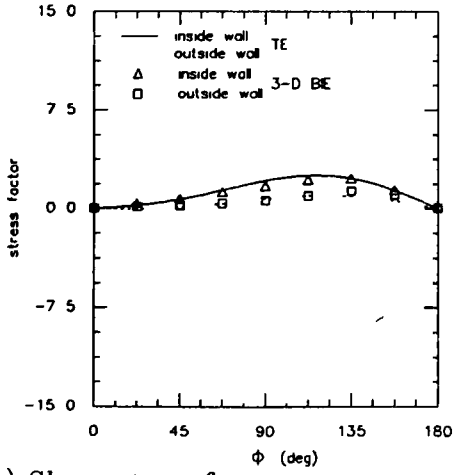

c) Shear stress factor

Figure 4.11· Stress factors for γ of 5 and t of 3.

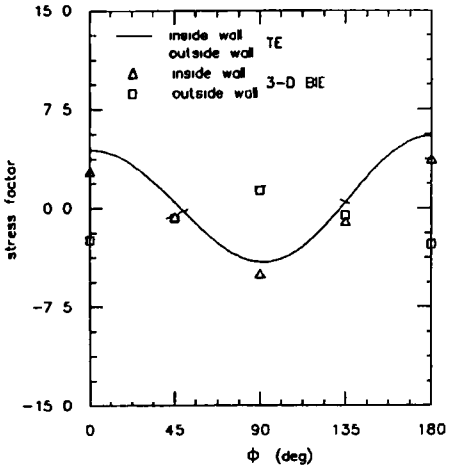

a) Circumferential stress factor

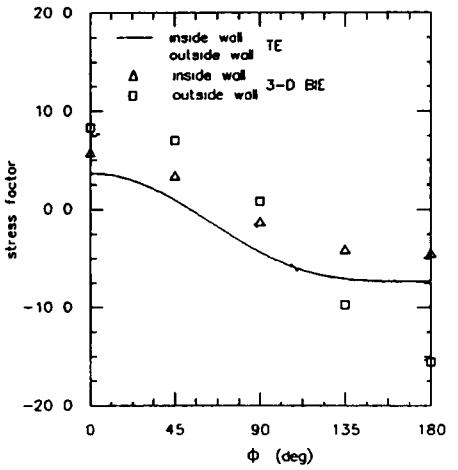

b) Longitudinal stress factor

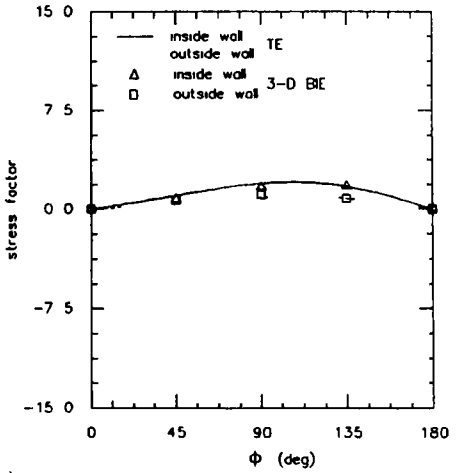

c) Shear stress factor

Figure 4.12· Stress factors for γ of 10 and t of 2.

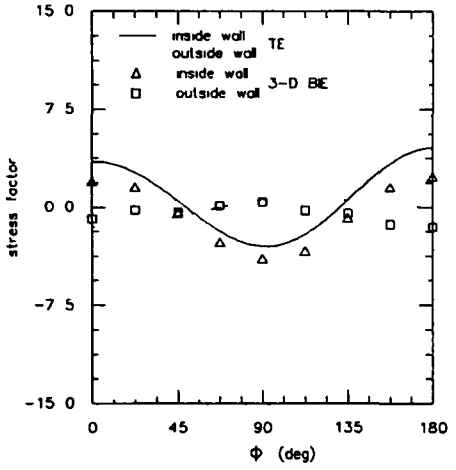

a) Circumferential stress factor

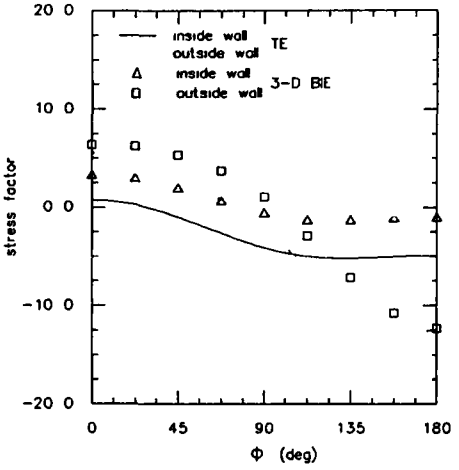

b) Longitudinal stress factor

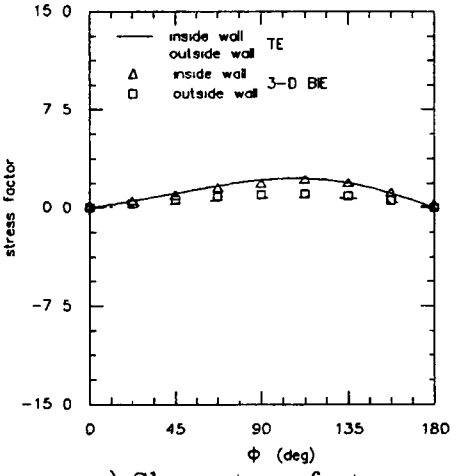

c) Shear stress factor

Figure 4.13. Stress factors for γ of 10 and t of 3

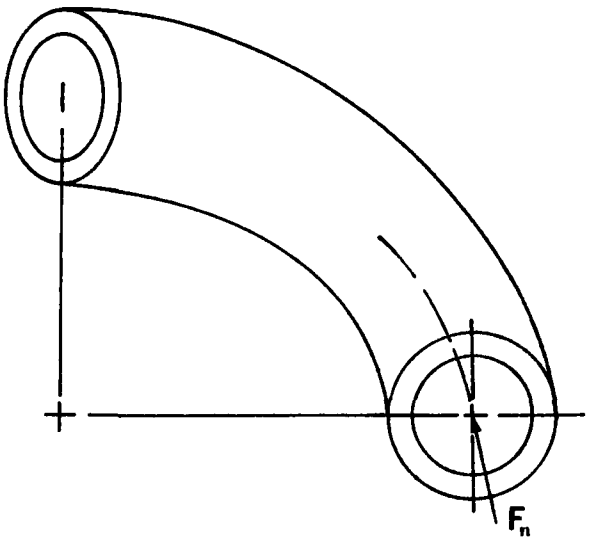

Figure 4.14: 90° Elbow subjected to an end normal force

It is shown that by adding a stress field, the agreement between the methods improved. Certainly adding second order stress fields throughout the TE solution would give a better improvement.

4.5 Normal Force Acting on a 90° Elbow

The problem considered next is a normal force, F_n, applied to the end at station θ of 0° of a hollow circular elbow which is fixed at the other end, as shown in Figure 4.14. Again there is one plane of symmetry and for the BIE solution half of the elbow is modelled. The applied force is uniformly distributed over the cross-section θ of 0°.

Lang [30] developed a total of eight stress fields for this problem. He considered an elbow with an end normal force acting at one end and an equilibriant system consisting of a shear force and a bending moment at the other end. The end normal force and the end shear force problems are dual problems. Lang simply converted the TE solution for the end shear force problem to the end normal force problem by adding a state of pure bending and by interchanging $\sin\theta$ and $\cos\theta$.

Lang [93] has submitted corrections to Ref. [30]. On page 166 of Ref. [30], δ_1 and δ_2 should be defined as $3/4(1+\nu)$ and $1/4(1+\nu)$, respectively. The corrections

γ	t	BIE σ_{max}	TE σ_{max}	Deviation (%)
5	2	2.8483	6.1439	115.7
10	2	5.2122	8.2058	57.4
5	3	2.6852	6.1744	129.9
10	3	3.7059	7.4841	101.9

Table 4.4: Peak stress factor for a normal force

applied to λ_1 in the previous section, should also be applied to this problem. The term δ in d_0 on page 170 should be replaced by 8. In equation $(\tau_{\phi\theta})_1$ on page 168, $\sin\theta$ replaces $\cos\theta$.

It is noticed that the sum of the eight stress fields did not satisfy the boundary conditions: a compressive normal force at station θ of 0° and a shear force combined with a bending moment at station θ of 90°. It is found that the initial stress field for pure bending was missing. The initial stress field for bending is given in Ref. [25].

As for the previous problem, the second-order stress field [26] defining the bending moment is added. Only the results with the added stress field are presented. The improvement of the added stress field is small at θ of 45°, because the terms defining the bending moment are multiplied by $(1 - \cos\theta)$.

Figures 4.15 to 4.18 show the computed σ_{ϕ_f}, σ_{θ_f} and $\sigma_{\phi\theta_f}$ by the TE and BIE methods for all cases. Only for $\sigma_{\phi\theta_f}$ do the methods correlate well. As t decreases the agreement improves for $\sigma_{\phi\theta_f}$ at the inside surface, especially for γ of 5. TE results for σ_{ϕ_f} at the inside surface follows a similar trend to the BIE results. The trend seems to improve as γ increases from 5 to 10. For σ_{ϕ_f} on the outside surface, the trend is not good for the cases with low values of γ. The case γ of 10 and t of 2 gives the best agreement. The agreement between both methods is reasonable at the inside surface for σ_{θ_f} between $\pi/2 \leq \phi \leq \pi$ whereas outside this region it is not. The overall σ_{θ_f} at the outside surface computed by the TE solution overpredicts the BIE method.

Similar to the end shear force problem, σ_{θ_f} on the outside surface at ϕ of 180° is the peak stress. Table 4.4 presents the peak stress factors for all cases considered. The TE solution overpredicts the BIE method by as much as 100%. The case γ of

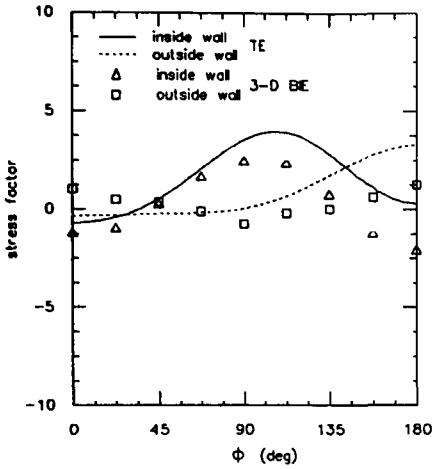

a) Circumferential stress factor

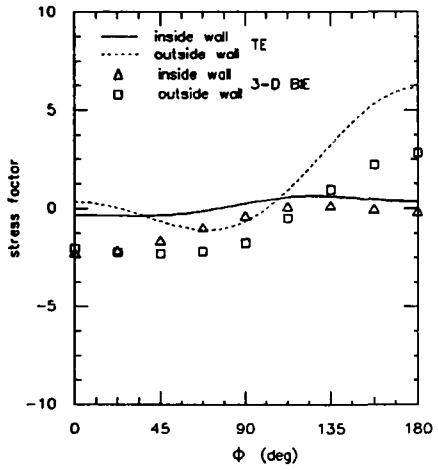

b) Longitudinal stress factor

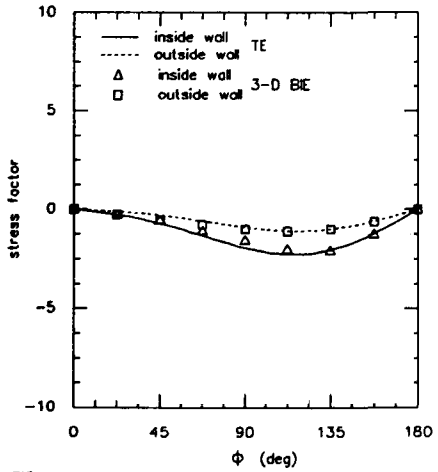

c) Shear stress factor

Figure 4.15: Stress factors for γ of 5 and t of 2.

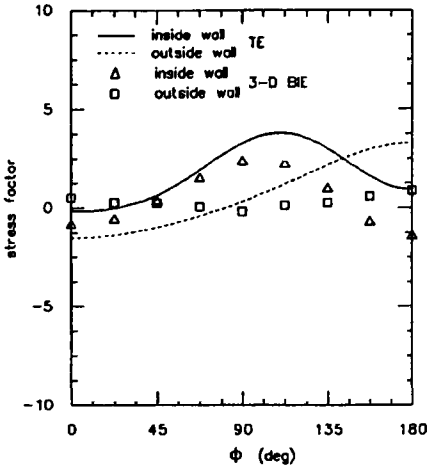

a) Circumferential stress factor

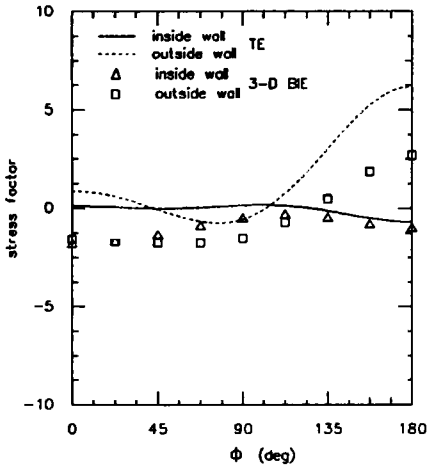

b) Longitudinal stress factor

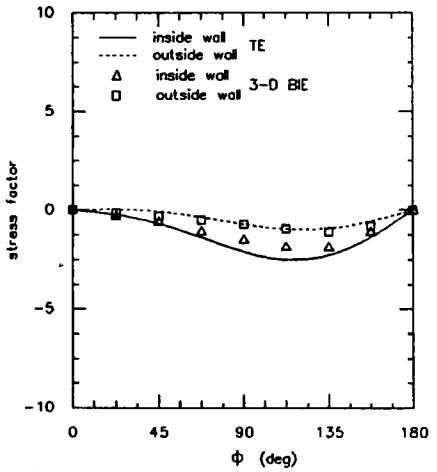

c) Shear stress factor

Figure 4.16: Stress factors for γ of 5 and t of 3.

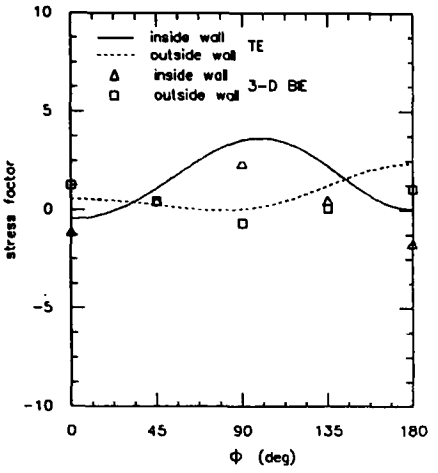

a) Circumferential stress factor

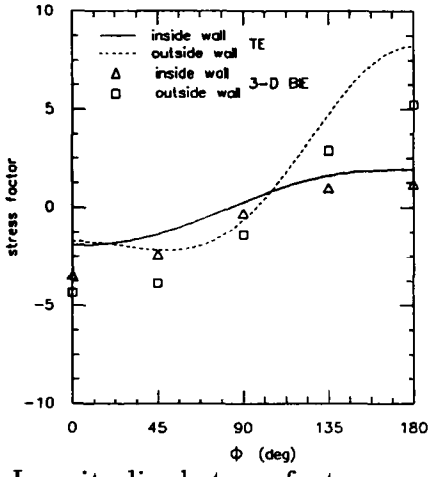

b) Longitudinal stress factor

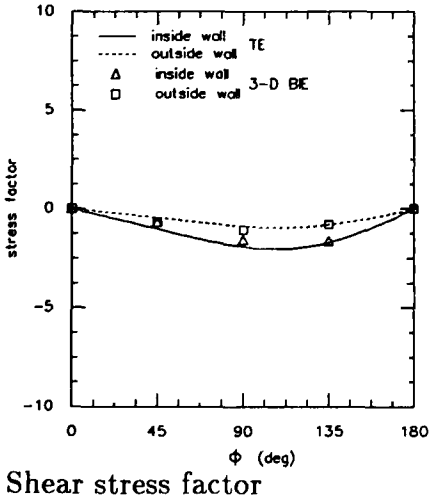

c) Shear stress factor

Figure 4.17: Stress factors for γ of 10 and t of 2.

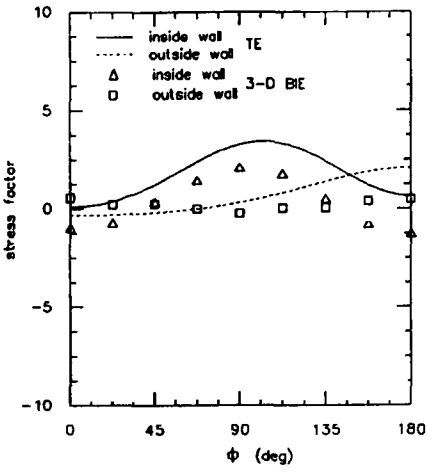

a) Circumferential stress factor

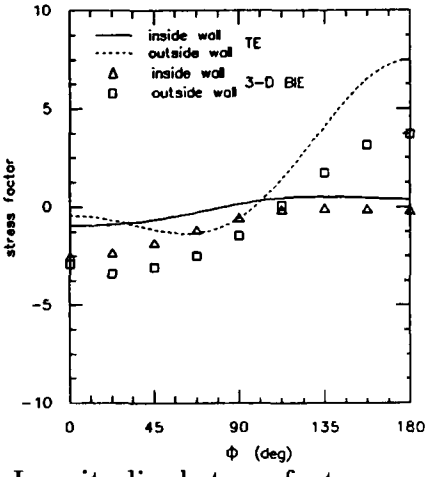

b) Longitudinal stress factor

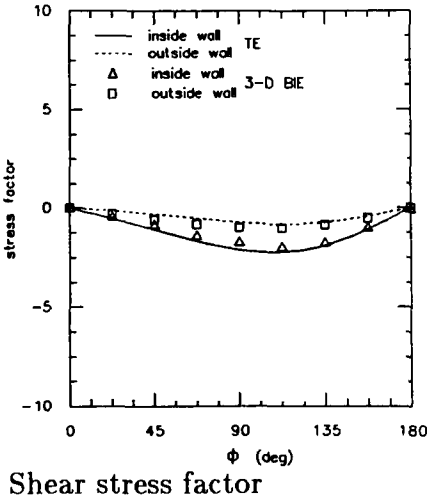

c) Shear stress factor

Figure 4.18: Stress factors for γ of 10 and t of 3.

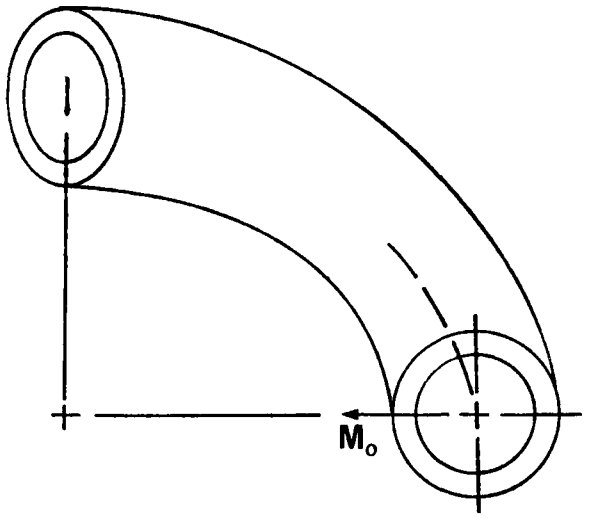

Figure 4.19: 90° Elbow subjected to an out-of-plane moment

10 and t of 2 is the only one that has a deviation less than 100%. The agreement between the peak stress computed by the methods seems to improve as γ increases and t decreases.

Certainly the TE solution needs more stress fields describing the normal forces acting on the elbow to predict the normal stresses with accuracy. This was also noticed for the end shear force problem.

4.6 Out-of-Plane Bending of a 90° Elbow

Figure 4.19 represents a 90° elbow subjected to an out-of-plane bending moment, M_o, at one end and fixed at the other end. However, due to the out-of-plane loading, there is no longer a horizontal plane of symmetry, which exists for in-plane loadings. Consequently, in the BIE analysis of the problem, the entire elbow needs to be modelled. A typical boundary element mesh is shown in Figure 4.20, and is composed of 128 elements and 384 nodal points. The moment is again defined in a strength of material manner, representing now a linear variation of the normal stress over the toroidal cross section, perpendicular to the plane of the elbow on the surface θ of 0°

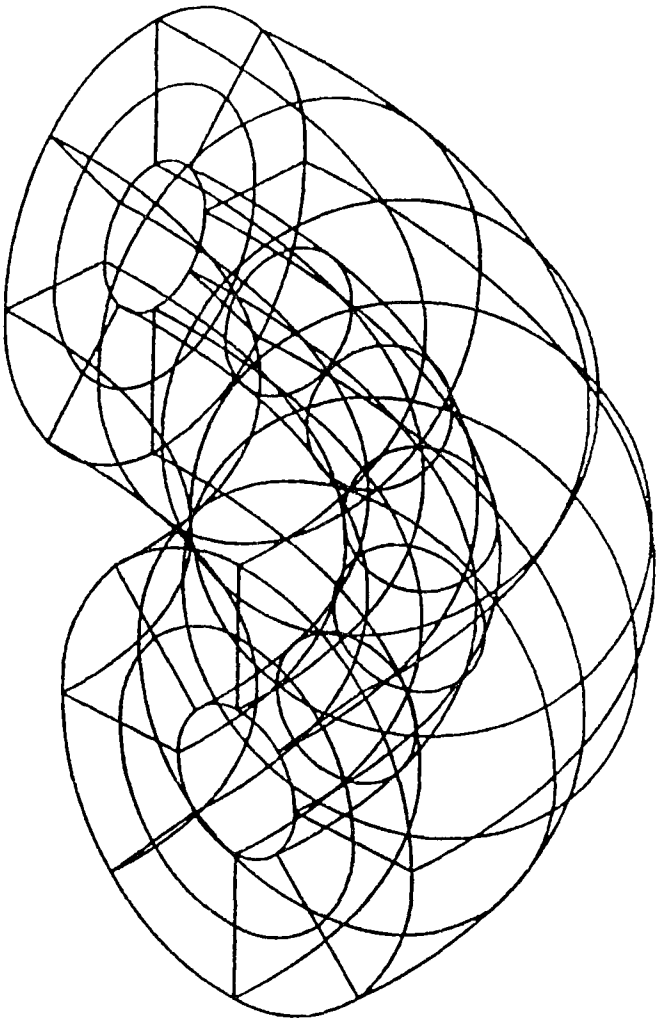

Figure 4.20: The BIE boundary mesh used for γ of 10 and t of 3, containing 128 elements and 384 nodes

Case	γ	t	ELEMENTS	NODES
1	5	2	128	384
2	5	3	96	288
3	10	3	128	384

Table 4.5: Mesh Distribution

Only two stress fields are developed by Lang [27] for this particular problem. He considered an elbow with out-of-plane bending arising from an end couple applied at one end. At the other end a twist bending moment is applied to maintain equilibrium.

Three cases are investigated, using the BIE and TE methods. The first two are for a radius ratio, γ, of 5 and a thickness ratio, t, of 2 and 3 and the third is for γ of 10 and t of 3. Table 4.5 gives the number of elements and nodes used for each configuration. The case γ of 10 and t of 2 would have required a mesh exceeding the capacity of the current program and was thus not calculated.

Figures 4.21 and 4.22 depict the stress factors σ_{ϕ_f}, σ_{θ_f} and $\sigma_{\phi\theta_f}$ as a function of ϕ in the middle cross section (θ of 45°) for γ of 5 and t of 2 and 3. It is observed from Figures 4.21b and 4.22b that both methods correlate well for σ_{θ_f}. For the circumferential stress shown in Figures 4.21a and 4.22a, the prediction of TE solution gives significantly greater value than BIE in the region $0 < \phi < \pi/2$ and $3\pi/2 < \phi < 2\pi$ at the inside surface. Reasonable agreement is obtained for σ_{ϕ_f} at the outside surface. Figures 4.21c shows reasonable agreement for $\sigma_{\phi\theta_f}$ between the methods whereas in Figure 4.22c the agreement is poorer, especially at the outside surface. Note that as t increases from 2 to 3 the agreement deteriorates between BIE and TE results.

In Figure 4.23, the circumferential, longitudinal and shear stress factors are presented for case 3. The TE results agree well with BIE results for the three stresses. Note that, just as for in plane bending and internal pressure loadings, the agreement between both methods improves as γ increases.

The maximum stress factor at the middle cross section (θ of 45°) is found to be the longitudinal stress factor on the outside surface at ϕ of 112.5° and 247.5°. Table 4.6 presents the peak stress factor for each case. The peak stress increases as t increases but decreases as γ increases.

The BIE results in Figures 4.21c, 4.22c and 4.23c, show that for γ of 10 and t of 3 $\sigma_{\phi\theta_f}$ is fairly uniform, but as γ decreases to 5 the shearing stress increasingly

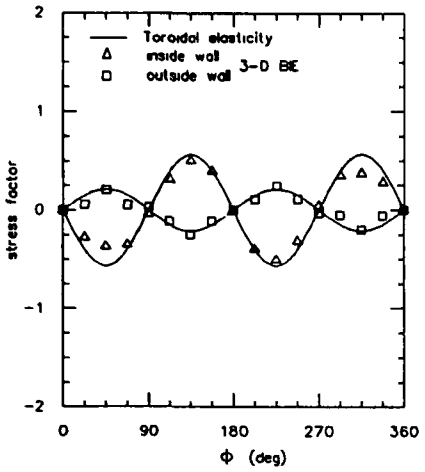

a) Circumferential stress factor

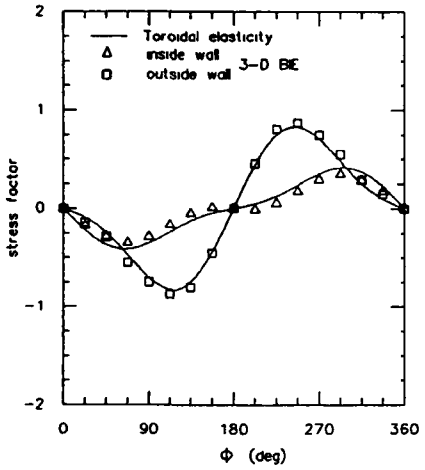

b) Longitudinal stress factor

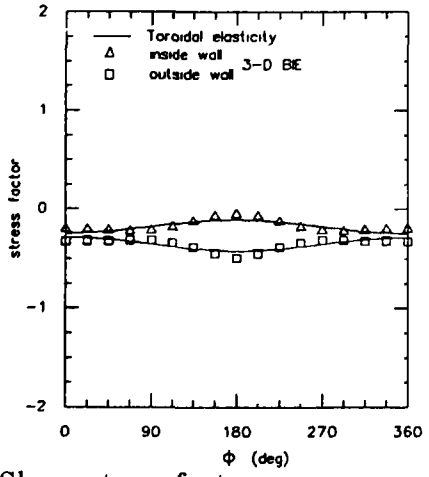

c) Shear stress factor

Figure 4.21: Stress factors for γ of 5 and t of 2.

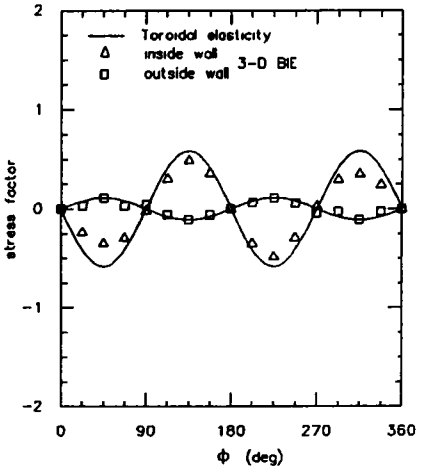

a) Circumferential stress factor

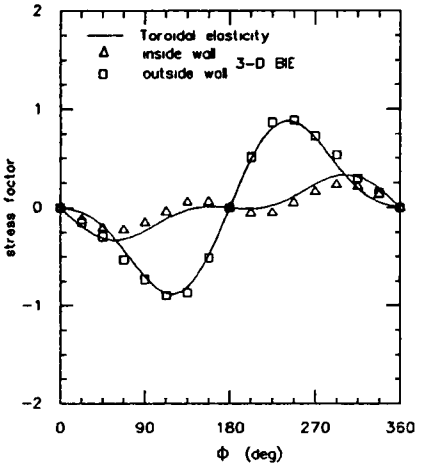

b) Longitudinal stress factor

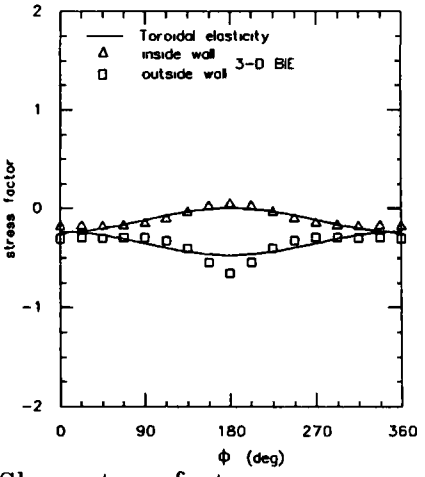

c) Shear stress factor

Figure 4.22: Stress factors for γ of 5 and t of 3.

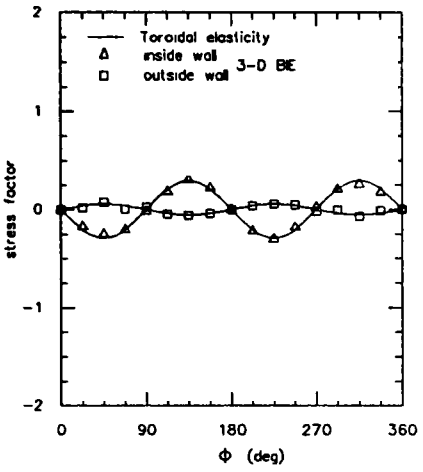

a) Circumferential stress factor

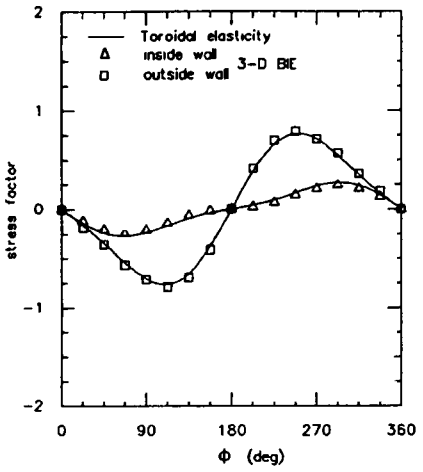

b) Longitudinal stress factor

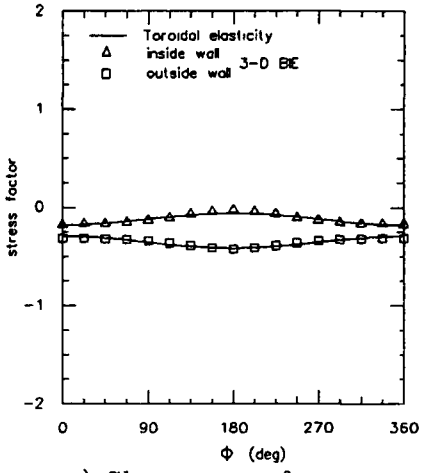

c) Shear stress factor

Figure 4.23: Stress factors for γ of 10 and t of 3.

γ	t	BIE σ_{max}	TE σ_{max}	Deviation (%)
5	2	0.8735	0.8283	5.17
5	3	0.8924	0.8803	1.36
10	3	0.7864	0.7639	2.86

Table 4.6: Peak stress factor for out-of-plane bending

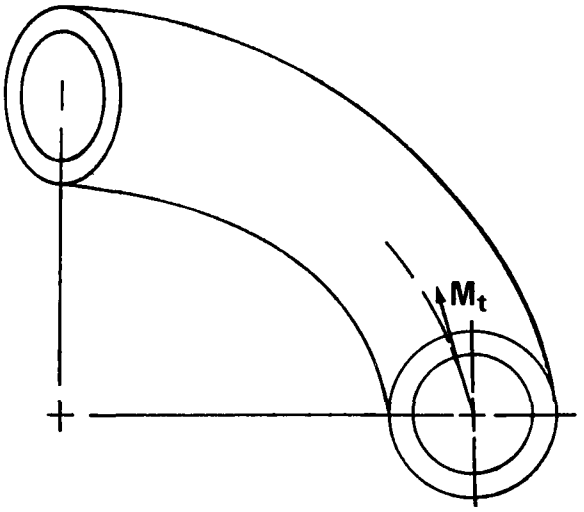

Figure 4.24: 90° Elbow subjected to a twist moment

varies with ϕ, especially for $3\pi/4 \leq \phi \leq 5\pi/4$ at the outside wall. However as t decreases from 3 to 2, $\sigma_{\phi\theta_f}$ varies less with ϕ. This effect is probably due to the much greater curvature in this region for higher values of t.

The BIE results give, for γ of 5 and t of 2, $\sigma_{\phi_{max}}$ greater than $\sigma_{\phi\theta_{max}}$. However, when t increases from 2 to 3, $\sigma_{\phi_{max}}$ is less than $\sigma_{\phi\theta_{max}}$. The TE solution underpredicts $\sigma_{\phi\theta_{max}}$ by 28% for case 2 compared to the BIE results.

4.7 Twist-Bending of a 90° Elbow

The problem considered in this section is shown in Figure 4.24. At the station θ of 0° a twist bending moment, M_t, is applied and at the station θ of 90° the elbow is fixed. Again there is no horizontal plane of symmetry and for the BIE solution the entire elbow needs to be modelled (Figure 4.20). The applied twist varies directly as the distance from the center of the section over the cross-section θ of 0°

The TE stress fields used in the previous section are modified for the twist loading case. The modification consists of interchanging $\sin\theta$ and $\cos\theta$ in every equation. This, in effect, places the twisting couple at the station θ of 0° and the bending moment at the station θ of 90°, so that the elbow is held in equilibrium.

The stress factors for twist bending are defined as

$$\sigma_f = \sigma / \frac{M_t b}{I_p}$$

where σ is the actual stress, b is the outside cross-section radius, M_t is the twist bending moment and I_p is the polar moment of inertia defined as $\pi/2(b^4 - a^4)$.

The circumferential, longitudinal and shear stress factors calculated by both BIE and TE are shown in Figures 4.25, 4.26 and 4.27, for the three cases studied. Similarly to the out-of-plane problem, reasonably good agreement is found between the methods for σ_{θ_f} in the three cases. From Figures 4.25c and 4.26c it is seen that as t increases, the TE solution for $\sigma_{\phi\theta_f}$ gives poorer agreement. Note that γ has just the opposite effect, when it increases the correlation improves between both methods, not only for the shearing stress, but also for normal stresses. As in the out-of-plane bending problem, the circumferential stress at the inside surface of an elbow having a γ of 5 obtained using TE is significantly greater in the region $0 < \phi < \pi/2$ and $3\pi/2 < \phi < 2\pi$ than the one obtained using BIE.

Looking at σ_{ϕ_f} and σ_{θ_f} results for both the out-of-plane bending problem (in the previous section) and the twist bending problem, it is seen that the normal stresses are inversed for twist bending. This is expected because the applied and reactive moments are interchanged. It is interesting to note that the BIE shearing stress for γ of 5 and t of 3 varies considerably at the outside surface for the out-of-plane bending problem whereas for the twist bending problem the variation is less.

The maximum longitudinal stress factor, at the cross section θ of 45°, is given in Table 4.7. The predictions for the peak stress values by the two theories differ only by about 5 to 10 percent. The agreement improves as γ is increased and deteriorates as t is increased. The $\sigma_{\theta_{max}}$ found by BIE, for the second case has shifted to ϕ of 135° and ϕ of 225° compared to the two other cases (ϕ of 112.5° and ϕ of 247.5°). The TE solution predicts $\sigma_{\theta_{max}}$ at ϕ of 112.5° and ϕ of 247.5° for the three cases.

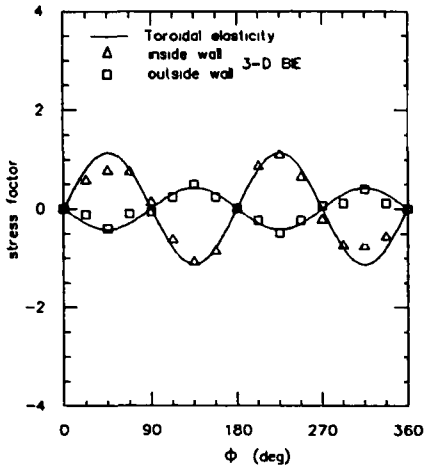

a) Circumferential stress factor

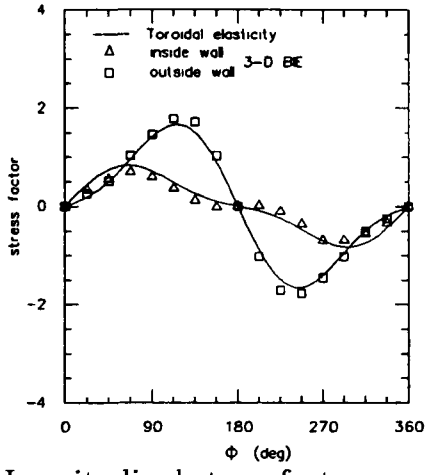

b) Longitudinal stress factor

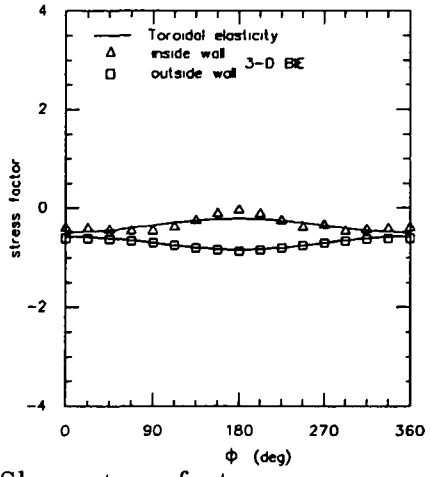

c) Shear stress factor

Figure 4.25: Stress factors for γ of 5 and t of 2.

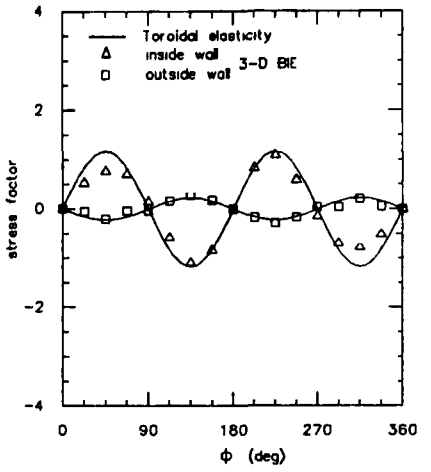

a) Circumferential stress factor

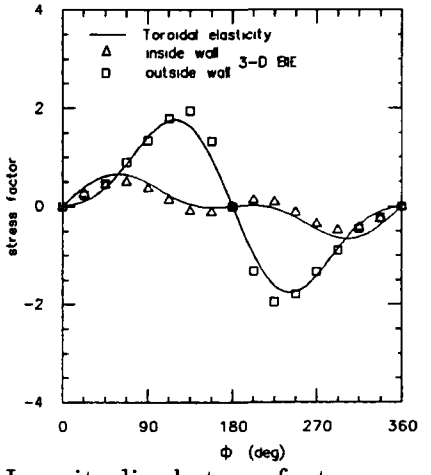

b) Longitudinal stress factor

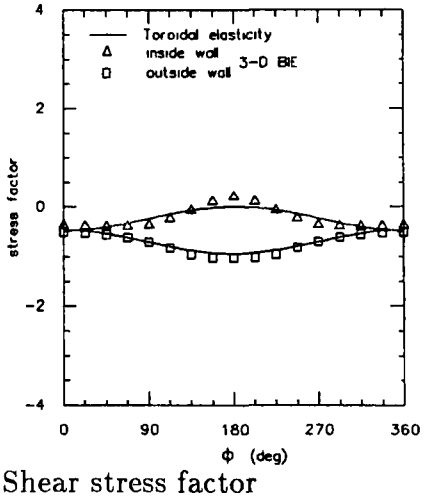

c) Shear stress factor

Figure 4.26: Stress factors for γ of 5 and t of 3.

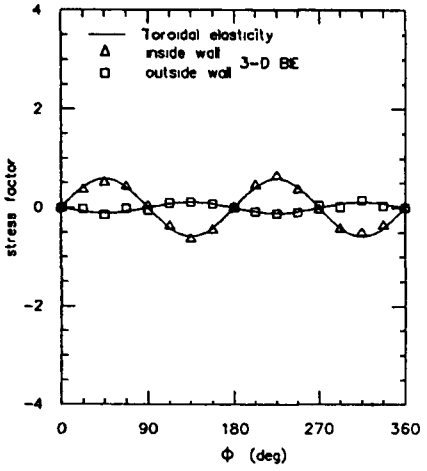

a) Circumferential stress factor

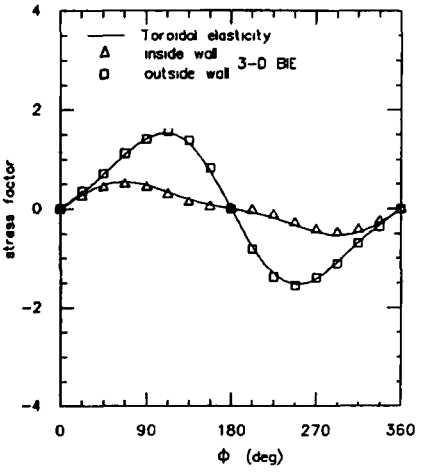

b) Longitudinal stress factor

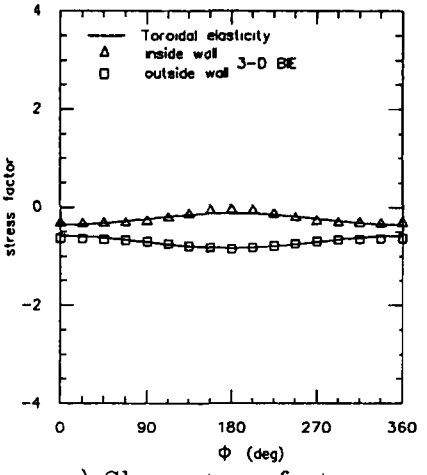

c) Shear stress factor

Figure 4.27: Stress factors for γ of 10 and t of 3.

γ	t	BIE σ_{max}	TE σ_{max}	Deviation (%)
5	2	1.7788	1.6566	6.87
5	3	1.9538	1.7441	10.73
10	3	1.5572	1.5253	2.05

Table 4.7: Peak stress factor for twist bending

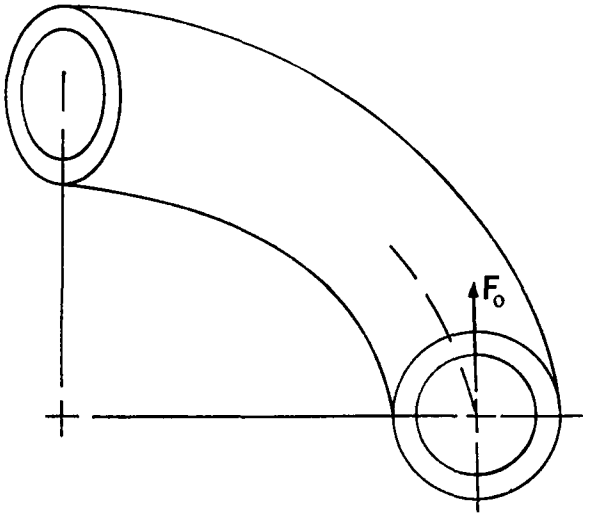

Figure 4.28: 90° Elbow subjected to an end shear force.

4.8 Out-of-Plane End Shear Force Acting on a 90° Elbow

The problem considered in this section consists of an end shear force acting on a 90° elbow, producing out-of-plane bending. The shear force, F_0, acts at the station defined by θ of 0° whereas the plane station θ of 90° is fixed (see Figure 4.28). The applied shear force, F_0, is assumed uniformly distributed over the cross section. Lang [28] determined the zero order and first order stress states for the TE solution. At θ of 90°, he considered that the elbow is maintained in equilibrium by a twisting moment and a bending moment. For this problem, again there is no symmetry and for the BIE solution the entire elbow needs to be modelled.

In Figures 4.29, 4.30 and 4.31, the circumferential, longitudinal and shear stress results of both methods are presented for the three geometries considered (see Table 4.5). The σ_{ϕ_f} results for the three cases show that for γ of 5 and t of 3 the agreement between both methods is the best. As the thickness ratio decreases the agreement deteriorates. This is also true as the radius ratio increases. The greatest difference between the computed σ_{ϕ_f} along the inner wall of the elbow is found at ϕ of 135° and 225°. The major discrepancy is for the case γ of 10 and t of 3,

γ	t	BIE σ_{max}	TE σ_{max}	Deviation (%)
5	2	7.0855	5.7495	18.85
5	3	5.6055	4.3010	23.27
10	3	9.4110	8.5153	9.52

Table 4.8: Peak stress factor for out-of-plane end shear force

where the TE solution underpredicts the BIE method by about 70%. Examining Figures 4.30a and 4.31a, it is seen that TE solution predicted the same results for both cases. The TE zero and first order stress fields developed by Lang for σ_ϕ are only functions of ϕ and θ and do not depend on the toroidal radius R. Probably the subsequent terms would depend also on R.

The TE stress fields developed for σ_θ depend on the three coordinates. The effects of thickness ratio and radius ratio on σ_{θ_f} are large. Figures 4.29b, 4.30b and 4.31b show that as the thickness ratio increases, σ_{θ_f} decreases. As the radius ratio increases, σ_{θ_f} also increases. Agreement between TE and BIE results improves as γ is increased. The peak stress is given by σ_θ at the outside surface. Note that, similar to the twist bending problem, the computed BIE peak stress for γ of 5 and t of 3 is not at the same location as for the other cases.

Figures 4.29c, 4.30c and 4.31c show the variation of the computed shear stress factor with ϕ. The TE results are in disagreement with the BIE results. The TE solution predicts almost a uniform value for $\sigma_{\phi\theta_f}$ at the outside surface whereas the BIE predicts a considerable variation. Notice that $\sigma_{\phi\theta_f}$ computed by the BIE method varies considerably for $\pi/2 < \phi < 3\pi/2$, giving a stress concentration effect at ϕ of π.

Table 4.8 compares the peak stress factors calculated by both methods. The peak stress has increased considerably compared to the problems of twist and bending of an elbow. The peak stress factors for the radius ratio of 5 are not in good agreement having a deviation of about 20%. The agreement improves as γ increases to 10. For this problem the TE solution with only two terms in the series does not give accurate predictions.

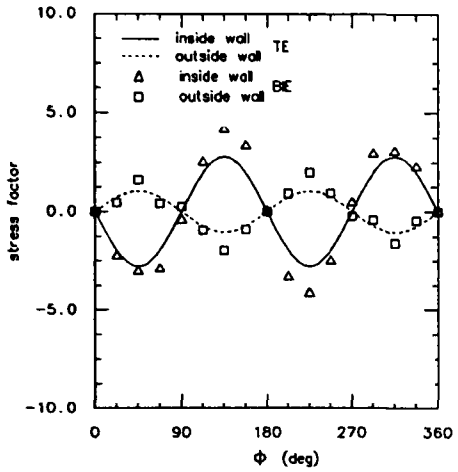

a) Circumferential stress factor

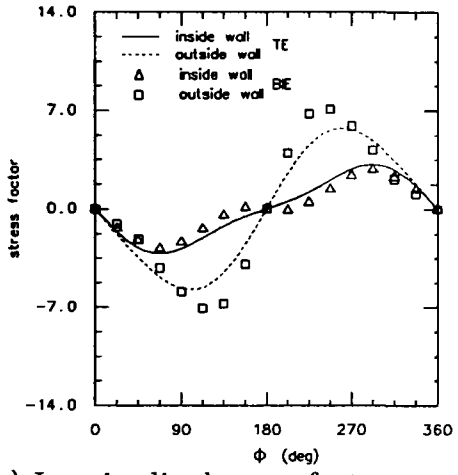

b) Longitudinal stress factor

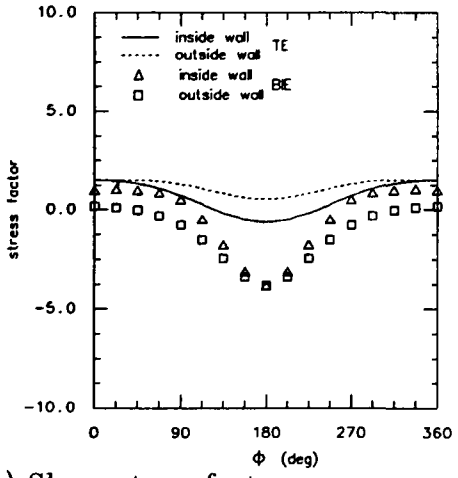

c) Shear stress factor

Figure 4.29: Stress factors for γ of 5 and t of 2.

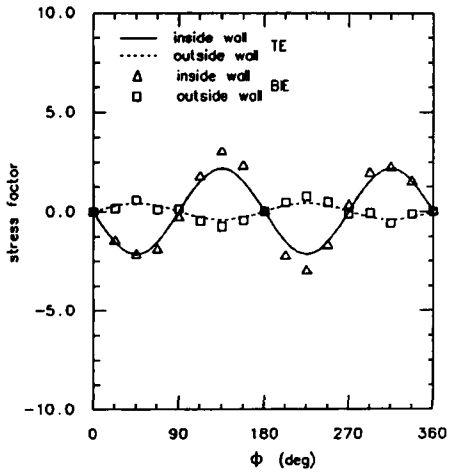

a) Circumferential stress factor

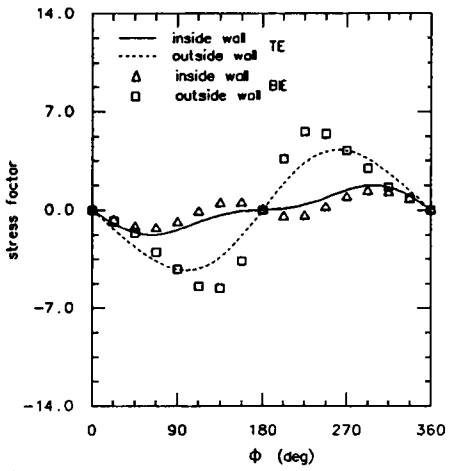

b) Longitudinal stress factor

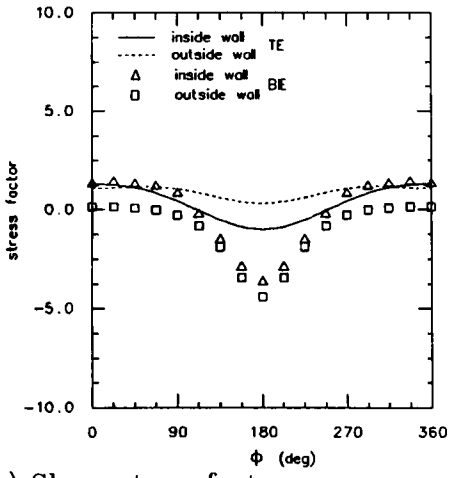

c) Shear stress factor

Figure 4.30: Stress factors for γ of 5 and t of 3.

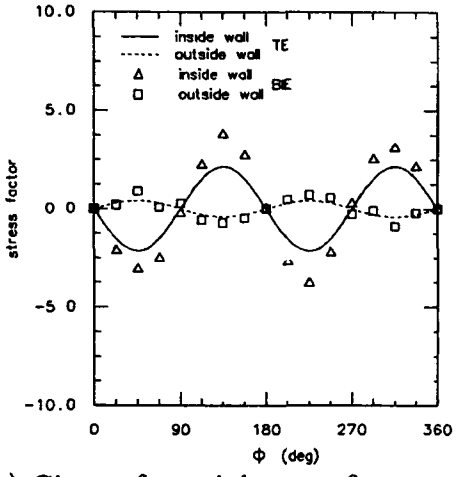

a) Circumferential stress factor

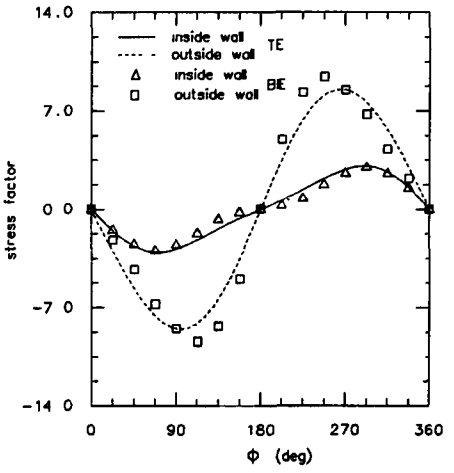

b) Longitudinal stress factor

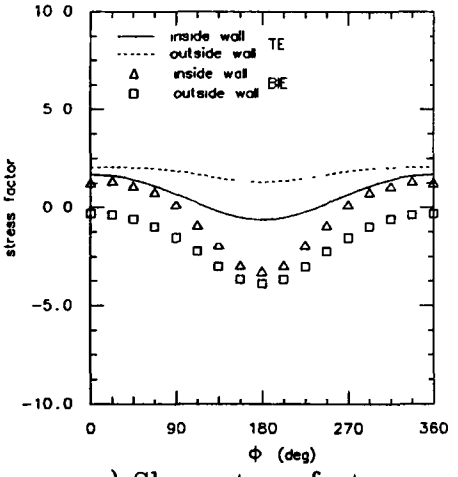

c) Shear stress factor

Figure 4.31: Stress factors for γ of 10 and t of 3.

Chapter 5

180° Pipe Bend with Tangent Pipes

Problems of thin-walled piping systems have been investigated by many researchers. However very little work has been concerned with thick-walled piping systems. The problem considered herein is a 180° thick-walled pipe bend, which has straight portions at both ends, subjected to in-plane bending and internal pressure, applied separately. Figure 5.1 shows the longitudinal section of the problem, where L is the length of each of the straight pipes, Z represents the longitudinal linear coordinate of the straight pipes and θ is the longitudinal angular coordinate of the pipe bend. For this particular problem, the total length L is equal to three times the outside pipe radius b and the wall thickness is assumed to be equal for both straight pipes and the pipe bend.

Figure 5.2 shows a typical BIE mesh used; only one quarter of the U-bend is modelled because of two planes of symmetry. Since there are only two planes of symmetry, the displacements are only constrained in two directions. The unconstrained displacement is in the Z direction. The line AB in Figure 5.2 is chosen to be constrained in the Z direction for the in-plane bending problem, having no load acting on this line. However this constraint can not be used for the internal pressure problem due to the Poisson ratio effect which creates extremely large stresses (because a line has zero surface area). To solve this problem, plain strain condition is assumed at the end of the straight pipes. So the entire cross-section at the pipe

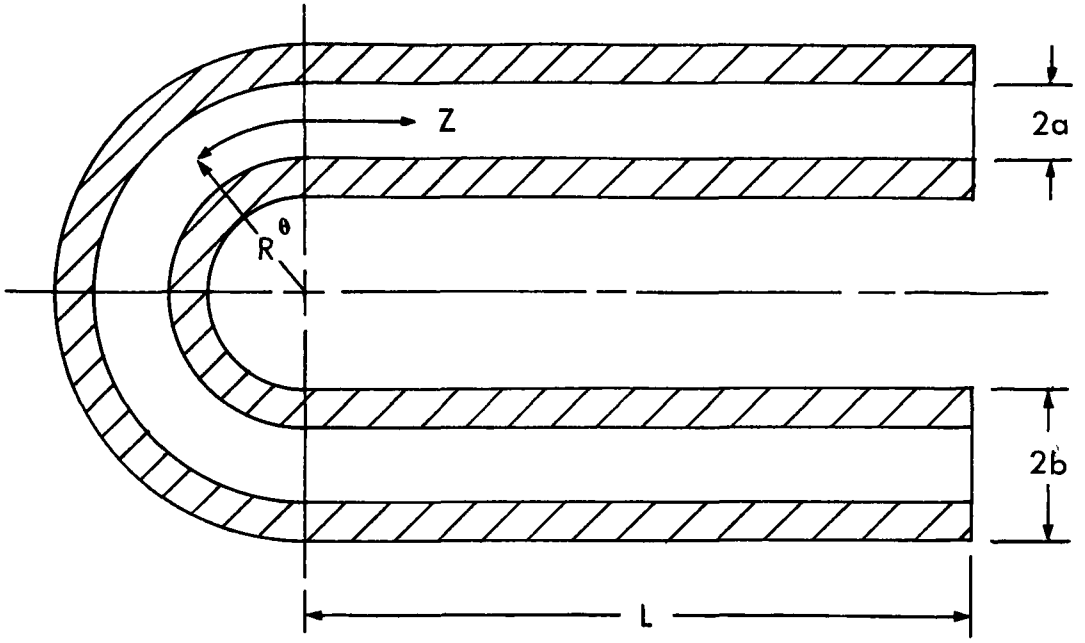

Figure 5.1: Longitudinal half-section of a U-bend.

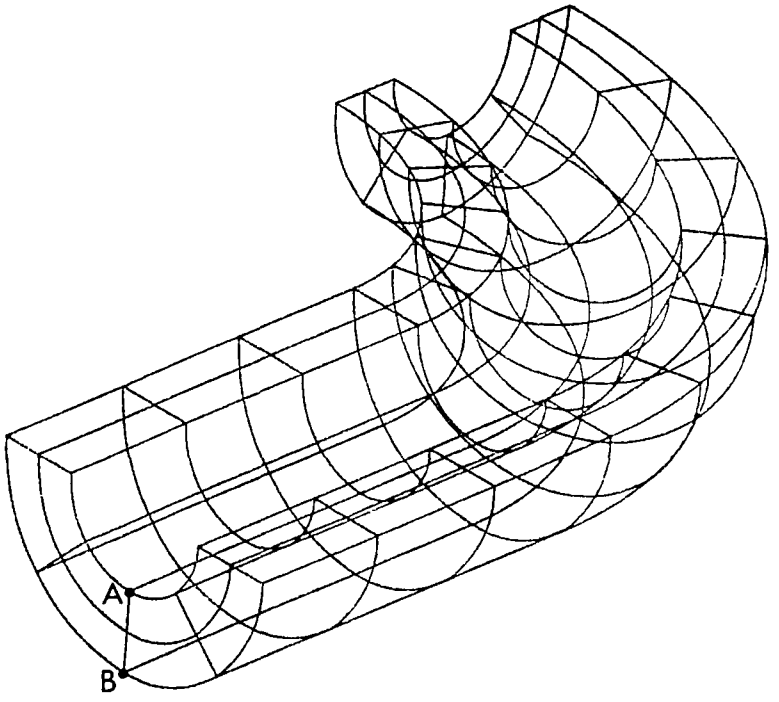

Figure 5.2: The BIE boundary mesh used for γ of 5 and t of 2, containing 124 elements and 374 nodes.

Case	γ	t	Elements	Nodes
1	5	2	124	374
2	5	3	100	302
3	10	3	124	374

Table 5.1: Mesh distribution for U-bends

end is constrained in the Z direction. Three cases are studied; Table 5.1 gives the geometric ratios and the number of elements and nodes used for each one.

5.1 In-Plane Bending Loading

The bending moment is defined in a strength of materials manner, representing a linear variation of the applied normal stress over the straight pipe cross-section, in the plane of the U-bend, on the surface $Z = L$.

Figure 5.3 shows the variation of the circumferential (σ_{ϕ_f}) and longitudinal (σ_{θ_f}) stress factors with the angle ϕ at the two cross-sections θ of 0° and θ of 90° for a U-bend having a γ of 5 and a t of 2. The results found in the previous chapter for a 90° elbow subjected to in-plane bending at θ of 45° are also presented. It is observed that at section θ of 0°, σ_{ϕ_f} is lower than at θ of 90°. For σ_{θ_f} at the inside surface, the values at section θ of 0° are similar to the ones found at section θ of 90° except in the region $3\pi/4 \leq \phi \leq \pi$ where σ_{θ_f} at section θ of 0° is larger than at θ of 90°. Notice that near the extrados, σ_{θ_f} at the outside surface at section θ of 0° is larger than at θ of 90° whereas at the intrados the reverse is true. Comparing the results obtained in the 90° elbow at θ of 45° with the ones obtained in the U-bend at θ of 90°, it is noticed that the values for σ_{θ_f} are almost identical whereas for σ_{ϕ_f} at the inside surface the BIE predicts slightly higher values for the U-bend.

The stress factors σ_{ϕ_f} and σ_{θ_f} for a t of 3 are shown in Figures 5.4 and 5.5 for γ of 5 and 10, respectively. Comparing with the previous results for a γ of 5 and t of 2, it is seen in Figure 5.4 that as t is increased the difference between σ_{θ_f} at cross-section θ of 0° and 90° has its greatest increase near the intrados. It is also observed that as t increases from 2 to 3, the values of σ_{θ_f} at the inside surface near

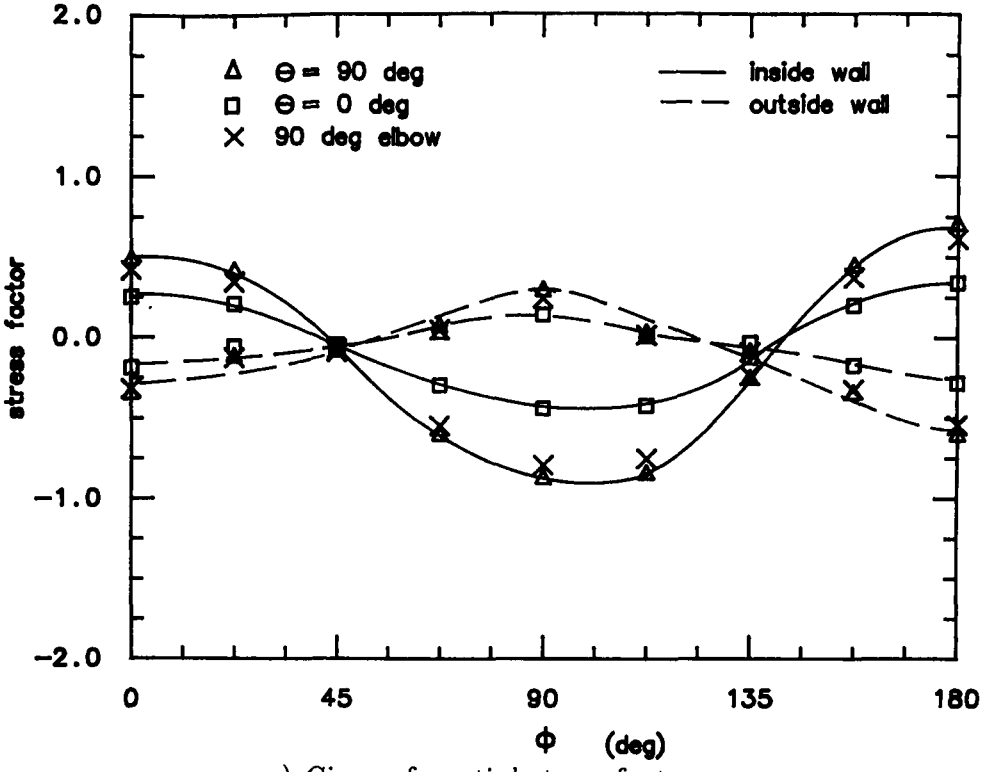

a) Circumferential stress factor, σ_{ϕ_f}

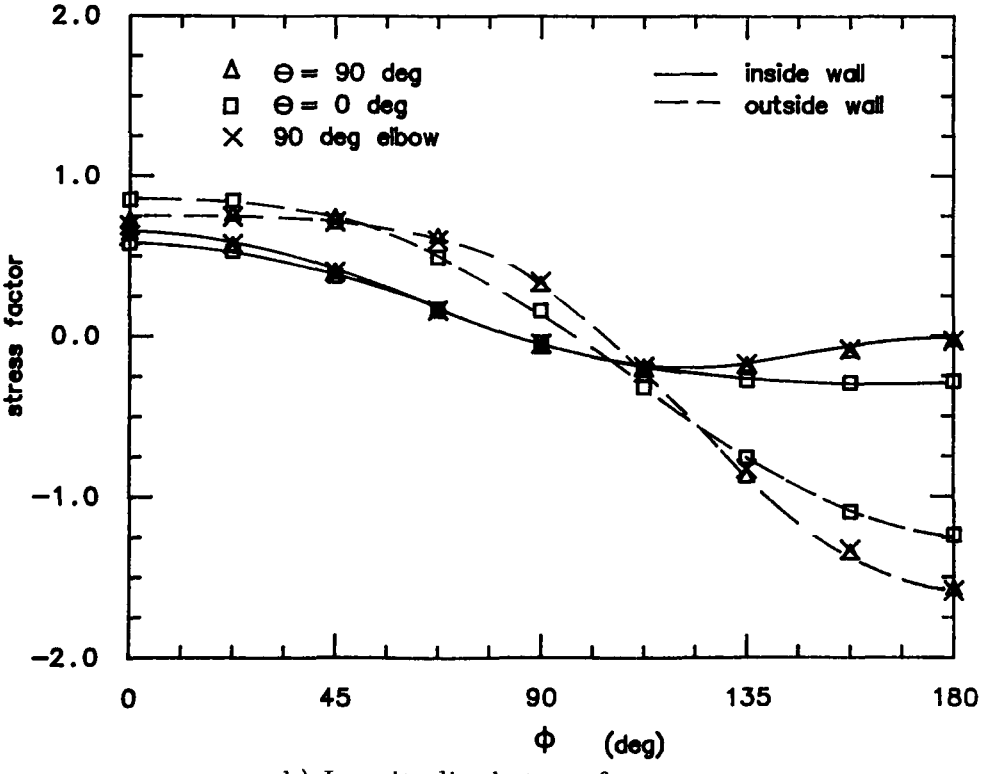

b) Longitudinal stress factor, σ_{θ_f}

Figure 5.3: Stress factors for γ of 5 and t of 2.

case	$\theta = 90°$ cross-section		$\theta = 0°$ cross-section		90° elbow ($\theta = 45°$)	
	$\sigma_{\phi_{max}}$	$\sigma_{\theta_{max}}$	$\sigma_{\phi_{max}}$	$\sigma_{\theta_{max}}$	$\sigma_{\phi_{max}}$	$\sigma_{\theta_{max}}$
1	-0.8808	-1.5833	-0.4387	-1.2396	-0.7929	-1.5838
2	-1.0099	-2.0140	-0.4992	-1.3403	-0.8468	-1.9061
3	-0.5373	-1.4033	-0.2578	-1.1681	-0.4978	-1.3322

Table 5.2: Peak stress factor for in-plane bending of a U-bend

the intrados at section θ of 0° is now lower than at θ of 90°. Notice that for σ_{ϕ_f} at the inside surface, the discrepancy between the values found in a 90° elbow at θ of 45° and in a U-bend at θ of 90° is greater as t is increased. It is observed from Figures 5.4 and 5.5 that as γ is increased the agreement between σ_{ϕ_f} in a 90° elbow at θ of 45° and in a U-bend at θ of 90° improves. Also as γ is increased the discrepancy between the values of σ_{θ_f} found in both section decreases.

The maximum circumferential and longitudinal stress factors are presented in Table 5.2 for θ equal to 0° and 90° sections of the U-bend and for θ equal to 45° section of the elbow. From the table, it is noted that the peak circumferential stress of the U-bend at θ of 90° is greater by about 50% than the one at θ of 0°. It is also observed that $\sigma_{\theta_{max}}$ and $\sigma_{\phi_{max}}$ increase when changing the problem from a 90° elbow to a 180° pipe bend with tangent pipes except for $\sigma_{\theta_{max}}$ of case 1 which is almost identical. Case 2 shows the greatest increase of $\sigma_{\theta_{max}}$ which is about 6%. This indicates that the computed $\sigma_{\theta_{max}}$ of a thick-walled 90° elbow at θ of 45° could be used as a good approximation for $\sigma_{\theta_{max}}$ of a thick-walled U-bend with straight pipes at θ of 90°; since it gives a value deviating by less than 10% from the true value.

Swanson and Ford [8] presented results done experimentally for this particular problem having circular and non-circular cross-sections. The problem of circular cross-section that they considered had a γ of 11.02 and a t of 1.83. This configuration was not studied using the BIE method because it would have required a mesh exceeding the capacity of the program. However, since it was shown that the stresses found in a 90° elbow at θ of 45° can be used as an approximation for the ones of a U-bend with straight pipes at θ of 90°, the results from Swanson and Ford

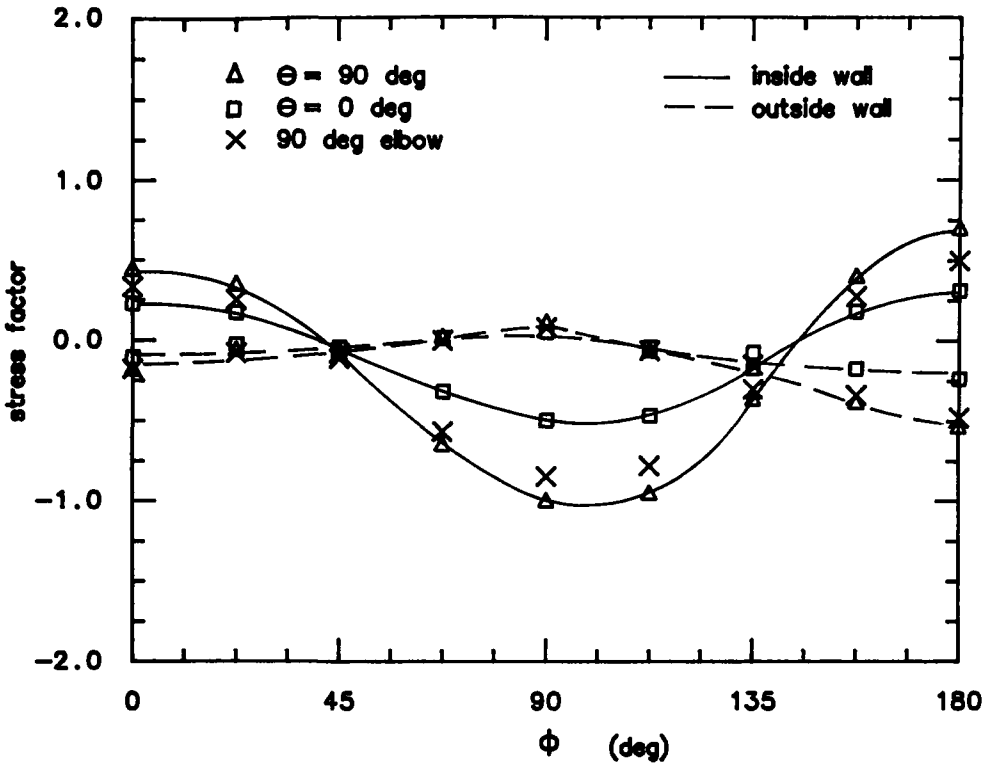

a) Circumferential stress factor, σ_{ϕ_f}

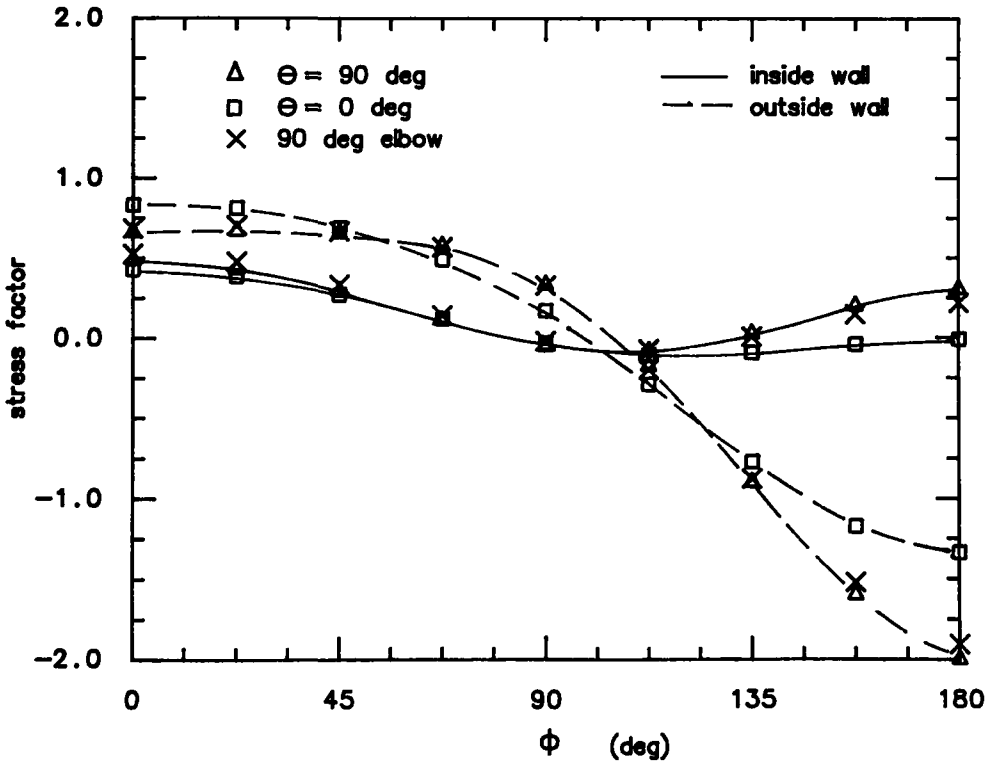

b) Longitudinal stress factor, σ_{θ_f}

Figure 5.4: Stress factors for γ of 5 and t of 3.

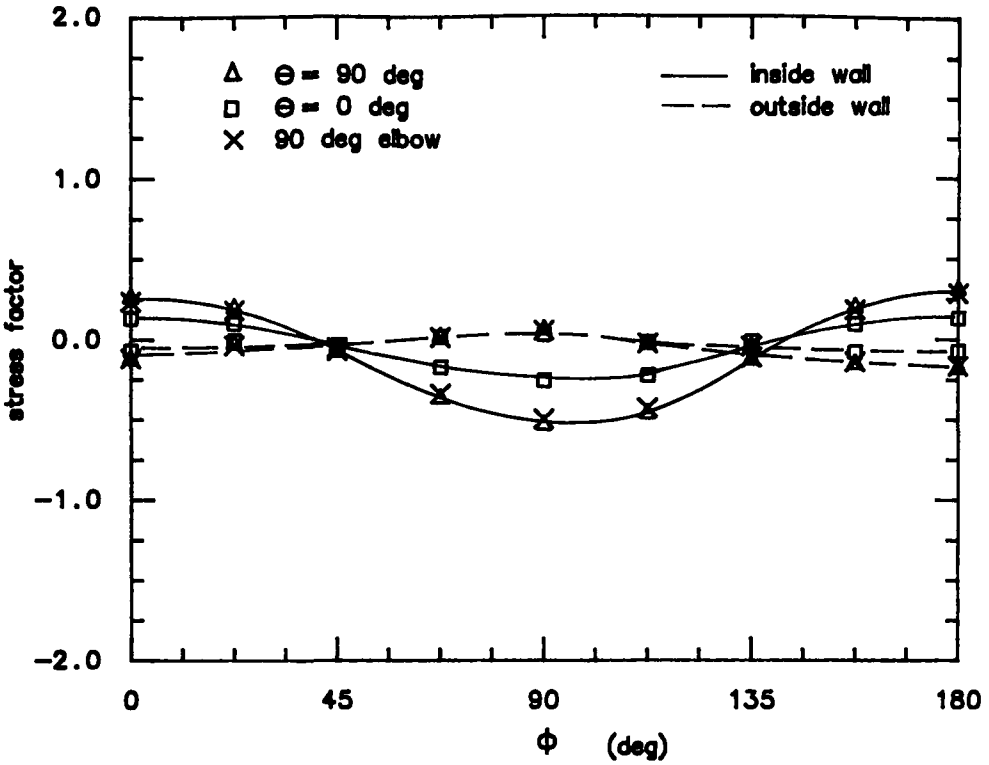

a) Circumferential stress factor, σ_{ϕ_f}

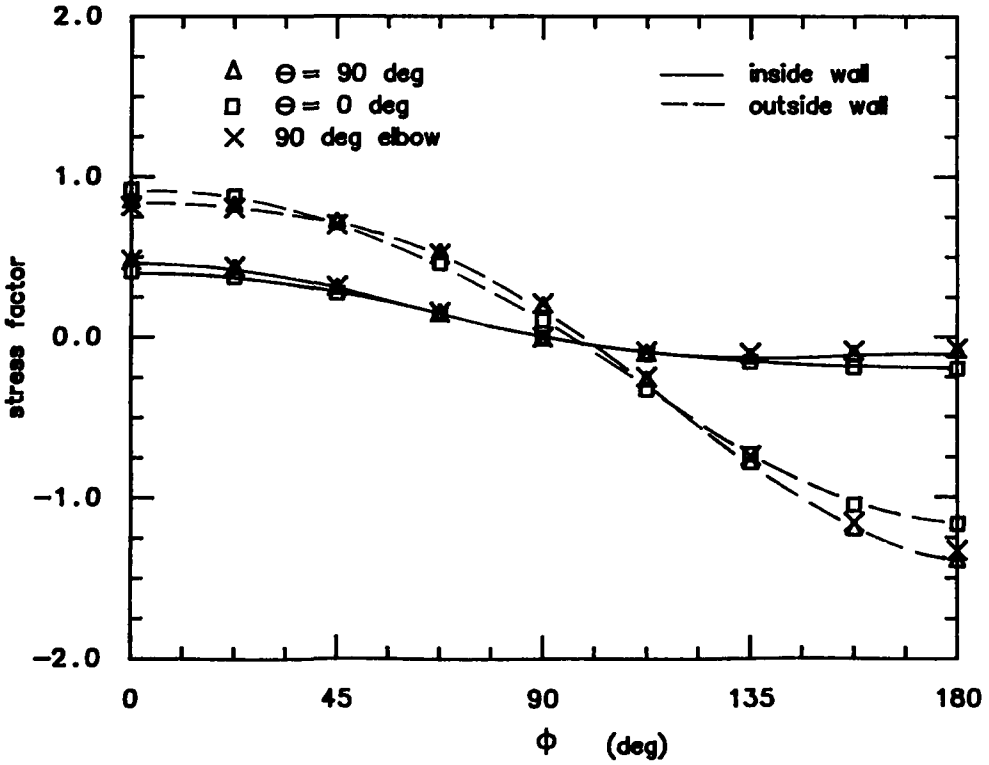

b) Longitudinal stress factor, σ_{θ_f}

Figure 5.5: Stress factors for γ of 10 and t of 3.

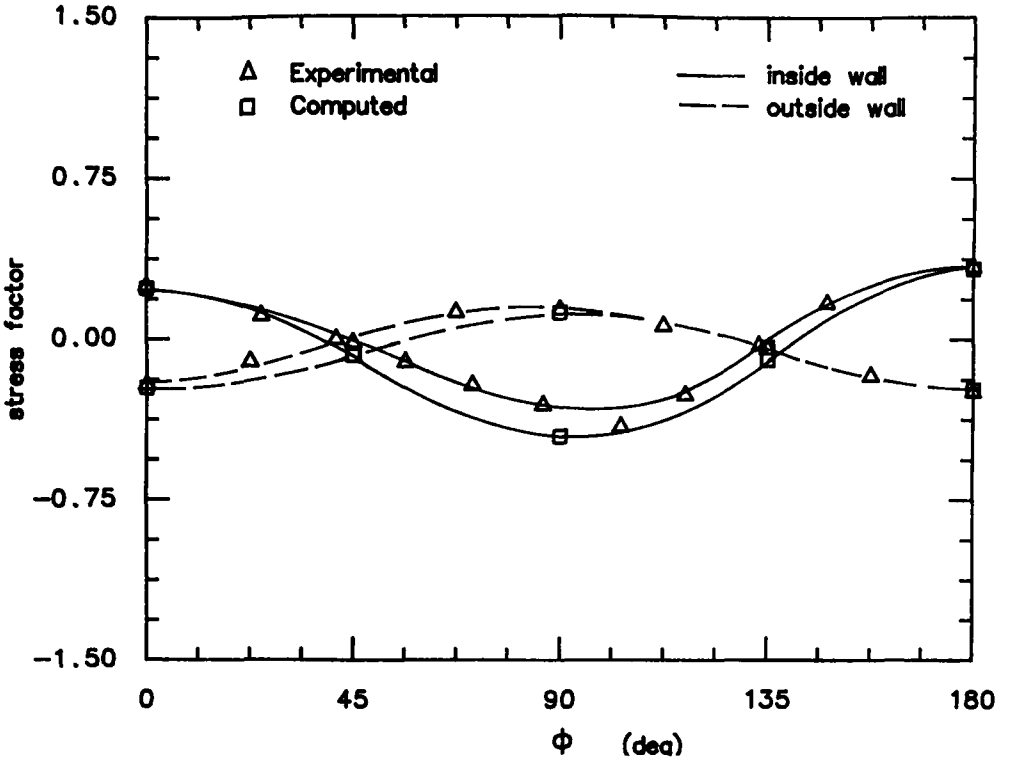

a) Circumferential stress factor, σ_{ϕ_f}

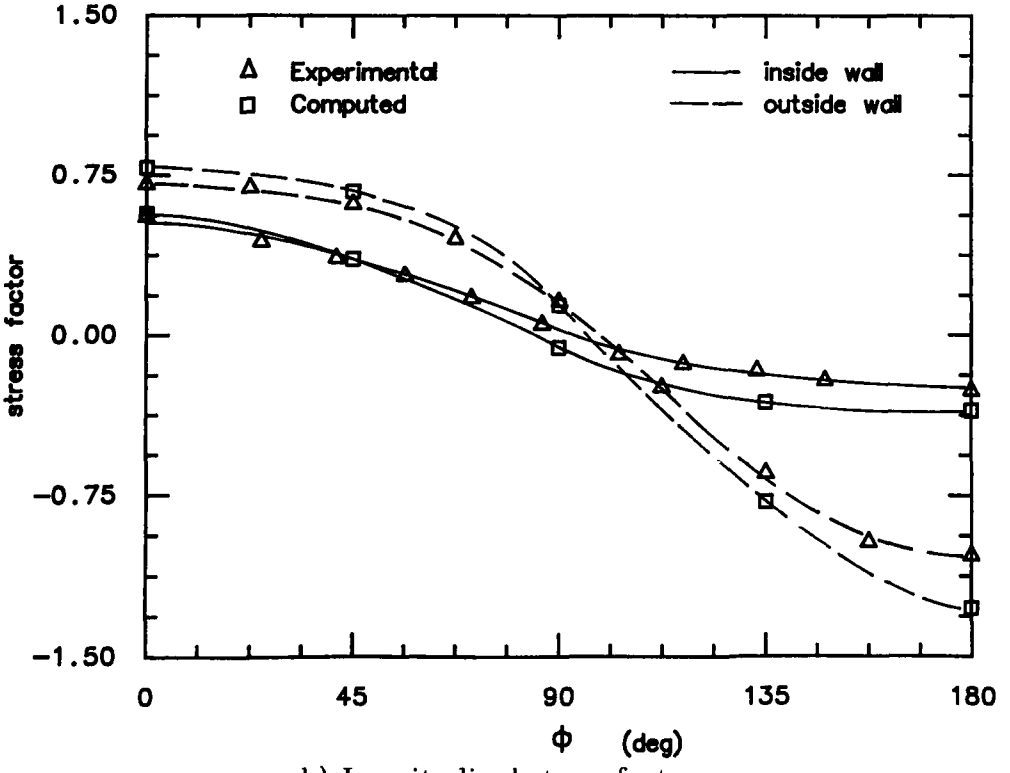

b) Longitudinal stress factor, σ_{θ_f}

Figure 5.6: Comparison between experimental and computed σ_{ϕ_f} and σ_{θ_f}

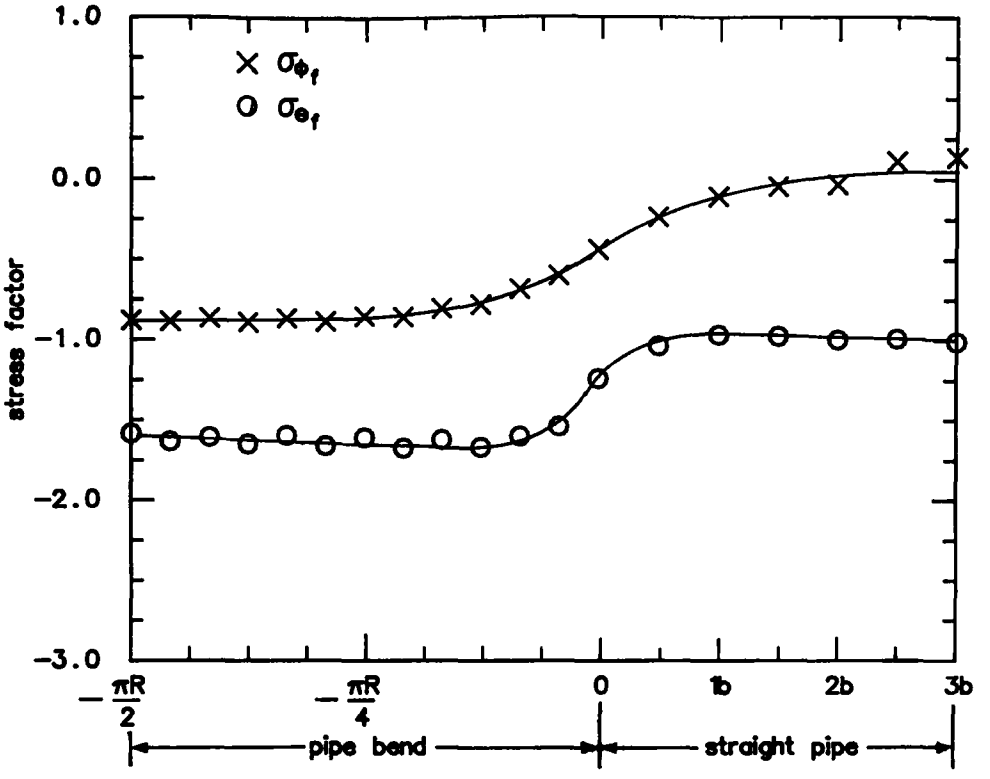

Figure 5.7: Circumferential and longitudinal stress factors along the mean pipe length for γ of 5 and t of 2.

are compared to a similar configuration (γ of 10 and t of 2 studied previously in chapter 4). Figure 5.6 presents the computed and experimental stress factors. It indicates that the BIE results follow the same trend as the experimental results. For a γ of 10 and a t of 2 the computed $\sigma_{\theta_{max}}$ equals 1.25 whereas for a γ of 11.02 and a t of 1.83 the experimental $\sigma_{\theta_{max}}$ equals 1.03. Figure 5.6 shows that as t increases and γ decreases $\sigma_{\phi_{max}}$ and $\sigma_{\theta_{max}}$ increase, which are as expected observing the effect of t and γ, separately.

In view that $\sigma_{\phi_{max}}$ and $\sigma_{\theta_{max}}$ found at both θ of 0° and 90° section are located at ϕ of 90° (inside surface) and 180° (outside surface) respectively, the variation of σ_{ϕ_f} at ϕ of 90° (inside surface) and of σ_{θ_f} at ϕ of 180° (outside surface) along the mean pipe length are shown in Figure 5.7 for case 1. Note that the stresses in the pipe bend fluctuate by about 5% from one point to the other. Moving away

from the middle section of the U-bend toward the straight pipe, σ_{θ_f} increases up to a peak which is about 5% greater than $\sigma_{\theta_{max}}$ at θ of 90° section. Notice that σ_{ϕ_f} contrary to σ_{θ_f} decreases steadily in the pipe bend. However, near the pipe bend and straight pipe connection both σ_{ϕ_f} and σ_{θ_f} decreased rapidly. It is observed that at b the computed σ_θ is lower than σ_θ applied at the end of the straight pipe. From b to $3b$ along the straight pipe axis the computed σ_θ increases and at $3b$ it equals the applied stress. The σ_{ϕ_f} decreases along the straight pipe approaching zero and near the pipe end it increases slightly above zero. These conclusions are also valid for the other two cases.

5.2 Internal Pressure Loading

The computed circumferential and longitudinal stress factors for the U-bend at the section θ of 0° and 90° and for a complete torus are shown in Figures 5.8 and 5.9, having a γ of 5 and t of 2 and 3 respectively. There is a close correlation between σ_{ϕ_f} at the outside surface found in a U-bend at section θ of 90° and in a torus whereas at the inside surface the computed values for the U-bend problem are slightly higher in the region $\pi/4 \leq \phi \leq 3\pi/4$. It is observed that σ_{θ_f} at the inside surface found in both the pipe bend at section θ of 90° and the torus is quite identical. However at the outside surface they are not. The circumferential stresses at the inside surface at the section θ of 0° are approximately the same than the ones at the section θ of 90° except in the region $3\pi/4 \leq \phi \leq \pi$. At the outside surface, σ_{ϕ_f} at θ of 0° is slightly greater than at θ of 90° near the extrados whereas near the intrados the contrary is true. The peak stresses are at the section θ of 90°. Similarly to the torus, the peak values of σ_{ϕ_f} and σ_{θ_f} for the U-bend are located on the inside wall at the intrados and extrados, respectively. It is observed that the greatest difference of stress between the two sections is found when comparing σ_{θ_f}.

Figure 5.10 presents σ_{ϕ_f} and σ_{θ_f} obtained in the U-bend having a γ of 10 and a t of 3 at the two cross-sections (0° and 90°). Results previously obtained for a complete torus are also presented. Note that contrary to the pipe bends with γ

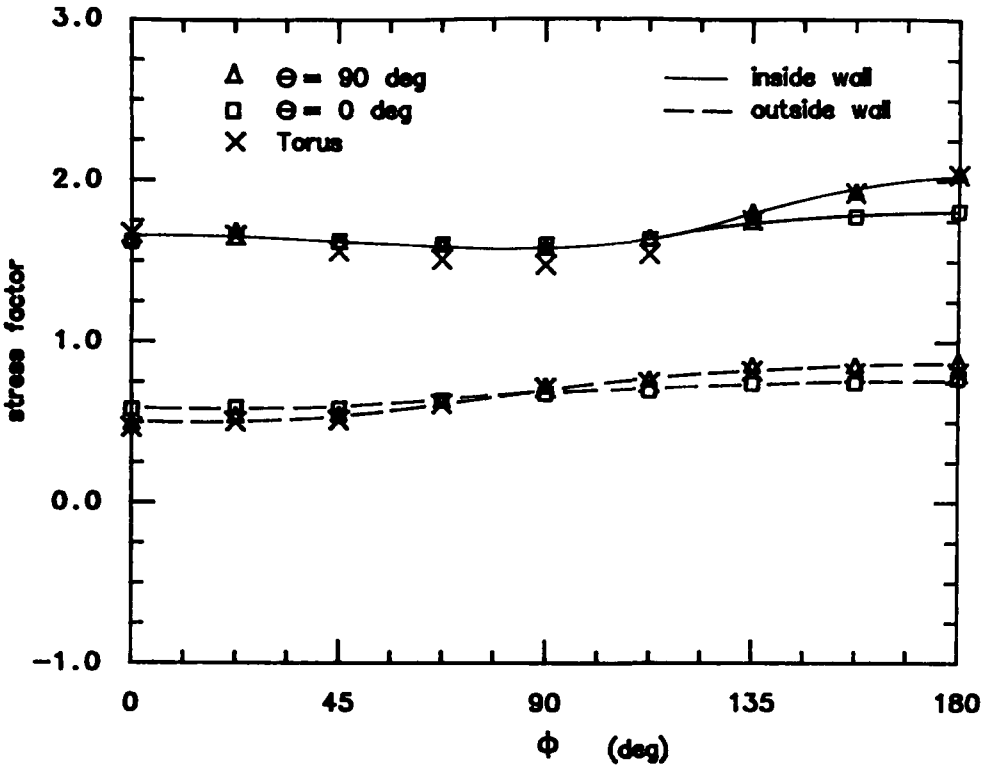

a) Circumferential stress factor, σ_{ϕ_f}

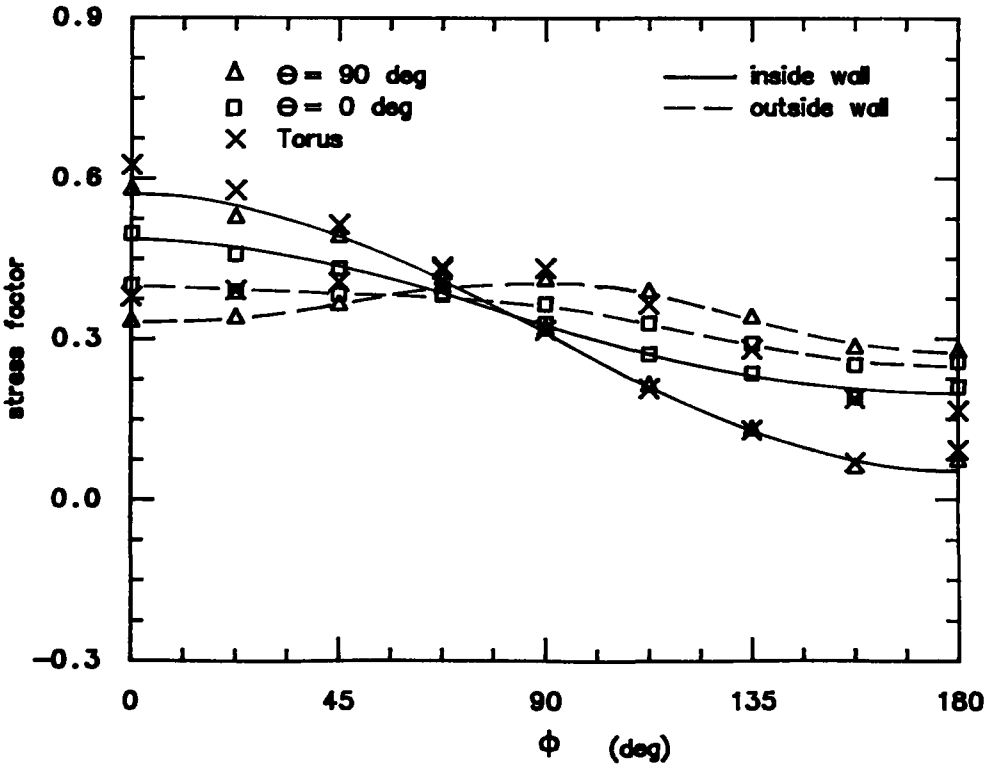

b) Longitudinal stress factor, σ_{θ_f}

Figure 5.8: Stress factors for γ of 5 and t of 2.

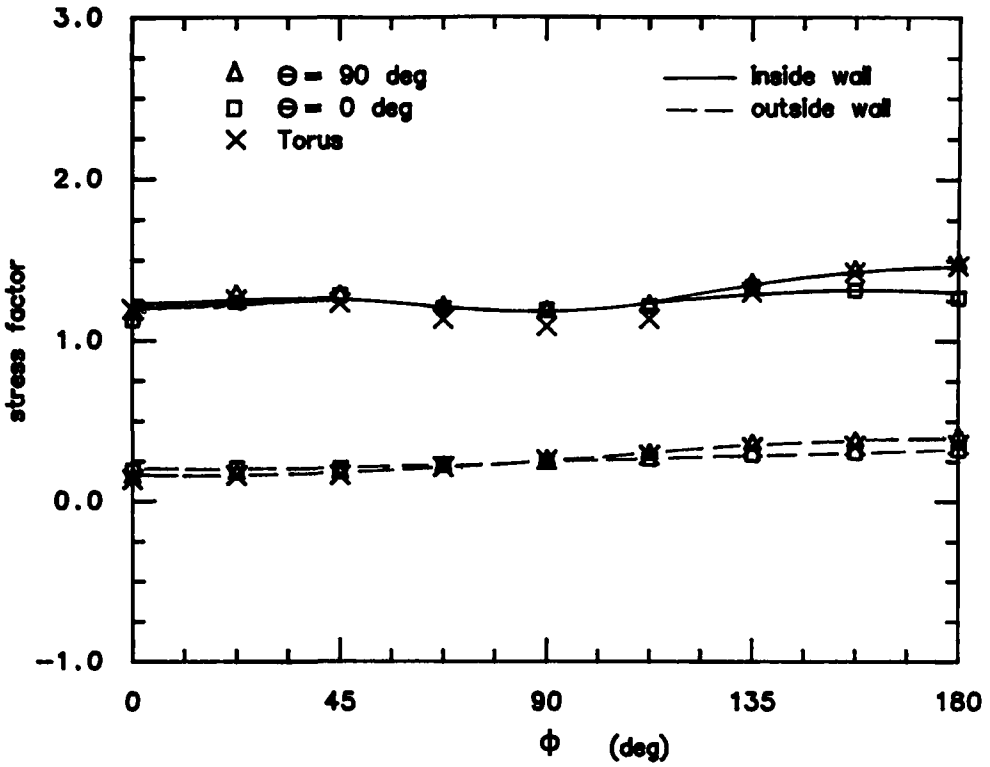

a) Circumferential stress factor, σ_{ϕ_f}

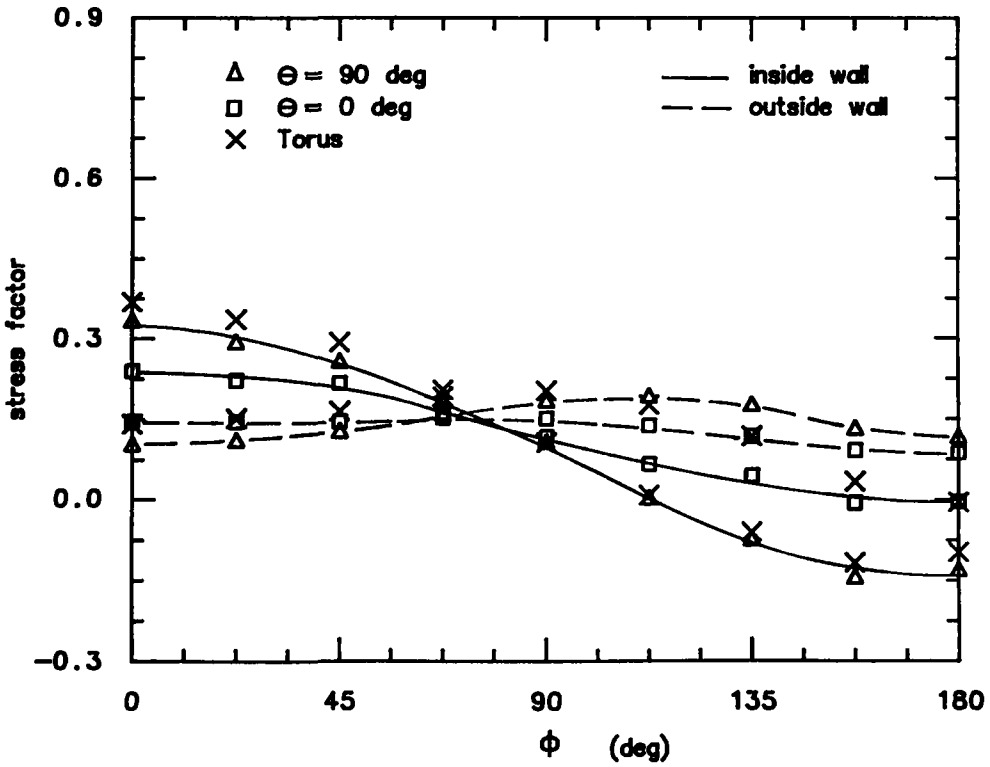

b) Longitudinal stress factor, σ_{θ_f}

Figure 5.9: Stress factors for γ of 5 and t of 3.

case	$\theta = 90°$ cross-section		$\theta = 0°$ cross-section		Torus	
	$\sigma_{\phi_{max}}$	$\sigma_{\theta_{max}}$	$\sigma_{\phi_{max}}$	$\sigma_{\theta_{max}}$	$\sigma_{\phi_{max}}$	$\sigma_{\theta_{max}}$
1	2.0311	0.5782	1.8101	0.4971	2.0374	0.6251
2	1.4802	0.3305	1.3378	0.2396	1.4664	0.3686
3	1.3871	0.2447	1.3415	0.1923	1.3452	0.2557

Table 5.3: Peak stress factor for a pressurized U-bend

of 5, σ_{ϕ_f} at the inside surface near ϕ of 90° found in a torus agrees better with the ones found in a U-bend at section θ of 0° than at 90°. At the outside surface, σ_{ϕ_f} obtained from the U-bend at both section and the torus are almost identical. Observing the above figures, σ_{ϕ_f} and σ_{θ_f} at the inside surface found in a torus are closely related to the ones found in a U-bend at the section θ of 90°. This is also true for σ_{ϕ_f} at the outside surface.

Table 5.3 presents the maximum circumferential and longitudinal stress factors of the U-bend at section θ of 0° and 90° and of the torus. Note that both $\sigma_{\phi_{max}}$ and $\sigma_{\theta_{max}}$ is smaller at θ of 0° than at 90°. Comparing the peak stress factors of the U-bend with the ones of the torus, it is observed that the value of $\sigma_{\phi_{max}}$ is almost identical, having only a maximum different of about 3%. However the discrepancy is greater for $\sigma_{\theta_{max}}$ where case 2 displays the maximum difference of about 11%. Notice that $\sigma_{\theta_{max}}$ decreases when changing the problem from a complete torus to a U-bend. Similarly to the torus, the peak value of σ_{ϕ_f} has moved from the intrados to ϕ of 135° for case 3. The $\sigma_{\phi_{max}}$ at the section θ of 0° for case 2 and 3 is also at ϕ of 135°.

Figure 5.11 depicts the variation of σ_{ϕ_f} at the intrados and σ_{θ_f} at the extrados at the inside surface along the mean pipe length for case 1. It is observed that the peak σ_{ϕ_f} is located at the middle cross-section of the U-bend ($\pi R/2$). Moving toward the straight pipe, σ_{ϕ_f} decreases slightly and then near the connection between the pipe bend and the straight pipe it decreases more rapidly. Note that σ_{θ_f} is uniform along the pipe and starts decreasing near the connection. From b to $3b$ along the straight pipe σ_{ϕ_f} is quite uniform and σ_{θ_f} slightly increases. At $3b$, σ_{ϕ_f} deviates by about 1% from the Lamé solution. These observations are also valid for the other

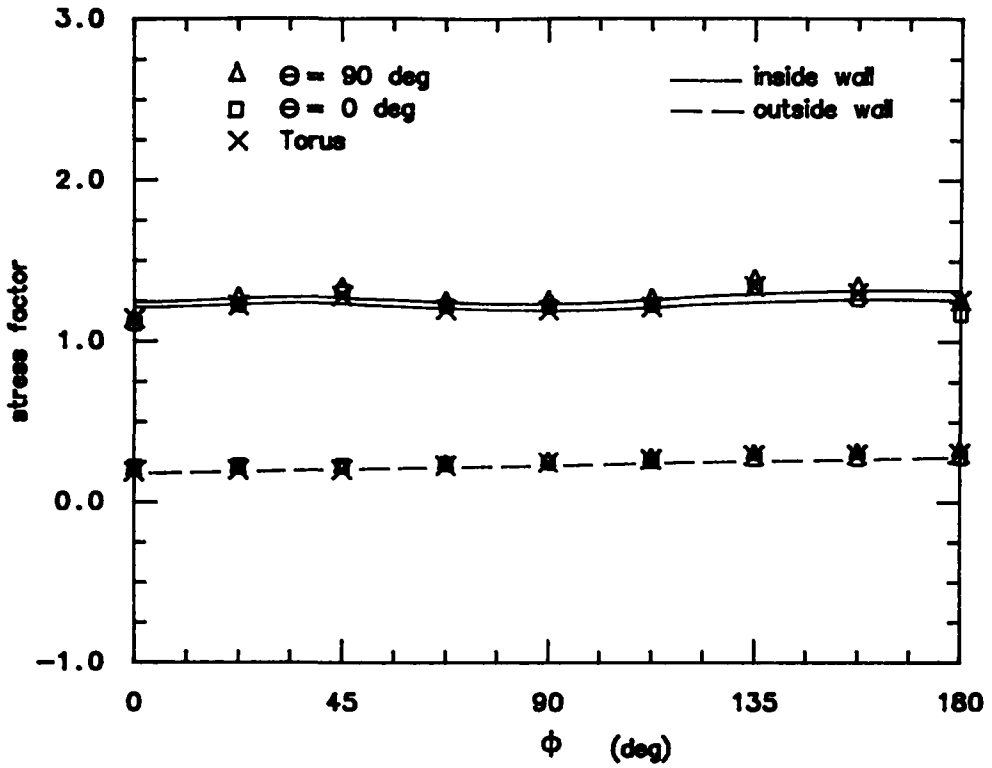

a) Circumferential stress factor, σ_{ϕ_f}

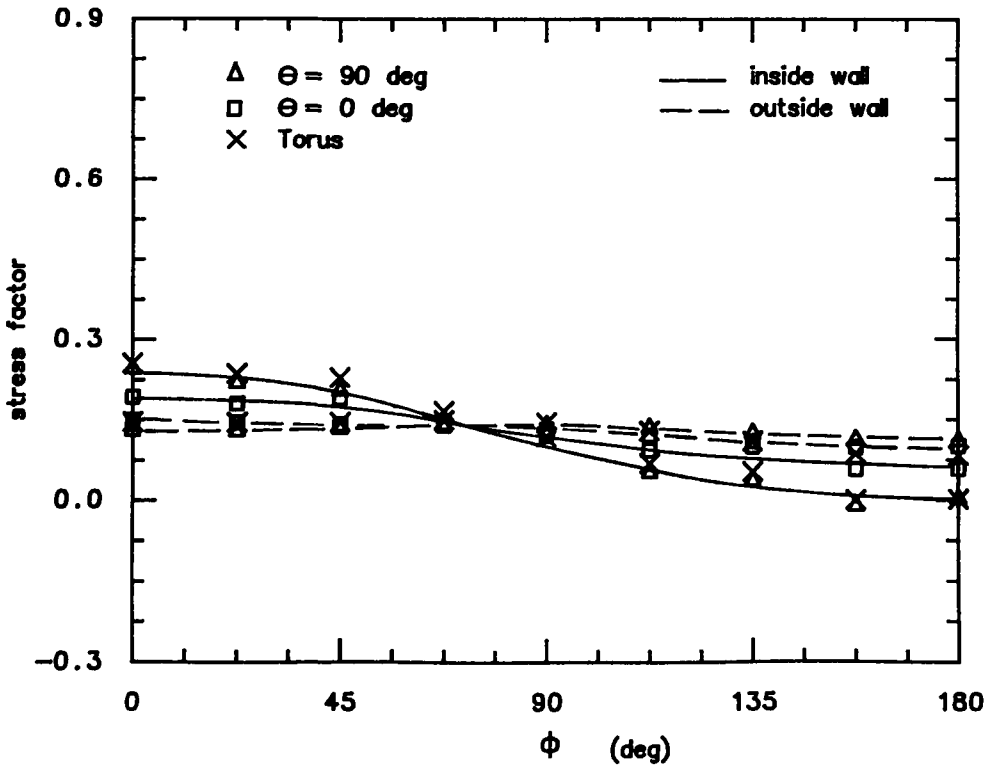

b) Longitudinal stress factor, σ_{θ_f}

Figure 5.10: Stress factors for γ of 10 and t of 3.

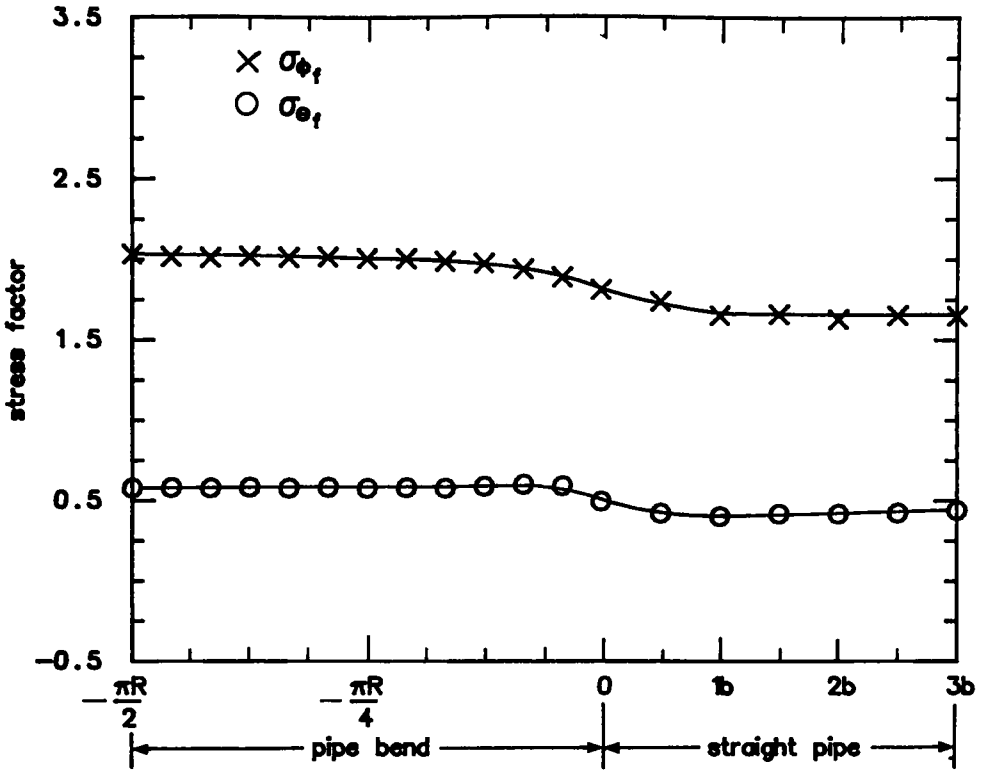

Figure 5.11: Circumferential and longitudinal stress factors along the mean pipe length for γ of 5 and t of 2.

two cases.

Chapter 6

Cylinder and Torus with Cross Bores

6.1 Thick-Walled Cylinder with Cross Bores

The problem of a cylinder with cross bores already solved by Tan and Fenner [50] was used to acquire experience in this field. Consideration of this problem enabled the determination of suitable mesh sizes and the calculation of reference stress values, to be used later in the analysis of tori.

The two problems considered are closed-end cylinders with a constant wall thickness. One cylinder has a single cross bore while the other has two cross bores. The loading in each case is internal pressure. Figures 6.1a and 6.1b show the longitudinal half section of the problems. In the figures a is the inside radius, b is the outside radius , $2H$ is the total length and R_s is the radius of the cross bore. The cross bore axis is radial to the main cylinder. The internal pressure, P_i, acting in the cross bore(s) is equal to the pressure acting in the cylinder. The closed-end boundary conditions are simulated in the numerical model by a uniform axial tensile stress applied on the cylinder ends which is given by

$$\sigma_l = \frac{P_i a^2}{(b^2 - a^2)}$$

Both problems studied have a cross-sectional radius ratio, b/a, of 2, a cross bore radius ratio, a/R_s, of 4 and b/H of 1. The cylinder with a single cross bore has only two planes of symmetry, so one quarter of the cylinder needs to be modelled. One

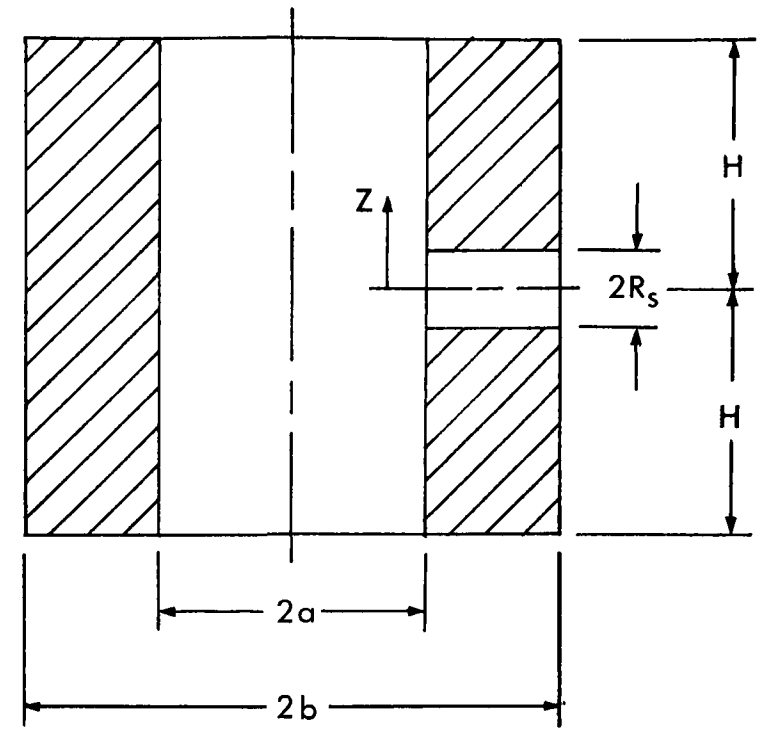

a) with one cross bore

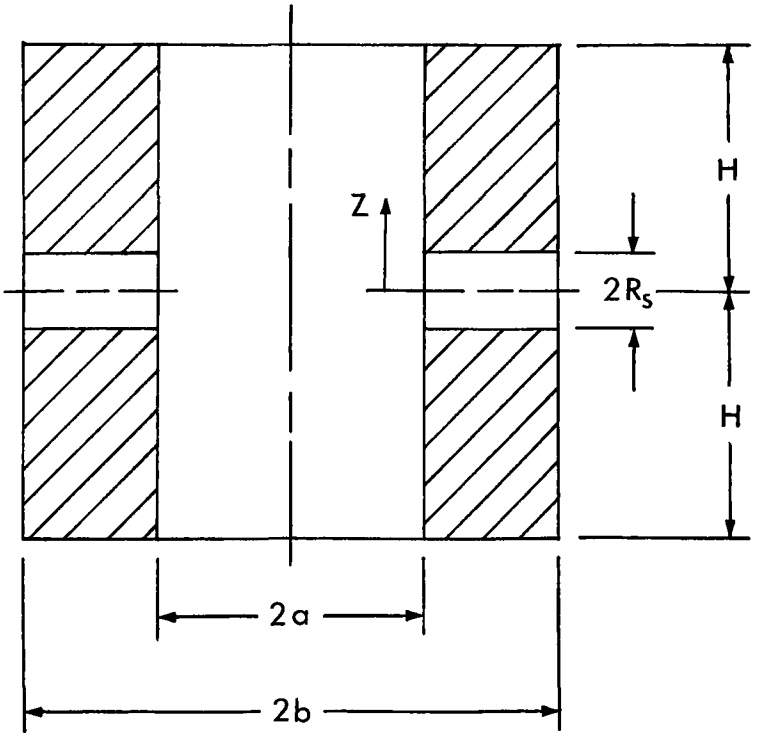

b) with two cross bores

Figure 6.1: Longitudinal half-section of a cylinder.

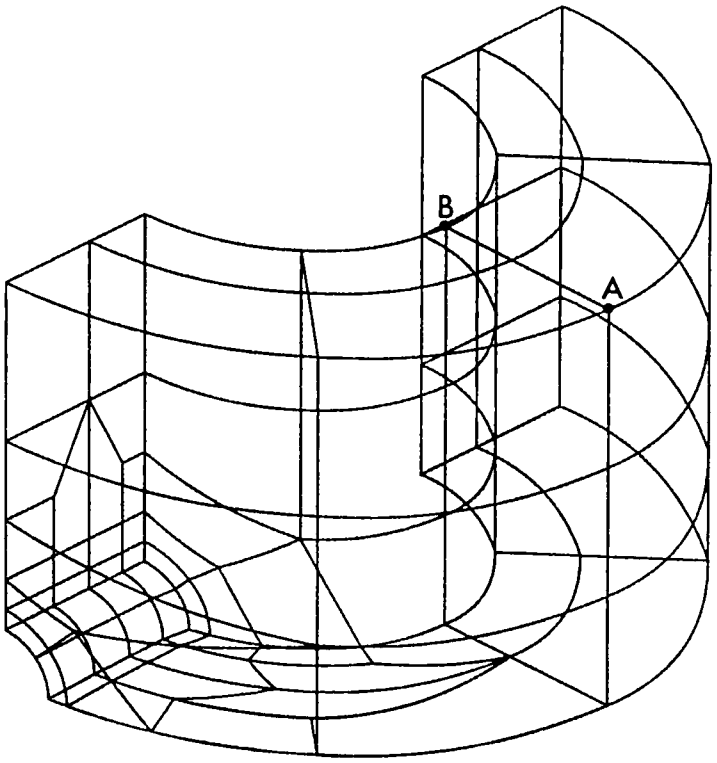

Figure 6.2: The BIE boundary mesh for a cylinder with a single cross bore.

plane is in the longitudinal section (shown in Figure 6.1a) and the second plane is the cross-section through the cross bore axis. Note that only one quarter of the hole needs to be modelled.

Having only two planes of symmetry means that the displacements in only two directions are constrained. The direction not constrained is parallel to the axis of the cross bore. It is difficult to constrain the displacement in that direction without having a major effect on the overall stress factors. Knowing that the effect of the holes diminishes as one goes further away from the cross bores, the displacement in the third direction is constrained on the plane $Z = H$. Figure 6.2 shows the boundary mesh chosen for this problem. There are 90 elements and 272 nodes. This problem is solved for two different ways of constraining the displacement in the third direction. The first case is such that only the point A is constrained whereas in the second case, the complete line AB is constrained (Shown in Figure 6.2).

The modelling of the hole is difficult, due to the fact that the circumference of

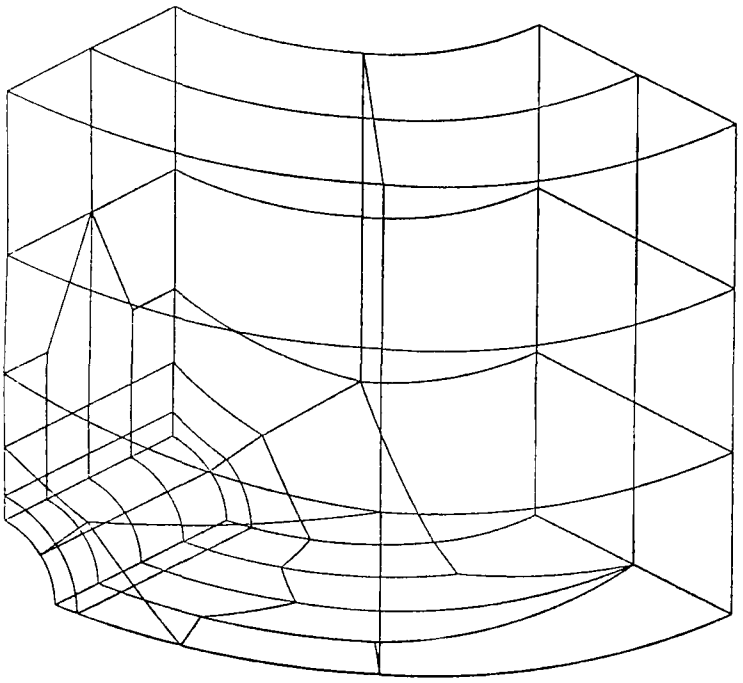

Figure 6.3: The BIE boundary mesh for a cylinder with two cross bores.

a hole on a curved surface is not represented by a circle but by an ellipse. Similarly to the torus with an elliptical cross-section problem, there is the need to use the elliptic integral of the second kind to find the actual distance between two points.

The problem of the bore crossing completly the cylinder walls, is easier to analyse because of the presence of three planes of symmetry, giving no difficulties in constraining the displacements in the three perpendicular directions. Only one eight of the cylinder is modelled. This boundary mesh is shown in Figure 6.3, with 70 elements and 212 nodes.

Figure 6.4 depicts the hoop stress factor variations with Z along the inner wall of the cylinder having a single cross bore. The maximum hoop stress in this figure increased by 3.6% in changing the line constraint to the point constraint. This means that the line constraint is too rigid for this problem. However, if the cylinder was of greater length, the difference between results of the line constraint and point constraint would be minimal because the effect of the hole would be less.

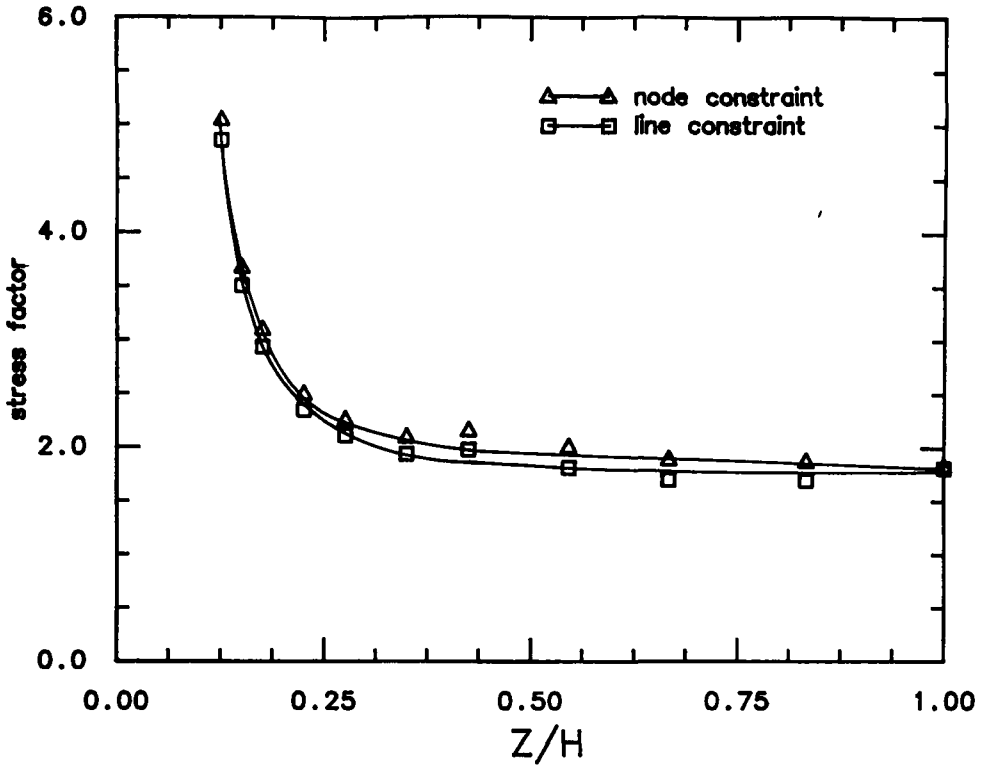

Figure 6.4: Hoop stress factor along the inner wall of a cylinder with a single cross bore.

The stress concentration factor, K_h, is defined as the maximum computed hoop stress expressed as a multiple of Lamé's solution value at the bore. The stress concentration factor is 2.91 and 3.02 for the line and point constraints, respectively. Tan and Fenner [50] found a K_h value of 2.90, which correlates well with the value found with the line constraint, meaning that they also used this constraint. But due to the rigidity of the line constraint for this particular problem, the results of the point constraint are more appropriate. Indeed, Tan [53] has very recently solved the same problem again using the point constraint and has obtained a value of 3.00 for the stress concentration factor using a slightly different mesh distribution. Gerdeen [47], using an approximate solution, found a value of 3.32 for K_h, which is about 9.9% higher than the BIE solution (for the point constraint).

Figure 6.5 shows the hoop stress variations for the double cross bore problems. The maximum hoop stress factor is 5.25, showing an increase of 4.2% compared to the single hole problem. The stress concentration factor is found to be 3.15 which

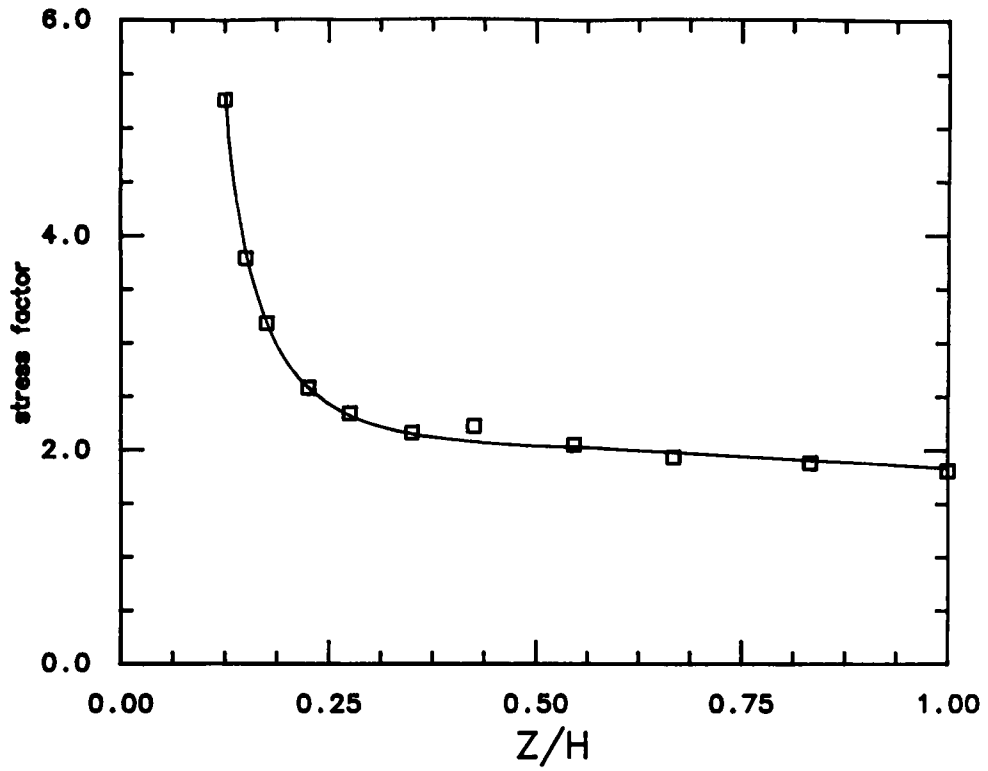

Figure 6.5: Hoop stress factor along the inner wall of a cylinder with two cross bores.

is the same as that found by Tan and Fenner [50].

For both problems studied herein the hoop stress at $Z = H$ plane agrees with the Lamé solution within about 9%. This indicates that the effect of the holes is still felt at the ends of the cylinder and that a greater length of cylinder is needed to obtained the same value as the Lamé solution.

6.2 Thick-Walled Torus with Cross Bores

The problem considered in this section, is that of obtaining the hoop stress in a complete torus with cross bores subjected to internal pressure. Figures 6.6a and 6.6b show the section in the plane of the torus of the two problems analysed. Figure 6.6a represents a complete torus with two identical and diametrically opposite cross bores at the intrados whereas Figure 6.6b represents a torus with cross bores at the extrados. In these figures, R is the mean toroidal radius, a and b are the cross sectional radii and R_s is the cross bore radius. The axis of the cross bores are radial in the cross-section of the torus. The internal pressure acting in the cross bores is equal to the pressure in the torus.

The problems analysed are for a toroidal radius ratio, γ, of 5, a thickness ratio, t, of 2 and two different cross bores ratios , a/R_s, of 4 and 8. For both problems considered, there are three planes of symmetry, so only one eight of the torus needs to be modelled. Figures 6.7 and 6.8 show the boundary mesh arrangements of quadrilateral and triangular elements, for the problems having the cross bores at the intrados and extrados, respectively. A maximum of 390 nodes and 130 elements are used.

Figure 6.9 depicts the hoop stress factor variation with θ along the inner wall in the planes of the torus for the cross bores positioned at the intrados. The hoop stress factor is at its peak near the cross bore and varies considerably for the first 10 degrees from the axis of the bores. Further away from the hole, its effect decreases giving a uniform stress between 45° and 90°. At 90° , the computed hoop stress approaches the hoop stress for a torus without cross bores, to within about 1%. The maximum hoop factor is about 6.25 and 5.89 for a/R_s of 4 and 8, respectively. Note that as the cross bores ratio decreases, the maximum stress factor increases.

Figure 6.10 shows the variation of the hoop stress along the internal surface of the torus in the longitudinal plane through the axis of the bores for the case where the cross bores are at the extrados. For this problem the cross bore ratio has a small effect on the peak stress whereas for the previous problem the effect

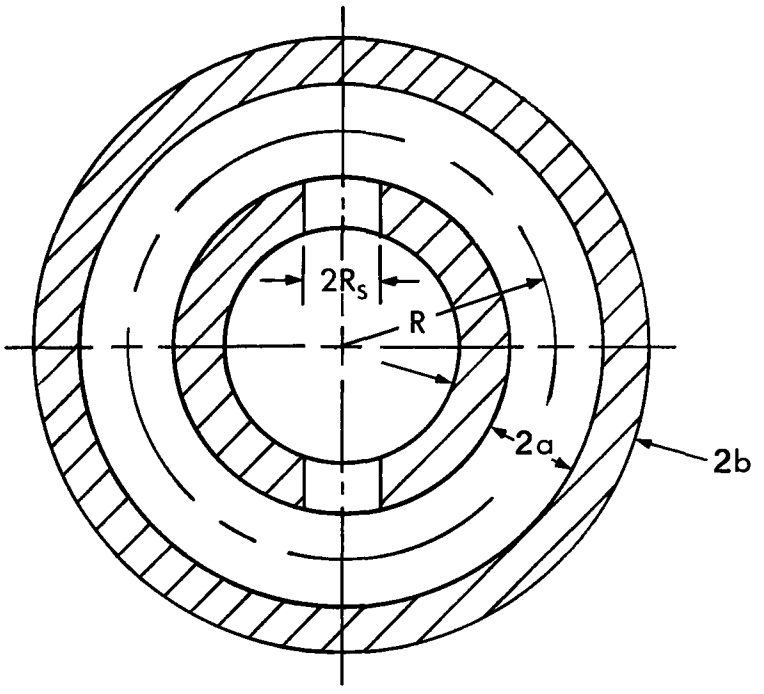

a) with the cross bores at the intrados

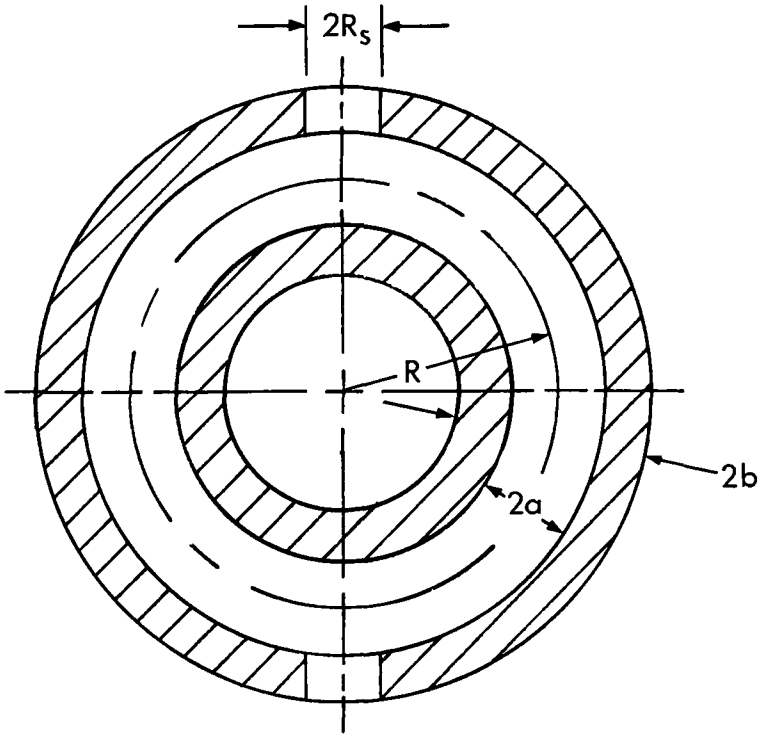

b) with the cross bores at the extrados

Figure 6.6: Longitudinal half-section of a torus.

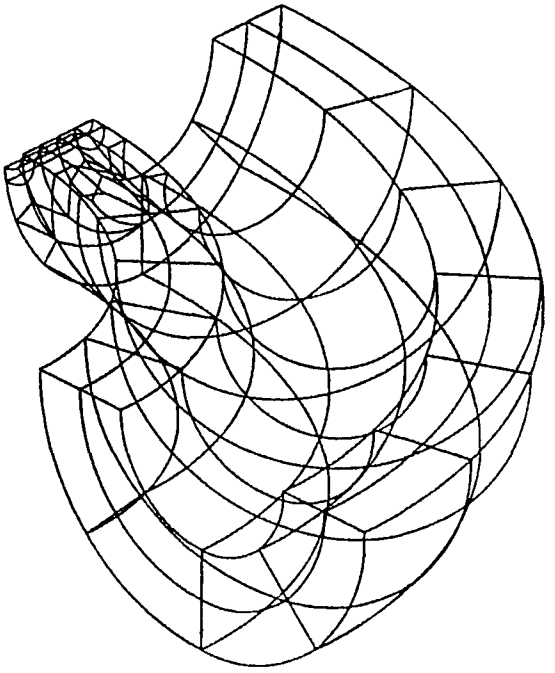

Figure 6.7: The boundary mesh used for a torus with cross bores at the intrados, containing 126 elements and 380 nodes.

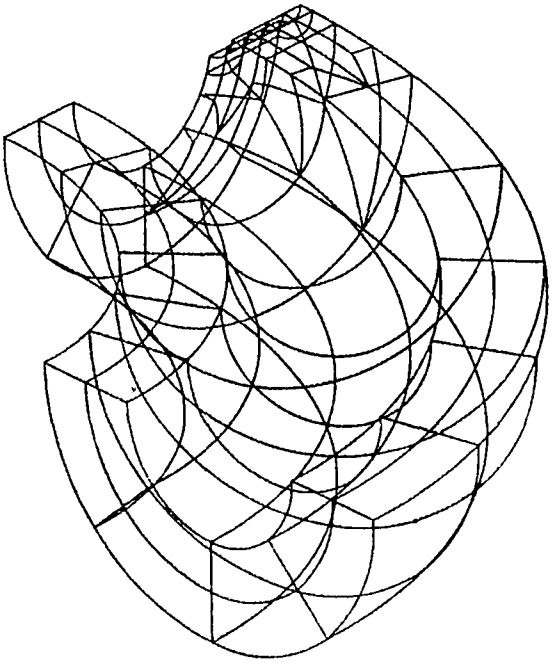

Figure 6.8: The boundary mesh used for a torus with cross bores at the extrados, containing 130 elements and 390 nodes.

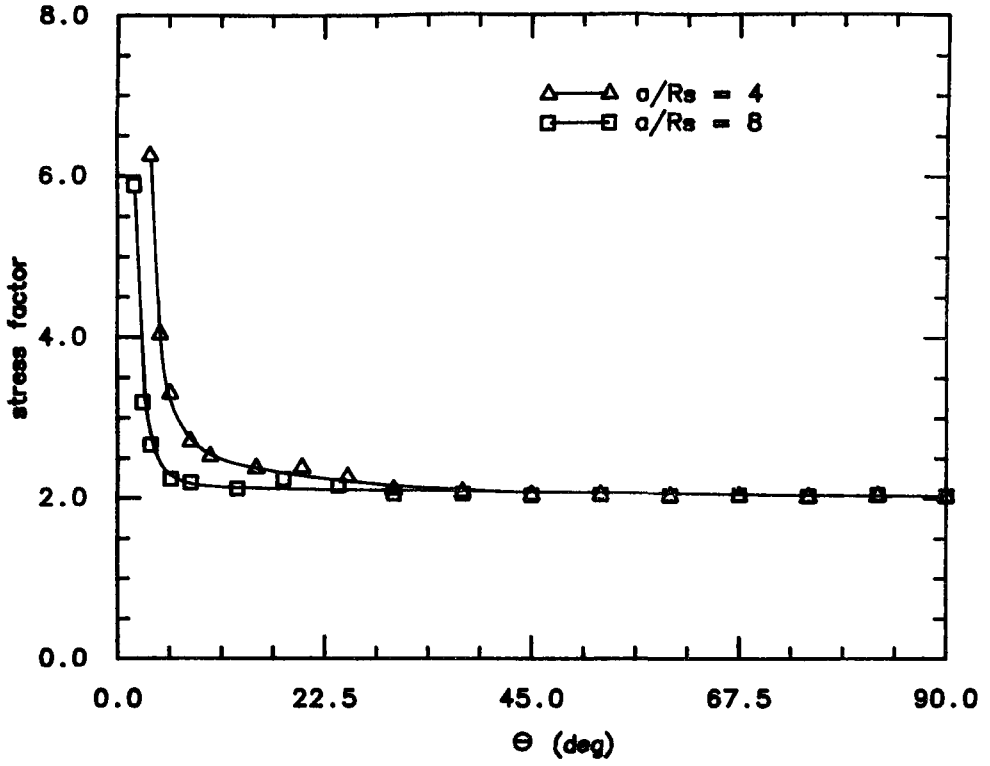

Figure 6.9: Hoop stress factor along the inner wall of the torus ($\phi = 180°$) with the cross bores at the intrados.

was considerable. The maximum hoop stress factor is about 2.65 times the hoop stress factor for a complete torus with no holes. Moving away from the hole it is seen that the effect of the cross bore over the stress decreases faster than for the previous problem, starting to be uniform at θ of 22.5°. Just as for the previous problem, the computed hoop stress at θ of 90° deviates from the hoop stress of a torus without holes only by about 1%. The results for the two problems show that there is almost no fluctuation of the computed hoop stress factor. This indicates that the mesh distributions chosen for both problems are satisfactory.

Unfortunately, no experimental results were available in the literature for comparison. Table 6.1 compares the stress concentration factor, K_h, of the tori with the one of the cylinders studied in this chapter. The torus with the cross bores at the extrados has the lowest K_h while the torus with the cross bores at the intrados the highest. The K_h value for the problem of the cylinder with two cross bores is about 19% higher than for the torus having the cross bores at the extrados.

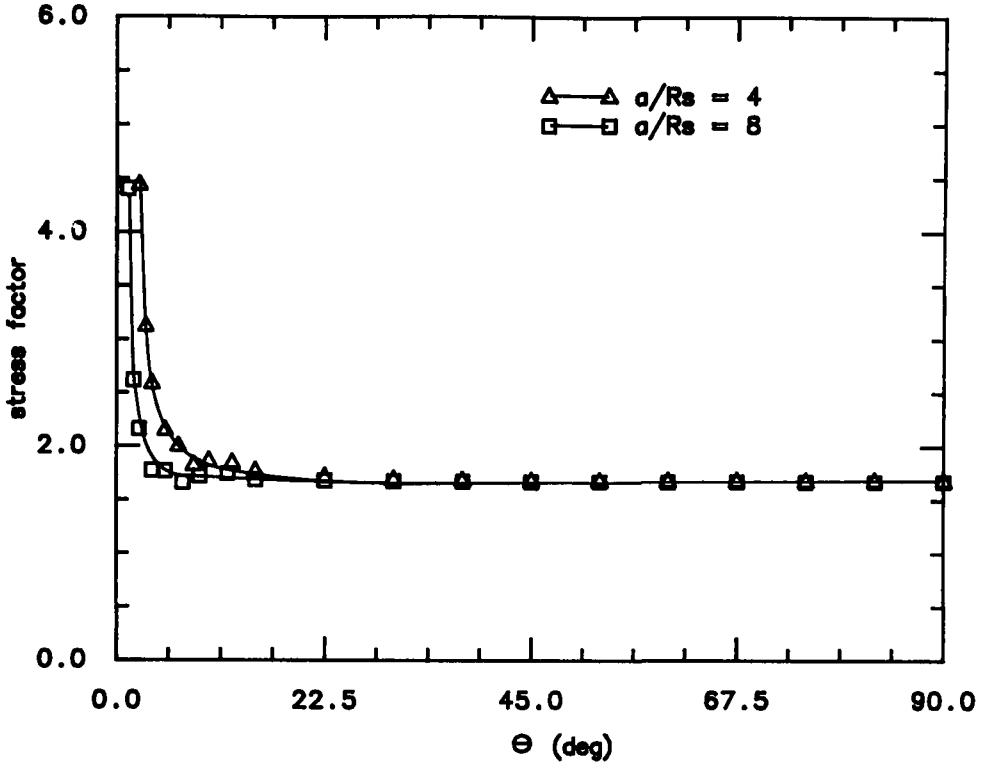

Figure 6.10: Hoop stress factor along the inner wall of the torus ($\phi = 0°$) with the cross bores at the extrados.

	Straight pipe		Torus with holes at			
	1 hole	2 holes	Intrados		Extrados	
a/R_s	4	4	4	8	4	8
K_h	3.02	3.15	3.75	3.53	2.65	2.64

Table 6.1: Stress concentration factors

Chapter 7

Conclusion

The present work has demonstrated effectively the power and versatility of the Boundary Integral Equation method for three-dimensional stress analysis of relatively simple and complicated thick-walled cylinder and toroidal geometries. It has particularly confirmed the usefulness of the BIE method for problems involving awkward boundary geometry and rapidly varying stress fields. Using a very modest number of boundary elements, it is possible to predict stresses and displacements with an accuracy that is adequate for most engineering purposes.

In the case of a torus under internal pressure, an excellent agreement between the three-dimensional BIE, axisymmetric BIE and axisymmetric FE results was found. It was observed that the BIE method significantly reduces the numerical problems over FE method. Within the range of parameters studied herein, the peak stress factor occurs near the intrados on the inside surface for a torus of circular cross-section. The peak stress factor increases as γ decreases and as t decreases. The torus with an oval cross-section presented a more complex situation. Initial ovality has significant effects on stresses and displacements. The stress and displacement factors vary considerably with ϕ. The peak stress now occurs at ϕ of 90° with an important increase compared to the ones of a circular cross-section. Contrary to the circular cross-section, the peak stress decreases with decreasing γ.

Results from the 3-D BIE method compared well with the TE results for the cases of a torus under internal pressure and a 90° elbow subjected to in-plane

bending moment when the zero, first and second order fields of stress are used in the TE solution. The peak stress factors found from both methods differ only by about 4%. For the in-plane bending problem, the peak stress occurs on the outside surface at the intrados which increases as t increases and/or γ decreases.

In the cases of a 90° elbow subjected to out-of-plane bending moment, twist bending moment and out-of-plane end shear force, reasonable agreement between the BIE and TE are obtained when the zero and first order fields of stress are used in the latter solutions. The agreement between the methods for the case of the end shear force is not as good as for the other two cases. This is especially true for $\sigma_{\phi\theta_f}$ for which the agreement is not good. The elbow having the geometric ratios γ of 5 and t of 3 gave the worst agreement between the methods for the peak stress which had a difference of about 5% for the out-of-plane bending moment, 10% for the twist bending moment and 23% for the out-of-plane end shear force. The peak stress for the three problems occurs near ϕ of 115° and ϕ of 250° on the outside surface. For the out-of-plane and twist bending problems, an increase in the peak stress was observed when t increased or γ decreased whereas for the out-of-plane end shear force problem the peak stress decreases for the same conditions.

Agreement between the normal stresses computed by the BIE and TE methods was not good in the cases of a 90° elbow subjected to in-plane end shear force and in-plane end normal force. However, reasonable agreement between both methods was found for $\sigma_{\phi\theta_f}$. The TE solution used has the zero, first and part of the second order fields of stress. Correlation between the peak stress factor was good only for the shear force problem. A maximum deviation less than about 8% was found for the shear force problem. For both problems, the BIE results showed that the peak stress increased with increasing γ whereas it decreased with increasing t.

A parametric study for the internal pressure and moment loading cases based on the TE solutions presented in this work should produce results suitable for engineering purposes. But the TE solutions for the force loadings studied in the present work are not adequate. A higher level of approximation is needed to obtain

suitable results.

Results of the peak stress factor presented in the cases of a U-bend with straight pipes subjected to in-plane bending moment and internal pressure showed that they would be well approximated by the peak stress obtained in a 90° elbow and a complete torus, respectively.

Results obtained for a pressurized cylinder with a single cross-bore showed the importance of the constraints when there are only two planes of symmetry. It was shown that by changing the line constraint to a point constraint, the stress concentration factor, K_h, increased, which indicated that the line constraint was too rigid. Results in the case of a cylinder with two cross-bores showed an increase of K_h by about 4% to the corresponding value for a cylinder with a single cross-bore. The cases of the torus with cross-bores at the intrados and extrados demonstrated that the K_h value for a torus with cross-bores at the extrados was the lowest even when it was compared to a cylinder with cross bore(s).

Further research is required to verify the applicability of the TE solutions for thin shell analysis. More work is also needed to develop extra stress fields to the TE solutions for the force problems in order to obtain suitable results for the problems considered herein. Having noted relatively few investigations concerning thick-walled pipe bends, piping systems and pipe bends with cross-bores, additional work in this field is necessary to know more about their behaviours under different kinds of loads.

Bibliography

[1] ASME,"Rules for Construction of Nuclear Power Plant Components, Section **III**","Rules for Construction of Pressure Vessels, Division 1 and Division 2, Section **VIII**", *ASME Boiler and Pressure Vessel Code* (1971).

[2] Von Karman, T.,"Über die Formönderung dünnwandiger Rohre, insbesondere federnde Ausgleichrohre," *Zeitschrift des Vereines deutscher Ingenieure* **55** (1911), 1889–1895.

[3] Vigness, I.,"Elastic properties of curved tubes," *ASME* **65** (1943), 105–120.

[4] Pardue, T. E. and Vigness, I. "Properties of thin walled curved tube of short-bend radius," *Trans. ASME,* **73** (1951), 77–87.

[5] Pardue, T. E. and Vigness, I., "Characteristic of pipe bends under applied moments," *Summary Report, Naval Research Lab.* **Report 4253** (1953).

[6] Vissat, P L. and Del Buono, A. J., "In-plane bending properties of welding elbows," *Trans. ASME* **77** (1953), 161–175.

[7] Rodabaugh, E. C. and George, H. H., "Effect of internal pressure on flexibility and stress-intensification factors of curved pipe or welding elbows," *Trans. ASME* **79** (1957), 939–948.

[8] Swanson, S. A. and Ford, H. "Stresses in thick-walled plane pipe bends," *J. Mech. Eng. Sci.* **1** (1959), 103–112.

[9] Turner, C. E. and Ford, H., "Examination of the theories for calculating the stresses in pipe bends subjected to in-plane bending," *Proc. I. Mech. E.* **171** (1957), 513–525.

[10] Barthelemy, J., "Etude de la deformation et des tensions internes des tuyaux a ligne moyenne plane soumis a des efforts exterieurs et a une pression interne," *Bull. Ass. Tech. Maritime* **46** (1947), 411.

[11] Thuloup, A., *Bull. Ass. Tech. Maritime* **41** (1937).

[12] Kornecki, A., "Stress distribution in a pressurized thick-walled toroidal shell–A three dimensional analysis," *College of Aeronautics, Cranfield, England* **Note 137** (1963).

[13] Smith, R. T. and Ford, H., "Experiments on pipelines and pipe bends subjected to three-dimensional loading," *Fl. Mech. Eng. Sci.* **9** (1967), 124.

[14] Smith, R. T., "Theoretical analysis of the stresses in pipe bends subjected to out-of-plane bending," *J. Mech. Eng. Sci.* **9** (1967), 115–123.

[15] Jones, N., "In plane bending of a short radius curved pipe bend," *J. Eng. Ind.* (1967), 271–277.

[16] Thailer, H. J. and Cheng, D. H., "In-plane bending of a U-shaped circular tube with end constraints," *Trans. ASME* **92** (1970), 792–796.

[17] McGill, D. J. and Rapp, I. H., "Axisymmetric stresses and displacements in thick-walled elastic torus," *J. Eng. Mech. Div., ASCE* **99** (1973), 629–633.

[18] Natarajan, R. and Blomfield, J., "Stress analysis of curved pipes with end restraints," *Comput. Struct.* **5** (1975), 187–196.

[19] Thompson, J. J., "Shell theory analysis of pure in-plane bending of a pipe bend," *Trans. Third Int. Conf. Struct. Mech. Reactor tech., London* **F6/1** , 1–9.

[20] Ohtsubo, H. and Watanabe, O., "Flexibility and stress factors of pipe bends - An analysis by finite ring method," *ASME J. Pres. Ves. Tech.* **2** (1977), 281–290.

[21] Whatham, J. F., "In plane bending of flange pipe elbows," *Inst. Eng. Au Civ. Eng. Trans.* **21** (1979), 80–85.

[22] Lang, H. A., "Stress analysis of pressurized elbows for nuclear components using toroidal elasticity," *Proc. Fourth Int. Conf. Pres. Ves. Tech. London* **2** (1980), 251–260.

[23] Natarajan, R. and Mirza, S., "Stress analysis of curved pipes with end restraints subjected to out-of-plane moments," *Proc. SMIRT Conf. Paris* **F2/8** (1981), 1–9.

[24] Lang, H. A., "Toroidal elastic stress fields for pressurized elbows and pipe bends," *Int. J. Pres. Ves. & Piping* **15** (1984), 291–305.

[25] Lang, H. A., "In-plane bending of a curved pipe or toroidal tube acted on by end couples," *Int. J. Pres. Ves. & Piping* **15** (1984), 27–35.

[26] Lang, H. A., "Stress fields for a curved pipe subjected to in-plane end couples," *Int. J. Pres. Ves. & Piping* **15** (1984), 93–104.

[27] Lang, H. A., "Twist-bending of a 90° elbow or pipe bend," *Int. J. Pres. Ves. & Piping* **16** (1984), 67–74.

[28] Lang, H. A., "Out-of-plane bending of an elbow or pipe bend under an end-loaded shear force," *Int. J. Pres. Ves. & Piping* **15** (1984), 205–212.

[29] Lang, H. A., "Stress fields for an in-plane end shear force acting on a 90° elbow or pipe bend," *Int. J. Pres. Ves. & Piping* **16** (1984), 263–284.

[30] Lang, H. A., "Stress fields for a normal force acting on the end of a 90° elbow or pipe bend," *Int. J. Pres. Ves. & Piping* **17** (1984), 163–172.

[31] Lang, H. A., "Twist of a circular toroidal tube," *Res Mechanica* **14** (1985), 245–259.

[32] Lang, H. A., "Mean stresses and mean displacements in thin-walled curved circular tubing," *Int. J. Pres. Ves. & Piping* **21** (1985), 67–78.

[33] Findlay, G. E. and Spence, J., "Bending of pipe bends with elliptic cross section," *Welding Research Council Bulletin* **164** (1971).

[34] Arav, F., "Evaluation of pipe bends having local corrugations," *Proc. Third Int. Conf. Pres. Ves. Tech. Tokyo* (1977), 193–205.

[35] Boyle, J. T. and Spence, J., "The non-linear analysis of pressurized curved pipes," *Proc. Third Int. Conf. Pres. Ves. Tech., Tokyo* (1977), 121–131.

[36] Spence, J. and Boyle, J. T., "The influence of shape imperfections on stresses in piping components," *Proc. I. Mech. E. Conf., on significance of deviations from design shapes, London* (1979), 71–79.

[37] Boyle, J. T. and Spence, J., "A simple analysis for oval pressurized pipe bends under external bending," *Proc. Fourth Int. Conf. Pres. Ves. Tech., London* **2** (1979), 201–207.

[38] Spence, J. and Findlay, G. E., "The effect of thickness variations on the behavior of smooth curved pipes under external bending," *J. Pres. Ves. Tech.* **102** (1980), 45–48.

[39] Thomas, K., "The effects of geometric irregularities on the design analysis of thin-walled piping elbows," *J. Pres. Ves. Tech.* **102** (1980), 410–418.

[40] Natarajan, R. and Mirza, S., "Flexibility analysis of pipes bends having variable thickness around the circumference," *Pres. Ves. Des.* **57** (1982), 101–106.

[41] Natarajan, R. and Mirza, S., "Effect of thickness variation on stress analysis of piping elbows under internal pressure," *Comput. Struct.* **18** (1984), 767–778.

[42] Moore, S. E., Dodge, W. G. and Bolt, S. E., " Experimental stress analysis of four machined 10-in. NPS piping elbows with specified geometric distortions," *Oak Ridge National Lab. TN Dept. of Energy, Washington* (1983).

[43] Fessler, H. and Lewin, B. H., "Stress distribution in a tee junction of thick pipes," *British J. Appl. Phys.* **7** (1956), 76–99.

[44] Lake, G. F., "Proc. Inst. Conf. Fatigue of Metals Inst.," *Mech. Eng. London* (1956), 743.

[45] Morrison, J. L. M., Crossland, B. and Parry, J. S. C., "Fatigue strength of cylinders with cross bores," *J. Mech. Eng. Sci.* **1** (1959), 207–210.

[46] Fidler, R., "A photoelastic analysis of oblique cylinder intersections subjected to internal pressure," *Welding Research Council Bulletin* **153** (1970), 81–85.

[47] Gerdeen, J. C., "Analysis of stress concentrations in thick cylinders with sideholes and crossholes," *J. Eng. Ind. Trans. ASME* **94** (1972), 815–824.

[48] Gerdeen, J. C. and Smith, R. E., "Experimental determination of stress concentration factors in thick-walled cylinders with cross holes and side holes," *Exp. Mech.* **12** (1972), 530–536.

[49] Stanley, P. and Day, B. V., "Stress concentrations at offset-oblique holes in thick-walled cylindrical pressure vessels," *Proc. Second Int. Conf. Pres. Ves. Tech., San Antonio* (1973), 167–181.

[50] Tan, C. L. and Fenner, R. T., "Boundary integral equation stress analysis of some problems in high pressure engineering," *Proc. Second Int. Sym. on Innovative Numerical Analysis in Applied Engineering Sciences, Montreal* (1980), 787–795.

[51] Stanley, P. and Day, B. V., "Stresses at offset-oblique holes in thick-walled cylinders subjected to torsional loading," *J. Strain Anal. Eng. Des.* **15** (1980), 175–182.

[52] Abdul-Mihsein, M. J. and Fenner, R. T., " Some boundary integral equation solutions for three-dimensional stress concentration problems," *J. Strain Analysis* **18** (1983), 207–215.

[53] Tan C. L., "Stress redistributions in thick-walled cylinders due to the introduction of a cross-bore after autofrettage," *J. Strain Analysis* **21** (1986), 177–183.

[54] Jaswon, M. A. and Ponter, A. R., " Integral equation methods in potential theory I," *Proc. Roy. Soc. Lond.* **A273** (1963).

[55] Symm, G. T., "Integral equation methods in potential theory 2," *Proc. Roy. Soc. Lond.* **A275** (1963).

[56] Rizzo, F. J., "An integral equation approach to boundary value problems of classical elastostatics," *Quart. Appl. Math.* **25** (1967), 83–95.

[57] Cruse, T. A., "Numerical solutions in three dimensional elastostatics," *Int. J. Sol. Struct.* **5** (1969), 1259–1274.

[58] Cruse, T. A. , "Application of the boundary integral equation method to three dimensional stress analysis, " *Comput. Struct.* **3** (1973), 509–527.

[59] Cruse, T. A. and Van Buren, W., "Three dimensional elastic stress analysis of a fracture specimen with an edge crack," *Int. J. Fract. Mech.* **7** (1971), 1–16.

[60] Cruse, T. A. and Rizzo, F. J., "A direct formulation and numerical solution of the general transient elastodynamic problem: I," *J. Math. Anal. Appl.* **22** (1968), 244–259.

[61] Cruse, T. A. and Rizzo, F. J., "A direct formulation and numerical solution of the general transient elastodynamic problem: II," *J. Math. Anal. Appl.* **22** (1968), 341–355.

[62] Swedlow, J. L. and Cruse, T. A., "Formulation of boundary integral equations for three dimensional elasto-plastic flow," *Int. J. Solids Struct.* **7** (1971), 1673–1683.

[63] Mendelson, A., "Boundary integral methods on elasticity and plasticity," *NASA TN D7418* (1973), 1–36.

[64] Mendelson, A. and Albers, L. U., " Application of boundary integral equations to elasto-plastic problems," *ASME Proc. AMD* **11** (1975), 47–83.

[65] Riccardella, P. C., "An improved implementation of the boundary integral technique for two dimensional elasticity problems," *Carnegie-Mellon Inst. of Technology, Pittsburgh* (1972).

[66] Cruse, T. A., "An improved boundary integral equation method for three dimensional elastic stress analysis," *Comput. Struct.* **4** (1974), 741–754.

[67] Boissenot, J. M., Lachat, J. C. and Watson, J. O., "Etude par equations integrales d'une eprouvette C.T. 15," *Revue de Physique Appliquee, Department D.T.E.-CETIM* **9** (1974), 611–615.

[68] Lachat, J. C., "A further development of the boundary integral technique for elastostatics," Ph.D. Thesis, University of Southampton (1975).

[69] Lachat, J. C. and Watson, J. O., " A second generation boundary integral equation problem for three dimensional elastic analysis," *ASME Proc. AMD.* **11** (1975), 85–100.

[70] Lachat, J. C. and Watson, J. O., " Effective numerical treatment of boundary integral equations," *Int. J. Num. Meths. Eng.* **10** (1976), 991–1005.

[71] Lachat, J. C. and Watson, J. O., " Progress in the use of boundary integral equations, illustrated by examples," *Comp. Meths. Appl. Mech. Eng.* **10** (1977), 273–289.

[72] Watson, J. O., "Advanced implementation of the boundary element method for two and three dimensional elastostatics," In: *Developments in Boundary Element Methods* **1** , Banerjee and Butterfield (Eds.), Applied Science Publisher Ltd., London (1979), 31–63.

[73] Rizzo, F. J. and Shippy, D. J., "An advanced boundary integral equation method for three dimensional thermo-elasticity," *Int. J. Num. Meths. Eng.* **11** (1977), 1753–1768.

[74] Banerjee, P. K. and Butterfield, R. (Eds.), "Developments in boundary element methods **1**," Applied Science Publisher Ltd., London (1979).

[75] Brebbia, C. A. (Ed.), "Boundary element methods," *Proc. Third Int. Conf. on Boundary elements, Irvine, California*, Springer-Verlag, New York (1981).

[76] Brebbia, C. A. (Ed.), "Boundary element methods in engineering," *Proc. Fourth Int. Conf. on Boundary elements*, Springer-Verlag, New York (1982).

[77] Brebbia, C. A., Futagami, T. and Tanaka, M. (Eds.), "Boundary element methods," *Proc. fifth Int. Conf. on Boundary elements, Hiroshima*, Springer-Verlag, New York (1983).

[78] Sokolnikoff, I. S. , "Mathematical theory of elasticity," Second Edition, McGraw Hill, Toronto (1956), 336–337.

[79] Love, A. E. H., "A treatise on the mathematical theory of elasticity," Fourth Edition, Dover publications, New York (1944), 245–246.

[80] Zienkiewicz, O. C., "The finite element method," Third Edition, McGraw Hill, Toronto (1977), 155–177.

[81] Tan, C. L. and Fenner, R. T., "Three-dimensional stress analysis by the boundary integral equation method," *J. Strain Anal.* **13** (1978), 213–219.

[82] Tan, C. L. and Fenner, R. T., "Elastic fracture mechanics analysis by the boundary integral equation method," *Proc. R. Soc. Lond.* **A369** (1979), 243–260.

[83] Tan, C. L. and Fenner, R. T., "Stress intensity factors for semi-elliptical surface cracks in pressurised cylinders using the boundary integral equation method," *Int. J. Fracture* **16** (1980), 233–245.

[84] Tan, C. L. and Shim M. L., "Stress intensity factor influence coefficients for internal surface cracks in Thick-Walled Cylinders," *Int. J. Pres. Ves. & Piping* **24** (1986), 49–72.

[85] Black, P. H., and Adams, O. E., "Machine design," Third Edition, McGraw Hill, New–York (1968), 237–241.

[86] Boresi, A. P., and Sibebottom, 0. M., Seely, F. B. and Smith, J. O., "Advanced mechanics of materials," Third Edition, , John Wiley and Sons, Toronto (1978), 471–480.

[87] Vogg, S. K. E., "Stress analysis using the ADINA package," University of Ottawa, May (1986).

[88] Selby, S., "Handbook of tables for mathematics," Fourth Edition, CRC Press, Ohio (1975), 792–795.

[89] Göhner, O., "Schubspannungsverteilung im querschnitt einer schraubenfeder," *Ingenieur Archiv.* **1** (1930), 619.

[90] Göhner, O., "Schubspannungsverteilung im querschnitt eines gedrillten ringstabs mit anwendung auf schraubenfedern," *Ingenieur Archiv.* **2** (1931), 1.

[91] Göhner, O., "Spannungsverteilung in einem an den endquerschnitten belasteten ringstabsektor," *Ingenieur Archiv.* **2** (1931), 381.

[92] Lang, H. A., "Private communication" MAY (1986).

[93] Lang, H. A., "Private communication" JULY (1986).

Appendix A

Transformation from cartesian to toroidal coordinate systems

First consider the transformation from the (x, y, z) cartesian coordinate axes to the (ρ, α, Z) cylindrical coordinate axes where the z-axis and the Z-axis remain coincident under the transformation. This represents a state of plane stress in the (x, y) plane which is parallel to the plane of the torus or elbow. Table A.1 gives the direction cosines between the axes in a transformation from the (x, y) coordinate axes to the (ρ, α) coordinate axes (Figure A.1). Hence, using Eqs. (1-4.1) and (1-4.3) in Ref. [86] on page 16–17, with Table A.1 yield the six stresses.

$$\begin{aligned}
\sigma_\rho &= \sigma_x \sin^2\alpha + \sigma_y \cos^2\alpha - 2\sigma_{xy}\cos\alpha\sin\alpha \\
\sigma_\alpha &= \sigma_x \cos^2\alpha + \sigma_y \sin^2\alpha + 2\sigma_{xy}\cos\alpha\sin\alpha \\
\sigma_Z &= \sigma_z \\
\sigma_{\rho\alpha} &= (\sigma_x - \sigma_y)\cos\alpha\sin\alpha + \sigma_{xy}(\sin^2\alpha - \cos^2\alpha) \\
\sigma_{\rho Z} &= \sigma_{yz}\cos\alpha - \sigma_{zx}\sin\alpha \\
\sigma_{\alpha Z} &= -\sigma_{yz}\sin\alpha - \sigma_{zx}\cos\alpha
\end{aligned} \tag{A.1}$$

	x	y	z
ρ	$l_1 = -\sin\alpha$	$m_1 = \cos\alpha$	$n_1 = 0$
α	$l_2 = -\cos\alpha$	$m_2 = -\sin\alpha$	$n_2 = 0$
Z	$l_3 = 0$	$m_3 = 0$	$n_3 = 1$

Table A.1: Direction cosines between (x, y, z) and (ρ, α, Z) axes.

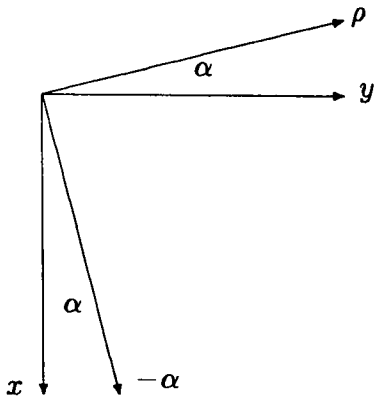

Figure A.1: Transformed (x, y) axes to (ρ, α) axes.

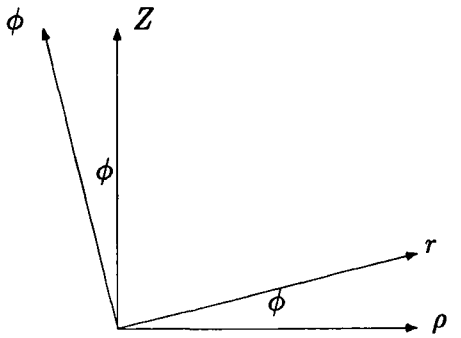

Figure A.2: Transformed (ρ, α) axes to (r, ϕ) axes.

Looking at Figure A.1 it is easily seen that the displacement transformation is given by

$$\begin{aligned} U_\alpha &= -U_x \cos\alpha - U_y \sin\alpha \\ U_\rho &= -U_x \sin\alpha + U_y \cos\alpha \\ U_Z &= U_z \end{aligned} \tag{A.2}$$

Now consider the transformation from the (ρ, α, Z) cylindrical coordinate axes to the (r, ϕ, θ) toroidal coordinate axes where the α-axis and the θ-axis remain coincident under the transformation. Similarly to the first transformation, this is a state of plane stress in the (ρ, Z). The plane (ρ, Z) is parallel to the torus or elbow cross-section plane where θ-axis is going inward. The direction cosines between the axes (see Figure A.2) in the transformation from (ρ, Z) coordinate axes to the (r, ϕ) coordinate axes are given in Table A.2. Again using Eqs. (1-4.1) and 1-4.3 in Ref. [86] in conjunction to Table A.2, we obtain

$$\begin{aligned} \sigma_r &= \sigma_\rho \cos^2\phi + \sigma_Z \sin^2\phi + 2\sigma_{Z\rho} \cos\phi \sin\phi \\ \sigma_\phi &= \sigma_\rho \sin^2\phi + \sigma_Z \cos^2\phi - 2\sigma_{Z\rho} \cos\phi \sin\phi \\ \sigma_\theta &= \sigma_\alpha \\ \sigma_{r\phi} &= -(\sigma_\rho - \sigma_Z) \cos\phi \sin\phi + \sigma_{Z\rho}(\cos^2\phi - \sin^2\phi) \end{aligned} \tag{A.3}$$

	ρ	α	Z
r	$l_1 = \cos\phi$	$m_1 = 0$	$n_1 = \sin\phi$
ϕ	$l_2 = -\sin\phi$	$m_2 = 0$	$n_2 = \cos\phi$
θ	$l_3 = 0$	$m_3 = 1$	$n_3 = 0$

Table A.2: Direction cosines between (ρ, α, Z) and (r, ϕ, θ) axes.

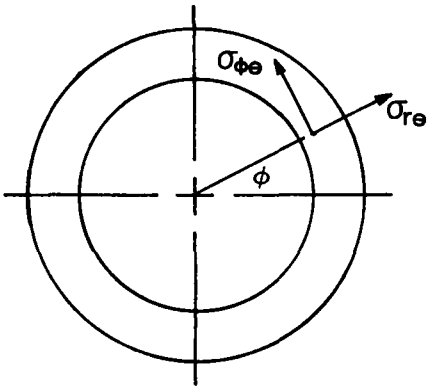

Figure A.3: Positive direction of $\sigma_{\phi\theta}$ and $\sigma_{r\theta}$.

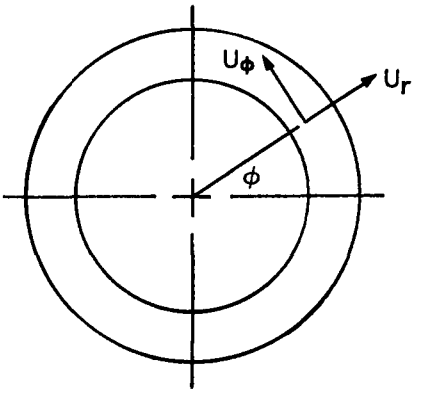

Figure A.4: Displacement U_ϕ and U_r.

$$\begin{aligned} \sigma_{r\theta} &= -1(\sigma_{\alpha Z}\sin\phi + \sigma_{\rho\alpha}\cos\phi) \\ \sigma_{\phi\theta} &= -1(\sigma_{\alpha Z}\cos\phi - \sigma_{\rho\alpha}\sin\phi) \end{aligned}$$

where $\sigma_{r\theta}$ and $\sigma_{\phi\theta}$ are multiplied by -1, so that they will be positive in the direction shown in Figure A.3.

Observing Figure A.4, the displacement transformation from cylindrical coordinate axes to toroidal coordinate axes is found to be

$$\begin{aligned} U_r &= U_\rho\cos\phi + U_Z\sin\phi \\ U_\phi &= -U_\rho\sin\phi + U_Z\cos\phi \\ U_\theta &= U_\alpha \end{aligned} \tag{A.4}$$

Substituting Eqs. (A.1) into Eqs. (A.3) and Eqs. (A.2) into Eqs. (A.4), transforms stress and displacement from cartesian coordinate system to the toroidal coordinate system.

Appendix B

Toroidal Elastic Stress Fields

Lang developed the toroidal elastic stress fields used in the present work for internal pressure problem, three end moment problems and three end force problems. Therefore, for completeness the references used ([24]–[30]) which describe Lang's work are presented in this Appendix.

B.1 Toroidal Elastic Stress Fields for Pressurized Elbows and Pipe Bends

Toroidal Elastic Stress Fields for Pressurized Elbows and Pipe Bends

H A Lang

Lang—Research West 1201 Idaho Avenue, Santa Monica CA 90403 USA

(Received 11 April 1983)

ABSTRACT

The zero order and first order stress fields are determined by toroidal elasticity methods for an elbow or pipe bend subjected to internal pressure The methods of toroidal elasticity, first introduced in 1980 at London, England are here made explicit These methods formed the basis for the numerical results presented in the earlier paper

The problem considered in this paper is one of the more difficult of the ten unit problems for a pressurized elbow or curved pipe acted upon by end loads and seismic accelerations All of these ten unit problems have now been solved The present paper complements the earlier paper The solution presented here was initially completed in 1978

NOMENCLATURE

r, ϕ, θ	Toroidal coordinates
$\sigma_r, \sigma_\phi, \sigma_\theta, \tau_{r\phi}$	Stress components
R	Toroidal radius
a	Internal radius
b	External radius
s	r/R
s_a	a/R
s_b	b/R
p	Internal pressure

Int J Pres Ves & Piping 0308-0161/84 $03.00 © Elsevier Applied Science Publishers Ltd England 1984 Printed in Great Britain

K	$ps_a^2/(s_b^2 - s_a^2)$
E, ν	Elastic constants
∇_0^2	$\frac{\partial^2}{\partial s^2} + \frac{1}{s}\frac{\partial}{\partial s} + \frac{1}{s^2}\frac{\partial^2}{\partial \phi^2}$
Θ	$\sigma_r + \sigma_\phi + \sigma_\theta$

INTRODUCTION

A serious defect of the formulae given by the ASME pressure vessel code for elbows and pipe bends is the absence of compatibility equations to determine topologically correct deformation fields The same criticism applies to finite element methods for curved pipe members From the standpoint of nuclear stress and safety, the matter deserves serious attention

It is now possible to make a rigorous numerical comparison of the stress and deformation fields of major elbows and pipe bends using the new tool of stress analysis called Toroidal Elasticity This new subject combines the three-dimensional mathematical (small strain) theory of elasticity with a toroidal geometry Its principal virtue is that it always determines the correct deformations and stresses because it contains a complete set of compatibility equations, expressed in terms of both stresses and strains The resulting model can, on both physical and mathematical grounds, be regarded as superior to methods in current use, and thus serves as a yardstick to assess if the current methods are indeed adequate

Toroidal elasticity, since it gives a consistent picture of all three displacements, all six strains and all six stresses, also generates a more accurate model of elbow ovalization This, in turn, should lead to a more accurate determination of the discontinuity stress fields between major elbows and contiguous cylindrical pipe Major sites of stress intensity can be investigated and thus may be significant for stress corrosion investigations

Since toroidal elasticity generates numerical results for 15 quantities, any complete stress analysis program is reasonably lengthy The complete analysis of a major elbow consists of ten problems—three end loaded forces, three end loaded moments, three seismic components, and pressure The present paper limits itself to the technically important problem of determining stress fields produced by internal pressure (Trivial changes can be made to account for external pressure as well)

It is a truism that the compatibility equations are lengthy However, the method of successive approximation can be applied to reduce all equations of the general theory to a set of working equations useful for solving boundary value problems in curved pipe This is the most expedient of several available approaches

The original analysis of the stresses in a pressurized elbow was completed in August 1978 An overview of the problem together with one set of numerical results (for a hockey stick heat exchanger or steam generator) was presented at the Fourth International Conference on Pressure Vessel Technology in London on 21 May 1980 [1] The solution of this problem within the scope of membrane theory had been given 20 years earlier by Flügge [2]

The present paper supplies the details of the analysis which makes use of the method of successive approximations The system of coordinates is shown in Fig 1 Each of the four stresses is represented by a series which can be expressed as

$$S(\text{total}) = S(0) + S(1) + S(0, 2) + S(2, 2) +$$

where S denotes any of the four stresses This analysis is limited to the first four terms of the series Further developments will be presented in subsequent papers

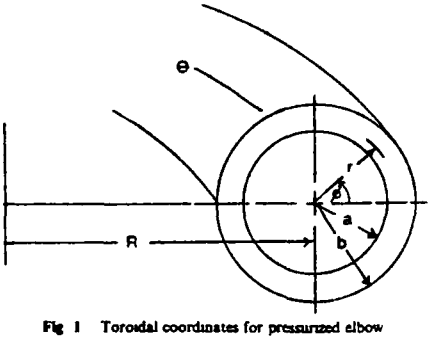

Fig 1 Toroidal coordinates for pressurized elbow

ANALYSIS

The initial stress field $S(0)$

The initial stress field $S(0)$ is identical to that for a straight cylindrical shell under internal pressure p, i e

$$\sigma_r = \frac{pa^2}{b^2 - a^2}\left(1 - \frac{b^2}{r^2}\right)$$

$$\sigma_\phi = \frac{pa^2}{b^2 - a^2}\left(1 + \frac{b^2}{r^2}\right)$$

$$\tau_{r\phi} = 0$$

To these we add the meridional stress $\sigma_\theta = pa^2/(b^2 - a^2)$ Dividing a and b by the toroidal radius R, the stresses become

$$\sigma_r = \frac{ps_a^2}{s_b^2 - s_a^2}\left(1 - \frac{s_b^2}{s^2}\right) = K\left(1 - \frac{s_b^2}{s^2}\right)$$

$$\sigma_\phi = \frac{ps_a^2}{s_b^2 - s_a^2}\left(1 + \frac{s_b^2}{s^2}\right) = K\left(1 + \frac{s_b^2}{s^2}\right)$$

$$\sigma_\theta = \frac{ps_a^2}{s_b^2 - s_a^2} = K$$

$$\tau_{r\phi} = 0$$

For convenience, we have introduced the constant $K = ps_a^2/(s_b^2 - s_a^2)$

Before continuing, we note that

$$El_r = K\left(1 - \frac{s_b^2}{s^2}\right) - \nu K\left(1 + \frac{s_b^2}{s^2}\right) - \nu K$$

and

$$El_\phi = K\left(1 + \frac{s_b^2}{s^2}\right) - \nu K\left(1 - \frac{s_b^2}{s^2}\right) - \nu K$$

For physically admissible deformations, the strain compatibility requirement is

$$\frac{\partial^2}{\partial s^2}(El_\phi) + \frac{2}{s}\frac{\partial}{\partial s}(El_\phi) - \frac{1}{s}\frac{\partial}{\partial s}(El_r) = 0$$

and is identically satisfied

To continue the analysis, we require

$$(\sigma_\theta - \sigma_r)\cos\phi = K\frac{s_b^2}{s^2}\cos\phi$$

and

$$(\sigma_\phi - \phi_\theta)\sin\phi = K\frac{s_b^2}{s^2}\sin\phi$$

These quantities constitute the right-hand sides of the next set of equilibrium equations which result from the application of the method of successive approximations

It is to be noted that the stress field $S(0)$ is an appropriate initial field of stress because it satisfies the strain compatibility requirement The incomplete toroidal elbow is in equilibrium under the action of the resultant forces due to pressure and to the stresses σ_θ acting on each of the two exposed cross sections

The stress field $S(1)$

The equilibrium equations assume the form

$$\left[\frac{1}{s}\frac{\partial(\sigma_r s)}{\partial s} + \frac{\partial\tau_{r\phi}}{\partial\phi} - \frac{\sigma_\phi}{s}\right]_1 = \frac{Ks_b^2}{s^2}\cos\phi$$

$$\left[\frac{1}{s}\frac{\partial(\sigma_\phi)}{\partial\phi} + \frac{1}{s^2}\frac{\partial}{\partial s}(\tau_{r\phi}s^2)\right]_1 = \frac{Ks_b^2}{s^2}\sin\phi$$

All terms on the left-hand side carry the subscript 1 associated with the next stress field

In addition, the stress compatibility equations are

$$\left[\nabla_0^2\sigma_r - \frac{4}{s^2}\frac{\partial\tau_{r\phi}}{\partial\phi} - \frac{2}{s^2}(\sigma_r - \sigma_\phi) + \frac{1}{1+\nu}\frac{\partial^2\Theta}{\partial s^2}\right]_1 = -2\frac{Ks_b^2}{s^3}\cos\phi$$

$$\left[\nabla_0^2\sigma_\phi + \frac{4}{s^2}\frac{\partial\tau_{r\phi}}{\partial\phi} + \frac{2}{s^2}(\sigma_r - \sigma_\phi) + \frac{1}{1+\nu}\left(\frac{\partial\Theta}{s\partial s} + \frac{1}{s^2}\frac{\partial^2\Theta}{\partial\phi^2}\right)\right]_1 = \frac{2Ks_b^2}{s^3}\cos\phi$$

$$[\nabla_0^2\sigma_\theta]_1 = 0$$

$$\left[\nabla_0^2\tau_{r\theta} + \frac{2}{s^2}\frac{\partial}{\partial\phi}(\sigma_r - \sigma_\phi) - \frac{4\tau_{r\phi}}{s^2} + \frac{1}{1+\nu}\left(\frac{1}{s}\frac{\partial^2\Theta}{\partial s\partial\phi} - \frac{1}{s^2}\frac{\partial\Theta}{\partial\phi}\right)\right]_1 = \frac{-2Ks_b^2\sin\phi}{s^3}$$

The terms on the right-hand side are, respectively, $-(\partial\sigma_\theta/\partial v)_0$, $-(\partial\sigma_\phi/\partial v)_0$, 0 and $(\sin\phi/s)(\sigma_r - \sigma_\phi)_0$ Here $\partial/\partial v$ is the operator $\cos\phi(\partial/\partial s)$ These terms arise from the method of successive approximations

Noting that $s\cos\phi$ and $(1/s)\cos\phi$ are both harmonic, the third compatibility equation determines

$$\sigma_\phi(1) = Ks_b^2(\cos\phi)\left(\lambda_1 s + \frac{\lambda_2}{s}\right)$$

We take $\sigma_\phi = -Ks_b^2(\cos\phi/s)$ as a particular solution of the equilibrium equations

From known solutions for $\nabla_0^4\Phi_1 = 0$ we select the stress function

$$\Phi_1 = Ks_b^2\left[\frac{A\lambda_0}{2s} - \frac{B\lambda_0}{2}s^3 + \lambda_0 s\ln s\right]\cos\phi$$

and define stresses

$$\sigma_r = \frac{1}{s}\frac{\partial\Phi}{\partial s} + \frac{1}{s^2}\frac{\partial^2\Phi}{\partial\phi^2}$$

$$\sigma_\phi = \frac{\partial^2\Phi}{\partial s^2}$$

$$\tau_{r\phi} = -\frac{\partial}{\partial s}\left(\frac{1}{s}\frac{\partial\Phi}{\partial\phi}\right)$$

The stress function ϕ identically satisfies the equilibrium equations and is derived directly from the theory of elasticity applicable to two-dimensional solutions in polar coordinates

Throughout the paper, stress functions Φ are introduced to provide the coefficients required for satisfying the boundary conditions

The stresses assume the form

$$\sigma_r = Ks_b^2(\cos\phi)\lambda_0\left(-\frac{A}{s^3} - Bs + \frac{1}{s}\right)$$

$$\sigma_\phi = Ks_b^2(\cos\phi)\left[\lambda_0\left(\frac{A}{s^3} - 3Bs + \frac{1}{s}\right) - \frac{1}{s}\right]$$

$$\sigma_\theta = Ks_b^2(\cos\phi)\left(\lambda_1 s + \frac{\lambda_2}{s}\right)$$

$$\tau_{r\phi} = Ks_b^2(\sin\phi)\lambda_0\left(-\frac{A}{s^3} - Bs + \frac{1}{s}\right)$$

where the particular solution has been added to σ_ϕ It remains to determine the constants λ_0, λ_1, λ_2, A and B from the compatibility equations and the boundary conditions

The boundary conditions reduce to

$$\sigma_r = 0 \quad \text{at } s = s_a \text{ and } s = s_b$$

$$\tau_{r\phi} = 0 \quad \text{at } s = s_a \text{ and } s = s_b$$

These determine

$$B = \frac{1}{s_b^2 + s_a^2} \qquad A = \frac{s_a^2 s_b^2}{s_b^2 + s_a^2}$$

The three compatibility equations are satisfied by choosing

$$\lambda_2 = (1 + 2\lambda_0\nu)$$

It remains to indicate how λ_0 and λ_1 are to be determined

It can be shown that the elbow is in equilibrium under the action of the pressure and the stress σ_θ on a cross-section Consequently subsequent solutions satisfy the condition of zero normal force, i e

$$\int_0^{2\pi}\int_{s_a}^{s_b}\sigma_\theta r\,dr\,d\phi = 0$$

or

$$\int_{s_a}^{s_b}\int_0^{2\pi}\sigma_\theta s\,ds\,d\phi = 0$$

This condition will determine λ_1 but only at the next step in the series solution

The value of λ_0 is fixed by the requirement that displacements in the cross-section are single-valued This condition is $\lambda_0 = 1/[4(1-\nu)]$

The stress field $S(0, 2)$

For the stress field (0, 2) we have $\tau_{r\phi} = 0$ and σ_r, σ_ϕ and σ_θ do not depend on ϕ. The single equilibrium equation is·

$$\left(\frac{1}{s}\frac{\partial(\sigma_r s)}{\partial s} - \frac{\sigma_\phi}{s}\right)_2 = \frac{\lambda_1 s}{2} + \frac{\lambda_0\nu}{s}$$

The three compatibility equations are

$$\left(\nabla_1^2\sigma_r - \frac{2}{s^2}(\sigma_r - \sigma_\phi) + \frac{1}{1+\nu}\frac{\partial^2\Theta}{\partial s^2}\right)_2 = \lambda_0\left(2B - \frac{1}{s^2}\right)$$

$$\left(\nabla_1^2\sigma_\phi + \frac{2}{s^2}(\sigma_r - \sigma_\phi) + \frac{1}{1+\nu}\frac{\partial\Theta}{s\partial s}\right)_2 = \lambda_0\left(2B + \frac{1}{s^2}\right)$$

$$(\nabla_1^2\sigma_\theta)_2 = \frac{4B\lambda_0}{1+\nu} - \frac{\lambda_1(2+\nu)}{1+\nu}$$

where

$$\nabla_1^2 = \frac{\partial^2}{\partial s^2} + \frac{1}{s}\frac{\partial}{\partial s}$$

For the particular solution, we take

$$\sigma_\theta = \alpha_1 s^2$$

$$\sigma_\phi = \alpha_2 s^2 + \alpha_3$$

$$\sigma_\theta = \alpha_4\ln\frac{s}{s_b} + \alpha_5 s^2$$

To satisfy the boundary conditions, we add solutions of $\nabla_0^4\Phi_0 = 0$ where

$$\Phi_0 = b_0\ln s + \frac{c_0}{2}s^2\ln s + \frac{a_0}{2}s^2$$

The stress field (0, 2) may be written in the form

$$\sigma_r = Ks_b^2\left(a_0 + \frac{b_0}{s^2} + c_0\ln\frac{s}{s_b} + \alpha_1 s^2\right)$$

$$\sigma_\phi = Ks_b^2\left(a_0 - \frac{b_0}{s^2} + c_0 + c_0\ln\frac{s}{s_b} + \alpha_2 s^2 + \alpha_3\right)$$

$$\sigma_\theta = Ks_b^2\left(\alpha_4\ln\frac{s}{s_b} + \alpha_5 s^2\right)$$

To determine the coefficients, we begin with the third compatibility equation from which

$$\alpha_5 = \frac{B\lambda_0}{1+\nu} - \frac{\lambda_1}{4}\left(\frac{2+\nu}{1+\nu}\right)$$

From the equilibrium equation, we find

$$\alpha_3 = -\lambda_0 \nu$$

and

$$3\alpha_1 - \alpha_2 = \frac{\lambda_1}{2}$$

The condition that the displacement u be single-valued reduces to $EI_\phi = E(\mathrm{d}/\mathrm{d}s)(sI_\phi)$ Expressed in terms of the stresses, this becomes the condition

$$\alpha_2(3+\nu) - \alpha_1(1+3\nu) - 2\lambda_5 = 0$$

From the two equations in α_1 and α_2, we obtain

$$\alpha_1 = \frac{B\lambda_0\nu}{4(1+\nu)} + \frac{\lambda_1}{16}\left(\frac{3+2\nu}{1+\nu}\right)$$

and

$$\alpha_2 = \frac{3B\lambda_0\nu}{4(1+\nu)} + \frac{\lambda_1(1-2\nu)}{16(1+\nu)}$$

The first compatibility equation is satisfied if

$$2c_0\nu - \alpha_4 = \lambda_0(1+\nu)(2\nu-1)$$

The condition that the displacement u is single-valued requires $2c_0 = \nu\alpha_4$ From these two equations

$$\alpha_4 = \lambda_0\frac{(1-2\nu)}{(1-\nu)}$$

$$c_0 = \frac{\nu\lambda_0(1-2\nu)}{2(1-\nu)}$$

The second compatibility equation is not required It leads to equations identical with those obtained from the first compatibility equation

The remaining two constants a_0 and b_0 are determined by the boundary condition

$$(\sigma_s)_1 = 0 \quad \text{at} \quad s = s_a \quad \text{and} \quad s = s_b$$

We find

$$a_0 = -c_0 s_a^2 \frac{\ln\left(\frac{s_b}{s_a}\right)}{(s_b^2 - s_a^2)} - \alpha_1(s_b^2 + s_a^2)$$

$$b_0 = \frac{c_0 s_a^2 s_b^2 \ln\left(\frac{s_b}{s_a}\right)}{(s_b^2 - s_a^2)} + \alpha_1 s_a^2 s_b^2$$

The last step to complete stress fields (1) and (0 2) consists of applying the condition

$$\int_{s_a}^{s_b} \sigma_\phi s\,\mathrm{d}s = 0$$

To remove the resultant force on a cross-section, we first obtain

$$\alpha_5(s_b^2 + s_a^2) = \alpha_4 - \frac{2\alpha_4 s_a^2 \ln\left(\frac{s_b}{s_a}\right)}{(s_b^2 - s_a^2)}$$

and then find

$$\lambda_1 = \frac{4B\lambda_0}{1+\nu} - \frac{4\lambda_0(1+\nu)(1-2\nu)}{(1-\nu)(2+\nu)}\frac{1}{(s_a^2+s_b^2)} + 8\lambda_0\frac{(1-2\nu)}{(2+\nu)}\frac{(1+\nu)}{(1-\nu)}\frac{s_a^2\ln\left(\frac{s_b}{s_a}\right)}{(s_b^4 - s_a^4)}$$

For the stress field (2, 2), we omit the common multiplier Ks_0^2

The stress field $S(2, 2)$

The equilibrium equations are

$$\left[\frac{1}{s}\frac{\partial\sigma_s}{\partial s} + \frac{1}{s}\frac{\partial\tau_{s\phi}}{\partial\phi} - \frac{\sigma_\phi}{s}\right]_2 = \cos 2\phi\left[\frac{\lambda_0 A}{s^3} + \frac{\lambda_0(\nu-1)}{s} + s\left(\frac{\lambda_1}{2} + B\lambda_0\right)\right]$$

$$\left[\frac{1}{s}\frac{\partial\sigma_\phi}{\partial\phi} + \frac{1}{s^2}\frac{\partial}{\partial s}(\tau_{s\phi}s^2)\right]_2 = \sin 2\phi\left[\frac{\lambda_0 A}{s^3} - \frac{\lambda_0\nu}{s} - \frac{3}{2s} - s\left(\frac{\lambda_1}{2} + B\lambda_0\right)\right]$$

In addition, the compatibility equations become

$$\nabla_0^2\sigma_r - \frac{4}{s^2}\frac{\partial\tau_{s\phi}}{\partial\phi} - \frac{2}{s^2}(\sigma_r - \sigma_\phi) + \frac{1}{1+\nu}\frac{\partial^2\Theta}{\partial s^2} = \cos 2\phi\left[-\frac{3\lambda_0 A}{s^4} - B\lambda_0 + \frac{2\lambda_0}{s^2}\right]$$

$$\nabla_0^2\sigma_\phi + \frac{4}{s^2}\frac{\partial\tau_{s\phi}}{\partial\Phi} + \frac{2}{s^2}(\sigma_r - \sigma_\phi) + \frac{1}{1+\nu}\left(\frac{1}{s}\frac{\partial\Theta}{\partial s} + \frac{1}{s^2}\frac{\partial^2\Theta}{\partial\phi^2}\right) = \cos 2\phi\left[\frac{3\lambda_0 A}{s^4} + B\lambda_0 - \frac{3}{s^2}\right]$$

$$\nabla_0^2\sigma_\theta = \cos 2\phi\left[\frac{3+2\lambda_0(1+\nu)}{s^2}\right]$$

$$\nabla_0^2\tau_{r\phi} + \frac{2}{s^2}\frac{\partial}{\partial\phi}(\sigma_r - \sigma_\phi) - \frac{4\tau_{s\phi}}{s^2} + \frac{1}{1+\nu}\left(\frac{1}{s}\frac{\partial^2\Theta}{\partial s\partial\phi} - \frac{1}{s^2}\frac{\partial\Theta}{\partial\phi}\right) = \sin 2\phi\left[-\frac{3A\lambda_0}{s^4} + \frac{\lambda_0}{s^2} + B\lambda_0 + \frac{3}{2s^2}\right]$$

The stress function Φ_2 satisfying $\nabla_0^4\Phi_2 = 0$ is

$$\Phi_2 = \left(\frac{a_2 s^4}{6} + \frac{b_2}{6s^2} + \frac{c_2 s^2}{2} + \frac{d_2}{2}\right)\cos 2\phi$$

The stresses are

$$\sigma_r = \frac{1}{s}\frac{\partial\Phi_2}{\partial s} + \frac{1}{s^2}\frac{\partial^2\Phi_2}{\partial\phi^2} = \cos 2\phi\left(-\frac{b_2}{s^4} - c_2 - \frac{2d_2}{s^2}\right)$$

$$\sigma_\phi = \frac{\partial^2\Phi_2}{\partial s^2} = \cos 2\phi\left(2a_2 s^2 + \frac{b_2}{s^4} + c_2\right)$$

$$\tau_{s\phi} = -\frac{\partial}{\partial s}\left(\frac{1}{s}\frac{\partial\Phi}{\partial\phi}\right) = \sin 2\phi\left(a_2 s^2 - \frac{b_2}{s^4} + c_2 - \frac{d_2}{s^2}\right)$$

We complete the stress field by adding

$$\sigma_r = \cos 2\phi\left(\beta_0 \ln\frac{s}{s_b} + \beta_1 + \beta_2 s^2 + \frac{\beta_3}{s^2}\right)$$

$$\sigma_\phi = \cos 2\phi\left(-\beta_0 \ln\frac{s}{s_b} + \beta_2 s^2 + \frac{\beta_3}{s^2} + \beta_4\right)$$

$$\phi_\theta = \cos 2\phi\left(\beta_5 + \beta_6 s^2 + \frac{\beta_7}{s^2}\right)$$

$$\tau_{s\phi} = \sin 2\phi\left(-\beta_0 \ln\frac{s}{s_b} + \beta_8\right)$$

to account for the particular solution

The complete stress field is

$$\sigma_r = \cos 2\phi\left[-\frac{b_2}{s^4} - c_2 - \frac{2d_2}{s^2} + \beta_0 \ln\frac{s}{s_b} + \beta_1 + \beta_2 s^2 + \frac{\beta_3}{s^2}\right]$$

$$\sigma_\phi = \cos 2\phi\left[2a_2 s^2 + \frac{b_2}{s^4} + c_2 - \beta_0 \ln\frac{s}{s_b} + \beta_2 s^2 + \frac{\beta_3}{s^2} + \beta_4\right]$$

$$\sigma_\theta = \cos 2\phi\left[\beta_5 + \beta_6 s^2 + \frac{\beta_7}{s^2}\right]$$

$$\tau_{r\phi} = \sin 2\phi\left[a_2 s^2 - \frac{b_2}{s^4} + c_2 - \frac{d_2}{s^2} - \beta_0 \ln\frac{s}{s_b} + \beta_8\right]$$

The equilibrium equations are satisfied by

$$\beta_1 + \beta_0 - \beta_4 + 2\beta_8 = \lambda_0(\nu - 1)$$

$$-2\beta_8 + 2\beta_4 + \beta_0 = \lambda_0\nu + \frac{3}{2}$$

$$\beta_2 = \frac{\lambda_1}{4} + \frac{B\lambda_0}{2}$$

$$\beta_3 = -\frac{\lambda_0 A}{2}$$

From the third compatibility equation, we find

$$\beta_5 = -\frac{1}{4}[3 + 2\lambda_0(1+\nu)]$$

The first compatibility equation determines

$$\beta_6 = -\frac{B\lambda_0}{2}(3+\nu) - \frac{\lambda_1}{2} + 2\nu a_2$$
$$\beta_7 = \tfrac{1}{2}\lambda_0 A(1-\nu) - 2d_2$$

The compatibility equations yield the three expressions

$$-6\beta_1 - 8\beta_8 + 2\beta_4 = 2\lambda_0$$
$$-6\beta_4 + 8\beta_6 + 2\beta_1 - \frac{4}{1+\nu}(\beta_1+\beta_4+\beta_5) = -3$$
$$-8\beta_8 - 4\beta_1 + 4\beta_4 + \frac{2}{1+\nu}(\beta_1+\beta_4+\beta_5) = \lambda_0 + \frac{3}{2}$$

and have the solutions

$$\beta_0 = \lambda_{01} - \frac{1}{2}\lambda_0 + \frac{3}{8}$$
$$\beta_1 = \frac{3}{4}$$
$$\beta_4 = 0$$
$$\beta_8 = -\frac{\lambda_0}{4} - \frac{9}{16}$$

The constants a_2 to d_2 are determined by the boundary conditions

$$\sigma_r = 0 \quad \text{at } s = s_a, s_b$$
$$\tau_{r\phi} = 0 \quad \text{at } s = s_a, s_b$$

Then knowing a_2 to d_2, the constants β_6 and β_7 are completely determined

The coefficients a_2, b_2, c_2 and d_2

A compact form for the coefficients is

$$f_0^2 a_2 = -6f_1 I_0 - f_2(\beta_1+\beta_8) - f_3\beta_2 + 2\beta_3$$
$$f_0^2 b_2 = 3f_1^2 f_2 I_0 + 2f_1^2(\beta_1+\beta_8) + 3f_2 f_1^2\beta_2 - f_1 f_2\beta_3$$
$$f_0^2 c_2 = s_a^2 f_4 I_0 + f_5\beta_1 + f_2 f_6\beta_2 - f_2\beta_3 + 2f_1\beta_8$$
$$f_0^2 d_2 = -2f_1 f_6 I_0 - f_1 f_2(\beta_1+\beta_8) - 2f_1 f_6\beta_2 + f_5\beta_3$$

where

$$I_0 = \frac{\beta_0 \ln(s_b/s_a)}{f_0} \qquad f_3 = (s_b^4 + s_a^4 + 4s_a^2 s_b^2)$$
$$f_0 = (s_b^2 - s_a^2) \qquad f_4 = (4s_b^4 + s_a^4 + s_a^2 s_b^2)$$
$$f_1 = (s_a^2 s_b^2) \qquad f_5 = (s_b^4 + s_a^4)$$
$$f_2 = (s_b^2 + s_a^2) \qquad f_6 = (s_b^4 + s_a^4 + s_a^2 s_b^2)$$

DISCUSSION

Toroidal elasticity is a new field using complete equations convenient for solving problems in toroidal geometries It is important to note that classical toroidal coordinates cannot be used for toroidal shells of uniform wall thickness In the present problem, the initial state of stress is admissible because it satisfies the strain compatibility requirement For state (1) it is convenient to introduce stress equilibrium and compatibility conditions For state (2), the right-hand sides of the equations contain a term $\cos^2\phi$ This must be rewritten as $\frac{1}{2}(1+\cos 2\phi)$ so that state (2) separates into a state (0, 2) and a state (2, 2) The reason why this must be done is to identify the solutions of $\nabla^4\phi = 0$ which are needed to satisfy the boundary conditions The state (0, 2) modifies the initial state Numerical calculations indicate that it is small compared with the initial state values

The next step in the converging series solutions contains $\cos^3\phi$ and is reduced to a term in $\cos\phi$ and a term in $\cos 3\phi$ We label these $S(1, 3)$ and $S(3, 3)$ respectively These terms will be presented in a subsequent paper

The essential feature of the present paper is to generate stresses at every point of an incomplete tore From the stresses, displacements are easily determined and detailed ovalization studies can be made

The work of W Flugge and others on internally pressurized toroidal shells normally ignores stress variation through the wall thickness Such work generally relies on toroidal membrane theory (and additional assumptions based on asymptotic methods in shell analysis) There is no assurance that the deformations are correct By contrast we always generate correct deformation fields because compatibility equations are applied to each term of the converging series solution

CONCLUDING REMARKS

The analysis of this paper forms the basis for numerical results presented in Ref 1 The analysis can be extended by the method of successive approximations to obtain the next two terms but the algebraic details become lengthy This extension together with a discussion of displacements and ovalization are planned for a subsequent paper

REFERENCES

1 Lang H A, Stress analysis of pressurized elbows for nuclear components using toroidal elasticity *Proc 4th Int Conf on Pressure Vessel Technology* London 1980 vol 2 pp 251–60
2 Flugge W *Stresses in Shells*, Springer-Verlag, Berlin, 1960

B.2 In-plane Bending of a Curved Pipe or Toroidal Tube Acted on by End Couples

In-plane Bending of a Curved Pipe or Toroidal Tube Acted on by End Couples

H A Lang

LANG—Research West 1201 Idaho Avenue,
Santa Monica CA 90403 USA

(Received 1 February 1983)

ABSTRACT

Stresses, strains and displacements are determined for a toroidal tube or pipe bend acted upon by end bending moments such that the deformation is in the plane of the tube The methods of toroidal elasticity are used so that the solution satisfies compatibility equations The analysis in this paper is limited to the first-order state resulting from application of the method of successive approximation

NOMENCLATURE

r, ϕ, θ	Toroidal coordinates
$\sigma_r, \sigma_\phi, \sigma_\theta, \tau_{r\phi}$	Stress components
$l_r, l_\phi, l_\theta, l_{r\phi}$	Strain components
u, v	Displacements
R	Toroidal radius
b	Outer radius
a	Inner radius
s	r/R
c	Constant
Φ	Stress function
E	Elastic constants
I_D	Moment of inertia
M	Bending moment
N	Normal force

Int J Pres Ves & Piping 0308 161 84 $03 00 © Elsevier Applied Science Publishers Ltd England 1984 Printed in Great Britain

INTRODUCTION

This paper considers a toroidal tube or pipe bend which is acted upon by end bending moments, M, as shown in Fig 1 Bending is in the plane of the tube The nomenclature for any cross-section is shown in Fig 2 which exhibits the toroidal radius R and the cross-section radii a and b The toroidal coordinates of a point are specified by r, ϕ while θ is the meridional coordinate but is not required for the problem of this paper The angle ϕ is positive in a counterclockwise sense as measured from an outer radial line

The analysis which follows is based on the theory of toroidal elasticity applied to isotropic materials The complete theory is expanded in powers of $1/R$ by the method of successive approximations This procedure generates the equilibrium and compatibility equations used in the present analysis

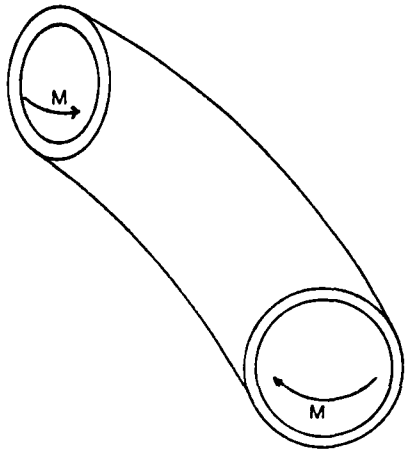

Fig 1 End couples acting on curved pipe

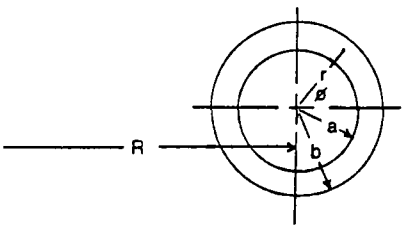

Fig 2 Nomenclature for pipe cross-section

THE INITIAL STATE (0)

Corresponding to pure bending of a prismatic bar, we assume an initial state of stress $\sigma_r = \sigma_\phi = \tau_{r\phi} = 0$ and $\sigma_{\theta_0} = cERs\cos\phi$ The normal force over a cross-section is

$$N = \int_a^b \int_0^{2\pi} \sigma_{\theta_0} r\,dr\,d\phi = R^2 \int_{s_a}^{s_b} \int_0^{2\pi} (\sigma_\theta)_0 s\,ds\,d\phi$$

or

$$N = cER^3 \int_{s_a}^{s_b} \int_0^{2\pi} s^2 \cos\phi\,ds\,d\phi = 0$$

The bending moment over a cross-section is

$$M = \int_a^b \int_0^{2\pi} (\sigma_{\theta_0} r\cos\phi) r\,dr\,d\phi$$

or

$$M = cER^4 \int_{s_a}^{s_b} \int_0^{2\pi} (s\cos^2\phi) s\,ds\,d\phi = cER^4\pi \int_{s_a}^{s_b} s^3\,ds$$

or

$$M = cER^4 \frac{\pi(s_b^4 - s_a^4)}{4} = cEI_D$$

Hence $cE = M/I_D$

THE STRESS STATE (1)

To determine the next stress field, we have the equilibrium equations of toroidal elasticity

$$\begin{aligned} \left(\frac{\partial(\sigma_r s)}{s\partial s} + \frac{\partial\tau_{r\phi}}{s\partial\phi} - \frac{\sigma_\phi}{s}\right)_1 &= cERs\cos^2\phi \\ \left(\frac{1}{s}\frac{\partial\sigma_\phi}{\partial\phi} + \frac{1}{s^2}\frac{\partial}{\partial s}(\tau_{r\phi}s^2)\right)_1 &= -cERs\sin\phi\cos\phi \end{aligned} \tag{1}$$

All terms on the left-hand side refer to the stress state (1)

For a particular solution, we take

$$\sigma_r = cER\left(\frac{3+2\nu}{16(1+\nu)}s^2\right) + cER\frac{s^2}{4}\cos 2\phi$$

$$\sigma_\phi = cER\left(\frac{1-2\nu}{16(1+\nu)}s^2\right) - cER\frac{s^2}{4}\cos 2\phi$$

$$\tau_{r\phi} = -cER(\sin 2\phi)\frac{s^2}{4}$$

The next step consists of satisfying the stress compatibility equations

Stress compatibility equations of toroidal elasticity

$$\begin{aligned} \left(\nabla_0^2\sigma_r - \frac{4}{s^2}\frac{\partial\tau_{r\phi}}{\partial\phi} - \frac{2}{s^2}(\sigma_r - \sigma_\phi) + \frac{1}{1+\nu}\frac{\partial^2\Theta}{\partial s^2}\right)_1 &= 0 \\ \left(\nabla_0^2\sigma_\theta + \frac{4}{s^2}\frac{\partial\tau_{r\phi}}{\partial\phi} + \frac{2}{s^2}(\sigma_r - \sigma_\phi) + \frac{1}{1+\nu}\left(\frac{1}{s}\frac{\partial\Theta}{\partial s} + \frac{1}{s^2}\frac{\partial^2\Theta}{\partial\phi^2}\right)\right)_1 &= 0 \\ \nabla_0^2\sigma_{\theta_1} = -cER\left(\frac{2+\nu}{1+\nu}\right) & \\ \left(\nabla_0^2\tau_{r\phi} + \frac{2}{s^2}\frac{\partial}{\partial\phi}(\sigma_r - \sigma_\theta) - \frac{4\tau_{r\phi}}{s^2} + \frac{1}{1+\nu}\frac{\partial}{\partial\phi}\left(\frac{1}{s}\frac{\partial}{\partial s} - \frac{1}{s^2}\right)\Theta\right)_1 &= 0 \end{aligned} \tag{2}$$

where $\Theta = \sigma_{r_1} + \sigma_{\phi_1} + \sigma_{\theta_1}$

and $\nabla_0^2 = \frac{\partial^2}{\partial s^2} + \frac{1}{s}\frac{\partial}{\partial s} + \frac{1}{s^2}\frac{\partial^2}{\partial\phi^2}$

Solutions for the compatibility equations may be found by taking solutions of $\nabla_0^4\Phi = 0$ where

$$\Phi = B_0 s^2 + C_0 \ln s + \cos 2\phi\left(A_2 s^2 + \frac{B_2}{s^2} + C_2 s^4 + D_2\right)$$

The associated stresses are

$$\sigma_r = \frac{1}{s}\frac{\partial\Phi}{\partial s} + \frac{1}{s^2}\frac{\partial^2\Phi}{\partial\phi^2} = 2B_0 + \frac{C_0}{s^2} + \cos 2\phi\left(-2A_2 - \frac{6B_2}{s^4} - \frac{4D_2}{s^2}\right)$$

$$\sigma_\phi = \frac{\partial^2\Phi}{\partial s^2} = 2B_0 - \frac{C_0}{s^2} + \cos 2\phi\left(2A_2 + \frac{6B_2}{s^4} + 12C_2 s^2\right) \quad (3)$$

$$\tau_{r\phi} = -\frac{\partial}{\partial s}\left(\frac{1}{s}\frac{\partial\Phi}{\partial\phi}\right) = \sin 2\phi\left(2A_2 - \frac{6B_2}{s^4} + 6C_2 s^2 - \frac{2D_2}{s^2}\right)$$

The coefficients $B_0, C_0, A_2, B_2, C_2, D_2$ are determined from the boundary conditions

$$\sigma_r = 0 \quad \text{at } s = s_a \quad \text{and} \quad s = s_b$$
$$\tau_{r\phi} = 0 \quad \text{at } s = s_a \quad \text{and} \quad s = s_b$$

for which the particular solutions are added to the stress field found from Φ

Summary of coefficients determined by boundary conditions

$$B_0 = -\frac{3+2\nu}{32(1+\nu)}(s_b^2 + s_a^2)$$

$$C_0 = \frac{3+2\nu}{1+\nu}\frac{s_a^2 s_b^2}{16}$$

$$A_2 = \frac{(s_b^2+s_a^2)(s_b^4+s_a^4+s_a^2 s_b^2)}{8(s_b^2-s_a^2)^2}$$

$$B_2 = \frac{s_a^4 s_b^4(s_b^2+s_a^2)}{8(s_b^2-s_a^2)^2}$$

$$C_2 = -\frac{1}{4}\frac{s_a^2 s_b^2}{(s_b^2-s_a^2)^2}$$

$$D_2 = -\frac{s_a^2 s_b^2(s_b^4+s_a^4+s_a^2 s_b^2)}{4(s_b^2-s_a^2)^2}$$

These results represent the conclusion of the present analysis Extension of the results to the next (second order) term is deferred for a subsequent paper It is also planned to present numerical results based on a computer program which uses the equations of this paper

Summary of stresses

$$\sigma_{r_1} = \frac{MR}{I_D}\left[\frac{(3+2\nu)s^2}{16(1+\nu)} + \left(\frac{3+2\nu}{1+\nu}\right)\frac{s_a^2 s_b^2}{16s^2} - \frac{1}{16}\left(\frac{3+2\nu}{1+\nu}\right)(s_b^2+s_a^2)\right]$$
$$+\frac{MR}{I_D}\cos 2\phi\left[-\frac{1}{4}\frac{s_b^2+s_a^2}{(s_b^2-s_a^2)^2}(s_b^4+s_a^4+s_a^2 s_b^2) - \frac{3}{4}\frac{s_a^4 s_b^4(s_b^2+s_a^2)}{s^4(s_b^2-s_a^2)^2}\right]$$
$$+\frac{MR\cos 2\phi}{I_D}\left[\frac{s_a^2 s_b^2(s_b^4+s_a^4+s_a^2 s_b^2)}{s^2(s_b^2-s_a^2)^2} + \frac{s^2}{4}\right]$$

$$\sigma_{\phi_1} = \frac{MR}{I_D}\left[\frac{(1-2\nu)s^2}{16(1+\nu)} - \frac{1}{16}\frac{(3+2\nu)(s_b^2+s_a^2)}{1+\nu} - \frac{(3+2\nu)s_a^2 s_b^2}{16(1+\nu)s^2}\right]$$
$$+\frac{MR}{I_D}\cos 2\phi\left[\frac{(s_b^2+s_a^2)(s_b^4+s_a^4+s_a^2 s_b^2)}{4(s_b^2-s_a^2)^2} + \frac{3}{4}\frac{s_a^4 s_b^4(s_b^2+s_a^2)}{s^4(s_b^2-s_a^2)^2}\right]$$
$$+\frac{MR}{I_D}\cos 2\phi\left[\frac{-3s^2 s_a^2 s_b^2}{(s_b^2-s_a^2)^2} - \frac{s^2}{4}\right]$$

$$(\tau_{r\phi})_1 = \frac{MR}{I_D}\sin 2\phi\left[-\frac{s^2}{4} + \frac{(s_b^2+s_a^2)(s_b^4+s_a^4+s_a^2 s_b^2)}{4(s_b^2-s_a^2)^2}\right.$$
$$\left.-\frac{3}{4}\frac{s_a^4 s_b^4(s_b^2+s_a^2)}{s^4(s_b^2-s_a^2)^2} - \frac{3}{2}\frac{s_a^2 s_b^2 s^2}{(s_b^2-s_a^2)^2} + \frac{s_a^2 s_b^2(s_b^4+s_a^4+s_a^2 s_b^2)}{2s^2(s_b^2-s_a^2)^2}\right]$$

$$\sigma_\theta = \frac{MR}{I_D}s\cos\phi + \frac{MR}{I_D}\left[\frac{2+\nu}{8(1+\nu)}(s_b^2+s_a^2) - \frac{(2+\nu)s^2}{4(1+\nu)} - \frac{s^2(1+\nu)}{2}\cos 2\phi\right]$$
$$+\frac{MR}{I_D}\cos 2\phi\left[-\frac{3\nu s_a^2 s_b^2 s^2}{(s_b^2-s_a^2)^2} + \frac{\nu}{s^2}\frac{s_a^2 s_b^2(s_b^4+s_a^4+s_a^2 s_b^2)}{(s_b^2-s_a^2)^2}\right]$$

Solution of compatibility equations

The solution of the third compatibility equation may be taken in the form

$$\sigma_{\theta_1} = -\frac{2+\nu}{4(1+\nu)}s^2 + \lambda_0 + \lambda_1(\cos 2\phi)s^2 + \lambda_2\frac{\cos 2\phi}{s^2}$$

where λ_0, λ_1 and λ_2 are to be determined

The first compatibility equation reduces to

$$\frac{2+\nu}{2(1+\nu)} - (1+\nu)\cos 2\phi - \nu\cos 2\phi\left(24C_2 - 24\frac{D_2}{s^4}\right) + \frac{\partial^2\sigma_{\theta_1}}{\partial s^2} = 0$$

This can be satisfied by

$$\lambda_1 = 12C_2\nu - \frac{1+\nu}{2}$$
$$\lambda_2 = -4D_2\nu$$

The coefficient $\lambda_0 = [(2+\nu)/8(1+\nu)](s_b^2+s_a^2)$, following from the condition that the normal force, N, over a cross-section vanishes The complete equation for σ_{θ_1} is

$$\sigma_{\theta_1} = cER\left[\frac{2+\nu}{8(1+\nu)}(s_b^2+s_a^2) - \frac{2+\nu}{4(1+\nu)}s^2 - s^2\frac{(1+\nu)}{2}\cos 2\phi\right]$$
$$+cER\nu\cos 2\phi\left[\frac{-3s_a^2 s_b^2 s^2}{(s_b^2-s_a^2)^2} + \frac{1}{s^2}\frac{s_a^2 s_b^2(s_b^4+s_a^4+s_a^2 s_b^2)}{(s_b^2-s_a^2)^2}\right]$$

The second and fourth compatibility equations are identically satisfied The equation for σ_{θ_1} does not lead to a resultant force, N, or a resultant bending moment, M

CONCLUSION

The stresses are summarized in the next section Knowing the stresses, the determination of strains is straightforward and obvious Then by differentiation and integration we may also find the two components of displacement, u and v

Summary of strains

$$l_{r_1} = cR\left[\frac{3(1+2\nu)s^2}{16} - \frac{2\nu(2+\nu)}{16(1+\nu)}(s_a^2+s_b^2) + 2B_0(1+\nu) + \frac{C_0}{s^2}(1+\nu)\right]$$
$$+cR\cos 2\phi\left[\frac{s^2}{4}(1+\nu)(1+2\nu) - 2A_2(1+\nu)\right.$$
$$\left.-\frac{6B_2}{s^4}(1+\nu) - 12C_2 s^2\nu(1+\nu) - \frac{4D_2}{s^2}(1-\nu^2)\right]$$

$$l_{\phi_1} = cR\left[\frac{(1+2\nu)s}{16} - \frac{\nu(2+\nu)}{8(1+\nu)}(s_a^2+s_b^2) + 2B_0(1-\nu) - \frac{C_0}{s}(1+\nu)\right]$$
$$+cR\cos 2\phi\left[\frac{s^2}{4}(1+\nu)(2\nu-1) + 2A_2(1+\nu)\right.$$
$$\left.+\frac{6B_2(1+\nu)}{s^4} + 12C_2 s^2(1-\nu^2) + \frac{4D_2}{s^2}\nu(1+\nu)\right]$$

$$l_{\theta_1} = cR\left[\frac{2+\nu}{8(1+\nu)}(s_a^2+s_b^2) - \frac{s^2}{2} - 4\nu B_0\right]$$
$$+cR\cos 2\phi(1+\nu)\left[12C_2 s^2 - \frac{s^2}{2} - \frac{4D_2}{s^2}\right]$$

$$l_{r\phi_1} = cR\sin 2\phi\left[-\frac{s^2}{2}(1+\nu) + 4A_2(1+\nu) - \frac{12B_2}{s^4}(1+\nu)\right.$$
$$\left.+12(1+\nu)C_2 s^2 - \frac{4D_2}{s^2}(1+\nu)\right]$$

$$l_{r_0} = l_{\phi_0} = -\nu cRs\cos\phi$$
$$l_{r\phi_0} = 0$$
$$l_{\theta_0} = cRs\cos\phi$$

Summary of displacements

$$u_1 = cR^2\left[\frac{1+2\nu}{16}s^3 - \frac{\nu(2+\nu)(s_a^2+s_b^2)s}{8(1+\nu)} + 2B_0 s(1+\nu) - \frac{C_0}{s}(1+\nu)\right]$$
$$+cR^2\cos 2\phi\left[\frac{s^3}{12}(1+\nu)(1+2\nu) - 2A_2 s(1+\nu) + \frac{2B_2}{s^3}(1+\nu)\right.$$
$$\left.-4C_2 s^3\nu(1+\nu) + \frac{4D_2}{s}(1-\nu^2)\right]$$

$$w_1 = cR^2 \sin 2\phi \left[-\frac{s^3}{6}(1-\nu^2) + 2A_2 s(1+\nu) + \frac{2B_2(1+\nu)}{s^3} + 2C_2 s^3(1+\nu)(3-2\nu) + \frac{2D_2}{s}(2\nu-1)(1+\nu) \right]$$

$$u_0 = -\nu c R^2 \frac{s^2}{2} \cos\phi$$

$$v_0 = -\nu c R^2 \frac{s^2}{2} \sin\phi$$

BIBLIOGRAPHY

Toroidal elasticity was introduced in

1 Lang, H A, Stress analysis of pressurized elbows for nuclear components using toroidal elasticity, *Proc 4th Int Conf Pressure Vessel Technology*, London, 1980, Vol 2, pp 251–60

The related problem of a solid circular ring sector was considered by Gohner in Refs 2–4

2 Gohner, O, Schubspannungsverteilung im Querschnitt einer Schraubenfeder, *Ing Archiv*, 1 (1930) 619

3 Göhner, O, Schubspannungsverteilung im Querschnitt eines gedrillten Ringstabs mit Anwendung auf Schraubenfedern, *Ing Archiv*, 2 (1931) 1

4 Göhner, O, Spannungsverteilung in einem an den Endquerschnitten belasteten Ringstabsektor, *Ing Archiv*, 9 (1938) 355

A compact account is given in

5 Timoshenko, S and Goodier, J N, *Theory of elasticity*, 2nd Ed, New York, McGraw–Hill, 1951, pp 395–8

B.3 Stress Fields for a Curved Pipe Subjected to In-plane End Couples

Stress Fields for a Curved Pipe Subjected to In-plane End Couples

H A Lang

LANG—Research West 1201 Idaho Avenue
Santa Monica CA 90403 USA

(Received 7 March 1983)

ABSTRACT

The present paper extends the stress fields derived in an earlier paper entitled 'In-plane bending of a curved pipe or toroidal tube acted on by end couples' (see Ref 1) The methods of Toroidal Elasticity are used Both the present and the earlier paper jointly provide the foundation for computer programs to determine not only stresses but strains displacements and ovalization effects

NOMENCLATURE

r, ϕ, θ	Toroidal coordinates
$\sigma_r, \sigma_\phi, \sigma_\theta$	Normal stresses
$\tau_{r\phi}, \tau_{r\theta}, \tau_{\phi\theta}$	Shear stresses
R	Toroidal radius
s	r/R
Θ	$\sigma_r + \sigma_\phi + \sigma_\theta$
∇^2	$\frac{\partial^2}{\partial s^2} + \frac{1}{s}\frac{\partial}{\partial s} + \frac{1}{s^2}\frac{\partial^2}{\partial \phi^2}$
$\frac{\partial}{\partial q}$	$\cos\phi \frac{\partial}{\partial s} - \frac{\sin\phi}{s}\frac{\partial}{\partial \phi}$
a	Inner radius
b	Outer radius

Int J Pres Ves & Piping 0308-0161/84/$03.00 © Elsevier Applied Science Publishers Ltd 1984 Printed in Great Britain

INTRODUCTION

When a hollow curved pipe is bent by end couples (Fig 1) in the plane of the pipe, the stress fields of toroidal elasticity may be expressed by a converging series

$$S(\text{Total}) = S(0) + S(1) + S(2) + S(3) +$$

where S is any stress The stresses $S(0)$ and $S(2)$ were determined in a previous paper [1] The objective of the present paper is to determine the stress fields $S(1)$ and $S(3)$

Toroidal elasticity was first introduced in 1980 [2] It is based on the toroidal elastic coordinates defined in Fig 2 The working equations of the current paper are developed by expanding the equilibrium and compatibility equations of toroidal elasticity in powers of $1/R$ where R is the toroidal radius

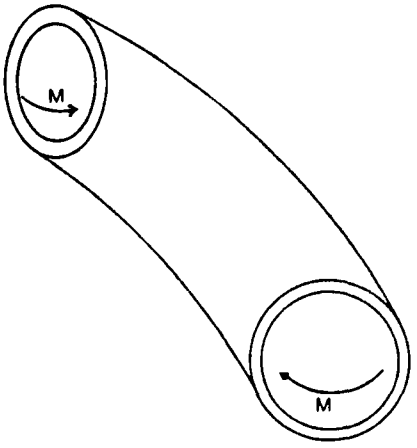

Fig 1 End couples acting on curved pipe

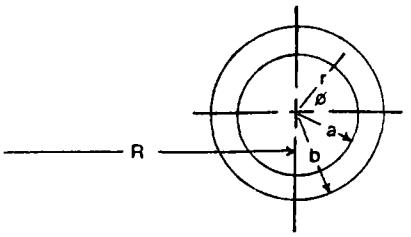

Fig 2 Nomenclature for pipe cross section

EQUILIBRIUM EQUATIONS

For the problem of a curved pipe bent by end couples the equilibrium equations are

$$\left[\frac{\partial(\sigma_r s)}{s\,\partial s} + \frac{1}{s}\frac{\partial \tau_{r\phi}}{\partial \phi} - \frac{\sigma_\phi}{s}\right]_{1,3} = N(1)$$
$$\left[\frac{\partial \sigma_\phi}{s\,\partial \phi} + \frac{1}{s^2}\frac{\partial(\tau_{r\phi} s^2)}{\partial s}\right]_{1,3} = N(2) \tag{1}$$

The functions $N(1)$ and $N(2)$ are developed in the Appendix Those functions separate into two parts One part is multiplied by functions $\cos\phi$ and $\sin\phi$ which determine the field of stress $S(1)$ The other part is multiplied by functions $\cos 3\phi$ and $\sin 3\phi$ which determine the field of stress $S(3)$

COMPATIBILITY EQUATIONS

The compatibility equations for the current problem are

$$\left[\nabla^2\sigma_r - \frac{4}{s^2}\frac{\partial \tau_{r\phi}}{\partial \phi} - \frac{2}{s^2}(\sigma_r - \sigma_\phi) + \frac{1}{1+\nu}\frac{\partial^2\Theta}{\partial s^2}\right]_{1,3} = V(1)$$
$$\left[\nabla^2\sigma_\phi + \frac{4}{s^2}\frac{\partial \tau_{r\phi}}{\partial \phi} + \frac{2}{s^2}(\sigma_r - \sigma_\phi) + \frac{1}{1+\nu}\left(\frac{1}{s}\frac{\partial\Theta}{\partial s} + \frac{1}{s^2}\frac{\partial^2\Theta}{\partial \phi^2}\right)\right]_{1,3} = V(2)$$
$$[\nabla^2\sigma_\theta]_{1,3} = V(3)$$

$$\left[\nabla^2\tau_{r\phi} + \frac{2}{s^2}\frac{\partial}{\partial \phi}(\sigma_r - \sigma_\phi) - \frac{4\tau_{r\phi}}{s^2} + \frac{1}{1+\nu}\left(\frac{\partial^2\Theta}{s\,\partial s\,\partial\phi} - \frac{1}{s^2}\frac{\partial\Theta}{\partial\phi}\right)\right]_{1,3} = V(4) \tag{2}$$

where

$$\nabla^2 = \frac{\partial^2}{\partial s^2} + \frac{1}{s}\frac{\partial}{\partial s} + \frac{1}{s^2}\frac{\partial^2}{\partial\phi^2}$$
$$\Theta = \sigma_r + \sigma_\phi + \sigma_\theta$$

The functions $V(1)$ to $V(4)$ are developed in the Appendix and also separate into two parts associated with the two solutions $S(1)$ and $S(3)$

STRESSES FOR TERMS IN $\cos\phi$ AND $\sin\phi$

To develop the field of stress corresponding to terms in $\cos\phi$ and $\sin\phi$ we assume that

$$\sigma_r = \beta_1 \cos\phi\left[s^3 + s_b^2 s_a^2 - s(s_a^2 + s_b^2)\right]$$
$$\sigma_\phi = \cos\phi\left[\beta_2 s^3 + \frac{\beta_3}{s} + \beta_4 s(s_a^2 + s_b^2)\right]$$
$$\sigma_\theta = \cos\phi\left[\beta_6 s^3 + \frac{\beta_7}{s}\right] \tag{3}$$
$$\tau_{r\phi} = \beta_5 \sin\phi\left[s^3 + \frac{s_b^2 s_a^2}{s} - s(s_a^2 + s_b^2)\right]$$

Note that σ_r and $\tau_{r\phi}$ vanish on the boundaries
The first equilibrium equation leads to

$$4\beta_1 + \beta_5 - \beta_2 = K_1 \tag{4}$$
$$\beta_5 s_a^2 s_b^2 - \beta_3 = K_3 \tag{5}$$
$$(-\beta_4 - 2\beta_1 - \beta_5)(s_b^2 + s_a^2) = K_2 \tag{6}$$

where the coefficients K_1 to K_4 are derived in the Appendix
The second equilibrium equation leads to two additional equations

$$5\beta_5 - \beta_2 = K_4 \tag{7}$$
$$-(\beta_4 + 3\beta_5)(s_a^2 + s_b^2) = -K_2 \tag{8}$$

Adding eqns (6) and (8) leads to

$$\beta_4 = -\beta_1 - 2\beta_5 \tag{9}$$

Taking $\beta_3 = \beta_5 s_a^2 s_b^2 - K_3$ the equilibrium equations remaining reduce to

$$\begin{aligned} 4\beta_1 + \beta_2 - \beta_2 &= K_1 \\ 5\beta_5 - \beta_2 &= K_4 \\ \beta_5 - \beta_1 &= \frac{K_2}{s_b^2 + s_a^2} \end{aligned} \tag{10}$$

These are not independent because the following relation exists

$$K_1 - K_4 = -\frac{4K_2}{s_b^2 + s_a^2}$$

This condition can be reduced to

$$\frac{1}{4} - 3C_2 = \frac{2A_2}{s_b^2 + s_a^2} \tag{11}$$

From the compatibility equation $\nabla^2\sigma_\theta = V(3)$, we obtain

$$8\beta_6 = \frac{15 + 13\nu + 2\nu^2}{2(1+\nu)} - 24C_2(1+\nu)$$

or

$$\beta_6 = -3C_2(1+\nu) + \frac{15 + 13\nu + 2\nu^2}{16(1+\nu)} \tag{12}$$

Forming linear combinations of the remaining three compatibility equations, a single equation results

$$\beta_2 + \beta_5 = \frac{1+2\nu}{16(1+\nu)} - 3C_2 \tag{13}$$

We thus find

$$\begin{aligned} \beta_5 &= \frac{K_4}{6} + \frac{1+2\nu}{96(1+\nu)} - \frac{C_2}{2} \\ \beta_2 &= -\frac{K_4}{6} + \frac{5(1+2\nu)}{96(1+\nu)} - \frac{5}{2}C_2 \end{aligned} \tag{14}$$

and then

$$\beta_1 = \frac{1+2\nu}{96(1+\nu)} - \frac{C_2}{2} - \frac{K_4}{12} + \frac{K_1}{4} \tag{15}$$

Finally, β_7 is determined from the compatibility equation

$$-s_a^2 s_b^2(2\beta_5 + \beta_1) + \beta_3 + \frac{1}{1+\nu}(\beta_3 + \beta_7 + 2\beta_1 s_a^2 s_b^2) = C_0 + D_2 \tag{16}$$

The coefficients β_1 to β_7 are summarized below

$$\begin{aligned} \beta_1 &= \frac{K_1}{4} - \frac{K_4}{12} - \frac{C_2}{2} + \frac{1+2\nu}{96(1+\nu)} \\ \beta_2 &= -\frac{K_4}{6} - \frac{5}{2}C_2 + \frac{5(1+2\nu)}{96(1+\nu)} \\ \beta_3 &= s_a^2 s_b^2 \beta_5 - K_3 \\ \beta_4 &= -\frac{K_1}{4} - \frac{K_4}{4} + \frac{3}{2}C_2 - \frac{1+2\nu}{32(1+\nu)} \\ \beta_5 &= \frac{K_4}{6} - \frac{C_2}{2} + \frac{1+2\nu}{96(1+\nu)} \\ \beta_6 &= \frac{3+\nu}{16(1+\nu)} + \frac{4+\nu}{8} - 3C_2(1+\nu) \\ \beta_7 &= (C_0 + D_2)(1+\nu) + (1+2\nu)\beta_5 s_a^2 s_b^2 + 2\beta_1 \nu s_a^2 s_b^2 + K_3(3+2\nu) \end{aligned}$$

STRESSES FOR TERMS IN $\cos 3\phi$ AND $\sin 3\phi$

To determine the field of stress corresponding to terms in $\cos 3\phi$ and $\sin 3\phi$, we assume that

$$\begin{aligned} \sigma_r &= \cos 3\phi\left[\bar\beta_1 s^3 + \frac{\bar\beta_2}{s} + \frac{\bar\beta_3}{s^3} - A_3 s - C_3 s^3 - \frac{5D_3}{s^3} - \frac{B_3}{s^5}\right] \\ \sigma_\phi &= \cos 3\phi\left[\bar\beta_4 s^3 + \frac{\bar\beta_5}{s} + \frac{\bar\beta_6}{s^3} + A_3 s + 5C_3 s^3 + \frac{D_3}{s^3} + \frac{B_3}{s^5}\right] \\ \tau_{r\phi} &= \sin 3\phi\left[\bar\beta_7 s^3 + \frac{\bar\beta_8}{s} + \frac{\bar\beta_9}{s^3} + A_3 s + 3C_3 s^3 - \frac{3D_3}{s^3} - \frac{B_3}{s^5}\right] \\ \sigma_\theta &= \cos 3\phi\left[\bar\beta_{10} s^3 + \frac{\bar\beta_{11}}{s} + \frac{\bar\beta_{12}}{s^3}\right] \end{aligned} \tag{17}$$

Here $\bar\beta_1$ to $\bar\beta_{12}$ will be determined by the particular solution while A_3 to D_3 are fixed by the boundary conditions

The third compatibility equation is

$$\nabla^2\sigma_\theta = V(3)$$

from which

$$\bar\beta_{11} = D_2(1+\nu) \tag{18}$$

The first equilibrium equation leads to

$$\begin{aligned} 4\bar\beta_1 + 3\bar\beta_3 - \bar\beta_4 &= K_5 \\ -2\bar\beta_3 + 3\bar\beta_9 - \bar\beta_6 &= 6B_2 \\ 3\bar\beta_8 - \bar\beta_5 &= (3-2\nu)D_2 \end{aligned} \tag{19}$$

The second equilibrium equation leads to

$$\begin{aligned} 5\bar\beta_7 - 3\bar\beta_4 &= -K_5 \\ \bar\beta_8 - 3\bar\beta_5 &= (1+2\nu)D_2 \\ -\bar\beta_9 - 3\bar\beta_6 &= 6B_2 \end{aligned} \tag{20}$$

We first find

$$\bar\beta_5 = -\nu D_2 \tag{21}$$

$$\bar\beta_8 = (1-\nu)D_2 \tag{22}$$

For a particular solution, the first compatibility equation requires

$$\bar\beta_{12} = -4\nu D_3 \tag{23}$$

The first compatibility equation can be reduced to

$$\begin{aligned} -12\bar\beta_9 - 2(\bar\beta_3 - \bar\beta_6) + \frac{12}{1+\nu}(\bar\beta_3 + \bar\beta_6) &= -24B_2 \\ -12\bar\beta_7 - \frac{96\nu C_3}{1+\nu} - 2(\bar\beta_1 - \bar\beta_4) + \frac{6}{1+\nu}(\bar\beta_1 + \bar\beta_4 + \bar\beta_{10}) &= 6C_2 - \frac{3}{4} \end{aligned} \tag{24}$$

From eqns (19), (20) and (24), we find

$$\begin{aligned} \bar\beta_3 &= \frac{\nu - 5}{2\nu} B_2 \\ \bar\beta_6 &= \frac{1-5\nu}{2\nu} B_2 \\ \bar\beta_9 &= \frac{3(\nu-1)}{2\nu} B_2 \end{aligned}$$

From eqns (19), (20) and (24), we also find

$$\begin{aligned} \bar\beta_{10} &= (1+\nu)(C_2 - \tfrac{1}{8}) + 4\nu C_3 \\ \bar\beta_1 &= \frac{2\nu - 1}{6\nu} K_5 \\ \bar\beta_4 &= \frac{5+2\nu}{6\nu} K_5 \\ \bar\beta_7 &= \frac{1}{2\nu} K_5 \end{aligned}$$

From a linear combination of the compatibility equations we find

$$\bar\beta_2 + \bar\beta_8 = D_2$$

or

$$\bar\beta_2 = \nu D_2$$

The remaining compatibility equations do not yield any new expressions for the coefficients $\bar\beta_1$ to $\bar\beta_{12}$.

Next, using the four boundary conditions,

$$\begin{aligned} \sigma_r &= 0 \qquad \text{at } s = s_a, s_b \\ \tau_{r\phi} &= 0 \qquad \text{at } s = s_a, s_b \end{aligned}$$

we determine A_3 to D_3. First take

$$\begin{aligned} \lambda_1 &= s_b^4 + s_a^4 + s_a^2 s_b^2 \\ \lambda_2 &= (s_b^4 + s_a^4)(s_a^2 + s_b^2) \\ \lambda_3 &= s_b^2 + s_a^2 \end{aligned}$$

and define functions

$$\begin{aligned} R_1 &= \lambda_2\bar\beta_1 + \lambda_3\bar\beta_2 + \bar\beta_3 \\ R_2 &= \lambda_1\bar\beta_1 + \bar\beta_2 \\ R_3 &= \lambda_2\bar\beta_9 + \lambda_3\bar\beta_8 + \bar\beta_9 \\ R_4 &= \lambda_1\bar\beta_7 + \bar\beta_8 \end{aligned}$$

Then

$$A_3=\frac{6\lambda_1R_1-10\lambda_1R_3+9\lambda_2(R_4-R_2)}{2(8\lambda_1^2-9\lambda_2\lambda_3)}$$

$$B_3=\frac{s_a^2s_b^2(\lambda_1\lambda_3(3R_1-5R_3)+R_4(9\lambda_2\lambda_3-4\lambda_1^2)+R_2(9\lambda_2\lambda_3-12\lambda_1^2))}{2(8\lambda_1^2-9\lambda_2\lambda_3)} \quad (25)$$

$$C_3=\frac{-3\lambda_3R_1+5\lambda_3R_3-4\lambda_1(R_4-R_2)}{2(8\lambda_1^2-9\lambda_2\lambda_3)}$$

$$D_3=\frac{R_1(2\lambda_1^2-3\lambda_2\lambda_3)-\lambda_1\lambda_2(R_4-R_2)-R_3(\lambda_2\lambda_3-2\lambda_1^2)}{2(8\lambda_1^2-9\lambda_2\lambda_3)}$$

CONCLUDING REMARKS

The present paper determines the stress field $S(1)$ and the stress field $S(3)$ where S is any one of the stresses σ_r, σ_ϕ, σ_θ, $\tau_{r\phi}$. Together with the stress fields $S(0)$ and $S(2)$ of Ref 1 we have the converging stress field

$$S(\text{Total})=S(0)+S(1)+S(2)+S(3)$$

The process can be continued to obtain additional terms but the algebraic details become cumbersome

Numerical results will be presented in a subsequent paper

REFERENCES

1 Lang H A In-plane bending of a curved pipe or toroidal tube acted on by end couples, *Int J Pres Ves Piping* 15 (1984) 27-35

2 Lang, H A, Stress analysis of pressurized elbows for nuclear components using toroidal elasticity, *Proc 4th Int Conf Pressure Vessel Technology* London, 1980 Vol 2, pp 251-60

The problem of Ref 1 for a solid circular ring sector was solved by

3 Göhner, O, *Ing Archiv*, 1 (1930) 619, 2 (1931) 1, 381

A compact account is given in

4 Timoshenko, S and Goodier, J N, *Theory of elasticity*, 2nd Ed New York, McGraw-Hill, 1951, pp 395-8

APPENDIX

Omitting the common multiplier cER, the stress fields from Ref 1 are

$$\sigma_{\theta_0}=s\cos\phi$$

$$\sigma_{r_1}=\frac{(3+2\nu)s^2}{16(1+\nu)}+2B_0+\frac{C_0}{s^2}+\cos2\phi\left(\frac{s^2}{4}-2A_2-\frac{6B_2}{s^4}-\frac{4D_2}{s^2}\right)$$

$$\sigma_{\phi_1}=\frac{(1-2\nu)s^2}{16(1+\nu)}+2B_0-\frac{C_0}{s^2}+\cos2\phi\left(-\frac{s^2}{4}+2A_2+\frac{6B_2}{s^4}+12C_2s^2\right)$$

$$\sigma_{\theta_1}=\frac{2+\nu}{8(1+\nu)}(s_b^2+s_a^2)-\frac{(2+\nu)s^2}{4(1+\nu)}-\frac{s^2(1+\nu)}{2}\cos2\phi$$
$$+\nu\cos2\phi\left(12C_2s^2-\frac{4D_2}{s^2}\right)$$

$$\tau_{r\theta}=\sin2\phi\left(-\frac{s^2}{4}+2A_2-\frac{6B_2}{s^4}+6C_2s^2-\frac{2D_2}{s^2}\right)$$

The coefficients B_0, C_0, A_2, B_2, C_2 and D_2 have been defined in Ref 1

The function $N(1)$ required for the first equilibrium equation is

$$N(1)=(\sigma_\theta-\sigma_r)_1\cos\phi-\tau_{r\theta_1}\sin\phi-\sigma_{\theta_0}s\cos^2\phi$$
$$=K_1s^2\cos\phi+K_2\cos\phi+K_3\frac{\cos\phi}{s^2}$$
$$+K_5s^2\cos3\phi+(3-2\nu)\frac{D_2\cos3\phi}{s^2}+\frac{6B_2}{s^4}\cos3\phi$$

The function $N(2)$ required for the second equilibrium equation is

$$N(2)=(\sigma_\phi-\sigma_\theta)_1\sin\phi-\tau_{r\phi_1}\cos\phi+\sigma_{\theta_0}s\cos\phi\sin\phi$$
$$=K_4s^2\sin\phi-K_2\sin\phi+K_3\frac{\sin\phi}{s^2}$$
$$-K_5s^2\sin3\phi+(1+2\nu)D_2\frac{\sin3\phi}{s^2}+\frac{6B_2\sin3\phi}{s^4}$$

The coefficients for $N(1)$ and $N(2)$ are listed below

$$K_1=(3+6\nu)C_2-\frac{31+30\nu+4\nu^2}{16(1+\nu)}$$

$$K_2=\frac{7+4\nu}{16(1+\nu)}(s_b^2+s_a^2)+2A_2$$

$$K_3=(1-2\nu)D_2-C_0$$

$$K_4=(6\nu-9)C_2+\frac{1}{16(1+\nu)}(13+2\nu-4\nu^2)$$

$$K_5=(6\nu-3)C_2-\left(\frac{2+\nu}{4}\right)$$

The functions required for the compatibility equations are

$$V(1)=-\frac{\partial\sigma_{r_1}}{\partial q}-\frac{2\tau_{r\phi_1}\sin\phi}{s}-2\sigma_{\theta_0}\cos^2\phi$$

$$V(2)=-\frac{\partial\sigma_{\phi_1}}{\partial q}+\frac{2\tau_{r\phi_1}\sin\phi}{s}-2\sigma_{\theta_0}\sin^2\phi$$

$$V(3)=-\frac{\partial\sigma_{\theta_1}}{\partial q}+\frac{1}{1+\nu}\frac{\partial\Theta_1}{\partial q}+\left(\frac{2+\nu}{1+\nu}\right)s\cos\phi\frac{\partial\sigma_{\theta_0}}{\partial q}+2\sigma_{\theta_0}$$

$$V(4)=-\frac{\partial\tau_{r\phi_1}}{\partial q}+\frac{\sin\phi}{s}[\sigma_r-\sigma_\phi]_1+\sigma_{\theta_0}\sin2\phi$$

where

$$\Theta_1=\sigma_{r_1}+\sigma_{\phi_1}+\sigma_{\theta_1}$$

and the operator is

$$\frac{\partial}{\partial q}=\cos\phi\frac{\partial}{\partial s}-\frac{\sin\phi}{s}\frac{\partial}{\partial\phi}$$

The functions $V(1)$ to $V(4)$ reduce to

$$V(1)=-\frac{3+2\nu}{8(1+\nu)}s\cos\phi+\frac{2C_0\cos\phi}{s^3}+\cos\phi\left(-6C_2s-\frac{7}{4}s+\frac{2D_2}{s^3}\right)$$
$$+\cos3\phi\left[\left(6C_2-\frac{3}{4}\right)s-\frac{10D_2}{s^3}-\frac{24B_2}{s^5}\right]$$

$$V(2)=-\frac{(1-2\nu)}{8(1+\nu)}s\cos\phi-\frac{2C_0\cos\phi}{s^3}+\cos\phi\left[\left(-18C_2-\frac{1}{4}\right)s-\frac{2D_2}{s^3}\right]$$
$$+\cos3\phi\left[\left(\frac{3}{4}-6C_2\right)s+\frac{2D_2}{s^3}+\frac{24B_2}{s^5}\right]$$

$$V(3)=-\frac{15+13\nu+2\nu^2}{2(1+\nu)}s\cos\phi-24C_2(1+\nu)s\cos\phi$$
$$-\frac{8D_2}{s^3}(1+\nu)\cos3\phi$$

$$V(4)=\frac{(1+2\nu)}{8(1+\nu)}s\sin\phi+\frac{2C_0}{s^3}\sin\phi+\sin\phi\left[\left(\frac{3}{4}-6C_2\right)s+\frac{2D_2}{s^3}\right]$$
$$+\sin3\phi\left[\left(\frac{3}{4}-6C_2\right)s-\frac{6D_2}{s^3}-\frac{24B_2}{s^5}\right]$$

B.4 Twist-Bending of a 90° Elbow or Pipe Bend

Twist-Bending of a 90° Elbow or Pipe Bend

H A Lang

LANG—Research West 1201 Idaho Avenue Santa Monica CA 90403 USA

(Received 25 June 1983)

ABSTRACT

Out of plane bending by an end couple applied to a 90° elbow or pipe bend of circular cross section is considered There is conversion of bending to twist so that at 90° the elbow is held in equilibrium by a twist couple Using the methods of toroidal elasticity, the six stresses of the first order stress field are determined from the zero order field The zero-order field constitutes a permissible initial deformation as verified by strain compatibility equations

The equations in the text are derived from the general theory of toroidal elasticity by applying the method of successive approximations The equations of the general theory are expanded in a series in 1/R (where R is the toroidal radius) This leads to the working equations given in the paper

NOMENCLATURE

r, ϕ, θ	Toroidal coordinates
$\begin{Bmatrix}\sigma_r, \sigma_\phi, \sigma_\theta \\ \tau_{r\phi}, \tau_{r\theta}, \tau_{\phi\theta}\end{Bmatrix}$	Stress components
$\begin{Bmatrix}e_r, e_\phi, e_\theta \\ e_{r\phi}, e_{r\theta}, e_{\phi\theta}\end{Bmatrix}$	Strain components
∇_0^2, p_1, p_3	Operators defined in the text

Int J Pres Ves & Piping 0308-0161/84/$03 00

a	Inner radius of cross-section
b	Outer radius of cross-section
I_p	Moment of inertia
K	$M_0 R/I_p$
M_0	End moment (twist or bending)
N	Normal force on cross-section
R	Toroidal radius
s	r/R
Θ	$\sigma_r + \sigma_\phi + \sigma_\theta$

INTRODUCTION

The problem considered in this paper is one of ten unit problems for a pressurized elbow acted upon by end loads A bending moment M_0 is applied at the station defined by $\theta = 0$ (see Fig 1) Equilibrium is maintained by an equal and opposite moment at the station $\theta = 90°$ This is a twisting moment so that there is conversion of bending to twist as the angle θ increases

The first order stress field is determined from the initial (zero order) stress field using the methods of toroidal elasticity The general theory of toroidal elasticity for isotropic material is expanded in a series in 1 R (where R is the toroidal radius) The method of successive approximations is then applied to determine the equilibrium and compatibility equations given in the paper

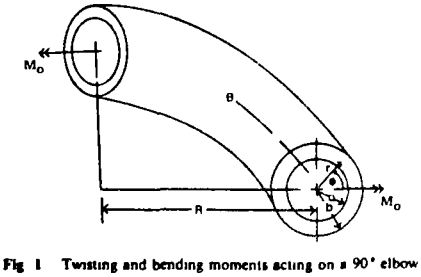

Fig 1 Twisting and bending moments acting on a 90° elbow

INITIAL ZERO ORDER STRESS FIELD

Consider an initial state of stress given by

$$\sigma_r = \sigma_\phi = \tau_{r\phi} = \tau_{r\theta} = 0$$
$$\sigma_\theta = 2As \sin\phi \cos\theta \tag{1}$$
$$\tau_{\phi\theta} = -Ks \sin\theta$$

As shown in Fig 1, this represents a bending moment at $\theta = 0$ such that $K = M_0 R / I_p$ In addition at $\theta = 90°$ there is a twisting moment $M_T = -M_0 = -(KI_p) R$

This state of stress satisfies the six strain compatibility conditions

$$\nabla_0^2 e_\theta = 0$$
$$p_1^2 e_\theta = 0$$
$$p_3^2 e_\theta = 0$$
$$p_1 p_3 e_\theta = 0$$
$$p_3\left(\frac{\partial e_{\phi\theta}}{\partial s} + \frac{e_{\phi\theta}}{s}\right) = 0$$
$$p_1\left(\frac{\partial e_{\phi\theta}}{\partial s} + \frac{e_{\phi\theta}}{s}\right) = 0$$

where

$$\nabla_0^2 = \frac{\partial^2}{\partial s^2} + \frac{1}{s}\frac{\partial}{\partial s} + \frac{1}{s^2}\frac{\partial^2}{\partial \phi^2}$$

and the operators are

$$p_1 = \cos\phi \frac{\partial}{\partial s} - \frac{\sin\phi}{s}\frac{\partial}{\partial \phi}$$
$$p_3 = \sin\phi \frac{\partial}{\partial s} + \frac{\cos\phi}{s}\frac{\partial}{\partial \phi}$$

the required strains are

$$e_\theta = \frac{2Ks \sin\phi \cos\theta}{E}$$
$$e_{\phi\theta} = \frac{-2Ks \sin\theta(1+\nu)}{E}$$

and the force and moment resultants are

$$N = \int_a^b \int_0^{2\pi} \sigma_\theta r \, dr \, d\phi = 0$$
$$M_0 = \int_a^b \int_0^{2\pi} (\sigma_\theta r \sin\phi) r \, dr \, d\phi = \frac{KI_p}{R}$$
$$M_T = M_0 = \int_a^b \int_0^{2\pi} (\tau_{\phi\theta} r) r \, dr \, d\phi = -\frac{KI_p}{R}$$

FIRST ORDER STRESS FIELD

Determination of shear stresses $(\tau_{r\theta})_1$ and $(\tau_{\phi\theta})_1$

The equilibrium equations for the stresses are

$$\left[\frac{1}{s}\frac{\partial(\tau_{r\theta} s)}{\partial s} + \frac{1}{s}\frac{\partial \tau_{\phi\theta}}{\partial \phi}\right]_1 = 0$$

In addition the two stress compatibility requirements are

$$\left(\nabla_0^2 \tau_{r\theta} - \frac{\tau_{r\theta}}{s^2} - \frac{2}{s^2}\frac{\partial \tau_{\phi\theta}}{\partial \phi}\right)_1 = \left(\frac{3+\nu}{1+\nu}\right) K \sin\phi \sin\theta$$
$$\left(\nabla_0^2 \tau_{\phi\theta} - \frac{\tau_{\phi\theta}}{s^2} + \frac{2}{s^2}\frac{\partial \tau_{r\theta}}{\partial \phi}\right)_1 = \left(\frac{3+\nu}{1+\nu}\right) K \cos\phi \sin\theta$$

All three equations are satisfied by

$$(\tau_{r\theta})_1 = -\frac{A}{8}\left(\frac{3+\nu}{1+\nu}\right)\left(s_a^2 + s_b^2 - s^2 - \frac{s_a^2 s_b^2}{s^2}\right) \sin\phi \sin\theta$$
$$(\tau_{\phi\theta})_1 = -\frac{A}{8}\left(\frac{3+\nu}{1+\nu}\right)\left(s_a^2 + s_b^2 - 3s^2 + \frac{s_a^2 s_b^2}{s^2}\right) \cos\phi \sin\theta \tag{2}$$

Determination of stress σ_{θ_1}

The stress compatibility condition is

$$\nabla_0^2 \sigma_{\theta_1} = 0$$

A solution consisting of harmonic terms can be found immediately

$$\sigma_{\theta_1} = \left(k_1 s^2 \sin 2\phi + \frac{k_2}{s^2} \sin 2\phi\right) \cos\theta \tag{3}$$

where k_1 and k_2 will be determined later from the compatibility equations

Determination of stresses σ_{r_1}, σ_{θ_1}, $\tau_{r\theta_1}$

The stresses σ_{r_1}, σ_{θ_1} and $\tau_{r\theta_1}$ satisfy the equilibrium equations

$$\begin{aligned}\left(\frac{1}{s}\frac{\partial}{\partial s}(\sigma_r s) + \frac{1}{s}\frac{\partial \tau_{r\theta}}{\partial \phi} - \frac{\sigma_\theta}{s}\right)_1 &= Ks \sin 2\phi \cos\theta \\ \left(\frac{1}{s}\frac{\partial \sigma_\theta}{\partial \phi} + \frac{1}{s^2}\frac{\partial}{\partial s}(\tau_{r\theta} s^2)\right)_1 &= Ks \cos 2\phi \cos\phi\end{aligned} \tag{4}$$

In addition there are three compatibility equations

$$\begin{aligned}\left(\nabla_0^2 \sigma_r - \frac{4}{s^2}\frac{\partial \tau_{r\theta}}{\partial \phi} - \frac{2}{s^2}(\sigma_r - \sigma_\theta) + \frac{1}{1+\nu}\frac{\partial^2 \Theta}{\partial s^2}\right)_1 &= 0 \\ \left(\nabla_0^2 \sigma_\theta + \frac{4}{s^2}\frac{\partial \tau_{r\theta}}{\partial \phi} + \frac{2}{s^2}(\sigma_r - \sigma_\theta) + \frac{1}{1+\nu}\left(\frac{1}{s}\frac{\partial \Theta}{\partial s} + \frac{1}{s^2}\frac{\partial^2 \Theta}{\partial \phi^2}\right)\right)_1 &= 0 \\ \left(\nabla_0^2 \tau_{r\theta} + \frac{2}{s^2}\frac{\partial}{\partial \phi}(\sigma_r - \sigma_\theta) - \frac{4\tau_{r\theta}}{s^2} + \frac{1}{1+\nu}\left(\frac{1}{s}\frac{\partial^2 \Theta}{\partial \phi \partial s} - \frac{1}{s^2}\frac{\partial \Theta}{\partial \phi}\right)\right)_1 &= 0\end{aligned} \tag{5}$$

We next write

$$\begin{aligned}\sigma_{r_1} &= \left(\frac{K}{2}s^2 - \frac{B}{s^4} - C - \frac{2D}{s^2}\right)\sin 2\phi \cos\theta \\ \sigma_{\theta_1} &= \left(\frac{K}{2}s^2 + 2As^2 + \frac{B}{s^4} + C\right)\sin 2\phi \cos\theta \\ \tau_{r\theta_1} &= \left(-As^2 + \frac{B}{s^4} - C + \frac{D}{s^2}\right)\cos 2\phi \cos\theta\end{aligned} \tag{6}$$

These satisfy the equilibrium equations The coefficients A, B, C and D are determined by the boundary conditions

$$\sigma_r = \tau_{r\theta} = 0 \quad \text{at } s = s_a \text{ and } s = s_b$$

$$\sigma_{\theta_1} = \left[(2A_1 - K)s^2 - \frac{2D_1}{s^2}\right]\sin 2\phi \cos\theta$$

$$\tau_{r\theta} = -\frac{K}{8}\left(\frac{3+\nu}{1+\nu}\right)\left(s_a^2 + s_b^2 - s^2 - \frac{s_a^2 s_b^2}{s^2}\right)\sin\phi \sin\theta$$

$$\tau_{\phi z} = -\frac{K}{8}\left(\frac{3+\nu}{1+\nu}\right)\left(s_a^2 + s_b^2 - 3s^2 + \frac{s_a^2 s_b^2}{s^2}\right)\cos\phi \sin\theta$$

where A B C and D are defined in eqns (7)

Both fields satisfy equilibrium equations compatibility equations and boundary conditions The methods of toroidal elasticity can be continued to obtain the next second order fields but the algebraic details are cumbersome

CONCLUSIONS

The zero and first order fields of stress can readily be computed by a simple Fortran computer routine The equations of the paper have already been programmed as one of a set of ten routines for the end loaded pressurized elbow

While the figures of this paper represent a 90° elbow the angle θ can easily be extended beyond 90° to represent a curved pipe bend with the load plane maintained at $\theta = 0$

It is also possible to interchange sin θ and cos θ in every equation This in effect places the twisting couple at the load plane $\theta = 0$ and the bending moment M_0 at the station $\theta = 90°$

BIBLIOGRAPHY

The theory of Toroidal Elasticity may be found in

Lang, H A , Stress analysis of pressurized elbows for nuclear components using toroidal elasticity, *Proc 4th Int Conf on Pressure Vessel Technology London*, 21 May, 1980 Vol 2, pp 251–60

Additional papers referring to a 90° elbow or pipe bend are available in the reports below

Lang H A , Toroidal elastic stress fields for pressurized elbows and pipe bends *Int J Pres Ves and Piping*, 15 (1984), 291–305

The coefficients are

$$\begin{aligned}A &= -\frac{K}{2}\frac{(s_b^6 + s_a^6 + 4s_a^2 s_b^2)}{(s_b^2 - s_a^2)^2} \\ B &= \frac{3}{2}\frac{K s_a^4 s_b^4 (s_a^2 + s_b^2)}{(s_b^2 - s_a^2)^2} \\ C &= \frac{K}{2}\frac{(s_b^2 + s_a^2)(s_b^4 + s_a^4 + s_a^2 s_b^2)}{(s_b^2 - s_a^2)^2} \\ D &= -\frac{K s_a^2 s_b^2 (s_a^4 + s_b^4 + s_a^2 s_b^2)}{(s_b^2 - s_a^2)^2}\end{aligned} \tag{7}$$

Considering only terms in s^2 all three compatibility equations lead to $k_1 = -K + 2A_1$ Considering only terms in $1/s^2$, all three compatibility equations lead to $k_2 = -2D_1$ This completes the determination of σ_{θ_1} The terms in B and C in the stresses σ_r σ_ϕ, and $\tau_{r\theta_1}$ satisfy the compatibility equations identically

SUMMARY OF STRESS FIELDS

Zero order field

$$\sigma_\theta = \frac{M_0 R}{I_p}(2s \sin\phi \cos\theta)$$

$$\tau_{\phi z} = -\frac{M_0 R}{I_p}(s \sin\theta)$$

First order field

$$\begin{aligned}\sigma_{r_1} &= \left(\frac{K}{2}s^2 - \frac{B}{s^4} - C - \frac{2D}{s^2}\right)\sin 2\phi \cos\theta \\ \sigma_{\theta_1} &= \left(\frac{K}{2}s^2 + 2As^2 + \frac{B}{s^4} + C\right)\sin 2\phi \cos\theta \\ \tau_{r\theta_1} &= \left(-As^2 + \frac{B}{s^4} - C + \frac{D}{s^2}\right)\cos 2\phi \cos\theta\end{aligned}$$

Lang, H A , Pure twist of a circular toroidal tube *Int J Pres Ves and Piping* (to be published)

Lang H A Out-of-plane bending of an elbow or pipe bend under an end loaded shear force *Int J Pres Ves and Piping* 15 (1984) 205–12

Lang H A In-plane bending of a curved pipe or toroidal tube acted on by end couples *Int J Pres Ves and Piping* 15 (1984) 27–35

Lang, H A , Stress fields for an in plane end shear force acting on a 90° elbow or pipe bend *Int J Pres Ves and Piping* 16 (1984) in press)

Lang H A Stress fields for a normal force acting on the end of a 90 elbow *Int J Pres Ves and Piping* in press

B.5 Out-of-plane Bending of an Elbow or Pipe Bend under an End-Loaded Shear Force

Out-of-plane Bending of an Elbow or Pipe Bend under an End-loaded Shear Force

H A Lang

LANG—Research West 1201 Idaho Avenue Santa Monica CA 90403 USA

(Received 8 March 1983)

ABSTRACT

There are ten unit problems for a 90° elbow subjected to pressure, seismic loads and end loads The unit problem considered in this paper consists of an end-loaded shear force which produces out-of-plane bending Equilibrium is maintained at the other end of the elbow by a twisting moment and a bending moment

The methods of toroidal elasticity are used to determine the zero order and first order stress states, the stress field being determined by a converging series The results are readily generalized to refer to a pipe bend In addition the results are applicable by a limit process to a solid circular ring sector

NOMENCLATURE

r, ϕ, θ	Toroidal elastic coordinates
$\sigma_r, \sigma_\phi, \sigma_\theta$	Normal stress components
$\tau_{r\phi}, \tau_{\phi\theta}, \tau_{r\theta}$	Shear stress components
R	Toroidal radius
s	r/R
a	Inner radius of elbow
b	Outer radius of elbow
M_B	Bending moment
M_T	Twisting moment
F_0	End shear force
K	Bending moment constant

Int J Pres Ves & Piping 0308-0161/84/$03 00 © Elsevier Applied Science Publishers Ltd, England, 1984 Printed in Great Britain

$\tilde{\tau}_0$	Twisting moment constant
τ_0	End shear force constant
∇_0^2	$\frac{\partial^2}{\partial s^2}+\frac{1}{s}\frac{\partial}{\partial s}+\frac{1}{s^2}\frac{\partial^2}{\partial\phi^2}$
p_1	$\cos\phi\frac{\partial}{\partial s}-\frac{\sin\phi}{s}\frac{\partial}{\partial\phi}$
p_3	$\sin\phi\frac{\partial}{\partial s}+\frac{\cos\phi}{s}\frac{\partial}{\partial\phi}$
Θ	$\sigma_r+\sigma_\phi+\sigma_\theta$

INTRODUCTION

Toroidal elasticity was first introduced in 1980 [1] It was applied to the determination of stresses in an elbow under internal pressure [2] This problem was the first of ten unit problems for an elbow subjected to both end loading and seismic effects—in addition to the pressure problem, the second unit problem discussed in-plane bending of an elbow acted upon by end couples [3]

The present paper represents the third unit problem An end shear force is applied to an elbow so that out-of-plane bending occurs The shear force acts in a load plane defined by $\theta = 0$ At $\theta = 90°$, equal bending and twisting moments exist in order to maintain equilibrium of the elbow (see Fig 1)

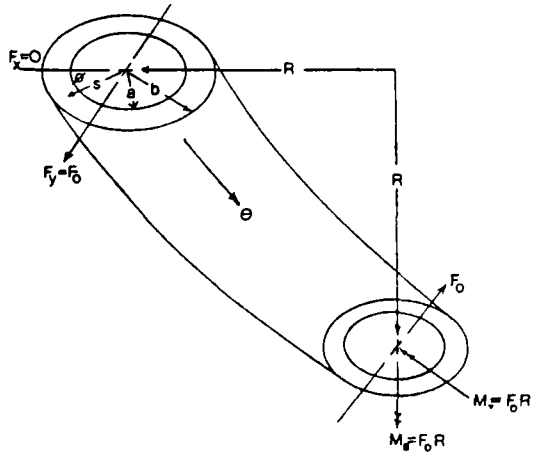

Fig 1. End shear force acting on 90° pipe elbow

There is conversion of the stress state (as we traverse the elbow) from the stress state at $\theta = 0$ to the stress state at $\theta = 90°$ Using the methods of toroidal elasticity we select an initial stress state and then determine the first order stress field

As shown in Fig 1, a 90° elbow is acted upon by a force F_0 acting at the upper face (defined by $\theta = 0$) At the lower face, $\theta = 90°$, equilibrium is maintained by an equal force F_0 In addition, we must have a twisting moment $M_T = F_0R$ and an out-of-plane bending moment $M_B = F_0R$ Selecting an initial stress state, we determine the first order stress field using the methods of toroidal elasticity

INITIAL STATE OF STRESS

The initial state of stress is

$$\sigma_r = \sigma_\phi = \tau_{r\phi} = 0$$

$$\sigma_\theta = -Ks\sin\phi\sin\theta$$

$$\tau_{r\theta} = \tau_0\left(s_a^2 + s_b^2 - s^2 - \frac{s_a^2 s_b^2}{s^2}\right)\sin\phi \tag{1}$$

$$\tau_{\phi\theta} = \tilde{\tau}_0 s(1-\cos\theta) + \tau_0\cos\phi\left(s_a^2 + s_b^2 - \frac{s^2}{3} + \frac{s_a^2 s_b^2}{s^2}\right)$$

This state of stress satisfies the boundary conditions

$$\sigma_r = 0 \qquad \text{at } s = s_b \text{ and } s = s_a$$

$$\tau_{r\phi} = 0 \qquad \text{at } s = s_b \text{ and } s = s_a$$

Moreover the strain compatibility equations are satisfied These are

$$\begin{aligned} \nabla_0^2 e_\theta &= 0 \\ p_1^2 e_\theta &= 0 \\ p_3^2 e_\theta &= 0 \\ p_1 p_3 e_\theta &= 0 \\ p_3\left[\frac{\partial e_{\phi\theta}}{\partial s} + \frac{e_{\phi\theta}}{s} - \frac{1}{s}\frac{\partial e_{r\theta}}{\partial\phi}\right] &= 0 \\ p_1\left[\frac{\partial e_{\phi\theta}}{\partial s} + \frac{e_{\phi\theta}}{s} - \frac{1}{s}\frac{\partial e_{r\theta}}{\partial\phi}\right] &= 0 \end{aligned} \tag{2}$$

The force resultants are

$$F_x = R^2\int_{s_a}^{s_b}\int_0^{2\pi}(\tau_{r\theta}\cos\phi - \tau_{\phi\theta}\sin\phi)s\,ds\,d\phi = 0$$

$$\begin{aligned} F_y &= R^2\int_{s_a}^{s_b}\int_0^{2\pi}(\tau_{r\theta}\sin\phi + q_{\phi\theta}\cos\phi)s\,ds\,d\phi \\ &= \pi R^2\tau_0\int_{s_a}^{s_b}[2(s_a^2+s_b^2) - \tfrac{4}{3}s^2]s\,ds \end{aligned} \tag{3}$$

or

$$F_y = \tfrac{2}{3}\pi R^2(s_b^4 - s_a^4)\tau_0 = F_0 \tag{4}$$

In addition, at the lower face, $\theta = 90°$

$$\begin{aligned} M_B &= -R^3\int_{s_a}^{s_b}\int_0^{2\pi}(\sigma_\theta s\sin\phi)s\,ds\,d\phi \\ &= R^3\int_{s_a}^{s_b}\int_0^{2\pi}(Ks^3\sin^2\phi)\,ds\,d\phi \end{aligned} \tag{5}$$

$$M_B = F_0R = \frac{K\pi R^4}{4}(s_b^4 - s_a^4)$$

and

$$\begin{aligned} M_T &= R^3\int_{s_a}^{s_b}\int_0^{2\pi}(\tau_{\phi\theta}\,s)s\,ds\,d\phi \\ &= R^3\frac{\pi\tilde{\tau}_0}{2}(s_b^4 - s_a^4) = F_0R \end{aligned} \tag{6}$$

If equilibrium can be maintained only by the initial state of stress then from eqns (4)–(6), we have

$$F_0 = \tfrac{2}{3}\tau_0\pi R^2(s_b^4 - s_a^4) = K\frac{\pi R^2}{4}(s_b^4 - s_a^4) = \frac{\bar{\tau}_0\pi R^2}{2}(s_b^4 - s_a^4)$$

or

$$K = 2\bar{\tau}_0 = \tfrac{8}{3}\tau_0$$

In determining the next field of stress we may retain the condition $K = 2\tau_0$ because of the equality between the end bending and twisting moments The condition $\tau_0 = \frac{4}{3}\tau_0$ does not hold however

STRESS STATE (1)

The equilibrium equation for stresses $\tau_{r\theta}$ and $\tau_{\phi\theta}$ is

$$\left(\frac{1}{s}\frac{\partial}{\partial s}(\tau_{r\theta}\, s) + \frac{1}{s}\frac{\partial \tau_{\phi\theta}}{\partial \phi}\right)_1 = 2\tau_0 s\sin\phi + \tau_0\sin 2\phi\left(\frac{2s^2}{3} + \frac{2s_a^2 s_b^2}{3s^2}\right) \tag{7}$$

The corresponding compatibility equations are

$$\begin{aligned}\left(\nabla_0^2\tau_{r\theta} - \frac{\tau_{r\theta}}{s^2} - \frac{2}{s^2}\frac{\partial \tau_{\phi\theta}}{\partial\phi}\right)_1 &= -\bar{\tau}_0\sin\phi + \left(\frac{3+\nu}{1+\nu}\right)\tau_0\sin\phi\cos\theta \\ &\quad + \tau_0\sin 2\phi\left(\frac{2s}{3} - \frac{2s_a^2 s_b^2}{s^3}\right)\\ \left(\nabla_0^2\tau_{\phi\theta} - \frac{\tau_{\phi\theta}}{s^2} + \frac{2}{s^2}\frac{\partial \tau_{r\theta}}{\partial\phi}\right)_1 &= -\tau_0\cos\phi + \left(\frac{3+\nu}{1+\nu}\right)\bar{\tau}_0\sin\phi\cos\theta \\ &\quad + \tau_0\cos 2\phi\left(\frac{2s}{3} + \frac{2s_a^2 s_b^2}{s^3}\right)\end{aligned} \tag{8}$$

A solution such that $\tau_{r\theta}$ vanishes on the boundary can be found

$$\begin{aligned}\tau_{r\theta_1} &= \tfrac{3}{4}\bar{\tau}_0\sin\phi\left[s^2 - (s_a^2 + s_b^2) + \frac{s_a^2 s_b^2}{s^2}\right] \\ &\quad - \frac{\nu}{4(1+\nu)}\bar{\tau}_0\sin\phi\cos\theta\left[s^2 - (s_a^2 + s_b^2) + \frac{s_a^2 s_b^2}{s^2}\right] \\ &\quad + \frac{\tau_0}{6}s\sin 2\phi\left[s^2 - (s_a^2 + s_b^2) + \frac{s_a^2 s_b^2}{s^2}\right]\end{aligned} \tag{9}$$

$$\begin{aligned}\tau_{\phi\theta_1} &= \tfrac{1}{4}\tau_0\cos\phi\left[s^2 - 3(s_a^2 + s_b^2) - \frac{3s_a^2 s_b^2}{s^2}\right] \\ &\quad + \frac{\nu}{4(1+\nu)}\bar{\tau}_0\cos\phi\cos\theta\left[-3s^2 + (s_a^2 + s_b^2) + \frac{s_a^2 s_b^2}{s^2}\right] \\ &\quad - \frac{\tau_0 s\cos 2\phi}{6}\left[(s_a^2 + s_b^2) + \frac{2s_a^2 s_b^2}{s^2}\right]\end{aligned} \tag{10}$$

The remaining four stresses σ_r, σ_ϕ, σ_θ and $\tau_{r\phi}$ satisfy the equilibrium equations

$$\begin{aligned}\left(\frac{1}{s}\frac{\partial}{\partial s}(\sigma_r s) + \frac{1}{s}\frac{\partial \tau_{r\phi}}{\partial\phi} - \frac{\sigma_\phi}{s}\right)_1 &= -\bar{\tau}_0 s\sin\theta\sin 2\phi \\ \left(\frac{1}{s}\frac{\partial}{\partial\phi}\sigma_\phi + \frac{1}{s^2}\frac{\partial}{\partial s}(\tau_{r\phi}s^2)\right)_1 &= -\bar{\tau}_0 s\sin\theta\cos 2\phi\end{aligned} \tag{11}$$

and the compatibility equations

$$\begin{aligned}\left[\nabla_0^2\sigma_r - \frac{4}{s^2}\frac{\partial\tau_{r\phi}}{\partial\phi} - \frac{2}{s^2}(\sigma_r - \sigma_\phi) + \frac{1}{1+\nu}\frac{\partial^2\Theta}{\partial s^2}\right]_1 &= 0 \\ \left[\nabla_0^2\sigma_\phi + \frac{4}{s^2}\frac{\partial\tau_{r\phi}}{\partial\phi} + \frac{2}{s^2}(\sigma_r - \sigma_\phi) + \frac{1}{1+\nu}\left(\frac{1}{s}\frac{\partial\Theta}{\partial s} + \frac{1}{s^2}\frac{\partial^2\Theta}{\partial\phi^2}\right)\right]_1 &= 0 \\ \nabla_0^2\sigma_{\theta_1} &= 0 \\ \left[\nabla_0^2\tau_{r\phi} + \frac{2}{s^2}\frac{\partial}{\partial\phi}(\sigma_r - \sigma_\phi) - \frac{4}{s^2}\tau_{r\phi} + \frac{1}{1+\nu}\left(\frac{1}{s}\frac{\partial^2\Theta}{\partial s\,\partial\phi} - \frac{1}{s^2}\frac{\partial\Theta}{\partial\phi}\right)\right]_1 &= 0\end{aligned} \tag{12}$$

A solution can be found by taking the particular solutions

$$\sigma_r = \sigma_\phi = -\bar{\tau}_0 s^2\sin\phi\cos\phi\sin\theta \tag{13}$$

and adding solutions of $\nabla_0^4\phi = 0$ The result may be written

$$\begin{aligned}\sigma_{r_1} &= \bar{\tau}_0\sin\theta\sin 2\phi\left(-\frac{s^2}{2} - \frac{6B}{s^4} - 2C - \frac{4D}{s^2}\right) \\ \sigma_{\phi_1} &= \bar{\tau}_0\sin\theta\sin 2\phi\left(-\frac{s^2}{2} + 12As^2 + \frac{6B}{s^4} + 2C\right) \\ \tau_{r\phi_1} &= -\bar{\tau}_0\sin\theta\cos 2\phi\left(6As^2 - \frac{6B}{s^4} + 2C - \frac{2D}{s^2}\right) \\ \sigma_{\theta_1} &= \bar{\tau}_0\sin\theta\sin 2\phi\left(\lambda_1 s^2 + \frac{\lambda_2}{s^2}\right)\end{aligned} \tag{14}$$

where $\lambda_1 = 12A$ and $\lambda_2 = -4D$ The boundary conditions of vanishing σ_r and $\tau_{r\phi}$ determine the coefficients A to D These are

$$\begin{aligned}A &= \frac{(s_b^4 + s_a^4 + 6s_a^2 s_b^2)}{12(s_b^2 - s_a^2)^2} \\ B &= -\frac{1}{4}\frac{s_a^4 s_b^4(s_a^2 + s_b^2)}{(s_b^2 - s_a^2)^2} \\ C &= -\frac{1}{4}\frac{(s_a^2 + s_b^2)(s_b^4 + s_a^4 + s_a^2 s_b^2)}{(s_b^2 - s_a^2)^2} \\ D &= \frac{s_a^2 s_b^2(s_b^4 + s_a^4 + s_a^2 s_b^2)}{2(s_b^2 - s_a^2)^2}\end{aligned}$$

The stress state (1) does not contribute to the twisting moment, M_T, or the bending moment, M_B Moreover, the resultant force F_{x_1} vanishes Equilibrium requires that $F_y = F_0$ at every cross-section and this condition is satisfied because the terms involving $\cos\theta$ in eqns (9) and (10) vanish The remaining terms lead to

$$\begin{aligned}F_{y_1} &= R^2\int_{s_a}^{s_b}\int_0^{2\pi}(\tau_{r\theta_1}\sin\phi + \tau_{\phi\theta_1}\cos\phi)s\,ds\,d\phi \\ &= -\tfrac{5}{16}\pi R^2\bar{\tau}_0(s_b^4 - s_a^4)\end{aligned}$$

For the stress states (0) + (1), we have

$$\begin{aligned}F_0 &= \tfrac{2}{3}\tau_0\pi R^2(s_b^4 - s_a^4) - \tfrac{5}{16}\pi R^2(s_b^4 - s_a^4)\bar{\tau}_0 \\ &= \frac{M_T}{R} = \frac{\pi R^2}{2}\tau_0(s_b^4 - s_a^4)\end{aligned}$$

Hence

$$\tfrac{2}{3}\tau_0 = \tfrac{13}{16}\bar{\tau}_0 \qquad \text{or} \qquad \tau_0 = \tfrac{32}{39}\bar{\tau}_0$$

CONCLUDING REMARKS

The selecting of $\theta = 90°$ is convenient in order to make the bending and twisting moments equal However, a little thought will make it evident that the solution holds for an incomplete hollow tore of less than 90° or for a pipe bend subtending an angle greater than 90°

The solution can also be readily applied to a solid curved ring sector by eliminating all terms in negative powers of s and setting $s_a = 0$ In eqns (14), the terms involving B and D vanish The limiting value of A is 1/12 and the limiting value of C is $-s_b^2/4$ The stress field which results then satisfies the boundary conditions $\sigma_r = \tau_{r\phi} = 0$ at $s = s_b$ for the circular ring sector

REFERENCES

1 Lang H A , Stress analysis of pressurized elbows for nuclear components using toroidal elasticity *Proc 4th Int Conf Pressure Vessel Technology*, London 21 May 1980 Vol 2 pp 251–60
2 Lang H A , Toroidal elastic stress fields for pressurized elbows and pipe bends, *Int J Pres Ves & Piping* 15 (1984) 93–104
3 Lang H A , In-plane bending of a curved pipe or toroidal tube acted on by end-couples *Int J Pres Ves & Piping* 15 (1984) 27–35

B.6 Stress Fields for an In-plane End Shear Force Acting on a 90° Elbow or Pipe Bend

Stress Fields for an In-plane End Shear Force Acting on a 90° Elbow or Pipe Bend

H A Lang

LANG—Research West 1201 Idaho Avenue
Santa Monica CA 90403 USA

(Received 21 August, 1983)

ABSTRACT

This paper develops the stress fields for a 90° elbow or pipe bend acted upon by an end shear force, W, which produces deformation primarily in the plane of the elbow. There are coupled fields of stress because the elbow is held in equilibrium by an end normal force N, and by a bending moment, M = WR. The solution makes use of a previous result for pure bending of an elbow.

The methods used are those of toroidal elasticity which requires the development of certain equilibrium functions N(i) and the development of certain compatibility functions V(i). These are listed in Appendices.

There appear to be a total of eight fields of stress. Three initial fields of stress generate five first-order fields of stress when the method of successive approximation is applied to the general theory of toroidal elasticity.

NOMENCLATURE

r, ϕ, θ	Toroidal coordinates
$\sigma_r, \sigma_\phi, \sigma_\theta$	Normal stresses
$\tau_{r\theta}, \tau_{r\phi}, \tau_{\phi\theta}$	Shear stresses
$\tau_{rz}, \tau_{\phi z}, \sigma_z$	Stresses in a cantilever beam
a	Internal radius of cross-section
b	External radius of cross-section

Int J Pres Ves & Piping 0308-0161/84/$03.00 © Elsevier Applied Science Publishers Ltd, England 1984 Printed in Great Britain

I	Moment of inertia
K	WR^2/I
K_0	K/κ
M	Bending moment
N	Normal force
$N(i)$	Equilibrium functions
R	Toroidal radius
ς	r/R
$V(i)$	Compatibility functions
W	Shear force
$\alpha\ \beta, \kappa, \delta_1, \delta_2$	Stress parameters

INTRODUCTION

This paper considers one of the ten unit problems of the 90° elbow. An end shear force, shown in Fig. 2, acts inwardly in the load plane, $\theta = 0$. The elbow is in equilibrium under this force W, and an equal normal force acting in the plane, $\theta = 90°$. Equilibrium also requires a bending moment WR at $\theta = 90°$. An initial field of stress generates, in part, stress $\tau_{r\theta}$ and $\tau_{\phi\theta}$ as shown.

To determine the first-order stress field, an initial state of stress is introduced. This state of stress is an extension and adaptation of the stress field in a straight cantilever beam acted upon by an end shear force (see Fig. 1), as given by Love [1]. Additional initial stress states must be assumed to satisfy the boundary conditions and toroidal geometry of the elbow.

The methods used depend on the general theory of toroidal elasticity first introduced by Lang [2]. The general theory is difficult to use directly for solving boundary value problems.

It is necessary to expand the general theory in a series in $1/R$ (where R is the toroidal radius) and apply the method of successive approximations. This procedure yields the zero-order equations and the first-order equations used in the present paper.

There is a coupling of the shear like stress field in the plane $\theta = 0$ and the normal like stress field in the plane $\theta = 90°$. This coupling is discussed in detail in the paper.

The determination of the first-order stress field also requires that we

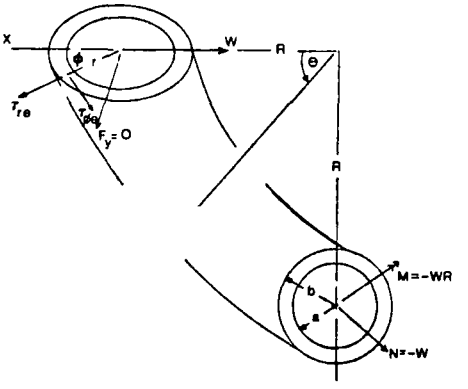

Fig. 2 Notation for 90° elbow acted on by an end shear force in the plane $\theta = 0$

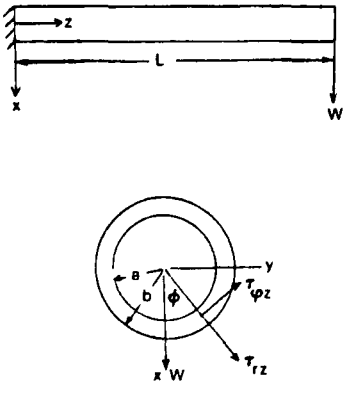

Fig. 1 End loaded shear force acting on a cantilever beam of circular cross section

add a state of stress due to end bending moments to the other fields of stress which arise. The solution for end bending moments (another unit problem of the elbow) was determined in two earlier papers [3,4]. The results are reproduced in their entirety in the present analysis.

In applying the method of successive approximations, terms appear on the right-hand side of the stress equilibrium and stress compatibility equations. We call these equilibrium functions $N(i)$ and compatibility functions, $V(i)$. The required functions are completely developed in Appendices 1 to 5.

INITIAL STRESS FIELD FOR $\tau_{r\theta}$ AND $\tau_{\phi\theta}$

To develop the initial stress field for stresses $\tau_{r\theta}$ and $\tau_{\phi\theta}$ we begin with a cantilever beam of circular cross-section acted upon by an end shear force W (as shown in Fig. 1). From Love[1] the stresses on any cross-section are

$$\tau_{rz} = -\frac{W}{2(1+\nu)I}\left[\frac{\partial\chi}{\partial r} + \cos\phi\left(\frac{1}{2}\nu x^2 + \frac{2-\nu}{2}y^2\right) + \sin\phi(2+\nu)xy\right]$$

$$\tau_{\phi z} = -\frac{W}{2(1+\nu)I}\left[\frac{1}{r}\frac{\partial\chi}{\partial\phi} + \cos\phi(2+\nu)xy - \sin\phi\left(\frac{1}{2}\nu x^2 + \left(\frac{2-\nu}{2}\right)y^2\right)\right]$$

where the function χ is

$$\chi = -\left(\frac{3+2\nu}{4}\right)b^2 r\cos\phi - \left(\frac{3+2\nu}{4}\right)a^2 r\cos\phi + \frac{1}{4}r^2\cos 3\phi - \left(\frac{3+2\nu}{4}\right)\frac{a^2b^2\cos\phi}{r}$$

Using $x = r\cos\phi$, $y = r\sin\phi$, the stresses become

$$\tau_{rz} = -\frac{WR^2}{2(1+\nu)I}\left[\left(\frac{3+2\nu}{4}\right)\cos\phi\left(s^2 - (s_a^2 + s_b^2) + \frac{s_a^2 s_b^2}{s^2}\right)\right]$$

$$\tau_{\phi} = -\frac{WR^2}{2(1+\nu)I}\left[\left(\frac{3+2\nu}{4}\right)\sin\phi\left(s_a^2 + s_b^2 + \frac{s_a^2 s_b^2}{s^2}\right) - \frac{1}{4}(1-2\nu)s^2\sin\phi\right] \quad (1)$$

The (downward) force is

$$F_z = \int_a^b \int_0^{2\pi} (\tau_{rz}\cos\phi - \tau_{\phi z}\sin\phi) r\,dr\,d\phi = W$$

In addition, there is bending stress

$$\sigma_z = -\frac{W(L-z)x}{I}$$

We generalize this result by replacing x by $r\cos\phi$ and $(L-z)$ by $\rho\sin\theta$ (where $\rho = R + r\cos\phi$) to obtain

$$\sigma_\theta = -\frac{WR^2\sin\theta}{I}[s\cos\phi(1+s\cos\phi)]$$

At $\theta = 90°$, we find

$$N = R^2\int_{s_a}^{s_b}\int_0^{2\pi}\sigma_\theta s\,ds\,d\phi = -W$$

$$M = R^3\int_{s_a}^{s_b}\int_0^{2\pi}(\sigma_\theta s\cos\phi)s\,ds\,d\phi = -WR$$

The assumed expression for σ_θ thus possesses the correct resultant force and the correct resultant moment

The transition of stresses from the cantilever of Fig 1 to the hollow toroidal elbow of Fig 2 is made by identifying the stresses according to the scheme

$$\tau_{rz} \to \tau_{r\theta}$$

$$\tau_{\phi z} \to \tau_{\phi\theta}$$

$$\sigma_z \to \sigma_\theta$$

We next modify the stresses $\tau_{r\theta}$ and $\tau_{\phi\theta}$ by adding the (respective) stress fields

$$\begin{aligned} &-\frac{WR^2}{2(1+\nu)I}\left[-\alpha\left(s^2-(s_a^2+s_b^2)+\frac{s_a^2s_b^2}{s^2}\right)\right]\cos\phi \\ &-\frac{WR^2}{2(1+\nu)I}\left[\beta s^2-\alpha\left(s_a^2+s_b^2+\frac{s_a^2s_b^2}{s^2}\right)\right]\sin\phi \end{aligned} \tag{2}$$

The (strain) compatibility conditions for strains $l_{r\theta}$ and $l_{\phi\theta}$ can be expressed by the single equation

$$\frac{\partial\tau_{\phi\theta}}{\partial s} + \frac{\tau_{\phi\theta}}{s} - \frac{1}{s}\frac{\partial\tau_{r\theta}}{\partial\phi} = 0$$

and this reduces to

$$-\frac{WR^2}{2(1+\nu)I}[2\nu s + (3\beta-\alpha)s]\sin\phi = 0$$

We satisfy this by imposing the condition

$$(3\beta-\alpha) = -2\nu$$

The (inward) force is

$$F_x = \int_a^b\int_0^{2\pi}(\tau_{r\theta}\cos\phi - \tau_{\phi\theta}\sin\phi)r\,dr\,d\phi$$

With the added stress fields this becomes

$$\begin{aligned} F_x = R^2\int_{s_a}^{s_b}\int_0^{2\pi}&\left[-\frac{WR^2}{2(1+\nu)I}\left(\frac{3+2\nu}{4}-\alpha\right)(s^2-(s_a^2+s_b^2))\cos^2\phi\right]s\,ds\,d\phi \\ &+R^2\int_{s_a}^{s_b}\int_0^{2\pi}\left[\frac{WR^2}{2(1+\nu)I}\right]\left\{\left(\frac{3+2\nu}{4}-\alpha\right)\left(s_a^2+s_b^2+\frac{s_a^2s_b^2}{s^2}\right)\right. \\ &\left.+[\beta-\tfrac{1}{4}(1-2\nu)]s^2\right\}\sin^2\phi\,s\,ds\,d\phi \end{aligned}$$

Performing the integration with respect to ϕ yields

$$\begin{aligned} F_x = &-\frac{WR^4\pi}{2(1+\nu)I}\int_{s_a}^{s_b}\left[\left(\frac{3+2\nu}{4}-\alpha\right)[s^2-(s_a^2+s_b^2)]\right]s\,ds \\ &+\frac{WR^4\pi}{2(1+\nu)I}\int_{s_a}^{s_b}\left[\left(\frac{3+2\nu}{4}-\alpha\right)(s_a^2+s_b^2)+[\beta-\tfrac{1}{4}(1-2\nu)]s^2\right]s\,ds \\ F_x = &\frac{WR^4\pi}{2(1+\nu)I}\left[\left(\frac{3+2\nu}{4}-\alpha\right)(\tfrac{1}{2}(s_b^4-s_a^4))+\beta\frac{(s_b^4-s_a^4)}{4}-\frac{(1-2\nu)}{16}(s_b^4-s_a^4)\right] \\ = &\frac{W}{2(1+\nu)}[2(1+\nu)-3\alpha+\beta] \end{aligned}$$

The last modification of the stresses $\tau_{r\theta}$ and $\tau_{\phi\theta}$ consists of replacing the factor $2(1+\nu)$ by κ where

$$\kappa = [2(1+\nu)-3\alpha+\beta]$$

Thus, finally

$$\begin{aligned} \tau_{r\theta} &= -\frac{WR^2}{\kappa I}\left[\delta_1\left(s^2-(s_a^2+s_b^2)+\frac{s_a^2s_b^2}{s^2}\right)\right]\cos\phi\cos\theta \\ \tau_{\phi\theta} &= -\frac{WR^2}{\kappa I}\left[-\delta_2 s^2+\delta_1\left[(s_a^2+s_b^2)+\frac{s_a^2s_b^2}{s^2}\right]\right]\sin\phi\cos\theta \end{aligned} \tag{3}$$

where

$$\delta_1 = \left(\frac{3+2\nu}{4}\right)-\alpha$$

$$\delta_2 = \left(\frac{1-2\nu}{4}\right)-\beta$$

The (inward) force $F_x = 2W$

We choose $\beta = 3\alpha$ so that $\kappa = 1+\nu$, one-half the value for the cantilever beam From the condition $3\beta-\alpha = -2\nu$ we have $\alpha = -\nu/4$ and $\beta = -3\nu/4$ Then

$$\delta_1 = \tfrac{3}{4}(1+\nu) \quad \text{and} \quad \delta_2 = \tfrac{1}{4}(1+\nu)$$

For future use, we note that

$$\frac{\delta_1}{\kappa} = \frac{3}{4} \quad \text{and} \quad \frac{\delta_2}{\kappa} = \frac{1}{4}$$

The initial stress, σ_θ

The stress σ_θ consists of two terms

$$\sigma_\theta = -\frac{WR^2}{I}s\cos\phi\sin\theta - \frac{WR^2}{I}s^2\cos^2\phi\sin\theta \tag{4}$$

Comparing with Appendix 2, the first term corresponds to sinusoidally varying pure bending of amount

$$cER = -\frac{WR^2}{I}$$

The associated stress, satisfying the boundary conditions, may be obtained from the stress field of pure bending by simply multiplying by $\sin\theta$ (see Appendix 3)

For the second term of σ_θ, we list the equilibrium and compatibility functions in Appendix 4

Additional shear stress due to sinusoidally varying bending

Bending varying as $\sin\theta$, produces an additional shear field of stress The equilibrium equation is

$$\frac{1}{s}\frac{\partial}{\partial s}(\tau_{r\theta}s) + \frac{1}{s}\frac{\partial\tau_{\phi\theta}}{\partial\phi} = \frac{WR^2}{I}s\cos\phi\cos\theta$$

The compatibility equations for these stresses are

$$\nabla_0^2\tau_{r\theta} - \frac{\tau_{r\theta}}{s^2} - \frac{2}{s^2}\frac{\partial\tau_{\phi\theta}}{\partial\phi} = \frac{WR^2}{I(1+\nu)}\cos\phi\cos\theta$$

$$\nabla_0^2\tau_{\phi\theta} - \frac{\tau_{\phi\theta}}{s^2} + \frac{2}{s^2}\frac{\partial\tau_{r\theta}}{\partial\phi} = -\frac{WR^2}{I(1+\nu)}\sin\phi\cos\theta$$

A solution can be found in the form

$$\begin{aligned} (\tau_{r\theta})_1 &= \frac{WR^2}{8I}\left(\frac{3+2\nu}{1+\nu}\right)\left[s^2-(s_a^2+s_b^2)+\frac{s_a^2s_b^2}{s^2}\right]\cos\phi\cos\theta \\ (\tau_{\phi\theta})_1 &= -\frac{WR^2}{8I}\left[\left(\frac{1-2\nu}{1+\nu}\right)s^2-\left(\frac{3+2\nu}{1+\nu}\right)\left((s_a^2+s_b^2)+\frac{s_a^2s_b^2}{s^2}\right)\right]\sin\phi\cos\theta \end{aligned} \tag{5}$$

This stress field has a resultant shear force (inward) of amount

$$F = -W\cos\theta$$

INITIAL NORMAL FORCE FIELD

We assume an initial field of stress expressed by

$$\begin{aligned} \sigma_r &= a_0\sin\theta\left[s^2-(s_a^2+s_b^2)+\frac{s_a^2s_b^2}{s^2}\right] \\ \sigma_\phi &= \sin\theta\left[b_0s^2-a_0(s_a^2+s_b^2)-a_0\frac{s_a^2s_b^2}{s^2}\right] \\ \sigma_\theta &= \sin\theta(\lambda_0+\lambda_0)(s_a^2+s_b^2)+\sin\theta(\lambda_1+\lambda_1)s^2 \end{aligned} \tag{6}$$

The strain compatibility conditions may be satisfied by

$$(3+\nu)b_0-(1+3\nu)a_0-2\nu(\lambda_1+\bar{\lambda}_1)=0$$

and

$$\lambda_1+\bar{\lambda}_1=\nu(a_0+b_0)$$

From these two equations we find the useful identity

$$(3-2\nu)b_0=(1+2\nu)a_0$$

The equilibrium and compatibility functions derived from this stress field are listed in Appendix 5

Because of the coupled stress fields it is necessary to introduce two terms in the expression for σ_θ This will be made evident in the subsequent analysis

Shear stress independent of ϕ

There is a state of stress, independent of ϕ, and given by

$$\frac{\partial}{s\partial s}(\tau_{r\theta}s)+\frac{1}{s}\frac{\partial\tau_{\phi\theta}}{\partial\phi}=\cos\theta[K_0(\delta_1+\delta_2)s^2-2K_0\delta_1(s_a^2+s_b^2)]+\cos\theta\left[\frac{WR^2s^2}{2I}-\bar{\lambda}_1s^2-\bar{\lambda}_0(s_a^2+s_b^2)\right]$$

with compatibility equations

$$\nabla_0^2\tau_{r\theta}-\frac{\tau_{r\theta}}{s^2}-\frac{2}{s^2}\frac{\partial\tau_{\phi\theta}}{\partial\phi}=\cos\theta\left[\frac{K_0s}{2}(3\delta_1-\delta_2)+\frac{WR^2s}{I(1+\nu)}-\frac{2\bar{\lambda}_1s}{\nu}\right]$$

$$\nabla_0^2\tau_{\phi\theta}-\frac{\tau_{\phi\theta}}{s^2}+\frac{2}{s^2}\frac{\partial\tau_{r\theta}}{\partial\phi}=0$$

We assume

$$(\tau_{r\theta})_1=d_0\left(s^3-s(s_a^2-s_b^2)+\frac{s_a^2s_b^2}{s}\right)\cos\theta$$
$$\tau_{\phi\theta}=0 \qquad (7)$$

and find

$$4d_0=K_0(\delta_1+\delta_2)+\frac{WR^2}{2I}-\bar{\lambda}_1$$

$$-2d_0=-2K_0\delta_1-\bar{\lambda}_0$$

$$8d_0=\frac{K_0}{2}(3\delta_1-\delta_2)+\frac{WR^2}{I(1+\nu)}-\frac{2\bar{\lambda}_1}{\nu}$$

The solution (for $\bar{\lambda}_1$, d_0, $\bar{\lambda}_0$, a_0 and b_0) is

$$\bar{\lambda}_1=-\frac{WR^2\nu^2}{2I(1-\nu^2)}-\frac{K_0\delta_1\nu}{4(1+\nu)}-\frac{5K_0\delta_2\nu}{4(1-\nu)}$$

$$d_0=\frac{WR^2}{8I(1-\nu^2)}+\frac{K_0}{16(1+\nu)}[(4-3\nu)\delta_1+(4+\nu)\delta_2]$$

$$\bar{\lambda}_0=\frac{WR^2}{4I(1-\nu^2)}+\frac{K_0}{8(1-\nu)}[(13\nu-12)\delta_1+(4+\nu)\delta_2] \qquad (8)$$

$$a_0=\frac{(3-2\nu)}{4\nu}(\nu_1+\bar{\nu}_1)$$

$$b_0=\frac{1+2\nu}{4\nu}(\nu_1+\bar{\nu}_1)$$

The value of ν_1 will be determined later

Field of stress in ($\cos 2\phi/\sin 2\phi$)

There is a shear field of stress including terms in $\cos 2\phi$ and $\sin 2\phi$ From the Appendices we have

$$\frac{1}{s}\frac{\partial(\tau_{r\theta}s)}{\partial s}+\frac{1}{s}\frac{\partial\tau_{\phi\theta}}{\partial\phi}=\cos\theta\cos 2\phi\left[\frac{WR^2s^2}{2I}+K_0(\delta_1-\delta_2)s^2+2K_0\delta_1\frac{s_a^2s_b^2}{s^2}\right]$$

$$\nabla_0^2\tau_{r\theta}-\frac{\tau_{r\theta}}{s^2}-\frac{2}{s^2}\frac{\partial\tau_{\phi\theta}}{\partial\phi}=\cos\theta\cos 2\phi\left[\frac{WR^2s}{I(1+\nu)}+\frac{K_0(\delta_1+\delta_2)}{2}s-2K_0\delta_1\frac{s_a^2s_b^2}{s^3}\right]$$

$$\nabla_0^2\tau_{\phi\theta}-\frac{\tau_{\phi\theta}}{s^2}+\frac{2}{s^2}\frac{\partial\tau_{r\theta}}{\partial\phi}=\cos\theta\sin 2\phi\left[-\frac{WR^2s}{I(1+\nu)}-\frac{K_0(\delta_1+\delta_2)}{2}s-2K_0\delta_1\frac{s_a^2s_b^2}{s^3}\right]$$

A solution can be found in the form

$$\tau_{r\theta}=\cos\theta\cos 2\phi\left[as^3-\frac{b}{s^3}+cs+\frac{d}{s}\right]$$
$$\tau_{\phi\theta}=\cos\theta\sin 2\phi\left[-fs^3-\frac{b}{s^3}-cs-\frac{g}{s}\right] \qquad (9)$$

where

$$g=-K_0\delta_1s_a^2s_b^2$$

$$d=-\frac{1}{2}K_0\delta_1s_a^2s_b^2$$

$$f=\frac{WR^2}{I}\frac{(1-\nu)}{12(1+\nu)}+\frac{K_0}{2}[3\delta_2-\delta_1]$$

$$a=\frac{K_0\delta_2}{2}+\frac{WR^2}{I}\frac{(2+\nu)}{12(1+\nu)}$$

$$c=\frac{\frac{1}{2}K_0\delta_1s_a^2s_b^2-a(s_b^4+s_a^4+s_a^2s_b^2)}{s_a^2s_b^2}$$

$$b=s_a^2s_b^2(-c-a(s_a^2+s_b^2))$$

Field of stress in ($\cos 3\phi/\sin 3\phi$)

There is a field of stress involving terms in $\cos 3\phi$ and $\sin 3\phi$ From the Appendices we have

$$\frac{\partial(\sigma_r s)}{s\partial s}+\frac{1}{s}\frac{\partial\tau_{r\phi}}{\partial\phi}-\frac{\sigma_\phi}{s}=-\frac{WR^2}{4I}s^2\cos 3\phi\sin\theta$$

$$\frac{1}{s}\frac{\partial\sigma_\phi}{\partial\phi}+\frac{1}{s^2}\frac{\partial}{\partial s}(\tau_{r\phi}s^2)=\frac{WR^2s^2}{4I}\sin 3\phi\sin\theta$$

The compatibility equations are

$$\nabla^2\sigma_r-\frac{4}{s^2}\frac{\partial\tau_{r\phi}}{\partial\phi}-\frac{2}{s^2}(\sigma_r-\sigma_\phi)+\frac{1}{1+\nu}\frac{\partial^2\Theta}{\partial s^2}=0$$

$$\nabla^2\sigma_\phi+\frac{4}{s^2}\frac{\partial\tau_{r\phi}}{\partial\phi}+\frac{2}{s^2}(\sigma_r-\sigma_\phi)+\frac{1}{1+\nu}\left(\frac{1}{s}\frac{\partial\Theta}{\partial s}+\frac{1}{s^2}\frac{\partial^2\Theta}{\partial\phi^2}\right)=0$$

$$\nabla^2\sigma_\theta=0$$

$$\nabla^2\tau_{r\phi}+\frac{2}{s^2}\frac{\partial}{\partial\phi}(\sigma_r-\sigma_\phi)-\frac{4\tau_{r\phi}}{s^2}+\frac{1}{1+\nu}\frac{\partial}{\partial\phi}\left[\frac{1}{s}\frac{\partial\Theta}{\partial s}-\frac{1}{s^2}\Theta\right]=0$$

A solution can be found in the form

$$\sigma_r=\cos 3\phi\sin\theta\left[-4As^3-\frac{12B}{s^5}-6Cs-\frac{10D}{s^3}-\frac{WR^2s^3}{12I}\right]$$

$$\sigma_\phi=\cos 3\phi\sin\theta\left[20As^3+\frac{12B}{s^5}+6Cs+\frac{2D}{s^3}-\frac{WR^2s^3}{12I}\right]$$

$$\tau_{r\phi}=\sin 3\phi\sin\theta\left[12As^3-\frac{12B}{s^5}+6Cs-\frac{6D}{s^3}\right] \qquad (10)$$

$$\sigma_\theta=\left(Fs^3\cos 3\phi+\frac{G}{s^3}\cos 3\phi\right)\sin\theta$$

where

$$F=16A\nu$$

$$G=-8D\nu$$

$$A=\frac{1}{6}\frac{WR^2}{I}\left[\frac{3\bar{\nu}_3(s_a^2+s_b^2)-4\bar{\nu}_2^2}{128\bar{\nu}_2^2-144\bar{\nu}_3(s_a^2+s_b^2)}\right]$$

$$B=\frac{1}{3}\frac{WR^2}{I}\left[\frac{2s_a^2s_b^2(\bar{\nu}_2^2-\bar{\lambda}_3\bar{\nu}_2(s_a^2+s_b^2))}{128\bar{\nu}_2^2-144\bar{\nu}_3(s_a^2+s_b^2)}\right] \qquad (11)$$

$$C=\frac{1}{3}\frac{WR^2}{I}\left[\frac{\bar{\lambda}_3\bar{\nu}_2}{128\bar{\nu}_2^2-144\bar{\nu}_3(s_a^2+s_b^2)}\right]$$

$$D=\frac{WR^2}{I}\left[\frac{\bar{\lambda}_3^2(s_a^2+s_b^2)-\bar{\lambda}_3\bar{\lambda}_2^2}{128\bar{\lambda}_2^2-144\bar{\nu}_3(s_a^2+s_b^2)}\right]$$

$$\bar{\lambda}_3=(s_b^4+s_a^4)(s_b^2+s_a^2)$$

$$\bar{\lambda}_2=s_b^4+s_a^4+s_a^2s_b^2$$

COUPLED TOROIDAL ELASTIC STRESS FIELD

The final field of stress consists of a coupling between the modified initial shear stress (of cantilever type) and the normal force field Using the Appendices, the equilibrium equations are

$$\frac{1}{s}\frac{\partial}{\partial s}(\sigma_r s)+\frac{1}{s}\frac{\partial \tau_{r\phi}}{\partial \phi}-\frac{\sigma_\phi}{s}=\cos\phi\sin\theta\left[K_0\delta_1(s_a^2+s_b^2)-K_0\delta_1 s^2-K_0\delta_1\frac{s_a^2s_b^2}{s^2}-\frac{3}{4}\frac{WR^2s^2}{I}+(\lambda_0+a_0)(s_a^2+s_b^2)+(\lambda_1-a_0)s^2-\frac{a_0s_a^2s_b^2}{s^2}\right]$$

$$\frac{1}{s}\frac{\partial}{\partial \phi}\sigma_\phi-\frac{1}{s^2}\frac{\partial}{\partial s}(\tau_{r\phi}s^2)=\sin\phi\sin\theta\left[K_0\delta_2 s^2-K_0\delta_1(s_a^2+s_b^2)-K_0\delta_1\frac{s_a^2s_b^2}{s^2}+\frac{1}{4}\frac{WR^2s^2}{I}+(b_0-\lambda_1)s^2-(a_0+\lambda_0)(s_a^2+s_b^2)-\frac{a_0(s_a^2s_b^2)}{s^2}\right]$$

The corresponding compatibility equations are

$$\nabla_0^2\sigma_r-\frac{4}{s^2}\frac{\partial \tau_{r\phi}}{\partial \phi}-\frac{2}{s^2}(\sigma_r-\sigma_\phi)+\frac{1}{1+\nu}\frac{\partial^2\Theta}{\partial s^2}=\sin\theta\cos\phi\left(-2a_0s+2a_0\frac{s_a^2s_b^2}{s^3}\right)$$

$$\nabla_0^2\sigma_\phi+\frac{4}{s^2}\frac{\partial \tau_{r\phi}}{\partial \phi}+\frac{2}{s^2}(\sigma_r-\sigma_\phi)+\frac{1}{1+\nu}\left(\frac{1}{s}\frac{\partial\Theta}{\partial s}+\frac{1}{s^2}\frac{\partial^2\Theta}{\partial\phi^2}\right)=\sin\theta\cos\phi\left(-2b_0s-\frac{2a_0s_a^2s_b^2}{s^3}\right)$$

$$\nabla_0^2\sigma_\theta=\sin\theta\cos\phi\left[-\frac{2\lambda_1 s(1+\nu)}{\nu}+\left(\frac{2+\nu}{1+\nu}\right)\left(\frac{2WR^2s}{I}\right)\right]$$

$$\nabla_0^2\tau_{r\phi}+\frac{2}{s^2}\frac{\partial}{\partial\phi}(\sigma_r-\sigma_\phi)-\frac{4\tau_{r\phi}}{s^2}+\frac{1}{1+\nu}\left[\frac{1}{s}\frac{\partial^2\Theta}{\partial s\partial\phi}-\frac{1}{s^2}\frac{\partial\Theta}{\partial\phi}\right]=\sin\theta\sin\phi\left[(a_0-b_0)s+2a_0\frac{s_a^2s_b^2}{s^3}\right]$$

From the compatibility equation for σ_θ, we have

$$\sigma_\theta=\cos\phi\sin\theta\left[k_1s^3+k_0s+k_2\frac{s_a^2s_b^2}{s}\right] \tag{12}$$

where

$$k_1=-\frac{\lambda_1}{4}\left(\frac{1+\nu}{\nu}\right)+\frac{1}{4}\frac{WR^2}{I}\left(\frac{2+\nu}{1+\nu}\right)$$

and the terms in k_0 and k_2 are harmonic

We assume the stress field

$$\sigma_r=a_1\left[s^3-s(s_a^2+s_b^2)+\frac{s_a^2s_b^2}{s}\right]\cos\phi\sin\theta$$

$$\sigma_\phi=\left[a_2s^3+a_3s(s_a^2+s_b^2)+a_5\frac{s_a^2s_b^2}{s}\right]\cos\phi\sin\theta \tag{13}$$

$$\tau_{r\phi}=a_4\left[s^3-s(s_a^2+s_b^2)+\frac{s_a^2s_b^2}{s}\right]\sin\phi\sin\theta$$

From the first equilibrium equation, on equating like terms, there results

$$4a_1-a_2+a_4=-K_0\delta_1-\frac{3}{4}\frac{WR^2}{I}+(\lambda_1-a_0) \tag{14a}$$

$$-2a_1-a_4-a_3=K_0\delta_1+\lambda_0+a_0 \tag{14b}$$

$$a_4-a_5=-K_0\delta_1-a_0 \tag{14c}$$

The same procedure applied to the second equilibrium equation leads to

$$5a_4-a_2=K_0\delta_2+\frac{1}{4}\frac{WR^2}{I}+b_0-\lambda_1 \tag{14d}$$

$$-a_3-3a_4=-a_0-\lambda_0-K_0\delta_1 \tag{14e}$$

$$a_4-a_5=-K_0\delta_1-a_0 \tag{14f}$$

We discard eqn (14f) which is the same as (14c), and form the sum and difference of eqns (14b) and (14e) to obtain

$$a_1+a_3+2a_4=0$$

$$-a_1+a_4=K_0\delta_1+\lambda_0+a_0$$

We also replace eqns (14a) and (14d) by their sum and difference The result is

$$a_1-a_4=-\frac{K_0(\delta_1+\delta_2)}{4}-\frac{WR^2}{4I}+\frac{\lambda_1(2\nu-1)}{4\nu}$$

$$2a_1-a_2+3a_4=\frac{K_0}{2}(\delta_2-\delta_1)-\frac{1}{4}\frac{WR^2}{I}+\frac{1}{2}(b_0-a_0)$$

The first compatibility equation leads to

$$6a_1-4a_4+2a_2+\frac{6}{1+\nu}[a_1+a_2+k_1]=-2a_0$$

$$2a_4+a_1+a_3=0$$

$$-4a_4-2a_1+2a_5+\frac{2}{1+\nu}[a_1+a_2+k_2]=2a_0$$

The second compatibility equation generates only one independent equation

$$6a_2+4a_4+2a_1+\frac{2}{1+\nu}(a_1+a_2+k_1)=-2b_0$$

The third compatibility equation does not yield any independent relations There are only three equations to consider since the second equation above was already derived from equilibrium considerations

The sum of eqns (14a) and (14d) is reducible to

$$a_1+a_2=-\frac{1}{4}\frac{WR^2}{I(1+\nu)}$$

The difference of the same two equations is reducible to

$$a_2+a_4=\frac{a_0}{8}-\frac{3b_0}{8}$$

From these, we obtain

$$a_1+a_4=-\frac{1}{4}\frac{WR^2}{I(1+\nu)}+\frac{3b_0}{8}-\frac{a_0}{8}$$

We have two expressions for the difference (a_1-a_4), one derived from the equilibrium equations and one derived from the compatibility equations Equating those two leads to an identity.

We also have

$$\lambda_1=\frac{K_0(\delta_1+\delta_2)}{8}+\frac{WR^2}{8I}\left(\frac{\nu}{1+\nu}\right)+\frac{4+\nu}{2(3-2\nu)}a_0$$

and

$$\lambda_1+\bar{\lambda}_1=\frac{4a_0\nu}{3-2\nu}$$

Solving for a_0 we find

$$a_0=\frac{2(3-2\nu)}{(4-7\nu)}\left[\frac{(5\nu^2-\nu)K}{8(1-\nu^2)}+\left(\frac{3\nu-1}{1-\nu}\right)\frac{K_0\delta_1}{8}+\frac{(11\nu-1)}{(1-\nu)}\frac{K_0\delta_2}{8}\right]$$

and then

$$b_0=\frac{2(1+2\nu)}{(4-7\nu)}\left[\frac{(5\nu^2-\nu)K}{8(1-\nu^2)}+\left(\frac{3\nu-1}{1-\nu}\right)\frac{K_0\delta_1}{8}+\frac{(11\nu-1)}{(1-\nu)}\frac{K_0\delta_2}{8}\right]$$

and

$$\lambda_1=\frac{K_0(\delta_1+\delta_2)}{8}+\frac{K\nu}{8(1+\nu)}+\left(\frac{4+\nu}{4-7\nu}\right)\left[\frac{(5\nu^2-\nu)K}{8(1-\nu^2)}+\frac{(3\nu-1)}{(1-\nu)}\frac{K_0\delta_1}{8}+\frac{(11\nu-1)}{4(1-\nu)}\frac{K_0\delta_2}{8}\right]$$

The coefficients can now be determined from the relations

$$\lambda_0=\frac{K}{4(1+\nu)}-K_0\delta_1-\frac{3b_0}{8}-\frac{7}{8}a_0$$

$$a_1=-\frac{5}{24}K_0\delta_1-\frac{1}{24}K_0\delta_2+\frac{\lambda_1}{4}-\frac{5a_0}{24}-\frac{b_0}{24}-\frac{K(2+\nu)}{6(1+\nu)}$$

$$a_2=-\frac{1}{4}\frac{K}{(1+\nu)}-a_1$$

$$a_4=\frac{a_0}{8}-\frac{3b_0}{8}-a_2$$

$$a_3=-2a_4-a_1$$

$$a_5=a_0+a_4+K_0\delta_1$$

$$k_2=(1+\nu)(a_0-a_5)+a_1\nu-a_2+2a_4$$

ADJUSTMENT OF THE RESULTANT NORMAL FORCE

The normal force is given by

$$N=R^2\int\int(\sigma_\theta s\,ds\,d\phi)=\pi R^2(s_b^4-s_a^4)\left(\bar{\lambda}_0+\lambda_0+\frac{\lambda_1}{2}+\frac{\bar{\lambda}_1}{2}\right)-W$$

reducing to $(WQ - W)$ where

$$Q = \frac{(-41\nu^2 + 63\nu - 25)}{(4 - 7\nu)(1 - \nu)} + \frac{(20 - 41\nu - 15\nu^2 + 30\nu^3)}{2(1 - \nu^2)(4 - 7\nu)}$$

In the solution of the problem of pure bending [3] a term

$$cER\lambda_0 = \frac{cER(2 + \nu)}{8(1 + \nu)}(s_b^2 + s_a^2)$$

was adjusted to give zero normal force We may now readjust this constant to eliminate the term WQ so that the resultant normal force is simply $-W$(compression) on the plane $\theta = 90°$

Let the increment in λ_0 be $\Delta\lambda_0$ We require

$$cER^3\pi(s_b^2 - s_a^2)\Delta\lambda_0 + \pi R^2(s_b^4 - s_a^4)\left(\tau_0 + \lambda_0 + \frac{\lambda_1}{2} + \frac{\tau_1}{2}\right) = 0$$

Using $cER = -WR^2/I$ we find

$$\Delta\lambda_0 = \frac{Q}{4}(s_b^2 + s_a^2)$$

In the solution for pure bending the equation for σ_θ is to be adjusted by replacing the term

$$\lambda_0 = \frac{2 + \nu}{8(1 + \nu)}(s_b^2 + s_a^2)$$

by the new value

$$\left[\frac{2 + \nu}{8(1 + \nu)} + \frac{Q}{4}\right](s_b^2 + s_a^2)$$

ADJUSTMENT OF THE RESULTANT MOMENT

The resultant moment (at $\theta = 90°$) is given by

$$\begin{aligned} M &= R^3 \int_{s_a}^{s_b}\int_0^{2\pi} (\sigma_\phi s\cos\phi)s\,ds\,d\phi - WR \\ &= R^3 \int_{s_a}^{s_b}\int_0^{2\pi} \cos^2\phi\left[k_1 s^3 + k_0 s + k_2\frac{s_a^2 s_b^2}{s}\right]s^2\,ds\,d\phi - WR \\ &= R^3\pi\left[k_1\frac{(s_b^6 - s_a^6)}{6} + k_0\frac{(s_b^4 - s_a^4)}{4} + k_2 s_a^2 s_b^2\frac{(s_b^2 - s_a^2)}{2}\right] - WR \end{aligned}$$

We select k_0 so the first term vanishes Hence

$$k_0 = -\frac{2k_2 s_a^2 s_b^2}{(s_b^2 + s_a^2)} - \frac{2}{3}\frac{k_1(s_b^4 + s_a^4 + s_a^2 s_b^2)}{(s_b^2 + s_a^2)}$$

CONCLUSION

Now that all coefficients in the stress equations have been determined, we may summarize the stress fields by equation numbers

σ_r = eqn (6) + eqn (10) + eqn (13) + Bending Term (Appendix 3)

σ_ϕ = eqn (6) + eqn (10) + eqn (13) + Bending Term (Appendix 3)

σ_θ = eqn (4) + eqn (10) + eqn (12) + Bending Term (Appendix 3)

$\tau_{r\phi}$ = eqn (10) + eqn(13) + Bending Term (Appendix 3)

$\tau_{r\theta}$ = eqn (3) + eqn (5) + eqn (7) + eqn (9)

$\tau_{\phi\theta}$ = eqn (3) + eqn (5) + eqn (9)

The procedure used in this paper can be continued but the next term is algebraically cumbersome We note that computer routines (in FORTRAN) are easily generated for the solution given here

APPENDIX 1

Equilibrium and compatibility functions

The three equilibrium functions for the initial shear stresses $\tau_{r\theta}$ and $\tau_{\phi\theta}$ are

$$N(1) = K_0\left[\delta_1(s_a^2 + s_b^2) - \delta_1 s^2 - \frac{\delta_1 s_a^2 s_b^2}{s^2}\right]\cos\phi\sin\theta$$

$$N(2) = K_0\left[\delta_2 s^2 - \delta_1(s_a^2 + s_b^2) - \frac{\delta_1 s_a^2 s_b^2}{s^2}\right]\sin\phi\sin\theta$$

$$\begin{aligned} N(3) = {} & K_0\cos\theta[-2\delta_1(s_a^2 + s_b^2) + (\delta_1 + \delta_2)s^2] \\ & + K_0\cos\theta\cos 2\phi\left[(\delta_1 - \delta_2)s^2 + \frac{2s_a^2 s_b^2}{s^2}\delta_1\right] \end{aligned}$$

The corresponding six compatibility functions are

$$V(1) = 0$$

$$V(2) = 0$$

$$V(3) = 0$$

$$V(4) = 0$$

$$V(5) = K_0\cos\theta\left[\frac{s}{2}(3\delta_1 - \delta_2) + \frac{1}{2}(\delta_1 + \delta_2)s\cos 2\phi - \frac{2s_a^2 s_b^2\delta_1\cos 2\phi}{s^3}\right]$$

$$V(6) = K_0\cos\theta\sin 2\phi\left[-\frac{1}{2}(\delta_1 + \delta_2)s - \frac{2s_a^2 s_b^2\delta_1}{s^3}\right]$$

APPENDIX 2

Functions for pure bending modified by $\sin\theta$

The initial state for pure bending is $\sigma_\theta = cERs\cos\phi$ When bending varies as $\sin\theta$, we have

$$\sigma_\theta = cERs\cos\phi\sin\theta$$

The three equilibrium functions for this stress field are

$$N(1) = cERs\cos^2\phi\sin\theta$$

$$N(2) = -cERs\cos\phi\sin\phi\sin\theta$$

$$N(3) = -cERs\cos\phi\cos\theta$$

The corresponding six compatibility functions are

$$V(1) = 0$$

$$V(2) = 0$$

$$V(3) = -cER\left(\frac{2 + \nu}{1 + \nu}\right)\sin\theta$$

$$V(4) = 0$$

$$V(5) = -\frac{cER\cos\phi\cos\theta}{(1 + \nu)}$$

$$V(6) = \frac{cER\sin\phi\cos\theta}{(1 + \nu)}$$

APPENDIX 3

Stress fields for pure bending modified by $\sin\theta$

$$\begin{aligned} \sigma_r = {} & -K\sin\theta\left\{\frac{(3 + 2\nu)s^2}{16(1 + \nu)} + \frac{(3 + 2\nu)}{(1 + \nu)}\frac{s_a^2 s_b^2}{16s^2} - \frac{1}{16}\left(\frac{3 + 2\nu}{1 + \nu}\right)(s_b^2 + s_a^2)\right\} \\ & - K\sin\theta\cos 2\phi\left[-\frac{1}{4}\frac{(s_b^2 + s_a^2)}{(s_b^2 - s_a^2)^2}(s_b^4 + s_a^4 + s_a^2 s_b^2) - \frac{3}{4}\frac{s_a^4 s_b^4(s_b^2 + s_a^2)}{s^4(s_b^2 - s_a^2)^2}\right] \\ & - K\sin\theta\cos\phi\left[\frac{s_a^2 s_b^2(s_b^4 + s_a^4 + s_a^2 s_b^2)}{s^2(s_b^2 - s_a^2)^2} + \frac{s^2}{4}\right] \end{aligned}$$

$$\begin{aligned} \sigma_\phi = {} & -K\sin\theta\left\{\frac{(1 - 2\nu)s^2}{16(1 + \nu)} - \frac{1}{16}\frac{(3 + 2\nu)(s_b^2 + s_a^2)}{(1 + \nu)} - \frac{(3 + 2\nu)s_a^2 s_b^2}{16(1 + \nu)s^2}\right\} \\ & - K\sin\theta\cos 2\phi\left[\frac{(s_b^2 + s_a^2)(s_b^4 + s_a^4 + s_a^2 s_b^2)}{4(s_b^2 - s_a^2)^2} + \frac{3}{4}\frac{s_a^4 s_b^4(s_b^2 + s_a^2)}{s^4(s_b^2 - s_a^2)^2}\right] \\ & - K\sin\theta\cos 2\phi\left[\frac{-3s^2 s_a^2 s_b^2}{(s_b^2 - s_a^2)^2} + \frac{s^2}{4}\right] \end{aligned}$$

$$\begin{aligned} (\tau_{\theta r})_1 = {} & -K\sin\theta\sin 2\phi\left\{-\frac{s^2}{4} + \frac{(s_b^2 + s_a^2)(s_b^4 + s_a^4 + s_a^2 s_b^2)}{4(s_b^2 - s_a^2)^2} - \frac{3}{4}\frac{s_a^4 s_b^4(s_b^2 + s_a^2)}{s^4(s_b^2 - s_a^2)^2}\right. \\ & \left. - \frac{3}{2}\frac{s_a^2 s_b^2 s^2}{(s_b^2 - s_a^2)^2} + \frac{s_a^2 s_b^2(s_b^4 + s_a^4 + s_a^2 s_b^2)}{2s^2(s_b^2 - s_a^2)}\right\} \end{aligned}$$

$$\begin{aligned} \sigma_\theta = {} & -K\sin\theta\left[\frac{2 + \nu}{8(1 + \nu)}(s_b^2 + s_a^2) - \frac{(2 + \nu)s^2}{4(1 + \nu)}\right. \\ & \left. + \frac{Q}{4}(s_a^2 + s_b^2) - \frac{s^2(1 + \nu)}{2}\cos 2\phi\right] \\ & - K\sin\theta\cos 2\phi\left[-\frac{3\nu s_a^2 s_b^2 s^2}{(s_b^2 - s_a^2)^2} + \frac{\nu}{s^2}\frac{s_a^2 s_b^2(s_b^4 + s_a^4 + s_a^2 s_b^2)}{(s_b^2 - s_a^2)^2}\right] \end{aligned}$$

APPENDIX 4

Functions for stress $\sigma_\theta = -\dfrac{WR^2}{I} s^2 \cos^2\phi \sin\theta$

The equilibrium functions are

$$N(1) = -\frac{WR^2}{I}\sin\theta\left(\frac{3}{4}s^2\cos\phi + \frac{s^2}{4}\cos 3\phi\right)$$

$$N(2) = \frac{WR^2}{I}\sin\theta\left(\frac{1}{4}s^2\sin\phi + \frac{s^2}{4}\sin 3\phi\right)$$

$$N(3) = \frac{WR}{I}\cos\theta\left[\frac{s^2}{2} + \frac{s^2\cos 2\phi}{2}\right]$$

The compatibility functions are

$$V(1) = 0$$

$$V(2) = 0$$

$$V(3) = \frac{2(2+\nu)}{1+\nu}\frac{WR^2}{I} s\cos\phi\sin\theta$$

$$V(4) = 0$$

$$V(5) = \frac{WR^2}{I(1+\nu)} s(1+\cos 2\phi)\cos\theta$$

$$V(6) = -\frac{WR^2}{I(1+\nu)} s\sin 2\phi\cos\theta$$

APPENDIX 5

Initial normal force stress field

The equilibrium functions are

$$N(1) = \sin\theta\cos\phi\left[(\lambda_0 + a_0)(s_a^2 + s_b^2) + (\lambda_1 - a_0)s^2 - \frac{a_0 s_a^2 s_b^2}{s^2}\right]$$

$$N(2) = \sin\theta\sin\phi\left[(b_0 - \lambda_1)s^2 - (a_0 + \lambda_0)(s_a^2 + s_b^2) - \frac{a_0 s_a^2 s_b^2}{s^2}\right]$$

$$N(3) = \cos\theta[-\lambda_1 s^2 - \lambda_0(s_a^2 + s_b^2)]$$

The compatibility functions are

$$V(1) = 2a_0\sin\theta\cos\phi\left[-s + \frac{s_a^2 s_b^2}{s^3}\right]$$

$$V(2) = 2\sin\theta\cos\phi\left[-b_0 s - a_0\frac{s_a^2 s_b^2}{s^3}\right]$$

$$V(3) = 2\sin\theta\cos\phi\left[-\frac{\lambda_1 s(1+\nu)}{\nu}\right]$$

$$V(4) = \sin\theta\sin\phi\left[(a_0 - b_0)s + 2a_0\frac{s_a^2 s_b^2}{s^3}\right]$$

$$V(5) = -2\cos\theta\frac{\lambda_1 s}{\nu}$$

$$V(6) = 0$$

REFERENCES

1 Love, A E H, *The mathematical theory of elasticity*, Oxford University Press, Oxford 4th Edition 1927, pp 330–5

2 Lang H A Stress analysis of pressurized elbows for nuclear components using toroidal elasticity *Proc 4th Int Conf on Pressure Vessel Technology*, London 1980 Vol 2 pp 251–60

3 Lang, H A, In-plane bending of a curved pipe or toroidal tube acted on by end couples, *Int J Pres Ves & Piping*, 15(1) (1984) pp 27–35

4 Lang H A, Stress fields for a curved pipe subjected to in-plane end couples, *Int J Pres Ves & Piping*, 15(2) (1984), pp 93–104

B.7 Stress Fields for a Normal Force Acting on the End of a 90° Elbow or Pipe Bend

Stress Fields for a Normal Force Acting on the End of a 90° Elbow or Pipe Bend

H A Lang

LANG—Research West 1201 Idaho Avenue
Santa Monica CA 90403, USA

(Received 3 January 1984)

ABSTRACT

In a previous paper, eight stress fields were determined for a 90° elbow or pipe bend acted upon by an end shear force directed inwardly. The present paper determines the eight stress fields when an end normal force acts on a 90° elbow or pipe bend. The two problems are dual problems in the sense that they differ only by adjustment of a stress field of pure bending.

NOMENCLATURE

a	Inner radius of cross section
b	Outer radius of cross section
E, ν	Elastic constants
I	Moment of inertia
K	$\frac{WR^2}{I}$
K_0	$\frac{K}{\kappa}$
M	Bending moment on end plane
Q	Function of ν defined in the text
R	Toroidal radius
r, ϕ, θ	Toroidal elastic coordinates (Fig 1)

Int J Pres Ves & Piping 0308-0161/84 $03.00 © Elsevier Applied Science Publishers Ltd England 1984 Printed in Great Britain

s	$\frac{r}{R}$
s_a	$\frac{a}{R}$
s_b	$\frac{b}{R}$
W	Normal force on end plane $\theta = 0$
$\kappa, \delta_1, \delta_2$	Functions of ν
$\sigma_r, \sigma_\phi, \sigma_\theta$	Normal stresses
$\tau_{r\phi}, \tau_{r\theta}, \tau_{\phi\theta}$	Shear stresses

INTRODUCTION

A normal force $N (= W)$ is applied to the end ($\theta = 0$) of a hollow circular elbow, as shown in Figs 1 and 2. Equilibrium is maintained by an end shear force W and by a bending moment $M = WR$ both acting at $\theta = 90°$.

We next apply a state of pure bending, for which stresses are known (from Ref 1). This gives the configuration in Fig 3. If we adjust the moment $M_0 = \bar{c}EI$ (where $\bar{c} =$ constant) so that $M_0 = M = WR$, the moments at $\theta = 90°$ cancel and the configuration becomes that of Fig 4. The solution to this set of loads is known (from Ref 2) where θ was measured from the end of the elbow acted on by a shear force. We now relabel this θ'. Then it is only necessary to interchange $\sin\theta$ and $\cos\theta$ to maintain the load plane at $\theta = 0$. In summary, the solution for end shear (Fig 4) can be converted to the solution for end normal force (Fig 2) by adding a state of pure bending and by interchanging $\sin\theta$ and $\cos\theta$.

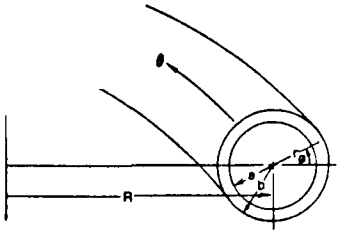

Fig 1. Cross-section coordinates of 90° elbow

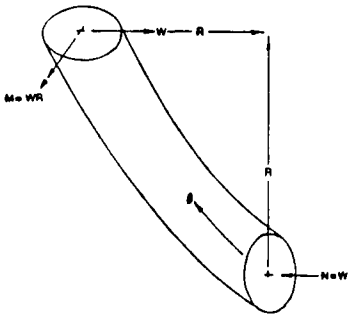

Fig 2. Normal compressive force acting on 90° elbow at load plane $\theta = 0$

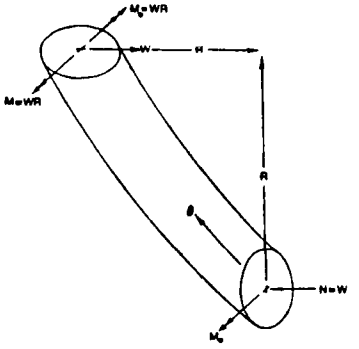

Fig 3. Addition of pure bending moment M_0, acting on 90° elbow

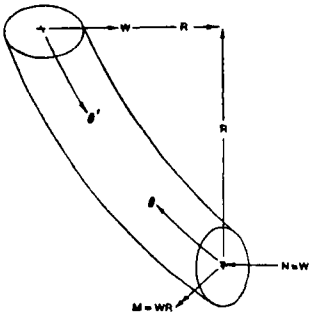

Fig. 4. In-plane end shear force, W, acting at load plane $\theta = 0$

Interchanging $\cos\theta$ and $\sin\theta$ from the eight stress fields of Ref 2 and adding the pure bending field from Ref 1 now leads to the eight stress fields described below.

THE EIGHT STRESS FIELDS

Stress field of initial (cantilever) type

$$(\tau_{r\phi})_0 = K_0\delta_1\left[(s_a^2 + s_b^2) - \frac{s_a^2 s_b^2}{s^2} - s^2\right]\cos\phi\sin\theta$$

$$(\tau_{\phi\theta})_0 = K_0\left[\delta_2 s^2 - \delta_1\left(s_a^2 + s_b^2 + \frac{s_a^2 s_b^2}{s^2}\right)\right]\sin\phi\sin\theta$$

$$(\sigma_\phi)_0 = -\frac{WR^2}{I}\cos\theta\left(s\cos\phi + \frac{s^2}{2} + \frac{s^2}{2}\cos 2\phi\right)$$

where

$$K_0 = \frac{WR^2}{I\kappa}$$

$$\kappa = 1 + \nu$$

$$\delta_1 = \tfrac{1}{4}(1 - 2\nu)$$

$$\delta_2 = \tfrac{1}{8}(1 - 2\nu)$$

This field of stress reduces to a shear force (at $\theta = 90°$) of amount $2W$(inwards) The normal force at $\theta = 0$ is $N = -W$ The bending moment at $\theta = 0$ is $M = -WR$ The stress term $-(WR^2/I)s\cos\phi\cos\theta$ generates a bending stress field varying as $\cos\theta$ The stresses from this term are combined later in the analysis, with the stresses from pure bending

Initial (normal force-like) stress field

$$\sigma_{r_0} = a_0\cos\theta\left[s^2 - (s_a^2 + s_b^2) + \frac{s_b^2 s_b^2}{s^2}\right]$$

$$\sigma_{\phi_0} = \cos\theta\left[b_0 s^2 - a_0(s_a^2 + s_b^2) - a_0\frac{s_a^2 s_b^2}{s^2}\right]$$

$$\sigma_{\theta_0} = \cos\theta[(\lambda_0 + \bar{\lambda}_0)(s_a^2 + s_b^2) + (\lambda_1 + \bar{\lambda}_1)s^2]$$

where

$$a_0 = \frac{2(3-2\nu)}{4-7\nu}\left[\frac{(5\nu^2-\nu)K}{8(1-\nu^2)} + \left(\frac{3\nu-1}{1-\nu}\right)\frac{K_0\delta_1}{8} + \left(\frac{11\nu-1}{1-\nu}\right)\frac{K_0\delta_2}{8}\right]$$

$$b_0 = \frac{2(1+2\nu)}{4-7\nu}\left[\frac{(5\nu^2-\nu)K}{8(1-\nu^2)} + \left(\frac{3\nu-1}{1-\nu}\right)\frac{K_0\delta_1}{8} + \left(\frac{11\nu-1}{1-\nu}\right)\frac{K_0\delta_2}{8}\right]$$

$$\bar{\lambda}_0 = \frac{WR^2}{4I(1-\nu^2)} + \frac{K_0}{8(1-\nu)}[(13\nu-12)\delta_1 + (4+\nu)\delta_2]$$

$$\bar{\lambda}_1 = -\frac{WR^2\nu^2}{2I(1-\nu^2)} - \frac{K_0\delta_1\nu}{4(1-\nu)} - \frac{5\delta_2 K_0\nu}{4(1-\nu)}$$

$$\lambda_0 = \frac{1}{4}\frac{WR^2}{I(1+\nu)} - \frac{3b_0}{8} - \frac{7a_0}{8} - K_0\delta_1$$

$$\lambda_1 = \frac{K_0(\delta_1+\delta_2)}{8} + \frac{K\nu}{8(1+\nu)} + \left(\frac{4+\nu}{4-7\nu}\right) \times\left[\frac{(5\nu^2-\nu)K}{8(1-\nu^2)} + \left(\frac{3\nu-1}{1-\nu}\right)\frac{K_0\delta_1}{8} + \frac{(11\nu-1)}{4(1-\nu)}\frac{K_0\delta_2}{8}\right]$$

This field of stress reduces, at $\theta = 0$, to a resultant force $N = WQ$ where

$$Q = \frac{-41\nu^2 + 63\nu - 25}{(4-7\nu)(1-\nu)} + \frac{20 - 41\nu - 15\nu^2 + 30\nu^3}{2(1-\nu^2)(4-7\nu)}$$

Shear field resulting from bending varying as $\sin\theta$

$$(\tau_{r\theta})_1 = \frac{WR^2}{8I}\left(\frac{3+2\nu}{1+\nu}\right)\left[s^2 - (s_a^2 + s_b^2) + \frac{s_a^2 s_b^2}{s^2}\right]\cos\phi\sin\theta$$

$$(\tau_{\phi\theta})_1 = -\frac{WR^2}{8I}\left[\left(\frac{1-2\nu}{1+\nu}\right)s^2 - \left(\frac{3+2\nu}{1+\nu}\right)\left(s_a^2 + s_b^2 + \frac{s_a^2 s_b^2}{s^2}\right)\right]\sin\phi\cos\theta$$

This field of stress represents a resultant shear force in the plane of the elbow. We have

$$F = R^2\int_{s_a}^{s_b}\int_0^{2\pi}(\tau_{r\theta}\cos\phi - \tau_{\phi\theta}\sin\phi)s\,ds\,d\phi$$

reducing to

$$F = -W\sin\theta$$

Stress field depending on $(\cos 2\phi/\sin 2\phi)$

$$(\tau_{r\theta})_1 = \sin\theta\cos 2\phi\left[as^3 - \frac{b}{s^3} + cs + \frac{d}{s}\right]$$

$$(\tau_{\phi\theta})_1 = \sin\theta\sin 2\phi\left[-fs^3 - \frac{h}{s^3} - cs - \frac{g}{s}\right]$$

where

$$a = \frac{K_0\delta_2}{2} + \frac{WR^2}{I}\frac{(2+\nu)}{12(1+\nu)}$$

$$b = -s_a^2 s_b^2(c + a(s_a^2 + s_b^2))$$

$$c = \frac{\frac{1}{2}K_0\delta_1 s_a^2 s_b^2 - a(s_b^4 + s_a^4 + s_a^2 s_b^2)}{s_a^2 + s_b^2}$$

$$d = -\tfrac{1}{2}K_0\delta_1 s_a^2 s_b^2$$

$$f = \frac{WR^2(1-\nu)}{12I(1+\nu)} + \frac{K_0}{2}(3\delta_2 - \delta_1)$$

$$g = -K_0\delta_1 s_a^2 s_b^2$$

This field of stress does not have a force resultant

First-order stress field depending on $(\cos\phi/\sin\phi)$

$$\sigma_{r_1} = a_1\cos\phi\cos\theta\left[s^3 - s(s_a^2 + s_b^2) + \frac{s_a^2 s_b^2}{s}\right]$$

$$\sigma_{\phi_1} = \cos\phi\cos\theta\left[a_2 s^3 + a_3 s(s_a^2 + s_b^2) + \frac{a_3 s_a^2 s_b^2}{s}\right]$$

$$(\tau_{r\phi})_1 = a_4\sin\phi\cos\theta\left[s^3 - s(s_a^2 + s_b^2) + \frac{s_a^2 s_b^2}{s}\right]$$

$$\sigma_{\theta_1} = \cos\phi\cos\theta\left(k_1 s^3 + k_0 s + k_2\frac{s_a^2 s_b^2}{s}\right)$$

where

$$a_1 = -\frac{5}{24}K_0\delta_1 - \frac{1}{24}K_0\delta_2 + \frac{\lambda_1}{4} - \frac{5a_0}{24} - \frac{b_0}{24} - \frac{K(2+\nu)}{6(1+\nu)}$$

$$a_2 = -\frac{1}{4}\frac{K}{(1+\nu)} - a_1$$

$$a_3 = -2a_4 - a_1$$

$$a_4 = \frac{a_0}{8} - \frac{3b_0}{8} - a_2$$

$$a_5 = a_4 + K_0\delta_1 + a_0$$

$$k_0 = -\frac{2k_2 s_a^2 s_b^2}{s_b^2 + s_a^2} - \frac{2}{3}\frac{k_1(s_b^4 + s_a^4 + s_a^2 s_a^2)}{s_b^2 + s_a^2}$$

$$k_1 = -\frac{\lambda_1}{4}\left(\frac{1+\nu}{\nu}\right) + \frac{1}{4}\frac{WR^2}{I}\left(\frac{2+\nu}{1+\nu}\right)$$

$$k_2 = (a_0 - a_5)(1+\nu) + a_1\nu - a_2 + 2a_4$$

This field of stress has no force or moment resultants

Stress field independent of ϕ

$$(\tau_{r\theta})_1 = d_0\left[s^3 - s(s_a^2 + s_b^2) + \frac{s_a^2 s_b^2}{s}\right]\sin\theta$$

$$(\tau_{\phi\theta})_1 = 0$$

where

$$d_0 = \frac{WR^2}{8(1-\nu^2)I} + \frac{K_0}{16(1-\nu)}[(4-3\nu)\delta_1 + (4+\nu)\delta_2]$$

This field of stress vanishes at the boundaries where $s = s_a$ or s_b It has no force resultant

First-order stress field depending on $(\cos 3\phi/\sin 3\phi)$

$$\sigma_{r_1} = \cos\theta\cos 3\phi\left(-4As^3 - \frac{12B}{s^5} - 6Cs - \frac{10D}{s^3} - \frac{WR^2 s^3}{12I}\right)$$

$$\sigma_{\phi_1} = \cos\theta\cos 3\phi\left(20As^3 + \frac{12B}{s^5} + 6Cs + \frac{2D}{s^3} - \frac{WR^2 s^3}{12I}\right)$$

$$\tau_{r\phi_1} = \cos\theta\sin 3\phi\left(12As^3 - \frac{12B}{s^5} + 6Cs - \frac{6D}{s^3}\right)$$

$$\sigma_{\theta_1} = \cos\theta\cos 3\phi\left(Fs^3 + \frac{G}{s^3}\right)$$

where

$$A = \frac{1}{6}K\left[\frac{3s_1(s_a^2 + s_b^2) - 4s_2^2}{128s_2^2 - 144s_1(s_a^2 + s_b^2)}\right]$$

$$B = \frac{1}{3}K\left[\frac{2s_a^2 s_b^2(s_2^3 - s_1 s_2(s_a^2 + s_b^2))}{128s_2^2 - 144s_1(s_a^2 + s_b^2)}\right]$$

$$C = \frac{1}{3}K\left[\frac{s_1 s_2}{128s_2^2 - 144s_1(s_a^2 + s_b^2)}\right]$$

$$D = K\left[\frac{s_1^2(s_a^2 + s_b^2) - s_1 s_2^2}{128s_2^2 - 144s_1(s_a^2 + s_b^2)}\right]$$

$$F = 16A\nu$$

$$G = -8D\nu$$

$$s_1 = (s_a^4 + s_b^4)(s_a^2 + s_b^2)$$

$$s_2 = s_a^4 + s_b^4 + s_a^2 s_b^2)$$

There is no resultant force or moment for this stress field

Combined field of bending stresses

$$\sigma_{r_1} = K(1-\cos\theta)\left[\frac{(3+2\nu)s^3}{16(1+\nu)} + \frac{3+2\nu}{16(1+\nu)}\frac{s_a^2 s_b^2}{s^3} - \frac{1}{16}\left(\frac{3+2\nu}{1+\nu}\right)(s_b^2+s_a^2)\right]$$
$$+ K(1-\cos\theta)\cos 2\phi\left[-\frac{1}{4}\frac{(s_b^2+s_a^2)}{(s_b^2-s_a^2)^2}(s_b^4+s_a^4+s_a^2s_b^2)+\frac{s^2}{4}\right.$$
$$\left.+\frac{s_a^2s_b^2}{s^2}\frac{(s_b^4+s_a^4+s_a^2s_b^2)}{(s_b^2-s_a^2)^2} - \frac{3}{4}\frac{s_a^4s_b^4(s_b^2+s_a^2)}{s^4(s_b^2-s_a^2)^2}\right]$$

$$\sigma_{\phi_1} = K(1-\cos\theta)\left[\frac{1-2\nu}{16(1+\nu)}s^2 - \frac{1}{16}\left(\frac{3+2\nu}{1+\nu}\right)(s_b^2+s_a^2) - \frac{3+2\nu}{16(1+\nu)}\frac{s_a^2s_b^2}{s^2}\right]$$
$$+ K(1-\cos\theta)\cos 2\phi\left[\frac{(s_b^2+s_a^2)}{4}\frac{(s_b^4+s_a^4+s_a^2s_b^2)}{(s_b^2-s_a^2)^2} - \frac{s^2}{4}\right.$$
$$\left.+\frac{3}{4}\frac{s_a^4s_b^4}{s^4(s_b^2-s_a^2)^2} - \frac{3s_a^2s_b^2s^2}{(s_b^2-s_a^2)^2}\right]$$

$$(\tau_{s\phi})_1 = K(1-\cos\theta)\sin 2\phi\left[-\frac{s^2}{4}+\frac{(s_b^2+s_a^2)}{4}\frac{(s_b^4+s_a^4+s_a^2s_b^2)}{(s_b^2-s_a^2)^2} - \frac{3}{4}\frac{s_a^4s_b^4(s_b^2+s_a^2)}{(s_b^2-s_a^2)^2}\right.$$
$$\left.-\frac{3}{2}\frac{s_a^2s_b^2s^2}{(s_b^2-s_a^2)^2}+\frac{s_a^2s_b^2(s_b^4+s_a^4+s_a^2s_b^2)}{2s^2(s_b^2-s_a^2)^2}\right]$$

$$\sigma_{f_1} = K(1-\cos\theta)\left[\frac{2+\nu}{8(1+\nu)}(s_b^2+s_a^2) - \frac{(2+\nu)s^2}{4(1+\nu)}\right]$$
$$-\cos\theta[(s_a^2+s_b^2)(\bar{\lambda}_0+\lambda_0)+(\lambda_1+\bar{\lambda}_1)s^2] + K(1-\cos\theta)\cos 2\phi$$
$$\times\left[-\frac{s^2(1+\nu)}{2} - \frac{3\nu s_a^2s_b^2s^2}{(s_b^2-s_a^2)^2} + \frac{\nu}{s^2}\frac{s_a^2s_b^2(s_b^4+s_a^4+s_a^2s_b^2)}{(s_b^2-s_a^2)^2}\right]$$

Thus field of stress has a resultant force $N = -WQ$ at $\theta = 0$. At 90°, the resultant is a bending moment of amount WR

RESULTANT FORCE AND MOMENT

The sum of all resultants from the eight fields of stress reduce to the compressive normal force $N = W$ at $\theta = 0$ and to a shear force W (inwards) at $\theta = 90°$ In addition, there is a bending moment $M = WR$ acting at $\theta = 90°$

REFERENCES

1 Lang, H A, In-plane bending of a curved pipe or toroidal tube acted on by end couples, *Int J Pres Ves & Piping*, 15 (1984), pp 27-35
2 Lang, H A, Stress fields for an in-plane end shear force acting on a 90° elbow or pipe bend, *Int J Pres Ves & Piping*, 16 (1984), pp 263-84